ASSESSMENT OF THERMAL AND FAST REACTOR DESIGNS BASED UPON THE ADVANCED GAS-COOLED REACTOR

RIDA Y. NUWAYHID

Environmental Safety Group
Nuclear Power Section
Department of Mechanical Engineering
Imperial College of Science, Technology and Medicine

A thesis submitted for

The degree of Doctor of Philosophy
of the University of London

and

The Diploma of Imperial College

March 1989

To my parents

and Rola

ABSTRACT

The physics performance parameters of a range of gas cooled reactors have been assessed using the codes WIMS-D4 and WIMS-E, both in the lattice cell approximation and as two or three dimensional whole cores. The extension of the normal use of the WIMS codes and library to fast cores was found to give rise to some uncertainties. Reactivity-lifetime tended to be overpredicted compared to the results of a dedicated fast reactor code.

In this study, the AGR has been taken as the basis of further gas cooled reactor developments. The major requirements of current AGR developement include an increase in discharge irradiation and higher availability. In the present work, new AGR variants of higher power density and longer fuel exposure have been investigated as possible routes for the continuation of the gas cooled/solid moderator reactor concept. A plutonium-burning variant and a variant with replacable graphite are compared and contrasted with AGR.

Further development of the AGR could result in a gas cooled breeder reactor if development and capital costs could be kept low. In this study the Existing Technology Gas Cooled Breeder reactor (ETGBR) has been considered; a low-rated design which uses established AGR components and technology where possible .

It is suggested in this work that ETGBR safety might be further enhanced by increasing the core thermal inertia. This might be achieved by the introduction into the core of non-fuel materials. Graphite and alumina are the principal diluents considered. Diluents can be introduced into the core in three different fashions: as integral subassemblies of diluent with circular fuel channels containing clustered rods, as subassemblies containing rods of both fuel and diluent, or as a heterogeneous core of subasssemblies of fuel and diluent. Such dilution, implemented sparingly to retain a sufficiently fast core, could result in an increase in the Doppler coefficient and a small decrease in breeding ratio. Using alumina as the diluent, while giving a higher conversion ratio, results in a shorter burnup for a given enrichment. In the present economic circumstances of low uranium prices, of relative abundance of plutonium from the operation of thermal reactors,

and of the delay in the fast reactor programme, the lower breeding ratios of the ETGBR variants might be justifiable. Partial 'blanketting' of the ETGBR variant core might be considered to obtain a 'near' or 'just' breeder.

Some scoping calculations were undertaken to show the relative difference in the thermal response of fuel pins, with and without moderator, in idealized transient situations. The inclusion of a small amount of diluent material was found to retard slightly the temperature rise in a defined depressurization transient. With alumina as diluent the greatest benefit in arresting the heat-up of the fuel and clad was noted. Finally, an established AGR thermal transient program was used to assess the effect of halving the graphite to fuel volume ratio in a typical AGR lattice. For a typical depressurization scenario this was found to produce larger temperature rises but as yet within safety limits.

ACKNOWLEDGMENTS

My gratitude and thanks must firstly go to my academic supervisor, Prof. A. J. H. Goddard, for his constant guidance, encouragement, and assistance throughout this research work.

Mr. C. P. Gratton of the AEEW has my thanks for his interest and suggestions concerning the work on gas cooled reactor design and particularly GCFR. Mr. W. Kemmish must also be acknowlged in this respect for his encouragement and the valuable advice he offered on ETGBR.

Many other individuals where helpful during the work and contributed information which cannot but be appreciated. I especially owe my thanks to Dr. R. Benodkar for his valuable assistance in the thermal modelling part of the work. Mr. S. P. Jayatissa of the CEGB also kindly provided the two KINAGRAX runs of chapter 7, in addition to his frequent useful advice regarding thermal modelling. Mr. M. Roth of AEE-Winfrith has my gratitude for his assistance in resolving difficulties with WIMS when they arose; his patience especially during the several phone calls is appreciated. I must also thank Dr. M. Javadi for his interest and helpful suggestions regarding neutronics aspects of the work.

Lastly, but definitely not least I would like to thank Rola Nuwayhid, my wife, for her help in typing and correcting a significant part of this thesis.

TABLE OF CONTENTS

LIST OF TABLES

LIST OF FIGURES

CHAPTER 1.

INTRODUCTION

1.1 THE PRESENT SITUATION - BACKGROUND

At the present time there appears to be no viable alternative to fossil fuels other than fission energy. The energy provided by fossil fuels is limited to a lifetime of the order of 90 years [1] depending on reserve status. With the least optimistic energy growth projection, and taking into account that the 'underdeveloped' world is striving for progress, the demand for electricity will in the early decades of the next century exceed the total proven uranium resources. It has been claimed that: "unless fast reactors are introduced from the year 2020 at a steady rate, thermal reactor capacity may continue to increase beyond the point that lifetime fuel supplies could be assured [2]". If the energy demand of the next century is to be met, nuclear energy must play a significant role. At present the world uranium market is depressed, with over-capacity on the supply side leading to low prices. Although the scene is not yet set for fast reactors, advantage is being taken of the low uranium prices through the use of thermal reactors. If it is to replace the thermal reactor early next century, viable fast reactor designs must be established today.

Two major nuclear accidents: Three Mile Island (TMI) and then Chernobyl have, however, caused a fundamental review of the public perception of nuclear power. Caution and the stringent monitoring of nuclear plants have become priorities. New designs will have to build on proved safety experience, if they are to be considered. The situation nuclear power finds itself in today is probably due to underestimation of the timescales needed for the introduction of new designs.

1.1.1 The U.K. Nuclear Programme Past to Present

The U.K. nuclear programme has suffered little technically from the two accidents referred to above; the U.K. systems are of a totally different design. The gas-cooled, graphite moderated design relies less on engineered safeguards than do the Pressurized-Water-Reactor (PWR) or the Russian steam-cooled, graphite-moderated design (RBMK). For example, there is no concern regarding a positive

void coefficient; a feature of the RBMK which was mainly to blame for the Chernobyl accident.

The lack of heavy water supplies and fuel enrichment facilities gave the impetus for the first gas-cooled, graphite-moderated designs. The physics of such systems and the inertness of the gas coolant allowed natural uranium to be used. The first U.K. commercial reactor of this type was the MAGNOX design, so-called because of the magnesium-aluminium alloy used for the cladding, selected in order to keep neutron absorption losses to a minimum. Fins on the can surface are neccesary to enhance heat transfer from the large fuel rods. A large core is nessitated by the physics of the natural uranium lattice, some 4000 channels, each containing one large 2.5 cm. diameter fuel rod make up the core. Magnox suffers from a few drawbacks: (1) the use of uranium metal fuel limits the maximum fuel temperature to about $650°C$ to avoid change in metallic phase. (2) the long neutron slowing down length in graphite results in a large core for natural uranium fuel (3) the metal fuel, limits burnup to a maximum of about 6000 MWd/t. (4) the low-melting point of the cladding further limits gas outlet temperature.

In order to utilize better the high temperature potential of the gas-cooled, graphite-moderated sytem, the AGR design was developed. This design had the benefit of fuel enrichment capability and could thus use ceramic fuel in the form of uranium dioxide. Oxide fuel, in addition to allowing safe extended burnup, also allows higher temperature operation due to the increased melting point. Using enrichments of the order of 2.5% U-235, the AGR achieves a burnup of 18 GWd/t, despite the use of stainless-steel cladding which, although giving significant parasitic neutron absorbtion, has improved thermal integrity compared with magnesium alloy clads. The high fuel rating and the low thermal conductivity of the fuel lead to the fuel being subdivided into smaller rods. The AGR element is thus a three ring cluster of 36 rods each of 1.5cm. diameter. The core is smaller than that of the Magnox reactor and has a lower graphite to fuel volume ratio.

Originally, the AGR fuel rod was to have beryllium (Be) cladding; reduced parasitic neutron absorption would have lead to lower enrichment. It was found

very early, however, that Be was too difficult to machine to be feasible as a clad material.

The latest AGR designs are planned to achieve burnups of 24 GWd/t using the new 'stage 2' fuel stringer design with a single graphite sleeve. It has been suggested that this limit may yet be exceeded, up to about 28 GWd/t, at which point the burnable poison requirement for reactivity control margin becomes the limiting factor [3].

1.1.2 Present Trends and the PWR

After two decades of the use of gas-cooled reactors, the U.K. today faces the question of whether to switch completely to PWR or else continue with AGR and other gas-cooled reactor types.

The CEGB are convinced that the PWR is the best choice [4]. The factors examined in this decision include: construction period, capital cost, plant availability, and plant lifetime. The capital cost of a PWR is lower than AGR but not significantly if it is noted that the AGR uses twin reactors each with 8 boilers whereas PWR is a single reactor with 4 steam generators. Planned construction period for both reactor types are similar but Dungeness-B gives a bad impression for AGR, due to prototype design features, and industrial relations problems during construction. Plant availability for the AGR should be better than that of the PWR if the design target of continuous refuelling at full power could be met. However, this is not the case and refuelling is performed at around 40% power. Refuelling at 70% power is, however, thought to be achievable in the very near term [5]. With higher-power refuelling, using single sleeve stringer design, AGR's could have a generating cost per kW(so) comparable (or lower) than PWR.

Design power output for single AGR reactors is typically 660 MW(e) though experience has shown this to vary from reactor to reactor. Hartlepool and Heysham-1, with their 'pod-boiler' design have had difficulty in increasing their output to the design target [6]. Hinkley Pt. B, on the other hand has achieved full design output and even surpassed 660 MW(e) per reactor. The newest AGR's

are expected to produce at least 660 MW(e) since they are based largely on the Hinkley Pt B design of core and boilers. Other minor problems encountered with Hinkley Pt B have led to design changes incorporated in the new AGR's.

The lower power output of the single AGR reactor compared to the PWR (660 vs 1150 MW(e)) inevitably gives economic penalties since smaller reactors must have substantially lower manufacturing costs in order to compensate for the lower output. On safety grounds, however, the lower power and power density is clearly an advantage and would tend to slow down any transient in accident situations. It is only now, after the recent nuclear accidents, that attention has been given to the potential of small and medium sized reactors.

Only countries with large electricity supply grids (> 9 GW(e)) could accept reactors with an output of above 900 MW(e). This is so because of the practice of the 10 percent rule regarding any single generating component of the electricity grid of a nation. Developing countries, on the other hand, will have capacities in the 5 to 6 GW(e) range in the next century and will then be capable of accepting reactors of up to 500 or 600 MW(e) [7].

With the above mentioned points considered and considering that AGR derivatives of the gas-cooled type are achievable, it is shown that the future for AGR and its derivatives is far clearer than presented sometimes.

An argument put forward in favour of PWR is that its adoption will bring the U.K. into line with the majority of nuclear users worldwide, as opposed to AGR in the use of which the U.K. stands alone. This argument has not been supported by those who believe that adopting the PWR will make the U.K. dependent on outside experience which it will need to draw on as a new user. Cost advantages set aside, PWR is considered on balance to be less of an inherently safe design than AGR(see reference 5 for example). The loss of the vast experience gained with gas-cooled reactors in the U.K. is likely unless a case can be made for new gas-cooled designs based on AGR.

1.2 FUTURE OPTIONS

1.2.1 The way ahead

Having been established as a viable option in the U.K., PWR, will be a partner of AGR in electricity generation in the late 1990's and early 2000's. With the last of the Magnox reactors being decomissioned around 2020, the 5.3 GW(e) they generate must be replaced. If this capacity is provided by PWR's (say 4 units), then replacement of the early AGR stations will become an issue. It is at that time that decisions will be required as to whether gas-cooled reactors will dissappear or continue to play a part in U. K. energy generation.

During the next 20 years, the possibility exists to develop the gas-cooled design while practical experience with AGR construction is available. It has been suggested that, for the AGR to continue, significant simplifications in design are warranted [8].

The AGR design is robust and could conceivably be modified for higher performance: extended burnup is an obvious aim, with up to about 28 GWd/t considered as economic and failure free. Reactor power output could be increased, if desired, with only the conventional equipement being the limiting factors. AGR derivative designs are a further possibility with the aim of achieving higher burnups [9]. Overcoming the low availability problem due to the current on-load refuelling system would be necessary. With regards to fuel rating, use of stainless-steel cladding implies a limit on outlet coolant temperature of about $675°C$ and a natural next step could be the use of an all ceramic core. With High Temperature Reactors: HTR, and 6-7% fuel enrichment, coolant outlet temperatures of about $750°C$ together with burnups of over 50 GWd/t are achievable. New fuel design and the extensive testing required may cause HTR acceptance to be a lengthy task although the current work in Germany is encouraging.

If plutonium fuel was to become used extensively, as U-235 stocks deplete and recycling increases, then fast spectrum reactors would be the most efficient fuel users. Figure (1.1) illustrates this fact by showing that η: the neutrons

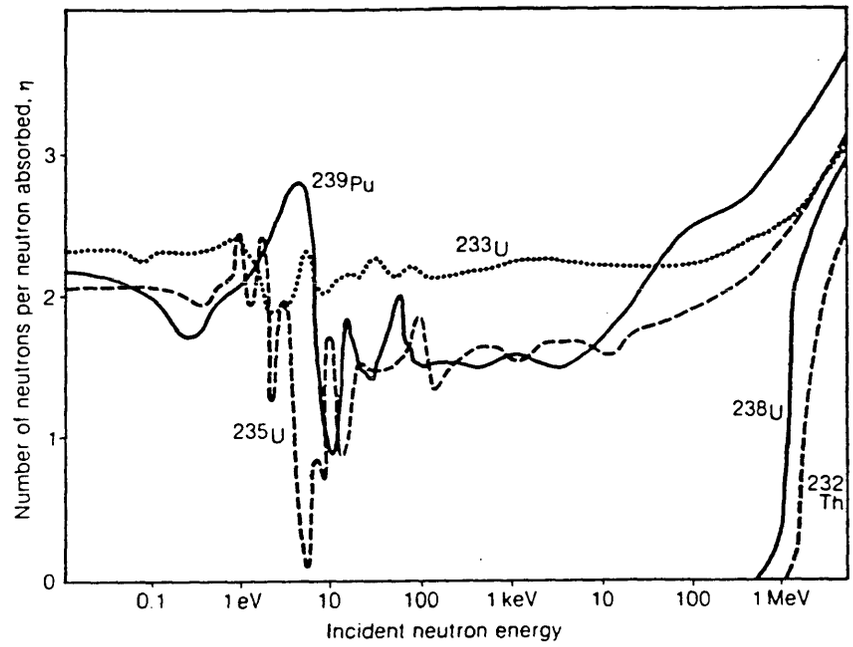

Figure 1.1. η versus energy for the major fuel nuclides

produced per neutron absorbed versus energy, for Pu-239, is greater than for U-235 at higher energies. Thus as an alternative to HTR having greater fertile material utilization, the Gas-Cooled Fast Reactor (GCFR), has been the subject of design studies. A design of GCFR which uses CO_2 coolant, with as much current AGR technology as possible, is the Existing Technology Gas Breeder Reactor (ETGBR). The ETGBR [10] concept has a relatively low rating and this, with other aspects, gives it potentially lower generating costs than a Liquid Metal Fast Breeder Reactor (LMFBR). The design takes into account a reduced need for breeding through the existence of larger Pu stocks.

The Diluted ETGBR is a concept investigated in this work which retains the ETGBR characteristics, but admits some diluent or moderator into the core as part of a study of safety benefits; the most convenient dilution is where a fuel channel is in an integral block of diluent. Another mode of dilution investigated, although in less detail, is the mixed pin subassembly. This uses a standard ETGBR subassembly containing both fuel and diluent rods, which serve to associate all fuel rods with close diluent. The bulk quantity of diluent is, however, for reactivity reasons considerably less than that in the integral block diluted design.

A mode of dilution that removes the need for stainless-steel cladding would bring higher temperatures and hence higher ratings. Such a fuel design would involove a dispersion fuel surrounded by a ceramic cladding as exemplified by HTR. This concept applied to fast reactors still remains a long range design target.

1.2.2 Economics of ETGBR

The situation today is that fissile fuel prices are low and the supply relatively plentiful. This is the case due to the continuing low rate of introduction of thermal reactors and the absence of general use of fuel recycle. Hence the accumulation of plutonium discharged from thermal reactors. The whole motive for the introduction of Fast Breeder Reactors may thus be questioned. With the dominant price constraint today being that of the fuel reprocessing, as opposed to fuel enrichment (see reference 10) , it appears that the use of high breeders is not justified at the present time. The GCFR with its harder neutron spectrum has a higher breeding gain than an equivalent LMFBR; this allows a GCFR to be designed with reduced rating and still mantain a significantly high fuel utilization through breeding, although the capital cost differences are uncertain. However, a GCFR design based on present gas cooled technology with low rating and reduced overall breeding is apparently attractive. With plutonium relatively plentiful, the higher core inventory may be tolerated on fuel cost grounds. The Existing Technology Gas Breeder Reactor (ETGBR), largly based on AGR plant component technology, is a fast reactor design attempting to take advantage of present circumstances. It may also be noted that proliferation control is improved by using fuel in the reactor which would otherwise be stockpiled.

1.2.3 Safety of ETGBR

The ETGBR is a relatively low rated system; this leads to a lower coolant pressure and slower heat-up rates under accident conditions. In common with other fast reactor designs, the ETGBR can operate over long burnups with little excess

reactivity present, due to the high conversion ratio. It follows that control investment need not be as high as in thermal reactors. Although in general continuous refuelling leads to higher discharge irradiation (DI) than for a batch case of similar enrichment, an ETGBR would be refuelled batchwise since the reactivity drop is small; this would simplify the refuelling apparatus. Proposed ETGBR designs retain SS316 cladding and embody the possible future introduction of SS20/25 TiN. Operating temperatures (and hence thermal efficency) are lower than those of AGR as a safety precaution. The absence of moderator removes the worry about its integrity but makes clad integrity of greater importance in light of the greater power density. The relative increase in fuel inventory and lowering of the fuel rating is a major safety enhancement. As in the AGR, depressurization under accident conditions is considered to take place over a long period due to the use of a pre-stressed concrete pressure vessel (PCPV). Special engineered safeguards in ETGBR design include the Core Auxilliary Cooling System (CACS), an added meanns of transient heat removal.

The diluted ETGBR designs introduced in this thesis are intended, among other aspects, to increase safety further by providing an in-core transient heat sink and to cause the Doppler coefficient of reactivity to be more negative than for the ETGBR itself.

1.3 SCOPE OF THE THESIS

The objective of the research described in this thesis is to investigate future options for advancing the gas-cooled reactor concept. Several AGR derivative designs, ranging from the thermal AGR itself to the fast ETGBR, are analyzed. The ETGBR offers the benefits of a fast system while being potentially of relatively low cost through the use of AGR component technology. The concept of a diluted ETGBR is introduced; its main feature is a degree of improved transient safety through the introduction of integral block subassemblies of diluent material, such as alumina, with drilled fuel channels containing regular ETGBR fuel rods. Alumina, as a diluent, is shown to be acceptable neutronically giving comparable fuel utilization as graphite cases, while being preferable to graphite on heat capacity and on grounds of non-ignition.

Chapter 1 of this thesis gives an outline to the problem and attempts to clarify the present circumstances of nuclear power. Chapter 2 presents the WIMS family of neutronic codes and discusses their applicability, especially to the fast and intermediate cores studied.

Chapter 3 reviews the present AGR and its status and discusses some of its features. The development potential of the AGR design is investigated, from a neutronic point of view, through the introduction of variant designs.

In chapter 4 the ETGBR design is highlighted. Some of its neutronic features are also reviewed with the aid of a study of the dependence of the calculations on the methods and assumptions used.

Chapter 5 is a study of the effect upon neutronics of diluting the ETGBR core using a integral block design. Both lattice cell and whole reactor calculations are performed.

In Chapter 6 calculations are performed on two further possible diluted variants of the ETGBR: pin-diluted and heterogeneous cores.

Chapter 7 gives a general and simplified assessment of the thermal (heat transfer) features of moderated and unmoderated cores in depressurization accident situations using a program written specifically to this end.

REFERENCES

1. Hoyle F. , *Energy or Extinction?*, p. 28, Open University Press, second edition, 1980

2. Quick J. , *Europe and the Fast Reactor*, Report from conference on the European approach to fast reactors (Oct 1987), Atom, p. 26, March 1988

3. Goode A. B. , *The fuel management of AGRs*, Nucl. Energy, Vol. 23, No. 3, pp. 149-160, 1984

4. Shackleton J. , *Britains Nuclear Future - economic and social appraisal*, MSc Thesis, Imperial College, September 1986

5. Pexton A. F. , *Improved characteristics of Scottish AGRs*, Nuclear Europe, No. 3, p. 30, 1985

6. Nuclear Europe, p. 36, No. 2, Febuary 1986

7. Atom, p. 22, April 1988

8. Eyre B. L. , Lecture at Imperial College, January 1986

9. Askew J. R. , Griggs M. A. , and Hutton JL, *Development potential of the AGR*, Proc. Conf. on gas cooled reactors today, p. 253, London 1982

10. Kemmish W. B. , *Gas cooled fast reactors*, Nucl. Energy, vol. 21, No. 1, p. 77, February 1982

CHAPTER 2.

WIMS METHODS AND MODELS

2.1 DESCRIPTION OF THE WIMS CODES

2.1.1 The lattice-cell code WIMS-D4

The WIMS code (Winfrith Improved Multi-Group Scheme) [1] provides a comprehensive scheme of reactor lattice calculations applicable to a wide range of reactor types. It is a 'fundamental mode' spectrum generation and fuel depletion code. The output of the code includes detailed reaction rates for the lattice and eigenvalues for cases where a simple buckling mode is required. As an alternative, spectrum weighted, leakage corrected averaged cell few-group constants are provided for use in overall reactor calculations.

The code has been written to use fundamental nuclear data only and is capable of performing calculations to different degrees of approximation. Thus, there is scope to vary the energy grouping as required (e.g. more groups for a fast system). Additional flexibility is provided in the solution of the transport equation as well as the geometrical representation.

WIMS was chosen for this work since it is adaptable to a broad range of reactor types, all using one single data library [2]. This allows consistent survey calculations and permits the study of any important features with increased accuracy if so desired.

The main transport calculation in WIMS-D4 is divided into two phases so that detailed spatial treatment of the cell is performed in a few main transport (MTR) groups instead of the initial 69 groups. An approximate spatial calculation in 69 groups using the SPECTROX method [3] is first carried out to determine the spectra needed for group condensation, followed by the detailed spatial treatment in few-groups. Transport solutions used are either the discrete ordinate method (S_N) or the collision probability method. Geometries available include slab, pin-cell, and cluster cell. Cluster geometry is of particular relevance to this work, since most cores studied, ranging from AGR to fast systems, involve clusters of rods.

In cluster geometry, WIMS offers two degrees of approximation in collision probability solution. PERSEUS uses a 'smeared ring of rods' approximation, whereas PIJ preserves rod heterogeneity. In the present calculations it was decided

that PERSEUS would be sufficient and this was confirmed for AGR by comparision with PIJ calculations. In addition, for the fast reactor calculation, there is no need to use PIJ since neutron path lengths are long and, a fully smeared cluster representation may be adequate. Figure (2.1) shows the calculational sequences available in WIMS-D4.

2.1.2 The WIMS-E Modular Code

The WIMS-E scheme for neutronic calculations was established to extend neutronic calculational facilities to cover a wider range of requirements and to permit more rapid adoptions to meet future requirements [4]. The scheme is 'modular' consisting of a set of computer programs each performing several calculations. Each program, or programs, is a self contained FORTRAN program and does not, in its operation, rely on any interaction with the other modules of the scheme except through a well defined interface. The integrated WIMS-E modular program contains the separate modules as overlay segments and a controlling routine which selects modules for execution in response to users commands. The transfer between modules is restricted to 5 files containing the most essential physical quantities. The five files (data sets) are: (1) Interface creation information (2) Microscopic cross-section (3) Number densities and macroscopic cross-sections (4) Geometry (5) Flux.

The earlier WIMS code (e.g. WIMS-D4), although rather general in concept, were mainly aimed at the representation of lattices consisting of regular arrays of pins or of clusters of pins. As in the original WIMS versions, the aim with WIMS-E is to treat different reactor types, using the same nuclear data library. Although the WIMS-D path may be selected as an option, the calculational route with WIMS-E is entirely determined by the user. WIMS-E has several options for the solution of the neutron transport equation. Collision probability methods are a normal approach and form the usual unit cell step although other options may be used. The main extension in WIMS-E compared to WIMS-D is the linkage to a three dimensional diffusion program SNAP as well as other options. The nuclear data library utilized in WIMS-E in this work is the same as that of WIMS-D. The

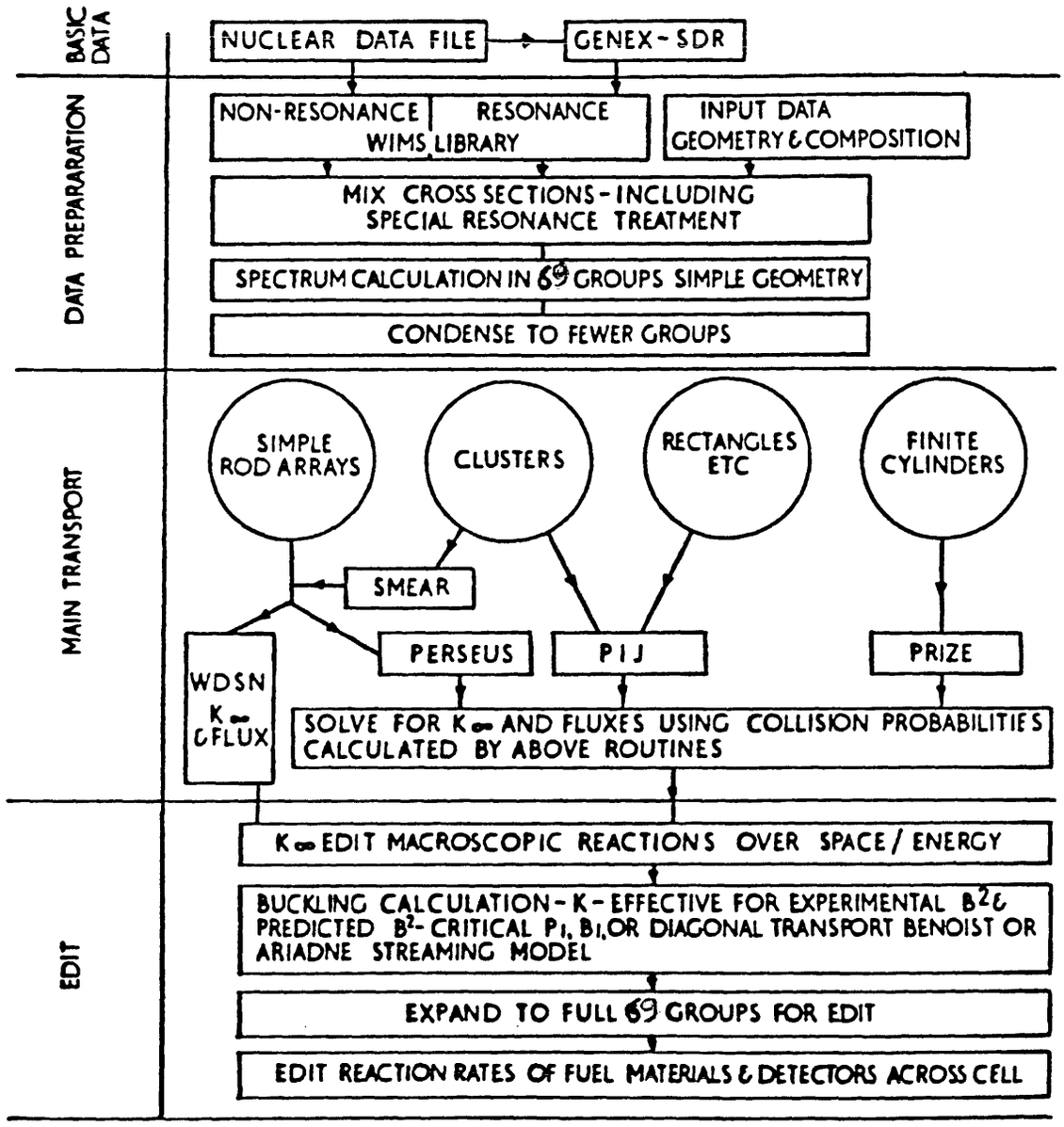

Figure 2.1. WIMS-D4 calculational sequences and options.

69 group library has in fact been converted directly from WIMS-D in order to maintain consistency [4].

WIMS-E has the capability, common to all WIMS versions of treating resonance capture by the equivalence model. The equivalence method provides average cross-sections over a pin for energy groups in the resonance range. This capability is within the WIMS-E module WHEAD and for present applications is deemed adequate as shall be shown in section 2.2. Further options exist in WIMS-E for refined resonance treatment and may be selected if desired.

The modules available in the present version of WIMS-E and a brief description of their main functions is given in table (2.1).

Table (2.1): WIMS-E modules and their function [5]

Module	Function
W-HEAD	Normally the first module in a calculation sequence, W-HEAD reads the geometry and material specification for a reactor cell, gets cross-sections from a nuclear data library and corrects them for the effects of resonant absorption. Establishes an interface for the reactor cell model.
W-MIX	Calculates macroscopic cross-sections, so that a partially written interface may be completed. The purpose of W-MIX is, in general, to allow modules that write a new interface to write only microscopic cross-sections, leaving to W-MIX the job of calculating macroscopic ones.
W-COND	Condenses cross-sections and fluxes over energy.
W-SMEAR	Averages cross-sections and fluxes over space. Includes a streaming calculation.
W-INTER	Prints, copies or writes interfaces.
W-MERGE	Merges several interfaces to produce a single new interface. Includes a multicell calculation.
W-FORTE	Reads output files from WIMSD4 or LWRWIMS and writes the same information in the format of a WIMS-E interface.
W-PONE	Writes a new interface by adding P1 scattering data from a WIMSD4 library to an old interface.

Table(2.1): continued

Module	Function
W-PRES	Prepares cross-sections in subgroups for a collision probability based shielding calculation.
W-RES	Forms group averaged shielded cross-sections based on a collision probability flux solution in subgroups.
W-THES	Calculates collision probabilities in slab geometry using Newmarch's method or in annular geometry using Bonalumi's method.
W-FLURIG	Calculates collision probabilities in annular geometry using Carlvik's method.
W-PIJ	Calculates collision probabilities in rod cluster geometry.
W-PROC	Calculates collision probabilities for grains in annular geometry.
W-WED	Prints a neutron balance edit.
W-WIRE	Prints reaction rates.
W-PIP	Calculates fluxes from a collision probability matrix.
W-PERS	Combines W-THES and W-PIP in a single calculation.
W-CRITIC	Modifies a given spatial flux solution by means of a fundamental mode critical spectrum calculation according to input buckling terms.
W-SNAP	One, two or three dimensional diffusion solution.
W-CHART	Flux solution using a characteristics formulation.
W-BRNUP	Calculates isotopic changes due to burnup.
W-LINK	Writes the SNAP fluxes to a WIMS-E interface, allowing for the possibility of writing fluxes from a two dimensional slice of the full three dimensional geometry of SNAP.

Because WIMS-D4 is particulary useful and simple in treating cluster geometry within a one dimensional annular approximation, the WIMS-E module WFORTE is used to transform the data for later use by further WIMS-E modules [6]. The practice adopted here is, therefore, one where the data is generated by

a local lattice calculation and is then followed by a reactor calculation if desired. This is the standard practice adopted by most workers [7].

2.2 VALIDITY OF WIMS LIBRARY AND METHODS

2.2.1 Discussion

Group averaged microscopic cross sections of the materials of fast reactors will depend on the composition and geometry of the reactor. A single set will therefore not suffice for all designs. For detailed design, a multigroup set of effective cross sections is normally developed for the particular reactor composition and geometry being analysed. For scoping studies, however, less detail is required and a single set may be applied to a range of designs, provided the compositions are not too different from the composition for which the set was originally developed [8].

The WIMS library [2] contains 69 energy groups; 14 fast groups, 13 resonance groups, and 42 thermal groups. Detail in thermal range arise from the fact that WIMS was intended as a thermal reactor code. Thermal region energy grouping ensures coverage of the low lying resonances of Pu-240 and Pu-241 and the influence of temperature and thermal absorbtion. For a fast reactor the fast groups may not be adequate and a new library would normally be required [9]. The group structure is such that important detail in the intermediate resonance region is well represented; this treatment would be adequate for intermediate spectrum reactors (ie. undermoderated reactors).

The WIMS 69 group averaged data were originaly produced from UKNDL using the GALAXY code with an undermoderated water system spectrum in the fast region and a 1/E spectrum in the resonance region. In the thermal region a Maxwellian distribution was used for group averaging. Resonance data for U-235, U-238, and Pu-239 were generated using the SDR code. Pu-240 and Pu-241 are taken to be non resonant in the current version of the WIMS library.

2.2.2 Resonance Treatment

In WIMS the principal resonant absorbers are U-235, U-238, and Pu-239. The resonance region is assumed to lie in the energy range from 9.118 KeV to 4.0 eV. Effective cross sections in this region are generated using flux evaluation for the energy self-shielding of the resonant nuclides. In the region the flux is closely approximated as a 1/E spectrum.

The WIMS library resonance tabulation is made up of , for each group, a resonance integral (RI) divided by the lethargy width of the group (τ) as a function of the potential scattering cross-section per atom of absorber (σ_p) and temperature for each fissile nuclide. As already mentioned the resonance integrals for the considered nuclides are calculated, using SDR, which solves the slowing down equations for homogeneous mixtures of hydrogen and the resonant absorber nuclide. Non- hydrogeneous moderators, which may be mixed with the fuel, such as oxygen or carbon, are taken into account in the equivalence theorem. The equivalence theorem is used to relate the tabulated (RI/τ) of the resonant nuclide to the particular heterogeneous problem. Resonance integrals, ie. $\int \sigma_a \phi dE$ for Pu-240, Pu-241, and U-234, are to be assumed infinitely dilute and are therefore not resonant self-shielded in WIMS.

The cut-off between fast and slowing down regions, 9.118 KeV in WIMS, is the energy above which U-238 capture is not resolved. It then appears that treatment above that energy in the unresolved range is neglected in WIMS. This, while probably justifiable for well thermalized systems, may be questionable for fast systems. Another possible difficulty is the fact that stainless-steel, which is a major constituent of fast reactor cores, has its cross sections treated as unshielded. This may be inadequate since iron has significant resonances above 10 KeV [10].

Resonance interaction is taken into account based on a simple correction. It is stated to be adequate for low enrichment systems but is untested for high Pu enrichment.

The resonance treatment assumes, for energy self-shielding a homogeneous reactor. For thermal systems, heterogeneity introduces significant spatial shielding

of the flux and this has to be treated. The rational approximation is utilized in WIMS to deal with this effect. For fast systems, although heterogeneity is of less importance, it nevertheless may be of benefit to use the capability. This may certainly be helpfull for comparative study of thermal, ranging through intermediate, to fast reactors.

2.2.3 Effect of WIMS Resonance Methods on Calculations of Gas-Cooled Fast Reactor Systems

WIMS Calculations for gas-cooled fast systems were subjected to scrutiny as far as the resonance treatment is concerned. It has been already pointed out that above 10 KeV the WIMS group structure may not be sufficient for 'hard' systems. In this section a simple test was performed wherein the fast core was calculated twice: once with the WIMS resonance treatment included and once with it suppressed. The quantity studied is the percent relative difference between the two calculations with the resonance calculated value as base. In this way, k_∞, absorbtion and fission rates of the fuel nuclides were studied.

It was verified that as the system gets 'harder' by increasing enrichment, the difference between the WIMS resonance and non-resonance calculations diminishes. With moderation (or dilution) varied, the core was again calculated twice as mentioned above. The calculations for cases with a range of diluent to fuel ratios and at three enrichments namely: 4.0, 9.0 and 16.5 % Magnox Pu showed that as the system gets 'harder' the effect is one of diminishing relative difference. It was noted that: (a) Absorption in U-238 varies the most. (b) The least relative difference is for the 'hardest' case (16.5 % enrichment and V_m/V_f of 1.0). (c) At V_m/V_f of 5.0 sufficient 'softening' of the neutron spectrum seems to lead to the relative difference to be equal for the three enrichments. These points are clarified by the figure shown in Appendix(1).

2.3 VALIDATION TESTS ON WIMS - VALIDITY FOR FAST SYSTEMS

The use of WIMS for fast reactors was adopted on the basis of a reccomendation that it should perform adequately for 'hard' systems to permit survey calculations [11]. With the shortfalls in the group structure already mentioned, it is obviously desirable to test its performance for systems ranging from fully 'fast' to 'intermediate' system. Three available cases were identified, although in the main lacking the information necessary for a thorough study. These test cases are the GBR-4 design study, LWHCR experiments, and early ETGBR calculations Further clarification of these casess is given in the relevant section.

2.3.1 The GBR-4 cell calculation

When this work was started, the only available gas-cooled fast reactor reference cases with enough data to allow a consistent check, were a few calculations reported on a GBR-4 pin-cell design [12]. GBR-4 is a helium-cooled highly rated gas-cooled fast reactor design. The major specifications of GBR-4 are given in table (2.2).

Table (2.2): Specifications of the GBR-4 unit pin-cell.

-Fissile Enrichment,%	12.84 (Atom)
-Fuel pin radius, cm	0.350
-Clad thickness, cm	0.035
-P/D	1.371
-Temperatures, K	
Fuel/Clad/Coolant	1100/900/700
-Fuel density, g/cc	9.35
-Fuel composition	
at equilibrium,%Wt. :	
U- 235	0.0742
U- 238	74.157
Pu-239	10.864
Pu-240	2.507
Pu-241	0.418
Pu-242	0.139
Oxygen	11.840

Table (2.2): Continued

-Clad composition (WIMS mat. 9056),%Wt,	density = 8.0 g/cc.
Iron	70.10
Nickel	10.00
Chromium	18.50
Manganese	0.80
Silicon	0.60
-Helium density g/cc at 700K and 90 atm,	0.055
-Core fuel rating (MW/tU),	82.0

WIMS-D4 was used to model the GBR-4 given the above parameters. The calculation was performed in a 9-group WIMS library structure corresponding in general, in the energy range of concern, to the 7-group structure used in reference 12. An S_4 discrete ordinate transport solution was used and was found to be adequate by comparison with higher order solutions. The WIMS REGULAR option was included to allow adequate estimation of the 'Dancoff Factors' for the lattice.

Rather than going through a detailed description and discussion of the calculations, it was thought more appropriate in the context of this chapter to highlight the WIMS calculated results and compare these, as far as possible, with reference values. In the remainder of this section several aspects of the nuclear characteristics of GBR-4 are presented: flux spectrum distribution, reactivity and performance indicators at BOL, and neutron balance at BOL.

Flux Spectrum Distribution

The relative flux spectra of the average GBR-4 cell as calculated by WIMS and as given in the reference, are shown in figure (2.2). The agreement in the spectral distribution is reasonable taking into account the difference in group boundaries of the two calculations. The median energy of the spectrum as calculated by WIMS is 185 KeV compared to 171 KeV reported in the reference.

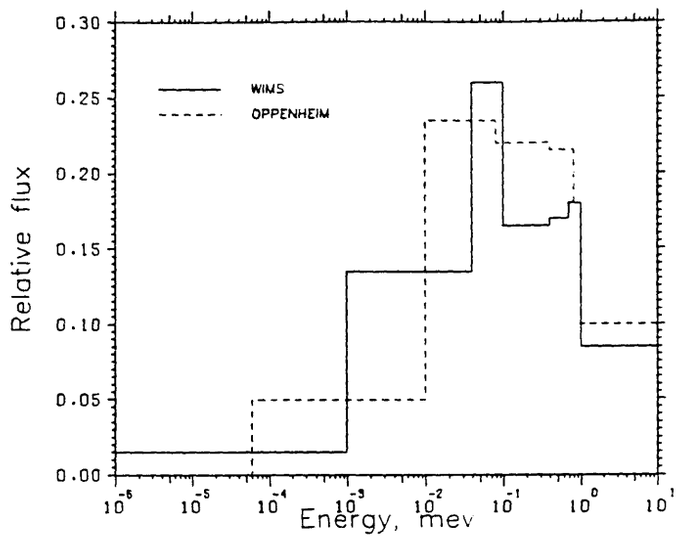

Figure 2.2. Comparison of the GBR-4 average cell relative flux spectrum as calculted by WIMS and reported in reference 12.

Reactivity and Nuclear Performance Indicators

Reactivity indicators :

Using WIMS-D4, the defined GBR-4 was found to have (at BOL)

k_∞ 1.3741

k_{eff} 1.0627 (with $B_r{}^2 = 1.55 \times 10^{-4}, B_z{}^2 = 5.035 \times 10^{-4}$)

The reference reports a k_∞ of 1.400 for the GBR-4 cell calculation; broadly in agreement with the WIMS-D4 value. No k_{eff} figure was reported in the reference to anable a comparison with the WIMS-D4 value.

Performance:

The WIMS calculated core conversion ratio was found to be 0.855. The breeding gain was calculated, using the reference isotopic weightings, as -0.125. The reference values for the core conversion and breeding gain are 0.870 and -0.100 repectively. It must be noted that the reference values are given for a 2-d calculational model, and these are used for lack of 1-d conversion figures.

Spectral Indices:

The WIMS-D4 deduced figures were:

ϵ 0.1857

α 0.2099

The 2-dimensional reference values of ϵ and α are reported as 0.179 and 0.228 respectively.

Neutron balance at BOL

The isotopic neutron balance as found by WIMS-D4 has beem compared to that reported by Oppenheim [12]. The WIMS-D4 lattice-cell calculation included leakage correction through the use of geometrical bucklings based on the GBR-4 radial and axial core dimensions. The reference calculation is reported to be carried out with the code ZERA using the KFKINR library (see reference 12 for details of the calculations). Table(2.3) shows the isotopic neutron balance comparison at BOL. It appears that WIMS gives results in general agreement with reference values, particularly with regards to the total fissions in the cell (0.3403 vs. 0.3407).

Table(2.3): Isotopic Neutron Balance for GBR-4 (Normalized to 1 neutron produced)

	WIMS		Oppenheim	
Material	Fissions	Captures	Fissions	Captures
U-235	0.00188	0.00047	0.0018	0.0005
U-238	0.05733	0.25684	0.0499	0.2538
Pu-239	0.25113	0.04759	0.2611	0.0549
Pu-240	0.01413	0.01570	0.0138	0.0110
Pu-241	0.01589	0.00188	0.0136	0.0027
Pu-242	-	5.6E-08	0.0006	0.0009
Oxygen	-	0.00383	-	0.0020
Clad	-	0.00798	-	0.0275
Total	0.34036	0.33429 *	0.3407	0.3735

* Note: Fission Product Captures Neglected

GBR-4 Conclusions

It is concluded that for the GBR-4 pin-cell WIMS gives results in general agreement with the reference calculation values. The greatest difference found, however, is in the non-fuel captures. This causes a large disagreement in the total captures in the cell (~8%).

2.3.2 The Light Water High Conversion Reactor (LWHCR) Calculation

Although this calculation is for a water-moderated case, it is nevertheless is useful in this work since:

(1) It is an undermoderated system with a moderator to fuel volume ratio (V_m/V_f) of only 0.3 compared to the PWR value of 2.0.
(2) It has a relatively high enrichment at 7.5 %fissile.
(3) It uses mixed Oxide Pu enrichment. PWR discharged fuel with a Pu vector as follows: 57.81 % Pu-239, 26.57 % Pu-240, 9.47 % Pu-241, and 6.15 % Pu-242

The calculation of the reactivity of LWHCR here is intended primarily as a check on the WIMS calculations as implemented in this work against the same calculation performed by other workers [13]. The sensitivity of LWHCR WIMS results (reactivity) to certain assumptions such as improved 'Dancoff Factors' and to externally input resonance cross- sections for Pu-240 and Pu-241, was also tested in the event. The LWHCR calculation is also of particular usefulness since the case was tested experimentally using the PROTEUS facility [14].

By using WIMS-D4 and WIMS-E it was possible to perform both lattice-cell and 2-d whole reactor determinations of reactivity for the LWHCR at BOL. The WIMS-D4 and WIMS-E input files are given in Appendix (2) for possible future reference. The most important features of the LWHCR cell and core are given in table (2.4).

Table (2.4): LWHCR characteristics

Outside Diameter (mm):	
Fuel Pellet	9.41
Cladding	10.21
Unit Cell	11.45
Pitch (mm)	10.90
Core Active Height(cm)	220.0
Core Diameter (cm)	378.8
Power Output (MWh)	3550

Ronen calculates, using WIMS-D4 for the leakage corrected core of the given size, a k_{eff} (BOL) of 1.0628. The present calculations gave a k_{eff} (BOL) of 1.0601 or 1.0596 depending on the WIMS leakage option used (Benoist and Transport

respectively). The only significant difference between Ronens usage of WIMS-D4 and that followed in this work, is the use of ENDF-BIV generated resonance region tabulations for Pu-240 and Pu-241 in the former. The present work utilized the '1981 WIMS library' default library with Pu-240 and Pu-241 considered to be unshielded. Both Ronen and the present work use the default 'Dancoff Factors' automatically calculated within WIMS. Ronen, however, does suggest that the reactivity is greatly influenced by the 'Dancoff Factors', and that WIMS-D4 over-predicts reactivity increasingly for large values of void fraction. This result, as a matter of fact, may be extended to conclude that for a gas-cooled reactor of comparable enrichment, the reactivity would be over-predicted. These last aspects are supported by other work such as that reported by Chawla et al [15] on the comparison of WIMS-D4 and experimental results for the LWHCR. The study indicated that, while the '1981 WIMS library' when applied to a voided core (ie a fast spectrum case) gives excellent agreement with experiment with regards to reaction rates (including capture in U-238 and fission in Pu-239 : which determine conversion ratio), there is an inadequacy in calculating captures in Pu isotopes and steel. These rates are reported to be underpredicted and to lead to a 4 % overprediction in k_∞ for a fast core. Based on the previous points Chawla et al recommend the refining of the WIMS library with respect to captures in Pu isotopes and steel.

The present LWHCR calculation did show that the inclusion of shielded resonance region cross-sections for Pu-240 and Pu-241 gave only a small difference from the usual unshielded calculation.

2.3.3 Validation of WIMS for a Gas Cooled Fast Reactor

The particular gas-cooled fast reactor studied here is the Existing Technology Gas Cooled breeder Reactor (ETGBR) which will be introduced in full in chapter 4. For the present purpose of WIMS validation, it suffices to define the general calculational characteristics of the ETGBR. Calculations for the ETGBR defined in AEEW-M1669 [16] are reported in this section as a further check on the use of WIMS and its data. A comparison was made between WIMS and COSMOS [17],

the latter having been used in AEEW-M1669. The COSMOS route followed in the reference utilizes the FD5 library containing 37 groups with tables of 'shielding factors' representing resonance shielding as a function of background cross-section and temperature [18]. The need to carry out a 'best-possible' comparison of WIMS against a code dedicated to fast reactor study, such as COSMOS, is emphasized by the disappointing over-prediction of reactivity for Pu-fuelled reactors reported in reference 14.

Methodology of Calculation

For the purpose of comparison with the COSMOS results, a specific WIMS-E route of calculation was devised. The WIMS-E calculation starts by setting pin-cells with the particular enrichment, radius, and pin pitch for each of the ETGBR regions. This is accomplished in the WIMS-E module WHEAD which also performs a resonance shielding calculation. Cell data are then collapsed to fewer groups using the module WCOND. Pin-cell regions are then smeared into single zones via the module WSMEAR. In the smearing stage the WSMEAR code word FACTORS is used to adjust the volume fractions of each of fuel, clad, and coolant in the resultant smeared material so that the resulting volume fraction are therby made to agree with those assumed in the COSMOS calculation. Few group data are finally passed on to the whole reactor diffusion module WSNAP. The ETGBR is modelled, as in COSMOS, in R-Z geometry. Figure (2.3) shows the reactor zones and dimensions.

As a general check on the WIMS-E calculational method an attempt was made to reproduce the same results for an ETGBR design in RZ geometry as was reported in AEEW-M1669 [ref 16] using the COSMOS scheme.

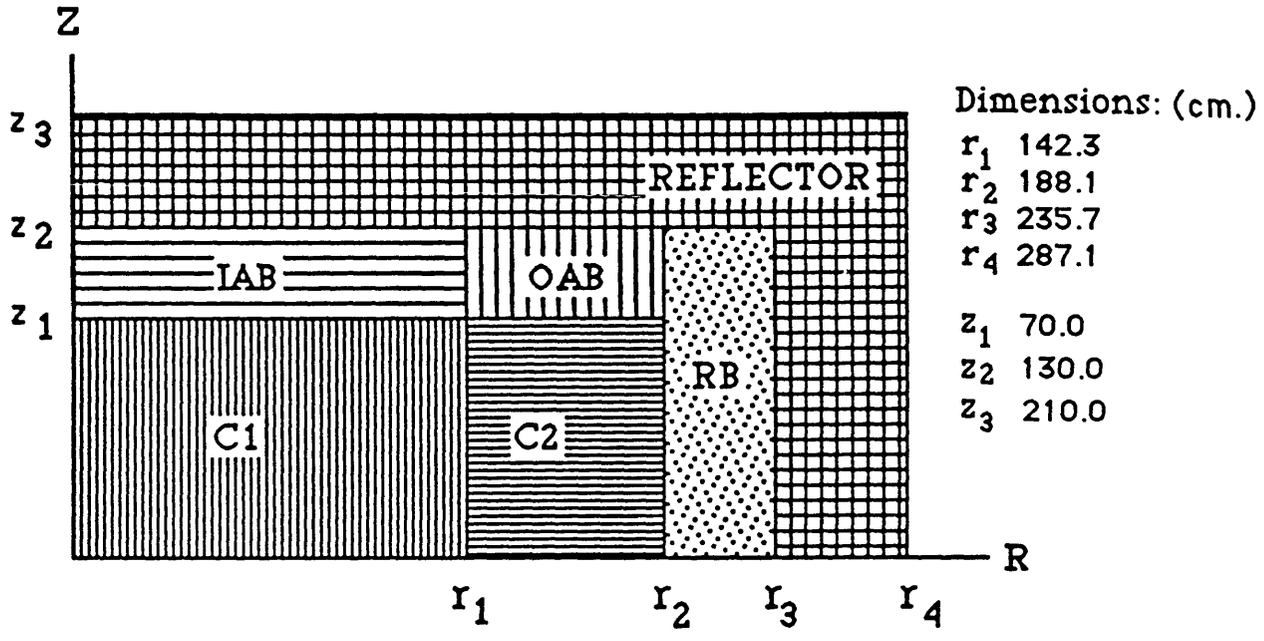

Figure 2.3. The RZ model of the ETGBR as defined in AEEW-M1669.

General Features of RZ Calculation

As already mentioned, a general check on the WIMS-E calculational methodology was attempted, in order to derive a WIMS-E route for the nucleonic study of a reactor design such as that of the ETGBR as reported in [AEEW-M1669]. Figure (2.4) outlines the computational sequence while Appendix(3) provides a listing of the WIMS-E input instructions.

a) ETGBR pin-cell: fuel radius(cm.) 0.3500
can radius(cm.) 0.3850
coolant radius(cm.) 0.5846
(Pitch/Diameter = 1.446)

b) The 2-d model of the ETGBR in this calculation is obtained by multiplying each of the fuel, can and coolant by factors in the smearing step such that the volume fractions of fuel, structure and coolant will be those given in AEEW-M1669. The zonal volume fraction corrections are as shown in the table below.

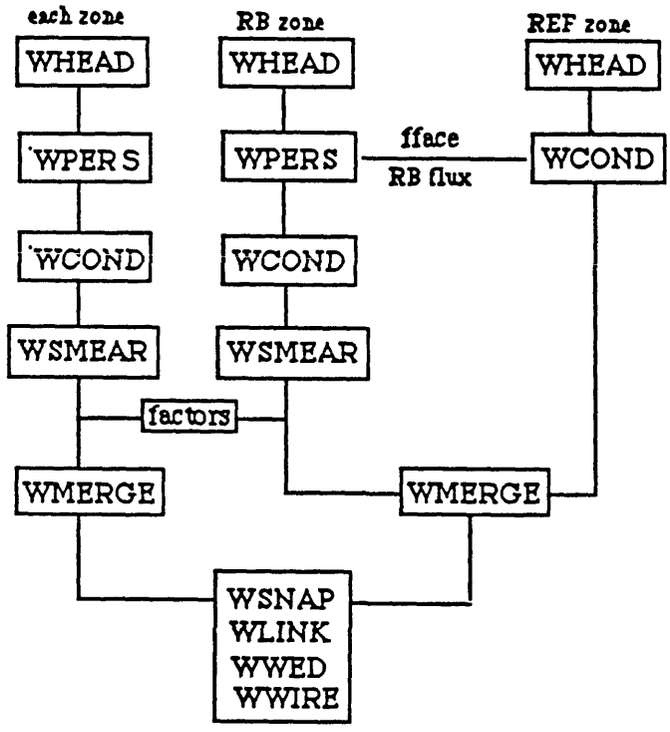

Figure 2.4. The WIMS-E modular sequence of calculations for the ETGBR.

Zone	WIMS-E FACTORS			Reference Volume Fractions		
	Fuel	Clad	Coolant	Fuel	Clad	Coolant
C1	0.5642	1.8519	1.1626	0.2022	0.1394	0.6584
C2	0.6182	1.8944	1.1227	0.2216	0.1426	0.6358
AB	0.6062	1.9077	1.0302	0.2173	0.1436	0.3812
RB	0.5941	3.5734	1.8154	0.4396	0.1792	0.6276

c) Resonance treatment is accomplished by either the default WIMS WHEAD calculation or by the WIMS-E option WPRES followed by WRES for U-238.

d) Reflector data is obtained by either the use of average flux spectrum in the adjoining radial breeder or via a WPERS 1-d calculation across the ETGBR centre-line plane.

Group Structure Selection

Because of excessive computing time, full 69 group calculations were not carried through to the spatial solution. In order to establish a minimum acceptable group structure, a 1-d WPERS calculation through the core midplane was carried

out. The resulting 69-group fuel flux of the 1-d ETGBR model is plotted in figure (2.5). The Pu-241 resonance at 1.0eV shows up clearly.

Most of the flux is shown, as expected, to lie above 1.0 eV, suggesting that the thermal groups may be condensed into a single group. Condensation using different groupings was performed on a semi-empirical basis and the error with respect to the full 69-group k_∞ value tabulated. The full group and condensed calculations were both taken to an iteration tolerance of 10^{-5}.

Table (2.5) below shows some results for k_∞ calculated for the 1-d ETGBR model; the percentage deviation from the result using the full (69 group) structure is also given.

Table(2.5): The dependence of ETGBR reactivity on group structure

Groups	Group Structure	k_∞	$\frac{k^g - k^{69}}{k^{69}} \times 100$
69	full WIMS library structure	1.649997	-
45	1-41 49 52 60 69	1.650138	0.00854
33	1-27 37 40 49	1.650128	0.00793
12	3 7 11 14 18 22 27 37 40 49 52 69	1.649710	0.01739
9	7 14 18 22 27 37 40 49 69	1.649717	0.01696
8	7 14 18 27 37 40 49 69	1.649714	0.01715
7	7 14 18 27 37 40 69	1.649706	0.01763
7	7 14 22 27 37 40 69	1.662216	0.74050
6	7 14 18 27 40 69	1.649707	0.01757
9	8 10 14 16 18 21 24 27 69	1.649985	0.00050
6	7 14 18 22 27 69	1.649686	0.01861
4	7 14 27 69	1.662189	0.73890

Some group structure sensitivity is apparent. It is clear that some detail is needed in the upper resonance region (note the 7 group result). The 4 group calculation shows significant error. Interestingly it appears that some of the fewer group cases gave generally better agreement with the full group value than did the more detailed groups cases. The best agreement found was the 9-group set. With the iteration on the full group case taken to 10^{-6} and on the condensed cases taken to 10^{-5}, the 6-group set gave best agreement. For finer coverage of zone events (eg. fissions..) it may be better to use the more detailed group structures.

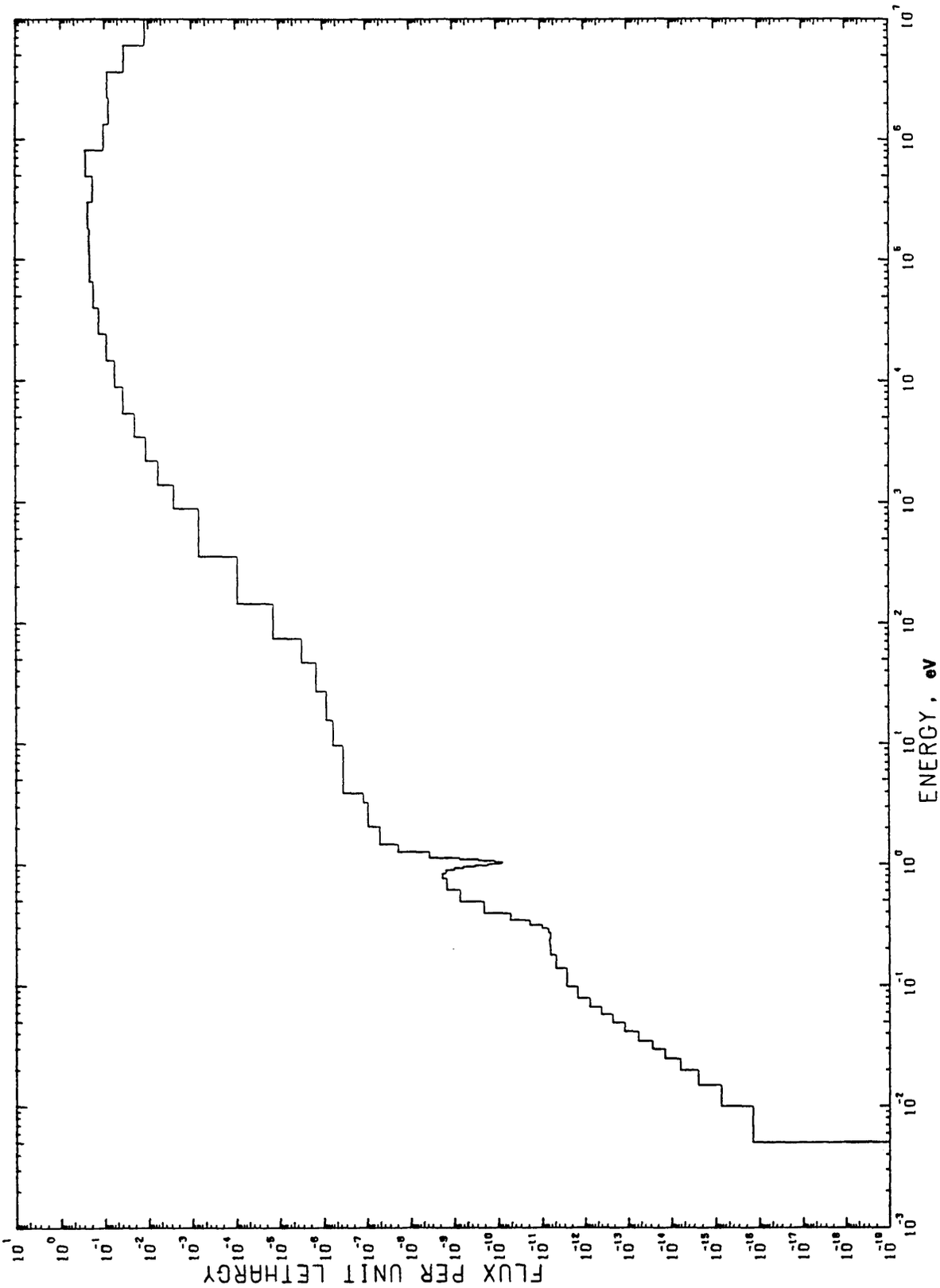

Figure 2.5. The neutron flux in the fuel of the ETGBR as determined by a 1-d calculation through the reactor midplane.

In general, it was shown that for this reactor design model, few groups, six or more, is quite adequate for our purposes.

As an extension of the group sensitivity study, the reactivity of the finite, leakage corrected ETGBR reactor as predicted using WIMS was calculated utilizing several group structures. A whole reactor R-Z calculation at BOL was carried out for the ETGBR using sizes and fractions given by AEEW-M1669. The model employed has already been shown in figure (2.3) previously. The 69 group k_{∞} values for the ETGBR pin-cell average zones, which were produced by WIMS were found to be as follows: C1: 1.3666, C2:1.6270, IAB & OAB: 0.2874, and RB: 0.2960 Table (2.6) shows the k_{eff} as calculated by WIMS-E using several group structures. This section will serve as a basis for the group structure choice which shall be declared in the immediately following section.

Table (2.6): R-Z whole reactor k_{eff} estimates for various group structures

Groups	k_{eff}	Group Structure
4	1.0479	7,14,27,69
7	1.0525	4,7,14,18,22,27,69
19	1.0549	2...14,16,18,22,24,27,69
28	1.0551	1...27,69

Discussion of WIMS-E Whole Reactor Results for the ETGBR

a) Reactivity:

The k values reported for the RZ calculation were compared with the values obtained using COSMOS and reported in AEEW-M1669. The reference result was given as k_{eff} =1.0658 using the uncondensed 37 group structure of the fast reactor specialized FD5 library. The few-group calculations of WIMS-E seem to show a relatively small dependence on the details of the group condensation as has been shown previously in table (2.6). Additionally, there appears to be a steady rise in the value of k_{eff} as the fast and resonance group structures become more detailed. The 19-group structure was chosen as the best compromise in accuracy and computing time which still gave full coverage of the available fast groups in WIMS, while considering a few resonance groups and a single thermal group.

Additionally, the significance of the resonance calculation was assessed using the 'subgroup' model within the WIMS-E modules WPRES and WRES. The result indicated no significant benefit, enhancing the fact that it is the energy region above 10 KeV and not the WIMS resonance region (4eV to 10KeV) that is significant in a fast core situation.

As a further test of accuracy, the meshing in the WSNAP diffusion step was checked. The 19-group case was rerun with the meshes doubled radially in all zones: k_{eff} showed little change, confirming the adequacy of the spatial meshing.

b) Reaction Rate Edits:

Reaction rates were produced on demand by the modules WLINK and WWED, after the WSNAP step in WIMS-E. The edit was performed for 7 and 19-groups whole reactor diffusion calculations. The results are shown in table (2.7).

Table(2.7): ETGBR neutron balance and k_{eff} using two different group structures

	7-group	19-group
Production	1.0572	1.0603
absorbtion	(absortion of 1.0 is normalization)	
Fissions	0.3617	0.3627
Captures	0.6383	0.6373
k_{eff}	1.0525	1.0549

The edit showed a small sensitivity to the grouping used in the estimation of reactivity, and tends to confirm the choice of 19 groups. Group dependent reaction rates were also examined for the three main energy ranges of the spectrum, in order to determine the energy regions of greatest importance for the ETGBR as shown in table (2.8) using two different group structures.

Table(2.8): Energy group dependence of neutron balance in ETGBR

Normalized to total absorbtion of 1.0

		7-group	19-group
	Fast	0.7309	0.7370
Absorbtions	Reson.	0.2675	0.2606
	Thermal.	0.0015	0.0023
	Fast	0.9204	0.9282
Productions	Reson.	0.1368	0.1320
	Thermal.	1.567×10^{-5}	1.938×10^{-5}

The 7 group structure predicts less events in the fast energy range, and more events in the resonance range, than does the 19 group structure. This accounts for the difference, although small (0.3%), in reactor reactivity prediction. This remaining sensitivity is a further argument in favour of the 19 group choice with full WIMS library groups used in the resonance and fast regions.

Comparison with COSMOS Results

The most detailed (28-group) WIMS reactivity calculation for the AEEW-M1669 design of the ETGBR using WIMS-E methods is shown to be lower than COSMOS results by some 1.07 %dk, with the 19 group calculation nearly identical. Taking into account the different calculational routes used by WIMS and COSMOS, the agreement at BOL appears to be very encouraging.

As a further comparison with AEEW-M1669 reaction rates, the following Table (2.9) shows the neutron absorbtions in each reactor zone as calculated by WIMS compared with reported results obtained with COSMOS. Agreement appears reasonable in all zones except the radial breeder (RB) zone, where a slightly different fuel composition (less U-235 and U-238) accounts for the inconsistency. With the better 19 group structure it is obvious that an improvement in consistency ensues.

Table (2.9): BOL Regional Absorbtion Fractions calculated by WIMS and COSMOS

	Absorbtions Per 1000 Fissions		
Zone	WIMS-E		COSMOS
	7-group	19-group	
C1	1218	1213	1182
C2	803	795	789
AB	342	350	348
RB	284	289	353
R	116	109	61

Further, the regional power distribution can be deduced from the edit at BOL and compared with data from AEEW-M1669 as shown in table (2.10) below. Again, as in the previous table, it appears that the agreement of the WIMS predictions with those of COSMOS are reasonable. The RB zone inconsistency is once again, as mentioned before due to the use of a different fuel composition.

Table (2.10): BOL Regional Power Contributions as calculted by WIMS and COSMOS

	Power (%)		
Region	WIMS-E		COSMOS
	7-grp	19-grp	
C1	53.74	53.93	52.40
C2	42.43	42.27	41.20
RB	1.75	1.70	3.10
AB	2.07	2.06	3.00

As a comparison over time of WIMS and COSMOS, tables (2.11) and (2.12) show the neutron balances for core zones (C1) and (C2) as calculated by both codes for the BOL and EOL. Although burnup is specifically covered in the next section, it was thought convenient to use the EOL neutron balance data in this section for completness. The EOL condition, as in the reference, was assumed to be after a full power burnup of 3.5 years. A noticeable difference is in the EOL fission contribution: WIMS gives higher Pu-239 (and Pu-241) fission contributions than does COSMOS.

Table (2.11): Inner Core Neutron Balance of ETGBR †

	B.O.L.				E.O.L.			
	Absorbtions		Fissions		Absorbtions		Fissions	
	WIMS	COSMOS	WIMS	COSMOS	WIMS	COSMOS	WIMS	COSMOS
Oxygen	0.36	0.26	-	-	0.43	0.26	-	-
Steel	5.76	6.33	-	-	5.58	6.40	-	-
235	0.35	1.27	0.28	1.01	0.20	0.73	0.10	0.58
238	44.82	42.60	5.20	6.29	42.64	40.11	5.10	5.72
239	42.75	43.64	34.05	34.44	41.04	40.54	33.15	31.95
240	3.58	3.83	1.36	1.56	4.37	4.86	1.71	1.96
241	2.37	2.01	2.06	1.65	2.17	2.10	1.91	1.73
242	1E-05	0.06	-	0.03	1E-05	0.10	1E-05	0.05
Fispd	-	-	-	-	3.57	4.87	-	-
Total	100	100	42.94	44.98	100	100	42.10	41.99

Table (2.12): Outer Core Neutron Balance of ETGBR †

	B.O.L.				E.O.L.			
	Absorbtions		Fissions		Absorbtions		Fissions	
	WIMS	COSMOS	WIMS	COSMOS	WIMS	COSMOS	WIMS	COSMOS
Oxygen	0.36	0.28	-	-	0.42	0.28	-	-
Steel	4.35	5.09	-	-	4.45	5.38	-	-
235	0.28	0.99	0.22	0.79	0.21	0.72	0.17	0.57
238	35.93	33.93	4.92	6.14	36.38	34.19	5.02	5.71
239	51.73	52.55	42.22	42.45	48.64	47.41	39.98	37.99
240	4.52	4.71	1.89	2.15	5.11	5.65	2.15	2.48
241	2.81	2.37	2.48	1.98	2.54	2.36	2.25	1.96
242	1E-05	0.08	-	0.04	1E-05	0.11	1E-05	0.06
Fispd	-	-	-	-	2.25	3.88	-	-
Total	100	100	51.7	53.5	100	100	49.5	48.77

†: Normalization is 100 absorbtions in the whole region considered.

An additional and important comparison, based on reaction rates, is the internal conversion ratio (ICR) and overall reactor breeding ratio (BR). These are defined, for the region of interest, as the ratio of captures in the fertile materials over the absorbtions in the fissile materials. WIMS, with the 19 group structure, gives an ICR of 0.748 and BR of 1.175 for the ETGBR at BOL, compared to 0.727 and 1.297 respectively deduced from COSMOS results for the two indicators respectively. It can be assumed that lower absorbtions in the radial breeder due to lower U-238 content, as shown to have been used previously, causes the reduced BR prediction with WIMS.

Burnup And Lifetime

A comparison between WIMS and COSMOS burnup predictions has been undertaken. In WIMS, burnup is handled at the pin-cell level followed by a whole reactor calculation performed with the generated few-group data. The general sequence of operations is shown in figure (2.6).

The burnup was carried out using both 7 and 19 groups with the following mean ratings assigned to each zone:

zone	Rating (MW/tHM)
C1	47.80
C2	38.30
IAB	2.72
OAB	2.72
RB	2.51

Fuel ratings used in each zone were obtained by carrying out a BOL R-Z whole reactor calculation for the ETGBR. Fission reactions edit gave fission events in each reactor zone, and these were then normalized to a maximum rating of 47.80 MW/t assigned to zone C1. This rating was deduced from ETGBR design information from Winfrith [19] where a reactor coolant mass velocity of 5500 Kg/s. was assumed. Reactivities calculated for enrichments of 15.17% C1 and 21.41% C2 at the end of a 3.5 year burnup are reported in table (2.13). The effect of calculating the spectrum every 213 days rather than 426 days is negligible.

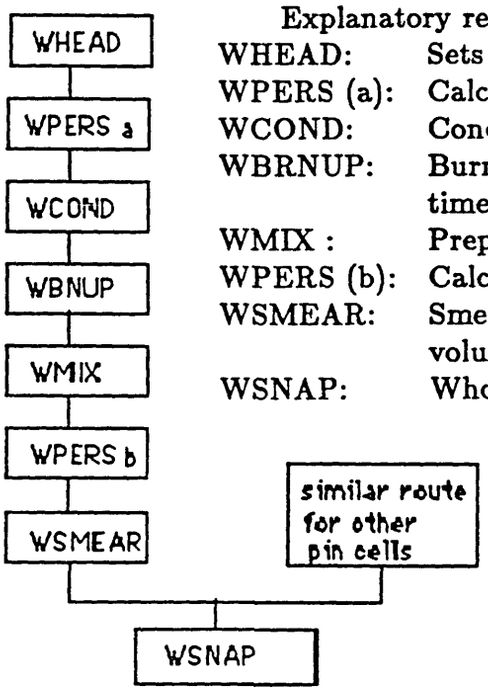

Explanatory remarks for figure (2.5):

WHEAD:	Sets up pin-cell and performs resonance calcs
WPERS (a):	Calcs 69-gp fluxes for pin-cell/for condensing
WCOND:	Condenses to few-groups
WBRNUP:	Burns pin-cell at a fixed rating for a given time using several spectrum recalculations
WMIX :	Prepares x-secs for subsequent steps.
WPERS (b):	Calcs few-group fluxes to use in region smear
WSMEAR:	Smears pin-cell into one region using given volume fractions
WSNAP:	Whole reactor diffusion calc. in RZ geom.

Figure 2.6. The WIMS-E calculational sequence for the burnup of a single zone of the ETGBR.

Table (2.13): Effect of spectrum recalculations (Cycles) on EOL k_{eff} of ETGBR

k_{eff} (BOL)	k_{eff} (EOL/3.5yrs) Cycles	
	3	6
1.0549	1.0271	1.0269

The reactivity of the reactor at the assumed 3.5 year EOL condition, is seen to be high and points to a longer life, for the same enrichments as the COSMOS reference. However, any conclusion regarding the WIMS prediction must take account of uncertainties in the validity of WIMS validity for fast systems.

Rather than undergoing an enrichment search in order to force agreement with the 3.5 year burnup yielded by of the COSMOS calculation, the burnup calculated by WIMS to EOL was determined, with EOL now indicating the time when k_{eff} (k_{datum}) is about 1.00. Figure (2.7) shows the reactivity-life curves

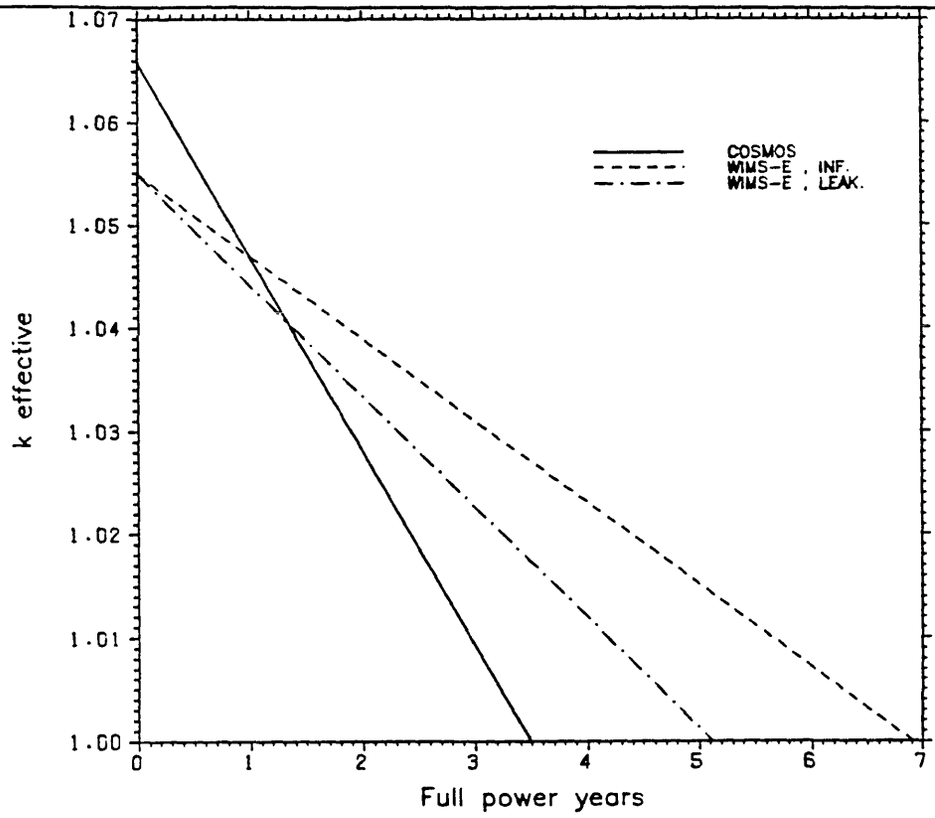

Figure 2.7. The burnup of ETGBR calculated by WIMS and compared to COSMOS (----)infinite spectrum data(-·-·-) leakage corrected data

predicted by WIMS and COSMOS. With WIMS either the infinite spectrum lattice data were used in the whole reactor calculation, or else the leakage corrected data was used. It is seen that even with the leakage correction (DB^2 addition to the absorbtion), the ETGBR reactivity-life predicted by WIMS-E is just over 5.0 years An average burnup fall of reactivity of 0.8 %dk per year is noted (5.5% over life) assuming a linear fall, as is shown to be the case.

Concluding Remarks:

It is apparent that WIMS-E overestimates the reactivity-life of the ETGBR as represented in AEEW-M1669. The reactivity at BOL predicted by WIMS is actually about 1 % lower than that reported for a COSMOS calculation and as burnup proceeds, WIMS increasingly over-predicts the reactivity of the ETGBR. It may be that this is a result of the non-resonance treatment of the unresolved region above 10 keV combined with leakage treatment uncertainties. For the chosen group

structure BOL data are in reasonable agreement with AEEW-M1669 COSMOS data. With these reservations, it is reasonable to employ WIMS for ETGBR survey calculations.

2.4 THE CALCULATIONAL MODELS ADOPTED IN THIS WORK-AN OVERVIEW

Two general models were used for the calculations reprted in this thesis. More details of the procedures used for each reactor core are given in the relevant chapter. A lattice-cell model with leakage correction, was used as a 'point' model of a bare core. This may be an adequate representation of a whole reactor or thermal and intermediate systems since reflector reactivity worth is relatively low. Secondly, for fast systems with small core sizes and high leakage, it is desirable to model multi-zone reactors including reflectors. To this end, a whole reactor calculation in 2 or 3 dimensions is required and WIMS-E's diffusion theory module WSNAP provides this capability.

2.5 CONCLUSIONS

The WIMS family of codes have been presented. The use of WIMS was an attempt to use a single calculational route for a range of reactors ranging in energy from thermal to fast. With no directly applicable benchmark cases available for the gas-cooled fast reactor systems, several comparisons with their methods had to suffice.

Reaction rate prediction was, in general, in reasonable agreement with other work. Burnup (ie. reactivity-lifetime) was found to be, even with the best leakage prescription included, overpredicted with WIMS. This was shown to be the case even with a reduced fuel loading considered.

The WIMS resonance treatment was shown to make little difference for very 'hard' cores. In brief, the WIMS high energy group structure is not adequately refined for fast sytems although it is assumed to be acceptable for the 'diluted' fast cores introduced in this thesis.

REFERENCES

1. Askew J. R. , Fayers F. J. , and Kemshell P. B. , *A General Description of the Lattice Code WIMS*, BNES, vol. 5, No. 4, p. 564, October 1966

2. Halsall M. J. , and Taubman C. J. , *The 1981 WIMS Nuclear Data Library*, AEE-Winfrith report AEEW-R1442, September 1983

3. Leslie D. C. , *The SPECTROX Method for Thermal Spectra in Lattice Cells*, J. Nucl. Energy, vol. 17, p. 293, 1963

4. Askew J. R. , and Roth M. J. , *WIMS-E , A Scheme for Neutronic Calculations*, AEE-Winfrith report AEEW-R1315, June 1982

5. Gubbins M. E. , Roth M. J. , and Taubman CJ, *A General Introduction to the Use of the WIMS-E Modular Program*, AEE-Winfrith report AEEW-R1329, June 1982

6. Roth M. J. , *The WIMS-E Module W-FORTE*, AEE-Winfrith report AEEW-R1688, September 1983

7. Tyror J. G. , Askew J. R. , *The United-Kingdom Approach to the Calculation of Burn-Up in Thermal Reactors*, Proc. of a Panel on Reactor Burnup Physics, p. 95, IAEA, Vienna, July 1971

8. Waltar A. E. , and Reynolds A. B. , *Fast Breeder Reactors*, p. 141, pergamon press, 1981

9. Roth M. J. , personal communication, 1986

10. Hughes D. , *Neutron Cross Sections*, Brookhaven National Laboratory Report BNL-325, 2*nd* Edition, 1958

11. Askew J. R. , Personal Communication, AEE-Winfrith, January 1984

12. Oppenhen C. , *GBR-4 Physics Performance*, GBRA, Brussels, 1973

13. Ronen Y. , Leibson M. J. , and Radkowsky A. , *On the Reactivity Void Response of an Advanced Pressurized Water Reactor*, Nuclear Technology, Vol. 80, p. 225, February 1988

14. Chawla R. , Gmur K. , and Hager H. , *Reactivity and Reaction Rate Changes with Moderator Voidage in a Light Water High Convertor Reactor Lattice*, Nuclear Technology, vol. 67, p. 360, December 1984

15. Chawla R. , Hsieh H. M. , and Halsall M. J. , *Effects of Recent WIMS Data Library Changes on Calculational Results for LWHCR Lattices*, Ann. Nucl. Energy, vol. 13, p. 523, 1986

16. MacBean I. J. , *A COSMOS Calculation of the Neutronics Performance of a 1670 MW(th) GCFR with 7 mm Fuel Pellets, and a comparison with Results of CEGB Calculation*, AEEW-M1669, Winfrith, April 1979

17. Brissenden R. J. , *The Compatible Open Shop Modular Operating system COSMOS*, Proc. Am. Nucl. Soc. Topical Meeting on Computational Methods in Nuclear Engineering, Charlestown, S. Carolina, 1975

18. Marshall W. , *Nuclear Power Technology - Volume 1 : Reactor Technology*, pp. 116-124, Oxford Science Publications, 1983

19. Askew J. R. , Gratton C. P. , and Goddard A. J. H. , Personal Communication, AEE Winfith, January 1984

Further References:

Roth M. J. , *The Collision Probability Modules of WIMS-E.*, AEE-Winfrith report AEEW-R1920, April 1985

Gratton C. P. , *The Gas-Cooled Fast Reactor in 1981.*, Nucl. Energy, Vol. 20, no. 4, p. 287, August 1981

CHAPTER 3.

THE AGR, ADVANCED AGR, AND DERIVATIVE CONCEPTS

3.1 THE CURRENT AGR

3.1.1 A Description and Review

The limitations inherent in the Magnox reactors using natural uranium fuel clad in magnesium alloy were recognized early in their operation. The metallurgical limitations of this type of fuel element restricts the reactor coolant outlet temperature to about 400C. A further limitation of Magnox is that burnup of the fuel is limited to some 5000 MWd/t, both because of reactivity limits, and due to swelling problems associated with the metal fuel.

Studies of improved designs emphasized ceramic fuel, which would be inert in carbon dioxide and which would not undergo any phase change. With ceramic oxide fuel came the need for enrichment. Initially, in order to keep the enrichment low, beryllium cladding was proposed. Beryllium, however, was found to be difficult to machine, in addition to doubts on its mechanical integrity in core. Stainless steel cladding, decided upon as a substitute, led to further enrichment of the fuel bieng needed to offset the increased absorbtions.

The immediate design aims of the new system were to be: increased fuel discharge burnup, and higher coolant outlet temperatures. The second goal has the advantageous effect of raising the plant thermal effeiciency (from about 30% for Magnox systems to some 40%). Of course, the new design was to benefit from Magnox reactor proven technology, such as the use of prestressed concrete pressure vessels (PCPV) in place of the earlier steel vessels.

The new design, having a greater power density and higher core temperatures than the Magnox reactor, had to have a fuel element subdivided into smaller diameter rods (of course the lower thermal conductivity of the ceramic oxide fuel is also a factor here). Additionally, the coolant pressure had to be raised from 10 bars in a typical Magnox reactor, to some 40 bars.

As a consequence of the new design, the amount of moderator in the core is reduced from that in a Magnox reactor - The graphite to fuel volume ratio is about 25 compared to 45. This, however, is not a drawback since the amount of

moderator is still large, and since the use of stainless steel cladding removes the possibility of clad ignition or failure at elevated temperatures.

With the above mentioned design features adopted, in addition to further aspects, the resulting concept was termed the Advanced Gas Cooled Reactor (AGR). With the Magnox reactors starting to be decommisioned, the AGR is today, and will be in the next decade the major nuclear power system in the U.K.

Ironically, the AGR which has the worse heat transfer medium (CO_2 vs H_2O for PWR), has the larger fuel rod diameter (roughly 15 cm. versus 10 cm.). The adverse effect of this, however, is somewhat alleviated by the central void in the rods [1]. Although the PWR core is significantly smaller, the AGR core itself has a notably smaller diameter than the Magnox core - 9.3 m. versus 14.2 m. respectively.

AGR is unique among reactors in having a 'gas-baffle' which allows seperate cooling of the graphite moderator. This is neccesary to control the positive moderator reactivity coefficient inherent in the design.

AGR was designed to be refuelled on-load at full power. This is potentially a valuable advantage in maximizing reactor overall availabilty. At present refuelling at Hinkley Point B is carried out at 40% power due to concern about graphite sleeve fracture. Plans for Heysham 2/Torness reactors indicate the possiblity of refuelling at 70% power using a new 'single-sleeve' stringer [2].

Because of the use of a 'just-critical' cycle (to be clarified in section 3.2.2) for AGR in-core fuel management, reactivity control is accomplished with little control rod usage. This also means that the reactor at no time has an overall excess reactivity of mor than 1.5%. The section on AGR fuel management (3.2.2) gives more information on these aspects.

Typical characteristics for an AGR are given in Table (3.1) while Figure (3.1) shows a typical AGR channel of 36 rods and the surrounding graphite structure.

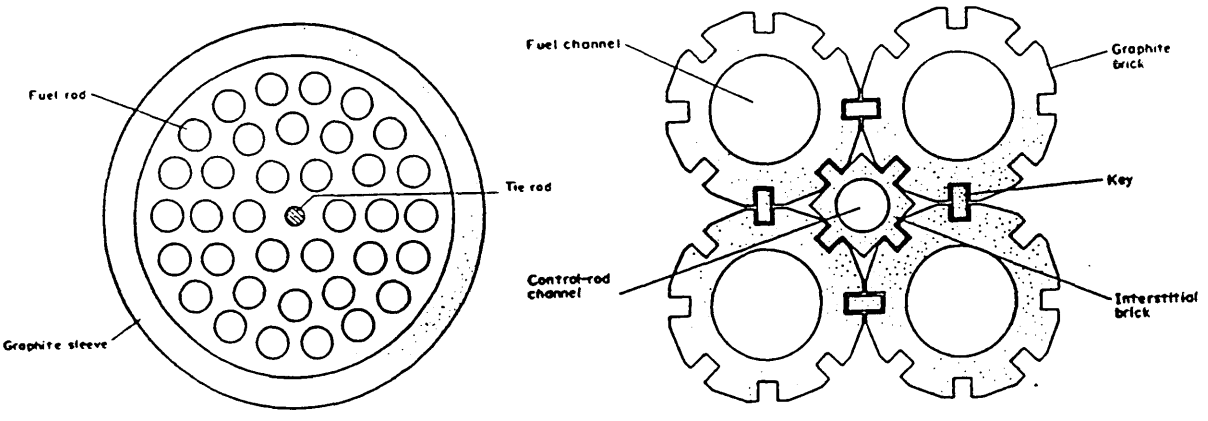

Figure 3.1 The AGR channel and block lattice.

Table (3.1): Typical commercial AGR characteristics.

Core Thermal Power Output MW	1510
Plant Thermal Efficiency %	42
Core:	
Diameter m.	9.3
height m.	8.2
Fuel Element:	
No. per Channel	8
Element Height m.	1.04
Pins per Element	36
Channel:	
No. in Core	332
Diameter m.	0.198
Diameter(OD) mm.	
Clad Thickness mm.	4.0
Enrichment:	
Inner Core %U235	2.078
Outer Core %U235	2.707
Average %U235	2.239

Table (3.1) : continued.

Control Rods	81
Rating MW/t	14.0
Power Density Mw/m^3	2.70
Discharge	
Irradiation MWd/t	18000
Coolant :	
Pressure Bar	41
Inlet Temperature (C)	318
Outlet Temperature (C)	651

3.1.2 Lattice Cell Calculations for the Standard AGR

Because the core is made up of a large number of identical cells, a reasonable method of calculating AGR core nuclear performance is by the use of a point model lattice calculation in cluster geometry. Neglecting the reflector,which accounts for little reactivity anyhow, this option is available in the WIMS-D4 code. To account for overall leakage the geometric bucklings based on AGR core dimensions has been used. Some particular inputs to the present calculation of the AGR are shown in Table (3.2).

Table (3.2): Data for assumed AGR design.

Core Diameter	910.0 cm.
Core Height	830.0 cm.
Radial Buckling	$1.43 \times 10^{-5} cm^{-2}$
Axial Buckling	$2.79 \times 10^{-5} cm^{-2}$
Fuel Enrichment	2.20 % U-235
Fuel Radius (Solid Pellet)	0.724 cm.
can outer Radius	0.766 cm.
Channel outer Diameter	44.34 cm.
Cluster Block Outer Diameter	17.78 cm.

The major difference from a commercial AGR is the assumption of a solid fuel pellet and the neglect of the interstitial graphite in order to simplify the lattice-cell calculation. The interstitial graphite control block may be represented directly in the lattice calculation by a multi-cell WIMS [3] set-up. The other possibiltiy to increase the main graphite block radius by an amount equivalent to the volume of

the interstitial block. In any event the present calculations neglect the interstitial block altogether and this is thought to have very small efect on the calculated parameters for the AGR.

The group structure used for the calculations on AGR and its derivatives is shown in table (3.3) and was chosen by minimizing the number of groups while preserving reactivity. Little sensitivity to group structure was noted for the AGR, with its well thermalized spectrum. The only provision made was to make sure that the low lying resonances of Pu-240 and Pu-241 were wholly within a group (groups 7 and 8).

Table (3.3): Eight group structure used in AGR lattice calculations.

Group	WIMS Groups	Energy Bounds
1	1 - 4	10.00 - 1.353 MeV
2	4 - 7	1.353 - 0.3025 MeV
3	7 - 14	302.5 - 9.118 KeV
4	14 - 24	9.118 - 0.027 KeV
5	24 - 27	27.0 - 4.0 eV
6	27 - 35	4.0 - 0.097 eV
7	35 - 50	1.097 - 0.300 eV
8	50 - 69	0.300 - 0.0 eV

The base case AGR was found to have, for a freshly fuelled channel, the following indices:

k_∞ 1.2171
k_{eff} 1.1854 (1.1784)
ICR 0.5124
α 0.2148
ϵ 0.0475

At the assumed datum k_{eff} of about 1.012, the AGR is taken to be at equilibrium at an irradiation of close to 10 GWd/t. The Conversion ratio (CR) is found then to be 0.5871 compared to the value shown above.

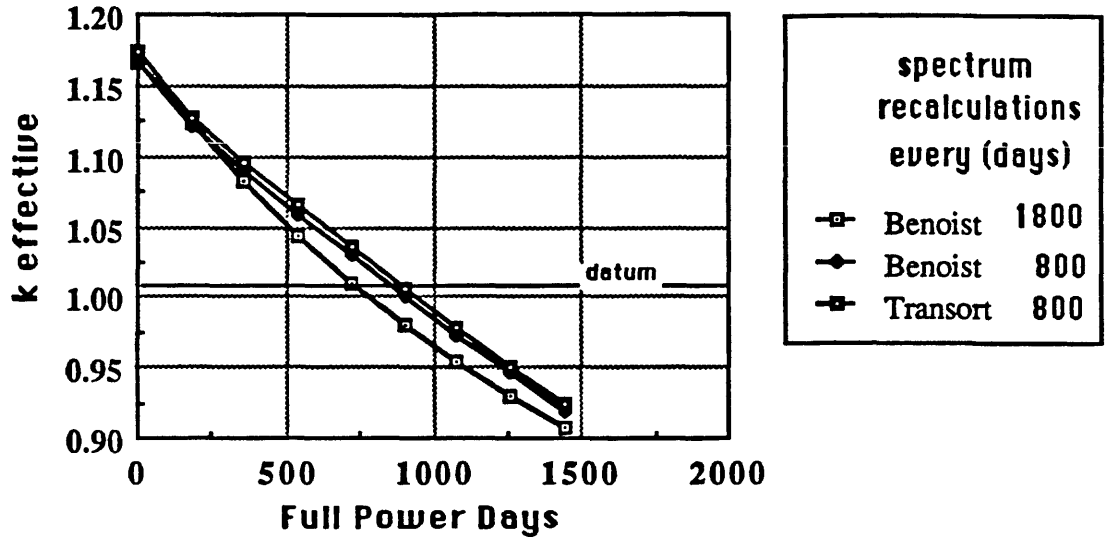

Figure 3.2. AGR burnup curves and effect of frequency of spectrum recalculation.

The reduction in the reactivity of a channel between loading and discharge is quite high at some 25 % dk. Although the BOL channel reactivity is high (about 20%), the fuel management is based on a 'just-critical' reactor cycle where the full reactor is maintained at an excess reactivity of around 1.5%. Reactivity control is accomplished by continuous refuelling of the channels as they reach the design discharge burnups.

The discharge irradiation calculated here was found to be slightly dependent on the treatment of leakage. A figure of 18500 MWd/t was found with the best WIMS Leakage formulation applied, whereas the default WIMS transport leakage calculation gave an overestimate of some 23500 MWd/t. The nature of the gas cooled design with large neutron streaming channels is respon sible for the sensitivity to the leakage treatment. The reactivity rundown of the AGR as calculated by the two WIMS leakage treatments and with different frequencies of spectrum recalculation, is shown in figure (3.2). Because of the nearly linear burnup, the discharge irradiation of the AGR in continuous-cycle is approximately given by twice the burnup at $k_{eff} = k_{datum} = 1.012$.

With the stress in this thesis being, with the medium term future in mind, on mixed plutonium fuelled systems, it is interesting to see what Magnox Pu enrichments are required to fuel a standard AGR. Table (3.4) shows the reactivities of a Pu fuelled AGR at several enrichments, together with discharge irradiation assuming continuous-cycle.

Table (3.4): Magnox Pu enriched AGR reactivity search.

Enrichment (%Magnox Pu)	k_∞	k_{eff}	Discharge Irradiation (GWd/t)
2.9	1.2425	1.2092	13.3
3.5	1.2637	1.2304	18.6
4.0	1.2782	1.2449	21.0
5.0	1.3014	1.2682	27.7

To obtain the same initial k_{eff} of about 1.18 as that of UO_2 fuelled AGR it is seen that just under 2.9% Magnox Pu is required for a standard AGR. For the AGR no worry about optimum moderator to fuel ratio exists as in the PWR when switching to Pu enrichment. This is due to the neutronic inertness of the CO_2 coolant as well as the effect of thermal expansion on the coolant being negligible. A Magnox Pu fuelled AGR would, however, require to be enriched to some 3.5 to 4.0 %Magnox Pu to give the same discharge irradiation as the normal AGR. The doppler coefficient for the Pu-fuelled AGR, however, must be checked; the doppler coefficients of both Pu and U-235 enriched AGR's are compared later in the section.

The neutron spectrum in an AGR channel (standard U-235 enriched) is well thermalized. The inner fuel ring spectrum is shown in figure (3.17) (in a coming section) as compared to that of the MSR (to be defined). This spectrum is also shown in figure (3.3) compared to that of the PWR. It is seen that the fuel zone of 'hardest' flux in an AGR is still softer than the flux in a PWR fuel rod - PWR having to use higher enrichment.

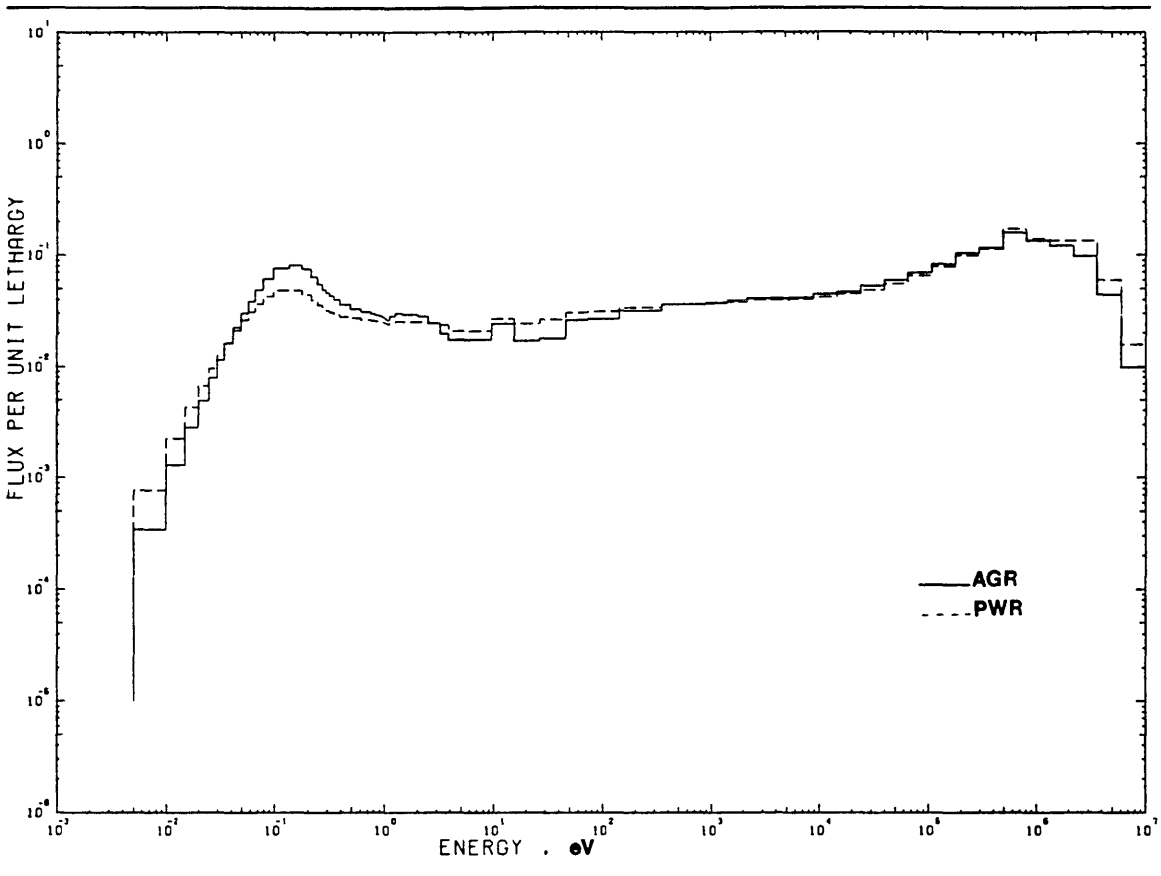

Figure 3.3. Inner fuel flux of AGR compared to PWR.

The BOL peaking factors of the 3 fuel rings are 0.84, 0.92 and 1.10 respectively, and these are of interest in the coming section on AGR developement; they are presented here for completeness of the AGR performance aspects. The peak ring rating (1.10) is the figure of most interest since it would be desirable in a new design to maintain this figure as close to 1.00 as possible.

Of interest is the isotopic concentration variation of the AGR fuel with irradiation. Figure (3.4a) shows this variation for the major heavy metal nuclides. In addition, the nuclide contribution to fission power as a function of irradiation is shown in figure (3.4b). The increasing contribution of the bred plutonium is clear (about 40% at EOL for a channel).

Regarding AGR temperature coefficients of reactivity, these have been determined for the 'just-critical' lattice. This is accomplished by burning the lattice to the operating datum level of k_{eff} of around 1.012. At this stage burnup is halted

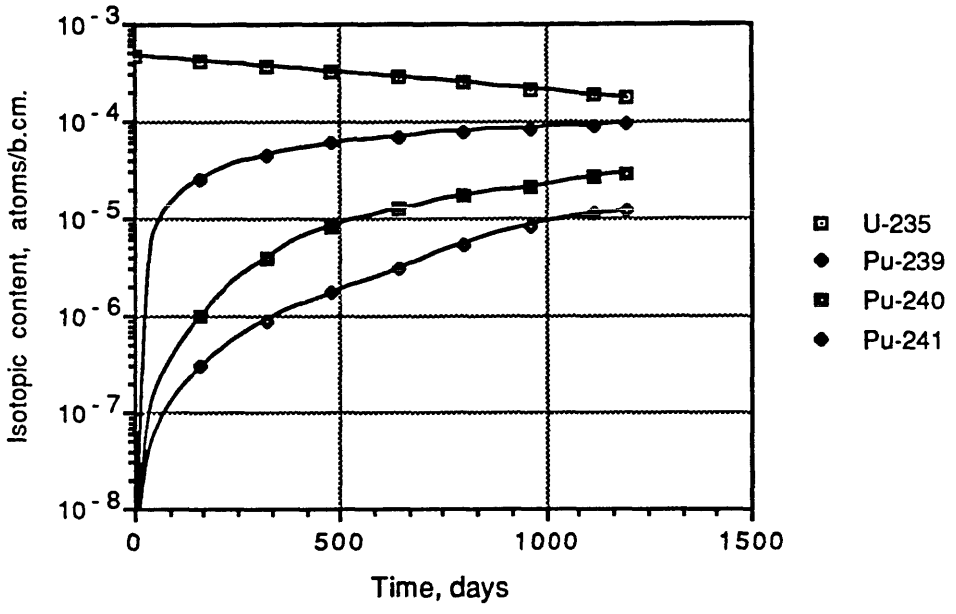

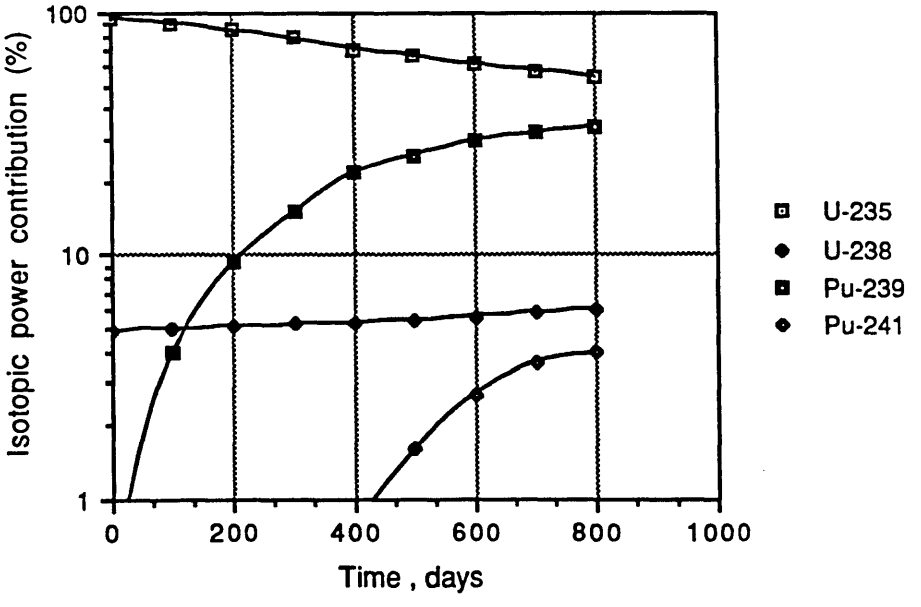

Figure 3.4. AGR (a) Isotopic change with burnup.(b) Isotopic power contribution change with burnup

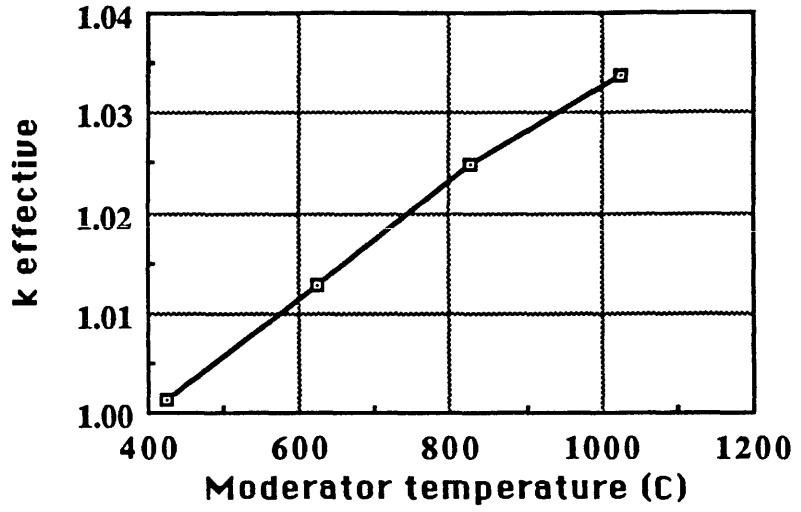

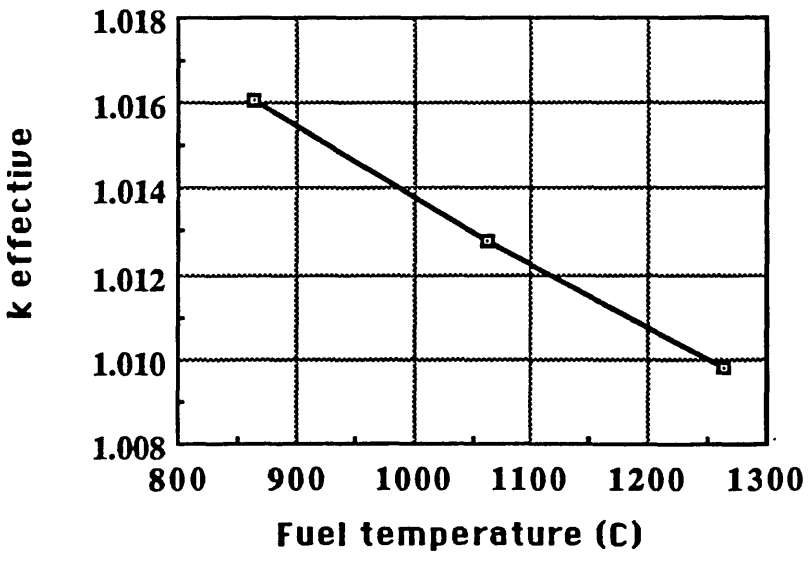

Figure 3.5. Effect of temperature on reactivity of AGR

and the materials of the lattice are subjected to temperature perturbations, once for each of fuel and moderator, yielding temperature coefficients of reactivity for the prescribed temperature ranges. Variation of the multiplication factor with either fuel or moderator temperature is shown in figure (3.5), while the calculated coefficients of reactivity are given in table (3.5). A simultaneous variation of fuel and moderator temperature, by 200K, gave an overall positive reactivity coefficient. However, a simultaneous change of the fuel and moderator temperature is unrealistic, since the moderator is largely isolated from the fuel. Separate cooling of the moderator causes its greater positive coefficient to be slow acting, while the fuel coefficient is rapid in its affect.

Table (3.5): AGR equilibrium coefficients of reactivity ($T\frac{dk}{dT}$) for 2.2% U-235 base AGR (K^{-1}).

Temperature range (K)	Fuel Coefficient	Moderator Coefficient	Overall Coefficient
fuel:1063-1263, moderator:425-625	-0.0174	+0.0298	+0.0124
fuel:1063-1263, moderator:625-825	-0.0174	+0.0432	+0.0258
Overall 1063-1263 Simultaneous	-	-	+0.0546
Overall 1000-1200, Simultaneous Magnox Pu at 2.9%	-	-	+0.0367

3.1.3 Whole Reactor Calculation of the AGR Core

In order to develop a more complete picture of AGR core physics, a 3 dimensional model is used. This procedure yields overall reactor flux profiles, power maps and an assesment of reactivity and nuclide utilization in the whole reactor. The calculational route followed is shown in figure (3.6).

Reactor zones have enrichments of 2.078 and 2.707% U-235 for the inner and outer cores respectively. WIMS-D4 data for each zone, in 13 groups, are translated into WIMS-E format, via the WIMS-E module WFORTE, using the procedure

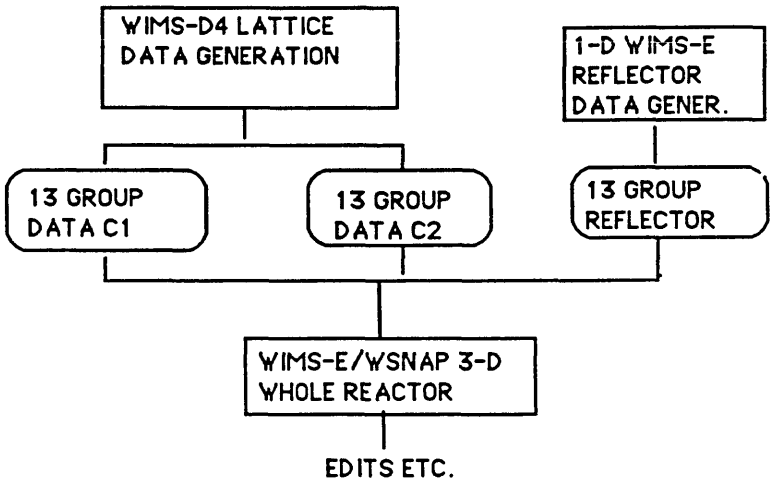

Figure 3.6. The WIMS route to an AGR whole reactor calculaton

described in chapter 2. The 3-d model for the AGR is in X-Y-Z geometry with each square mesh representing a lattice unit. One quadrant of the core is modelled. The core studied had 332 channels (216 in zone 1 and 116 in zone 2) as shown in figure (3.7).

To model approximately, the equilibrium core, where the AGR channels are on the average evenly distributed in irradiation (see figure 3.12a), burnup is carried out to roughly half the expected discharge irradiation (DI). Hence for the standard AGR a burnup of about 10 GWd/t is performed, at which point the data is transferred to WIMS-E. Table (3.6) gives the major neutronic indicators, calculated both for a core of 0 GWd/t burnup (freshly loaded) and for a core with channels at 10 GWd/t, calculated in whole reactor geometry with a row of steel reflectors included.

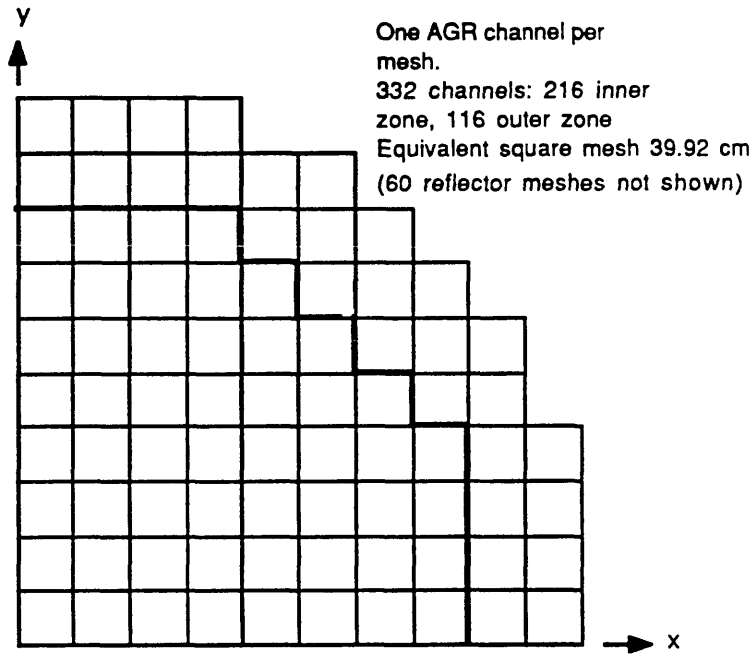

Figure 3.7. The AGR quadrant and its dimensions

Table(3.6): Derived neutronic indicators for zero burnup and equilibrium AGR - whole core.

	0 GWd/t burnup	equilibrium 10 GWd/t
k_∞ , inner	-	1.192
k_∞ , outer	-	1.272
k_{eff}	1.171	1.017
CR , inner	0.395	0.461
CR , outer	0.110	0.116
CR , average	0.296	0.340
ϵ, inner	0.052	-
ϵ, outer	0.050	-
ϵ, average	0.051	-
α, inner	0.214	-
α, outer	0.219	-
α,average	0.216	-

The average channel power is found to be 4.61 MW with a radial peaking factor of 1.42; this compares with reported values of 4.87 MW and 1.32 respectively for the Hinkley Pt B reactor [4]. A sample WIMS calculated power distribution is

shown in figure (3.8), for a freshly fuelled AGR core, whole reactor power output of 1500 MW(th).

Figure (3.8): Power map of equilibrium AGR core quadrant (MW), WIMS-E/WSNAP X-Y-Z calculation in 13 groups

3.05	2.91	2.61	2.06						
4.34	4.17	3.84	3.34	2.69	1.80				
4.45	4.34	4.12	3.81	3.91	3.27	2.29			
4.93	4.83	4.64	4.39	4.10	4.19	3.40	2.29		
5.37	5.28	5.10	4.86	4.57	4.21	4.19	3.27	2.05	
5.75	5.67	5.50	5.25	4.94	4.57	4.10	3.91	2.70	
6.32	6.24	6.07	5.82	5.50	5.10	4.64	4.12	3.90	2.61
6.07	5.99	5.82	5.57	5.25	4.86	4.39	3.81	3.41	2.06
6.32	6.24	6.07	5.82	5.50	5.10	4.64	4.12	3.90	2.61
6.49	6.41	6.24	5.99	5.67	5.28	4.83	4.34	4.21	2.91
6.58	6.49	6.32	6.07	5.75	5.37	4.93	4.45	4.36	3.05

3.2 DEVELOPMENT AND EXTENSION OF AGR

3.2.1 Background

In recent years nearly all U.K. research effort has shifted from AGR to other reactor types; to the Steam Generating Heavy Water Reactor, PWR, and Fast Reactors. In this section, it is attempted to show that the AGR has by no means become the end of the line for the steel-clad UO_2, CO_2 cooled graphite reactor.

In studying the development potential of the AGR, concentration will be upon the design of the reactor core and its fuel - less risk being involved and innovation being easier in this area than in other system components. In the following sections, WIMS-D4 is used to perform all the neccesary reactor physics calculations - the details of each calculation being given as required in the relevant section.

3.2.2 AGR Prospects

A primary goal in AGR developement must be extending the efficiency of extraction of energy from the fuel. A burnup close to the PWR figure of 30 GWd/t would be an ideal target. This together with the higher availability due to the on-load refuelling of AGR would definitely put it ahead of its rivals. In reality, extension of the discharge irradiation (DI) is not so simple with burnable poison requirement becoming both costly and difficult to implement without change to the present fuel design (ie using toroids of burnable poison wrapped round the fuel cluster within the grid and braces of each fuel element). Further limits on burnup arise from cladding behaviour and the lack of available fission gas pressure void space in the fuel pins.

Disregarding, for the present all other limits, the extension of DI may be accomplished by the use of higher enrichment feed fuel assuming no change to the fuel element geometry and heat transfer area. Figure (3.9a) shows the neccesary enrichments required for a given DI (there is a small difference between these

and equivalent calculations reported by Askew [1] presumably due to the use of slightly different AGR models).

The same information provided by figure (3.9a) may be obtained by noting the fissile feed requirement of AGR as a function of discharge irradiation. This is shown in figure (3.9b) together with the discharged and overall consumption of fissile. It can be seen that with higher enrichment, a reduction in fissile feed requirement per unit of energy extracted is achieved (the fission of pure U-235 produces about 1 GWd/kg of heat). The discharged fissile content falls however, as the U-235 is burned further while bred Pu only slightly increases in net. The discharged percentage of the fissile nuclides are listed in table (3.7).

Table (3.7) : Discharged fissile content in AGR for higher feed enrichment.

Feed Enrichment (%U-235)	Fraction of Initial Heavy Metal		
	U-235	Pu-239	Pu-241
2.2	0.0058	0.0037	0.0007
2.9	0.0047	0.0038	0.0010
4.0	0.0032	0.0039	0.0012

With higher enrichment, the refuelling frequency is less and the difference in rating between a newly loaded channel and its neighbours is larger. This channel-to-channel peaking problem is solved by the introduction of burnable poisons (Gd_2O_3). This is a further cost component that must be considered. Overall, it appears that the AGR may be designed neutronically for considerably higher fuel use (DI). Fissile usage, however, is almost independent of irradiation above 30 GWd/t with more of the plutonium produced during the cycle being consumed and therefore imposing an upper limit on burnup.

Figure (3.10) shows the simultaneous (change to fuel and moderator temperatures) overall coefficients of reactivity for the AGR with increasing enrichment. The most interesting result is that at 4.0%, the overall coefficient is actually negative. This is presumably due to the spectrum being shifted significantly into the

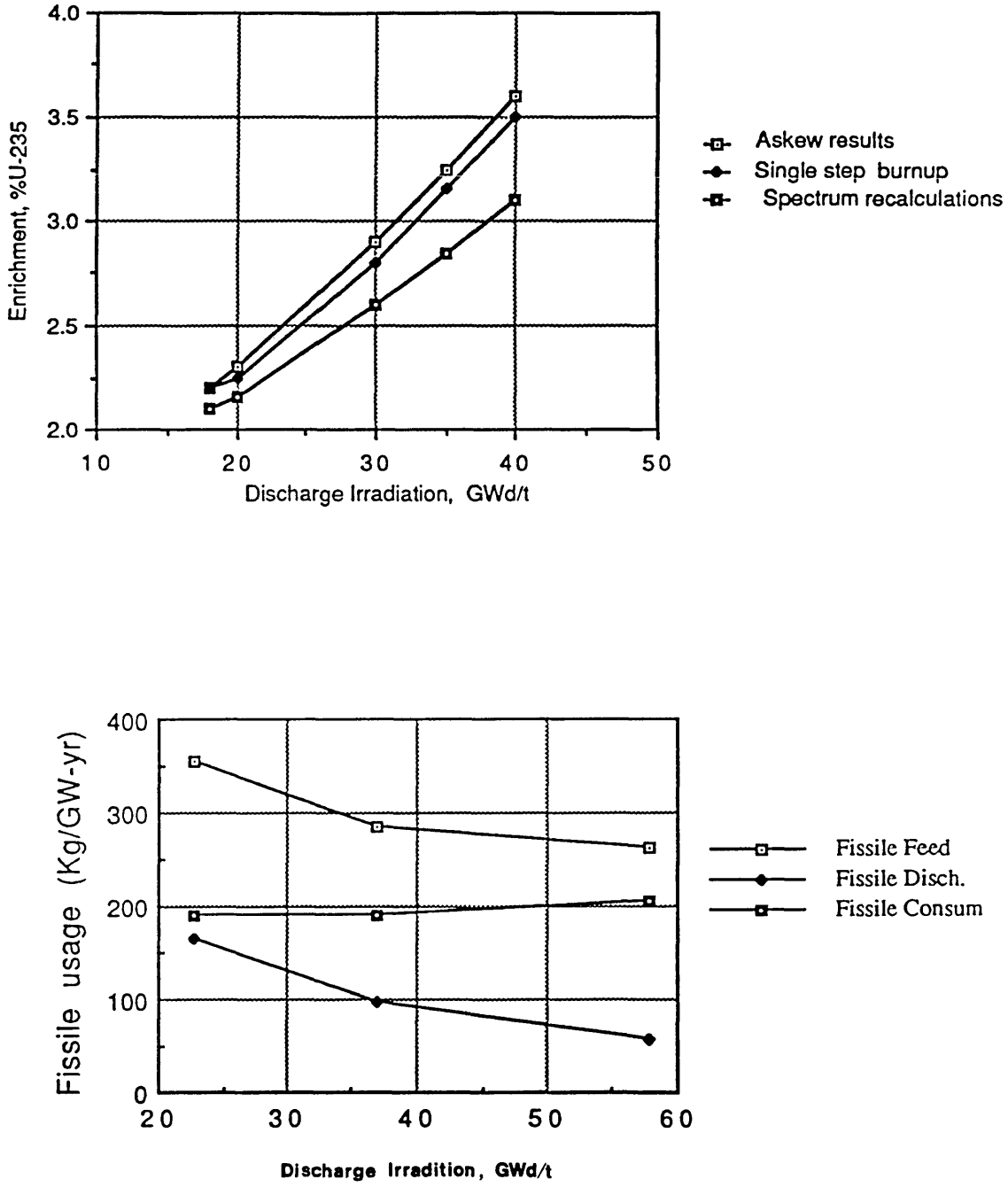

Figure 3.9. (a) Enrichment requirement to extend AGR burnup. (b) AGR fissile usage at extended burnups.

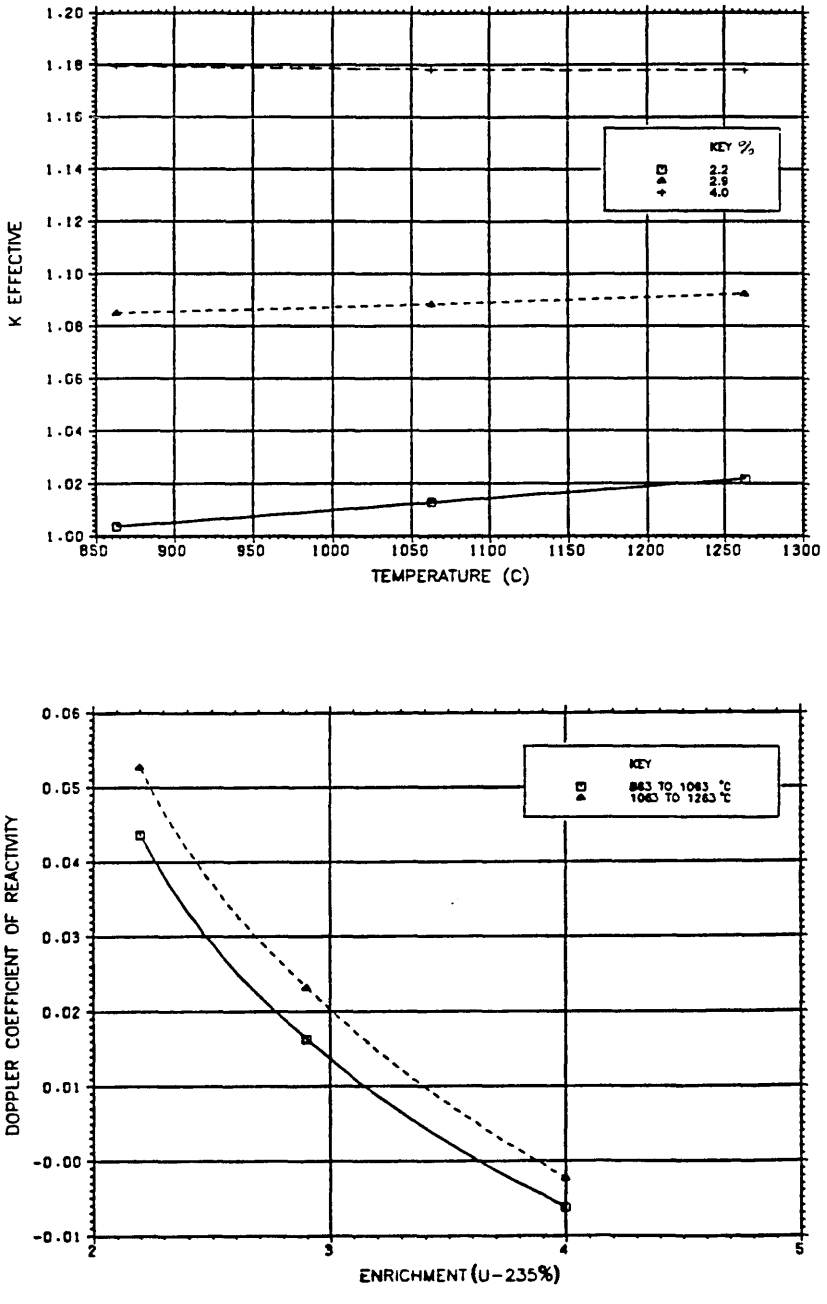

Figure 3.10. (a) Variation of AGR effective multiplication factor with temperature for each AGR enrichment. (b) Doppler coefficient of reactivity versus AGR enrichment.

resonance region. Study of the fuel spectra in figure (3.11) helps appreciation of the upward energy shift.

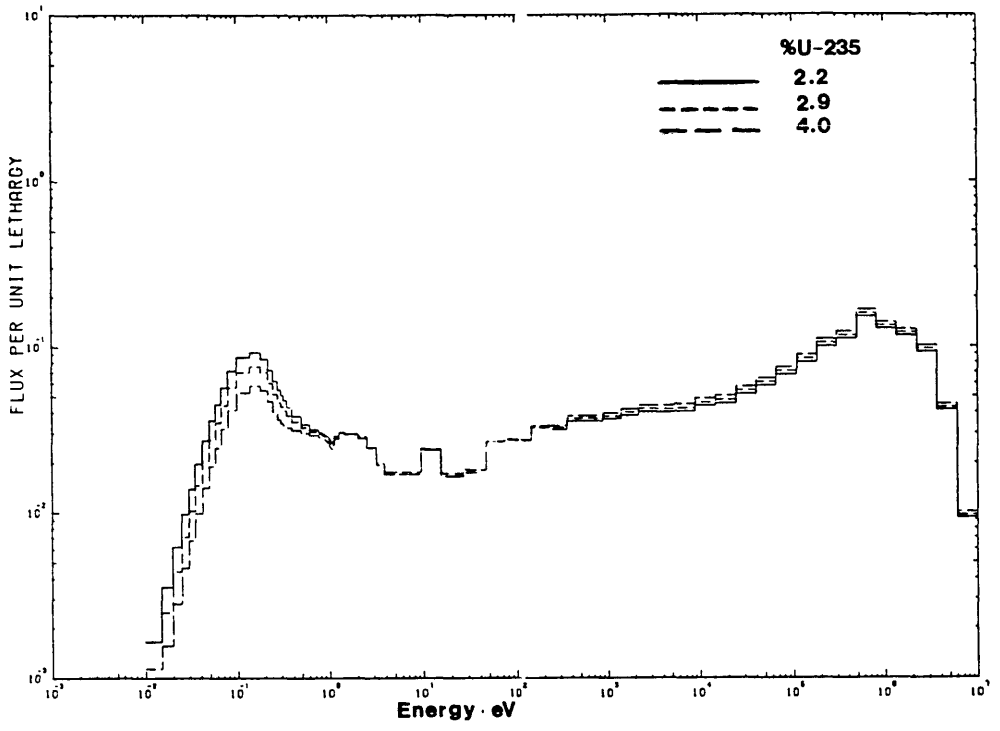

Figure 3.11. Inner fuel flux spectra of AGR at increasing enrichment.

An aspect of the AGR that should be noted, especially in comparison with, say, a PWR is that because of the method of continuous refuelling, at no time is there a large excess reactivity in the system.

With graphite present in the high temperature field of the AGR, core life becomes dependant on moderator integrity. The most straightforward solution proposed is the use of replaceble graphite moderator bricks. Askew et al [5] proposed , for an advanced AGR concept, the use of an integral fuel block based on HTR sizes, but incorporating an AGR standard channel with more pins of smaller diameter. Other proposals concerning moderator integrity maintenance, opt for a solution involving the reduction of the operating temperatures. This is vital if designs are sought which reduce the amount of moderator in the core, hence reducing the heat sink available during unplanned transients.

In the longer term ,the stainless steel cladding is an obstacle to both high temperature operation and general safety. The HTR solution of removing cladding completely is the obvious way ahead but some material integrity issues still need to be solved. Alternatively, the use of other materials for cladding is on the menu as well but extensive experience is required before these may be introduced fully.

In brief the improvements sought for the advanced AGR are:

1. Longer Neutronic Burnups (DI)
2. Better Material Integrity (clad)
3. Better Material Integrity (moderator)
4. Higher Conversion Ratios (CR) - fuel use efficiency
B. About as high a Temperature operation (efficiency)
6. At least as good a Transient response of temperatures
7. Minimal cost increase in core (Control,structure...)
8. Minimal cost increase out of core (boiler/circulator)
9. Relaxation of CO_2 Coolant Chemistry Control

3.2.3 AGR In-Core Fuel Management and its Variations

Progress from the AGR design can only be achieved if its special features are understood, especially if the inherent as well as the hard won engineered advantages are to be utilized. As mentioned previously, the AGR enjoys a feature unavailable to cores that must be enclosed in steel pressure vessels (PWR) - the ability to adopt a continuous on-load refuelling scheme. Starting with an AGR of given geometry and loading, WIMS-D4 will be utilized when required to calculate the performance indices of an AGR lattice.

The incentive is to achieve high burnup of the fuel at as high a rating as possible without violating metallurgical criteria [6]. For the AGR these criteria include: can corrosion, fission gas pressure, and irradiation damage. Since temperature controls the first two aspects, we may consider it as an effective criterion for fuel endurance. The performance limits may be roughly maintained by controlling the peak ratings in the core. It follows that the form factor (peak to average ratings) must be minimized. Since the power output of a reactor is normally fixed, this is then equivalent to minimizing the value of fuel and can temperatures. Fuel

lifetime must not be sacrificed and therefore the spread of discharge irradiations for the channels must be kept narrow. The two points have opposing effects and a balanced choice must be set. The use of absorbers is one of the methods to achieve the objectives.

Reactor design is usually set in terms of fuel cycle eqiulibrium, which is the state of the reactor after some years when the initial starting conditions have been 'forgotten'. This equilibrium state is represented as a point in time for an on-load fuelled system or by a burnup cycle in a batch, off-load reactor [7].

As already mentioned continuous refuelling of AGR is not adopted in practice since this would be tedious and with reduced power presently neccesary, would subject the system to frequent thermal cycling. The use of a delayed several batch scheme, a currently adopted practice, introduces a reactivity penalty. Reactivity penalty is defined as the difference between batch and continuous cycle reactivity as shown in figure (3.12).

Theoretically, AGR designs are operated on a 'just-critical' cycle. As the core burns up, new fuel is continuously fed in on-load to make up the loss of reactivity. Ideally, frequent and continuous refuelling is best, however, this is difficult and uneconomic since power level must be reduced (to some 30% presently). Therefore, refuelling is performed several channels at a time giving less overall power loss. The delayed scheme impliesthe need for higher enrichment feed fuel and thus a higher reactivity swing on refuelling. The more channels are refuelled at a time, the longer the delay and hence the greater the reactivity swing.

In the present calculations it is assumed that the datum reactivity of the AGR core is 1.5%dk. This is the margin adopted in this work for full xenon and temperature override [8].

The following discussion provides a simplified review of AGR in-core fuel management and explores some variations on current practice. In addition to a straight-forward extension of discharge irradiation, a scheme is sought where several channels are refuelled in a batch at a given time delay and giving the same discharge irradiation as the continuous cycle case. Another option is the adoption

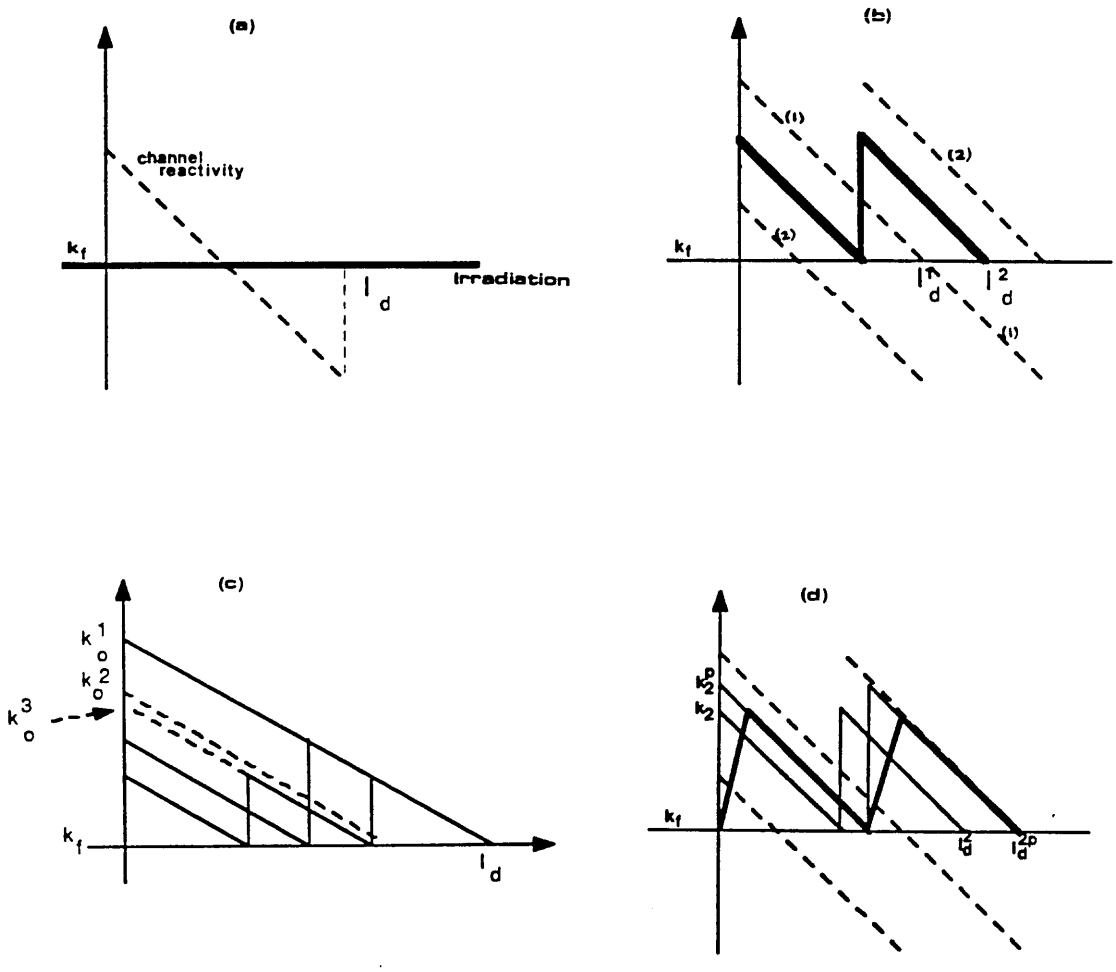

Figure 3.12. AGR versus batch refuelling and reactivity penalty

of a wholly batch scheme. In addition there are AGR derivates of new design; these are discussed in following sections.

The use of higher enrichment feed fuel in an equilibrium cycle is the straightforward method to extend DI. In practice, this requires burnable poisons to keep regulating rod movement no greater than in the base case (i.e. limit the control range to that of the current AGR). Also, poison keeps the age-factor (largest to average reactivity ratio) limited to the base value.

It is assumed that k_{eff} changes linearly with irradiation. Since the channels are taken to be similar, they are assigned equal weighting, and for a finite system the operating reactivity is given as:

$$k_{eff} = 1/n \sum^{n} k_e{}^i = \frac{k_e^1 + k_e^2 + ... + k_e^n}{n}$$

$$= n k_e^{datum}/n = k_e^{datum},$$

Where i is a channel, $k_e^1 = k_e^2 = ...k_e^n$, and n is the total number of channels. For equilibrium cycle continuous refuelling, the channels are distributed evenly in burnup; with one channel at zero burnup and one about to be discharged at a burnup of DI.

WIMS-D4 burnup calculations where performed using a 2.15% average enrichment, giving a DI of 17.48 GWd/t as the base continuous cycle case. This case had a fuel dwell time of 1248 full power days. The refuelling interval is given as :

$$Refuelling\ interval = \frac{Dwell\ time}{n},$$

where n is the number of channels in the core. For a 324 channel case such as Hartelepool, the interval is 3.85 days per channel. Hence, a channel is refuelled every 3.85 days to maintain the datum reactivity of the core. This is equivalent to 1.81 channels per week. If refuelling were to be performed every week, an enrichment increase would be needed to compensate for the missing refuelling.

If increased enrichment is considered in order to extend DI, the information in figure (3.9a) of the previous section may be used to study the extension of the refuelling interval. The table below shows this information for a desired doubling of refuelling interval:

Refuelling Interval (days)	Dwell Time (days)	Discharge Irradiation (GWd/t)	Enrichment (%U-235)
3.85	1248	17.48	2.15
7.70	2496	34.96	3.10

The table shows that, in order to refuel 1 channel per week, an enrichment of 3.10% is required, an icrease of 40 % over the base AGR case. The reactivity penalty is such that an investment in burnable poison is required. This reduced refuelling frequency is beneficial in power availibilty (if refuelling is carried out at reduced power as is the case presently), and in reduction of refuelling machine use; however, a penalty in enrichment and poison cost is incurred.

It is the function of the regulating rods in an AGR to preserve the radial flux distribution during refuelling of individual channels. Channel power will differ due to flux level and due to the age-factor. Channels at equilibrium cycle are nearly evenly distributed between zero age and those at DI and in normal operation rods are at a mean insertion of 50% (15% to 85% is their range). On refuelling a number of rods are inserted further to balance the local reactivity introduced by the feed fuel; other rods further away are adjusted slightly outwards also [9].

It is of interest to consider a hypothetical batch refuelled AGR, where refuelling is delayed substantially and where large portions of the core are refuelled. Obviously, an on-load scheme would not be realistic in this case due to the vast numbers of channels involved. For 3 batches for instance, refuelling would take place every 624 days. The reactivity penalty would be only half that of a single batch scheme (ie. $RP = 2(k_0 - 1)/(n + 1)$, where n is the number of batches). It is clear that as the the number of batches increase we approach continuous cycle refuelling and for the same feed enrichement, more batches means longer DI.

When refuelling is discretized, reactivity swings are introduced and figure (3.12c) shows 1,2 and 3 batch schemes for a similar DI. For a target DI, and a given reactivivity refuelling criterion k_f, the less batches are refuelled together; the higher the feed enrichment needs to be. The reactivity penalty is given by the difference between $k_0^i - k_0^{cc}$, where the second term is the continuous cycle feed k_{eff}. Relative to the DI of the continuous cycle base AGR, the obtainable batch DI is given by:

$$DI(i) = 0.85 \times (i/i+1) \times DI(c.c.)$$

Hence, for a 3 batch scheme of the same enrichment as the base AGR, and DI(c.c.) of 17.48 GWd/t , the achievable DI is about 11.14 GWd/t. This is quite low and in order to achieve a DI equal to DI(c.c.) the feed enrichment must be such that:

$$DI(3) = 0.85 \times (3/4) \times DI(c.c.) = 17.48$$

and therefore DI(c.c.) = 27.42 GWd/t

Using figure (3.9a) and the above value of DI(c.c.) , a feed enrichment of 2.65% is required compared to the base value of 2.15% - an enrichment increase of 23%. For this to be accomplished, burnable poison is required, if DI is to be extended without violating the maximum control range.

3.2.4 The Mixed-Spectrum AGR Variants

With the routine production of Plutonium from the burnup of current thermal reactors, it is possible to envisage a switch to Pu fuelled cores. Using Pu, neutronic efficiencies may be obtained as long as the neutron spectrum is sufficiently 'hard' (see figure (1.1)). If, a fast reactor is not the immediate aim, then the possibility exists of a so-called Hybrid or Mixed Spectrum Reactor (designated MSR). Here, zones with a 'hard' neutron spectrum are mixed with zones with a relatively thermalized spectrum.

When considering the possibility of using larger fuelled channel sizes in an AGR derivative, it may be noted that, as the fuelled channel became sufficiently large, the pins in the innermost part are in a fast spectrum regime. The pins nearer to the moderator fall into a thermalized regime. This suggests the possible use of Pu, at least in the innermost zone. Such a design was suggested by Askew et al [1] as a developement of current AGR. A change from the simple cluster block design of current AGR was proposed.

In order to keep refuelled units relatively small a hexagonal subassembly of 90 pins was the basic building block. A module was then made up of 7 fuelled subassemblies surrounded by 12 hexagonal subassemblies of pure moderator. The MSR unit module is shown below in figure (3.13).

Channel volume ratio of moderator to fuel is about 2, giving an effective moderator to fuel volume ratio of 3.5. Pin size is similar to that of a PWR, with a diameter of 11.0 mm. The can is stainless steel of 3.5 mm. thickness.

Calculations carried out for the MSR with WIMS-D4 treat a cylindrical model of the module with a fuel zone radius of 19.80 cm. and an outer moderator radius of 32.62 cm. The module was thus approximated by a large cluster of 630 of rods arrange in cylindrical rings. No account was taken of intervening wrapper material between hexagonal subassemblies. A case with the same mass of fuel as in an AGR was considered. The resulting MSR core had an equivalent diameter of 397.0 cm with a height, as in AGR, of 800.0 cm. The MSR core was hence required to have 37 modules arranged in 3 rings as shown in figure (3.13). It should be noted that the resulting core height to diameter ratio is quite high, at about 2, which is larger than usual practice values of around 0.5 . With the same fuel type, fuel mass, and power output, the MSR was assigned the same specific rating as the AGR : 14 MW/t. The core power density is, however, much higher at 15.25 MW/m^3 due to the smaller core diameter.

With such a large fuelled zone in the module it is inescapable that there will be a large difference in the relative power production of the inner rings of rods and

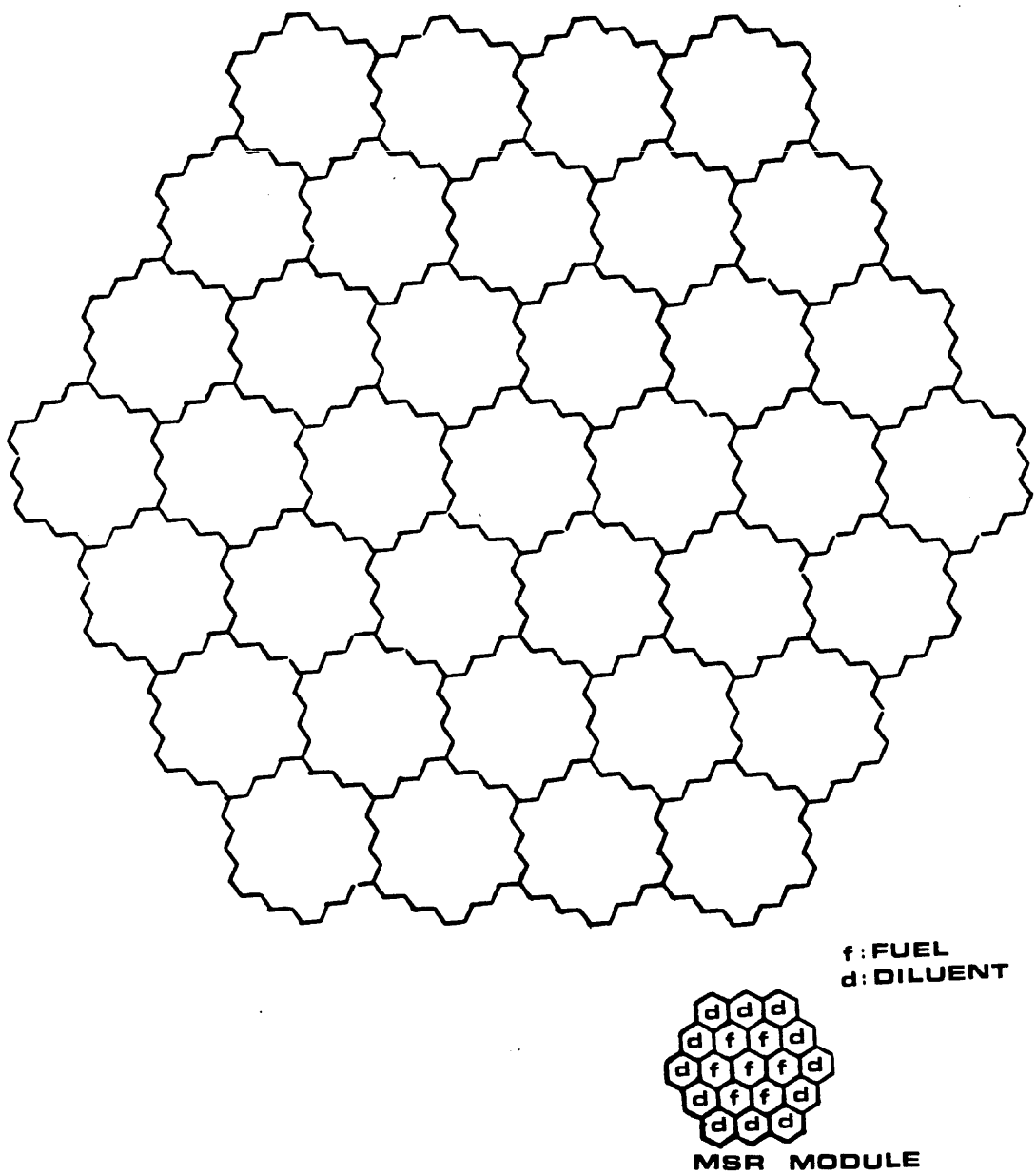

Figure 3.13. The MSR module and 3 ring core

those close to the moderator. In order to alleviate this problem, differential enrichment from ring to ring is attempted. The BOL reactivity and relative peaking factors were studied for a range of enrichment variation. To avoid the complexity of each ring having its own enrichment (as suggested by Askew), differential enrichment was only attempted on a subassembly level. The inner subassembly would have a high enrichment and the 6 outer ones would have one lower enrichment. This is approximated in the WIMS-D4 calculation by the first 5 rings having one enrichment and the next rings 6 to 14 having a lower enrichment.

The peaking factor of the MSR outer ring of rods is relatively high in all cases studied, being over 2.8, compared with the value of 1.10 of a standard AGR. It is apparent that adopting only 2 enrichment zones per module, with the attraction of minimum complexity and cost, may not be sufficient to flatten adequately the power peaking. A fully differential enrichment scheme was studied. A case was tested where the inner subassembly had an enrichment of 15% and the outer subassemblies differential enrichment as follows: 12,12,9,9,7,7,5,5,5 for rings 6 to 14 respectively in % Magnox Pu. The resulting peaking factor reduces to 2.62 still a high value. In addition to monitoring the power peaking,an enrichment search was carried out for a critical system at BOL and the results are shown in table (3.8).

Table (3.8): Reactivity and peaking factor of differentially enriched MSR module (%Magnox Pu enrichment) †

Inner zone Enrichment	Outer zone Enrichment	k_∞	k_{eff}	Outer ring peaking factor
7.0	7.0	1.1578	1.1044	3.200
7.0	5.0	1.0868	1.0346	3.095
9.0	5.0	1.0952	1.0428	3.044
12.0	5.0	1.1073	1.0548	2.969
15.0	5.0	-	-	-
18.0	5.0	1.1309	1.0782	2.822

†The MSR (and later alumina-MSR) case enrichments are identified heron by inner/outer figures (%Magnox Pu) for the inner and outer hexagons of a module (e.g. MSR 12/5).

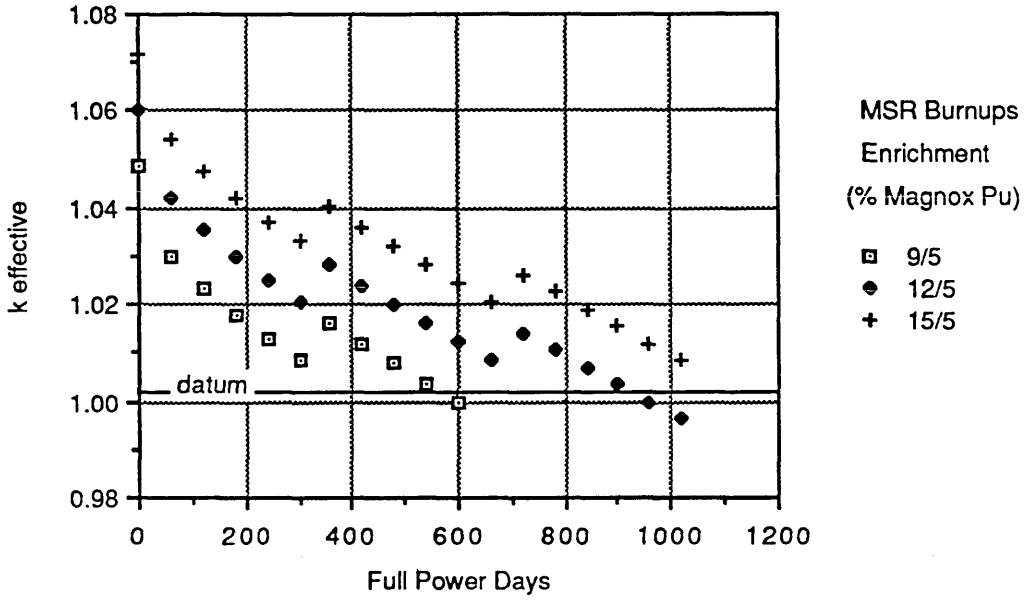

Figure 3.14. MSR burnup at several enrichments

If the power peaking problem is then taken to be solvable in the fashion discussed, burnup may next be studied to determine reactivity rundown of MSR cores. The core is one of relatively low neutron leakage with infinite and finite multiplication differing by some 5% (For an AGR this is about 3%). Thus while the core diameter is small, the large height and the large graphite zones radially account for the the low leakage.

From many trials it was found that MSR cores with 12 or 15 % inner and 5% outer enrichments gave reasonable burnups (discharge irradiations). Figure (3.14) shows the reactivity rundown of these (where the discontinuities are due to spectrum recalculations).

The discharge irradiation depends on whether a batch or continuous refuelling scheme is adopted. For continuous refuelling, the MSR design may not be

Table (3.9): Discharge irradiation of MSR for single batch burnup.

Case	Dwell Time (days)	DI (GWd/t)
9/5	540	7.56
12/5	900	12.60
15/5	1200	16.80
16.5/5	1440	20.16

appropriate, since numerous hexagonal subassemblies would have to be moved individually from each module. A more feasible design would be the integral block AGR derivative (to be discussed in section 3.2.5).

The discharge irradiations of the MSR variants for both refuelling methods are shown in table (3.9). With a datum k_{eff} of around 1.005 used, the discharge irradiation is given by $(2N/N + 1) \times DI_{datum}$, where N is the number of batchs and is infinite for continuous cycle.

In addition, graphite life must be a consideration if re-entrant cooling is not used or no separate cooling is provided for the moderator block. The integral block design (section 3.2.5) solves this by using integral blocks which allow the moderator and fuel to be replaced together.

The BOL nuclear indices for the MSR are compared with those of a standard AGR (at same zero burnup) and shown in table (3.10). The MSR conversion ratio, as well as α and ϵ, are greater than in an AGR core due to the 'harder' neutron spectrum resulting from higher enrichment requirement. This is further shown by the higher median energy of the the flux spectrum (E-median) for the innermost fuel ring of each of MSR and AGR.

Table (3.10): MSR and AGR nuclear indices (BOL).

	MSR(12/5)	AGR
k_∞	1.1073	1.1892
k_{eff}	1.0548	1.1573
ICR	0.8559	0.4931
α	0.4823	0.2115
ϵ	0.1412	0.050
E-median(inner fuel)	184 (15/5)	27

The flux spectrum in the centre fuel ring of the MSR has been compared to that of the AGR and these are shown in figure (3.17), in a following section, together with that of another concept (Alumina-MSR). A 'harder' spectrum than AGR, is once again apparent.

Regarding fissile fuel utilization, the MSR (12/5) is found to consume less and discharge more fissile material. At the same time it requires a larger fissile inventory for a continuous cycle discharge irradiation of some 30.0 GWd/t. Table (3.11) below compares MSR and AGR fuel utilization. Discharged fissile content of the MSR is 8.97% in the single inner subassembly and 2.78% in the 6 outer subassemblies of the fuel zone. This is compared to a figure of 1.21% discharged from the AGR. The percentages relate to total fissile content.

Table (3.11): Fissile fuel utilization (kg/GW-yr) of MSR's as compared to AGR.

	Feed	Discharge	Consumption	D/F(%)	C/F(%)
AGR	436	229	207	52.0	47.0
Cont. cycle:					
MSR 12/5	596	447	149	75.0	25.0
MSR 16.5/5	508	456	52	89.0	10.0
One Batch:					
MSR 16.5/5	1015	956	59	94.0	6.00

The MSR has a relatively high Pu inventory (feed figure in table 3.11), while consumption of fissile material is improved (reduced) below that of the standard AGR. There is, however, an optimization to be arrived at between increasing DI and reducing fissile feed loading. The more highly enriched MSR (16.5/5.0), although allowing an extended one batch DI, uses a higher fissile loading and a

resultant high discharge. Further insight into fissile usage is gained in table (3.12) where the Pu-239 inventory is shown for MSR and AGR.

Table (3.12): Pu-239 inventory change over life of MSR and AGR in kg per kg initial heavy metal.

	Feed	Primary Discharge	Bred Discharge	Primary D/F	DI
AGR	0.022	0.0058	0.0037	26.3	18.00(CC)
MSR(12/5)	0.0481	0.0377	0.0115	78.3	30.24(CC)
MSR(16.5/5)	0.0534	0.0347	0.0139	65.0	20.16(SB)
MSR(16.5/5)	0.0534	0.0239	0.0213	44.0	40.32(CC)
For the same last entry the following is for the outer fuel rings					
	0.0400	0.0110	0.0215	27.5	

It may be noted that the MSR seems not to utilize its fissile fuel well. Indeed, compared with the standard AGR, MSR's operating on a one batch cycle come to the end of their core lifes with fissile contents typically of more than 65% of feed. This figure is improved if we consider the outer hexagons of the module, at lower enrichment. If reasonable fissile usage is to found then a longer DI must be found for the MSR. On a continuous cycle refuelling scheme the 16.5/5.0 MSR would give 44.0% D/F on average and 27.5% for the outer rings, a much improved usage of primary fissile. At the same time up to 50% of initial feed fissile material is bred during fuel life, compared to a figure of 17% for AGR. The AGR bred Pu-239, however, is possibly not recoverable, since it is less than 0.7%, whereas MSR might provide a source of Pu recycle.

3.2.5 Alumina Moderated MSR

As an alternative to graphite, alumina moderation (more appropriately alumina dilution) was investigated. The motive behind this was to remove graphite/CO_2 reaction concerns and the possibility of graphite ignition. Additionally, a non-moderator such as alumina would significantly suppress the module flux peaking problem and allow the possibility of using a single enrichment. This may offset the cost of higher enrichment needed for such a core.

Table (3.13) : Alumina-MSR enrichment search (%Magnox Pu)

Inner enrichment	Outer enrichment	k_∞	k_{eff}	Outer ring peaking	Outer ring power fraction
15.0	9.0	0.9548	0.9238	1.726	23.00
12.0	12.0	-	1.0103	-	-
15.0	12.0	1.0545	1.0215	1.724	22.98
16.5	12.0	1.0643	1.0310	-	-
18.0	12.0	1.0715	1.0357	-	-
14.0	14.0	-	1.0736	1.729	23.00

For a system of sufficient reactivity, enrichments more typical of fast reactors are required. Table (3.13) shows reactivity and power peaking factors of the Alumina-MSR at a range of enrichments.

Illustrating the reduced flux peaking in the alumina-MSR module, figure (3.15) plots the radial group 1 (fast) and total flux across the module. The nearly flat total flux for the alumina-MSR is apparent. The difference between infinite and effective mutiplication factor is about 3%, which is less than that for the graphite MSR. Increased absorption in alumina for this design leads to reduced leakage, but of course reactivity is reduced.

The nuclear indices for the Alumina-MSR lattice of the same size (same gemetric buckling) as the MSR, and with enrichments selected to give burnups at least as good as for the MSR, are found to be as follows :

k_∞	1.0545
k_{eff}	1.0215
ICR	0.8515
α	0.4062
ϵ	0.1893
$E_{median}(innerfuel)$	201 keV

It is seen in figure (3.17) that the flux spectrum of the alumina-MSR is 'harder' than that of MSR due both to its higher average fuel enrichment and much reduced moderation effect of alumina. The initial conversion ratio is not very different from that of MSR and the capture to fission ratio is reduced somewhat. A comparison of the reactivity rundown of Alumina-MSR with MSR shows a shallow drop due to the much 'harder' spectrum. A longer discharge irrradiation and reduced control requirement may be possible. Figure (3.16) shows this fact.

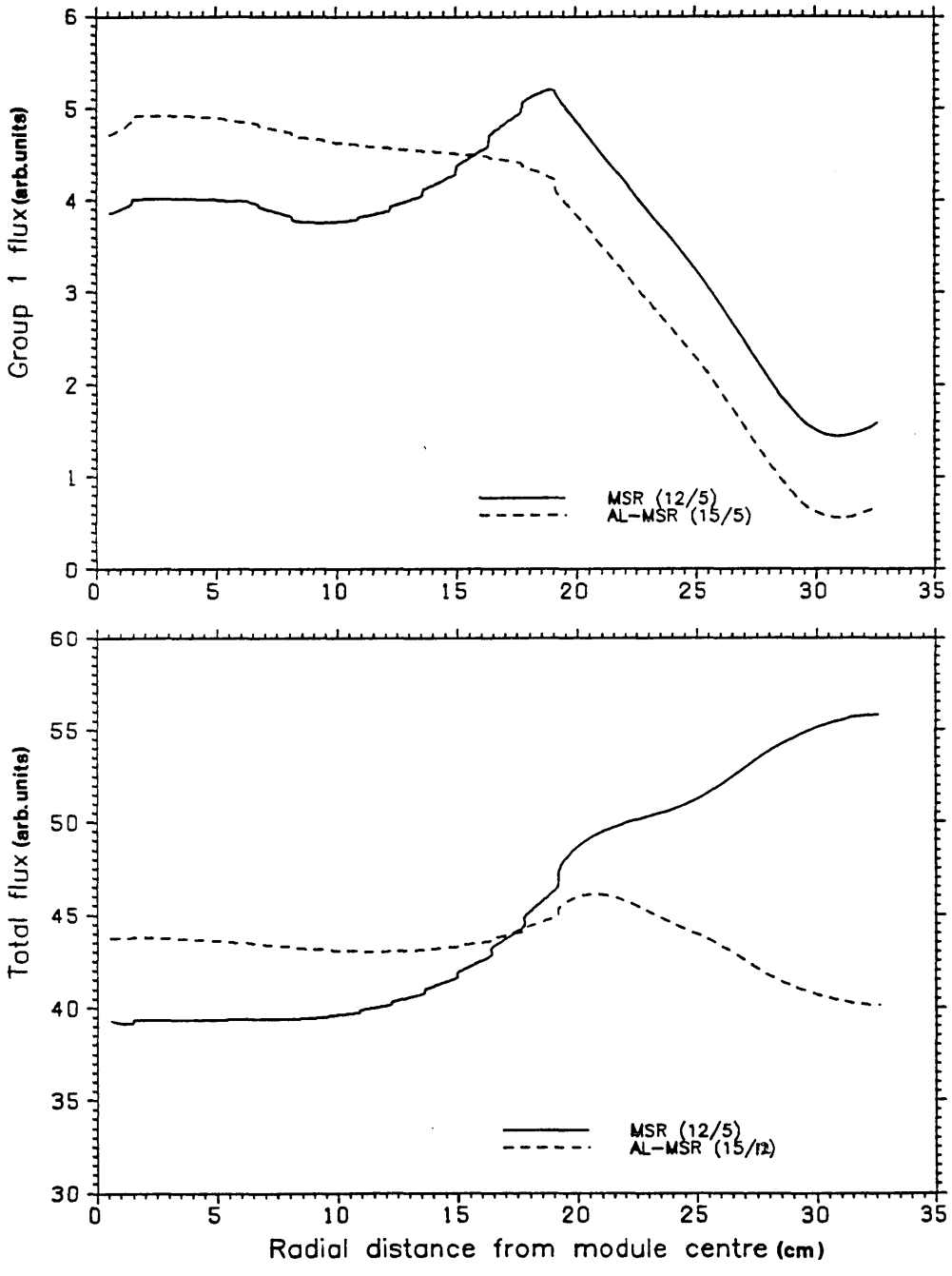

Figure 3.15. The radial flux profile across the MSR and alumina-MSR modules

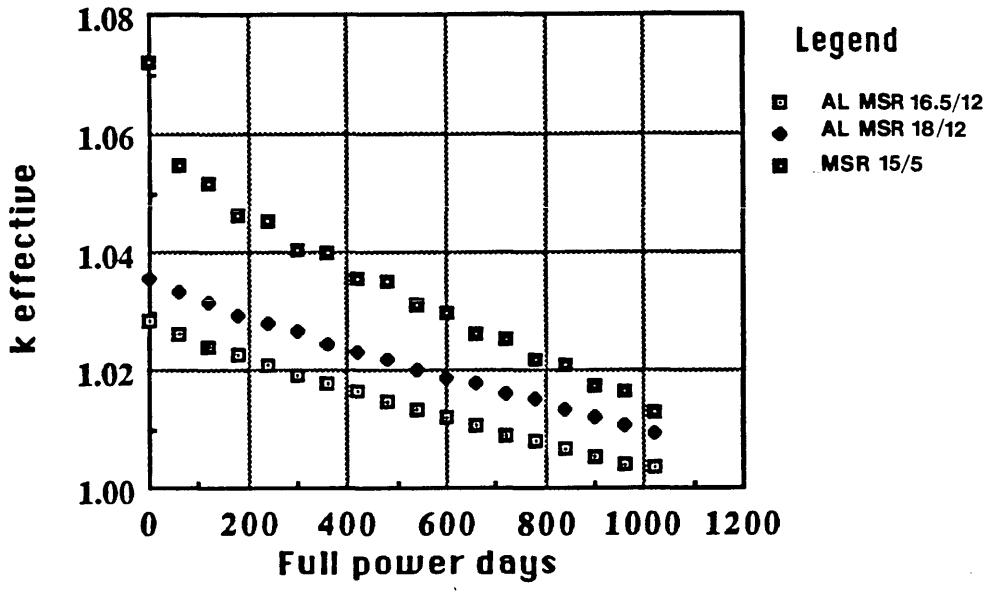

Figure 3.16. Alumina-MSR burnup compared to MSR

The fissile fuel usage in the Alumina-MSR, considering single batch refuelling is not as good as that of the graphite MSR. Values for the Alumina-MSR, at two inner subassembly enrichments, levels are given in table (3.14).

Table (3.14): Fissile fuel utilization of Alumina-MSR (Kg/GW-yr) using a single batch cycle.

Enrich.	Feed	Discharge	Consumption	C/F	D/F
16.5/12	2874	2822	53	0.02	0.98
18/12	2229	1876	352	0.16	0.84
15/12	1060	973	87	0.08	0.91

The high fissile enrichment required together with the relatively low DI of these batch cases cause the feed figures to be high. However, cases with a relatively fast spectrum have a correspondingly high fissile discharge. Continuous refuelling can be ruled out inpractice due to the large number of subassemblies in the fuel zone.

It is convenient at this point to study the coefficients of reactivity for both the MSR and the Alumina-MSR. It is possible to see in table (3.15) that the fuel

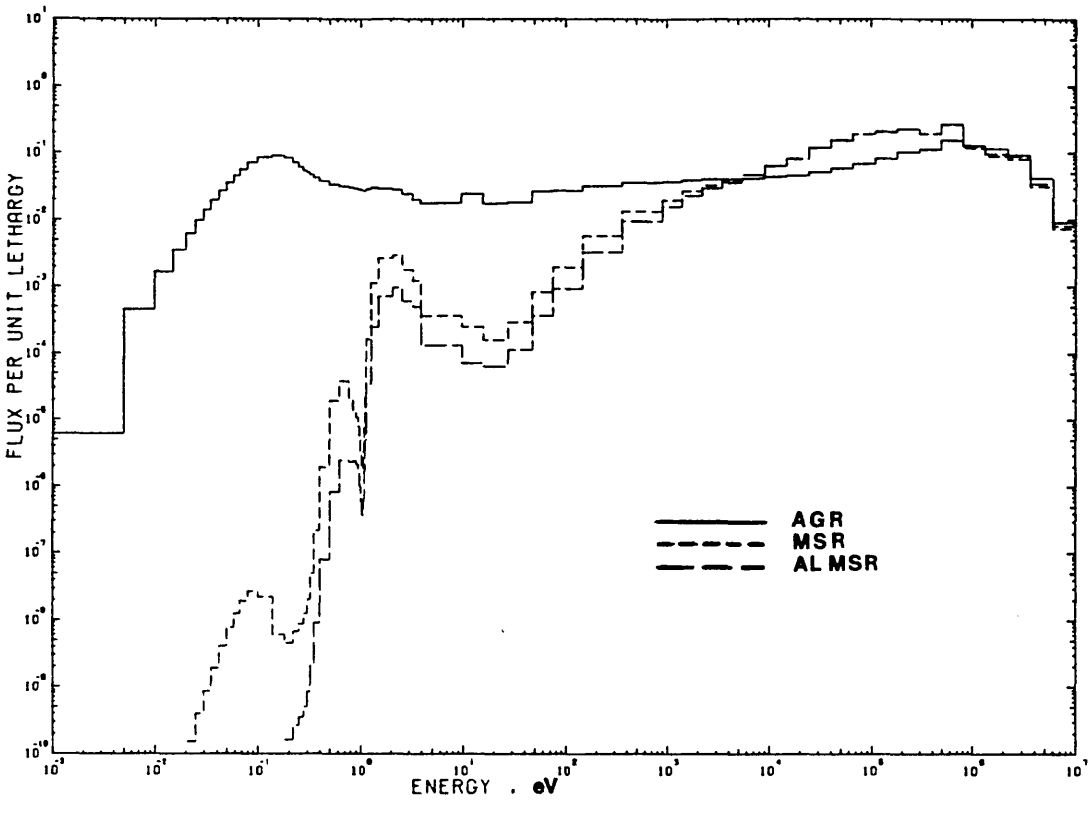

Figure 3.17. The flux spectrum of the Alumina-MSR compared to those of MSR and AGR

coefficients are always negative for both systems. The moderator coefficient of the MSR seems to be less positive than that of the alumina MSR. In fact the MSR has a negative moderator coefficient at BOL. The coefficients are listed in table (3.15) below; the overall coefficients are all negative.

Table (3.15): Temperature coefficients of reactivity for fuel and moderator of MSR and Al-MSR at different temperatures.

		Fuel Coefficient	Moderator Coefficient	Overall Coefficient
I.	MSR(15/5)			
	Tf 800-1000			
	Tm 450-650	-0.0224	-0.0098	-0.0322
BOL				
	Tf 1000-1200			
	Tm 650-850	-0.0235	-0.0160	-0.0395
	Tf 800-1000			
	Tm 450-650	-0.0197	+0.0010	-0.0187
EOL				
	Tf 1000-1200			
	Tm 650-850	-0.0037	-0.0164	-0.0201
II.	Al-MSR(16.5/12)			
	Tf 800-1000	-0.0152	+0.0052	-0.0100
	Tm 450-650			
BOL				
	Tf 1000-1200	-0.0164	+0.0037	-0.0126
	Tm 650-850			
	Tf 800-1000	-0.0143	+0.0049	-0.0094
	Tm 450-650			
EOL				
	Tf 1000-1200	-0.0148	+0.0048	-0.0099
	Tm 650-850			

3.2.6 The Prismatic Block AGR Variant

This concept was outlined by Askew et al [5] as a possible development of the AGR; the aim was to increase power output and to give the possibility of replacing moderator together with the fuel inorder to minimize material damage. It is appropriate to close this chapter with the presentation of this concept since progress towards this is much simpler than towards other AGR variants.

In this Integral Block AGR (i.e. IBAGR) design the channel size was kept the same as that of AGR, but fuel pins were reduced in diameter to limit centre temperatures. Additionally, the fuel mass per channel was retained at the AGR value and a 60 pin cluster thus emerges. Features of the IBAGR are given in Table

(3.16) together with data for the concept used by Askew [5] as well as for the AGR (both as defined here and as quoted in reference 5).

A small increase in gas pressure was envisaged, from the AGR value of 40 bars, to about 47 bars. Together with the smaller clusters (i.e. more channels) this leads to a near doubling of power output to some 3100 MW(th). The gas velocity and core size are kept at the standard AGR values. The power density is, as a result of the above changes, increased to near double that of AGR, giving an increased graphite oxidation rate. This lead to the adoption of this integral fuel/moderator block design.

Table (3.16): Present model prismatic AGR specifications compared with AGR and reference [5] model.

	IBAGR	IBAGR[Askew]	AGR	AGR [design]
Pins/cluster	60	60	36	36
Fuel pin radius(cm)	0.455		0.724	
Blocks in core	564	564	332	332
Channel radius(cm)	8.89	9.5	8.89	9.5
Cluster cell outer radius(cm)	18.90	18.0	22.17	23.0
Core Height (m)	8.30	8.00	8.30	8.00
Core Diameter(m)	9.10	9.40	9.10	9.40
Fuel mass in Core (tonne)	185.4	178.8	165.7	129.0
V_g/V_f	22.3	18.8	21.9	28.8
Ratio of graphite to fuel mass	3.75	3.15	3.66	4.82
Average Fuel Rating (GW/t)	18.95	19.75	13.20	14.0

The prismatic AGR used in these calculations differs slightly in design detail from the concept of Askew [5]. A basic difference is the greater graphite to fuel ratio, due to the use by Askew of sizes typical of the hexagonal bricks of the Fort St. Vrain HTR. The present study, setting aside the practical aspects of using established HTR dimensions, attempted to retain a large graphite volume in going from AGR to IBAGR. The nuclear performance parameters appeared to be only slightly sensitive to small variations in graphite block volume - i.e. a smaller block radius of 18 cm. gave little change in BOL k_{eff} and in core reactivity

lifetime. Interestingly, the IBAGR model adopted in this work differs from the reference case in having about the same V_g/V_f as the standard AGR, while the reference model gives a reduced value. This may be judged to be, based on AGR experience, an advantage with regards to transient safety.

The burnup behaviour of the IBAGR was studied with various enrichments; two selected cases are shown in Table (3.17).

Table (3.17): Prismatic AGR (IBAGR) enrichment and burnup.

Enrichment (%U-235)	Dwell Time (days)	D.I.(1 batch) (GWd/t)	k_{eff} (BOL) (1 batch)	k_{eff} (3 batch) (same DI)
2.9	1065	20.00 (3 yrs)	1.2578	1.128
4.0	1610	30.50 (4.5 yrs)	1.3348	1.167
For a reduced graphite outer radius to 18 cm (V_g/V_f of 18.8)				
4.0	1450	.....(4.0 yrs)	1.2886	-

If continuous cycle refuelling were adopted then discharge irradiations of about twice the single batch values would be obtained. Although this is a substantial improvement, the high power densities rule out these long dwell times, due to graphite irradiation, and batch refuelling must be used. A single batch cycle may not be reasonable since it involves too large a BOL excess reactivity: control range (see above k_{eff}'s). If a 3 batch refuelling scheme were adopted then, for the 2.9% and 4.0% cases, batch cycle lengths of approximately 1 year and 1.5 years respectively would be obtained and lead to discharge irradiations of 30.5 and 45.7 GWd/t respectively (according to $DI_n = DI_1(2n/n+1)$, where n=3). With a batch life of 1.5 years, the batch k_{eff} (k_n) for the 2.9% case, becomes 1.128; while for the 4.0% case k_n becomes 1.167. These are obtained according to $(k_1 - 1/T) = (k_n - 1/t_n)$, where k_1 is the batch initial k_{eff}, T is the single batch burnup, and t_n is the cycle length for the batch scheme.

For the 2.9% enrichment case the fuel usage is given in table (3.18), for both the one batch and continuous cycle schemes.

Table (3.18): Fissile usage for 2.9% IBAGR - kg/GW-yr.

	One Batch	Continuous-Cycle
Feed	518	269
Discharge	286	82
Consumption	232	187
Total Fissile: Dis/Feed (%)	55	30

The fissile usage in the case of continuous cycle gives a reduction in feed requirement relative to the standard AGR (see table 3.11). The discharged fissile material is low, indicating good usage (consumption of feed is 70% whereas in the case of AGR it was 47%). The discharged fissile enrichment is . For a 1 batch case, disregarding limitations of control, the IBAGR fissile usage is about the same as that of the standard AGR.

The conversion ratio of the IBAGR as a function of irradiation time is given in table (3.19) where it is compared to the CR of of a standard AGR at several possible enrichments.

Table (3.19): Conversion ratio vs burnup of 2.9% IBAGR and AGR.

	time, days			
	0	360	720	1080
AGR :				
2.2%	0.516	0.542	0.587	0.641
2.9%	0.438	0.467	0.505	0.548
4.0%	0.367	0.448	0.529	-
IBAGR	0.437	0.483	0.540	0.606

The IBAGR at 2.9% enrichment has an increase in CR versus time greater than for the standard AGR of the same enrichment. It appears that the 'harder' spectrum gives more fertile conversion.

3.3 CONCLUSIONS

The gas-cooled family, exemplified by the AGR, has not yet reached the limit of its development. Furthur development could be towards longer burnups, higher availability, and general simplification of design. Higher costs for enrichment and

excessive burnable poison requirement and cost impose a limit on burnup achievable by present AGR designs. Higher availabilty would be possible if the design plan for full power, on-load refuelling could be achieved. The major argument put against AGR today, that it is a difficult system to construct, is being challenged as the latest AGRs are being constructed to time. The design itself, although in need of some simplification, is robust and cannot be held to blame for a myriad of problems that have arisen during construction of the older AGRs. The technical problems have been manageable, and the latest AGR designs are based on experience gained with the AGRs which have performed best.

New AGR variants, aiming for 'harder' neutron spectra may be contemplated. This may be achieved by adopting larger fuelled channels. A mixed spectrum reactor (MSR) design, or hybrid as it may be called, is possible; here the fuel zone is sufficiently large so that the central rods are in a very 'hard' spectrum, while those next to the moderator are in a thermalized spectrum. The use of mixed plutonium oxide fuel in the inner part of the fuel zone becomes efficient, as a result. This system features a low moderator to fuel ratio and a moderate average enrichment leading to enhanced conversion ratios and longer burnups. An increased flux peaking factor across the large fuelled zone may be solved by adopting differential enrichment. Two enrichments are feasible for each fuelled zone of an MSR module, without further differential enrichment, however the peaking factor is still relatively high.

A mixed spectrum reactor, using alumina in place of graphite for the 'moderator' hexagonal blocks, shows a significant reduction in peaking factor. This, however, was accomplished through the non-moderating nature of alumina and the generally 'harder' spectrum created. The increased parasitic absorption in alumina neccesitates the use of higher enrichment if reasonable burnups are to be achieved.

With less ambitious development of AGR design being simpler, the problem of graphite damage due to higher power density and longer burnups requirements, is alleviated by the use of an integral block (or prismatic) design of AGR (named

IBAGR). The design is based on HTR and is a direct development of AGR, retaining the same fuel channel size but using smaller fuel rods and a smaller moderator to fuel ratio. The general features of this design are higher fuel rating and conversion ratio giving longer burnups, and a doubling of reactor power, accomplished with a small increase in the coolant pressure.

REFERENCES

1. Askew J. R. , Griggs M. A. , and Hutton J. L. , *Devolpement potential of the AGR*, Gas Cooled Reactors Today, BNES, London, 1982

2. Pexton A. F. , *An up-to-date assessment of AGR-and some comparisons with PWR-part 1*, CME, p. 23, january 1986

3. Massimo L. , *Physics of high-temperature reactors*, P. 88, Pergamon Press, 1976

4. Day J. W. , and Vaughan R. I. , *Performance aspects of the fuel cycle in a mark II gas cooled reactor*, JBNES, p. 155, vol. 11, 1972

5. Askew J. R. , Thorpe G. , *Possible developements from the AGR*, Nucl. Energy, Vol. 25, No. 1, pp. 41-46, feb. 1986

6. Smith P. R. , *In-core reactor fuel management*, Queen Mary College Lecture Notes, QMC ET6032

7. Tyror J. G. , and Fayers F. J. , *General considerations in fuel management for thermal reactors*, JBNES, p. 25, vol. 11, 1972

8. Dickinson N. , Ghilardotti G. , and Haubert P. , *Fuel cycles for the HTR*, Symposium on Advanced and High Temperature Gas-Cooled Reactors, p. 742, Julich, 1968.

9. Goode A. B. , *The fuel management of AGRs*, Nucl. Energy, Vol. 23, No. 3, P. 149-160, 1984

Additional references:

Cutts B. , *A study of fuel cycles and fuel cycle problems for advanced gas-cooled graphite moderated reactors*, Proc. 3rd. Intl. Conf. on Peacefull Uses of Atomic Energy, U. N. , Vol. 3, p. 364 , 1964

Buckler A. N. , *Methods for studying fuel management in advanced gas cooled reactors*, Jnl. Br. Nucl. Energy Soc. , vol. 11, no. 2, p. , 1972

Stewart H. B. , Richard C. L. , and Melese G. B. , *Gas-cooled reactor technology*, Advances in Nuclear Science & Technology, Vol. 4, p. , 1968

CHAPTER 4.

THE GAS-COOLED FAST REACTOR (GCFR)

4.1 BACKGROUND

There is no doubt that the continued use of low-conversion thermal reactors is a waste of nuclear fuel resources. If nuclear power is to be a long term contributor to energy production then breeders or high conversion reactors must be the next step, although when this step is adopted will depend upon economic factors.

As an alternative to LMFBR, the Gas-Cooled Fast Reactor (GCFR) has been studied for over two decades but as yet no demonstration plant has been constructed. General Atomics was first to complete several studies on GCFR feasibility starting in 1962. A significant milestone was the setting up, in the late 1960's of the European Gas-Breeder Reactor Association (*GBRA*) in order to carry out commercial size GCFR studies.

As a fast reactor, the GCFR naturally has some similarities with the LMFBR. The two designs do, however, differ in many important aspects, and it was to alleviate some concerns associated with LMFBR that GCFR designs were considered. Fuel rating is a basic point of difference. In GCFR designs it tends to be lower than LMFBR because of the inferior thermal qualities of the gas coolant. This implies a higher fuel inventory for the same output and a longer doubling time than might be expected from the high breeding ratio. Features of the GCFR design, described in section 4.3 tend to alleviate this problem.

Due to the maintained momentum for LMFBR many demonstration plants have been built. In the case of GCFR, its position in the 'shadow' of LMFBR, the consequent lack of funds, and the then (late 1960's) untested nature of PCPV type gas cooled designs, all explain the untried status of GCFR designs.

4.2 FEATURES OF GCFR VERSUS LMFBR

4.2.1 Advantages

In this section a helium cooled GCFR is discussed since this coolant was the initial choice due to its good thermal properties. Most GCFR designs employ helium cooling including the GBRA's GBR-4 design [1].

A major advantage of gas cooling is the minimal neutron absorbtion and moderation in the coolant, compared with sodium. This results in more neutrons being available for fission and for breeding in the harder neutron spectrum. This low coolant neutron absorbtion and scattering yields a system relatively insensitive to lattice size, giving the possibility of more open lattices and the avoidance of blockages in accident situations. Enhanced leakage does however need to be borne in mind.

Helium is chemically inert and this removes any worry of material compatibility, for example the potential coolant reaction with water or moist air, a severe worry in LMFBR, is overcome by gas cooling. Additionally, there is no need for an intermediate heat exchanger (as in LMFBR); which must give a significant saving in capital cost. Most gas coolants remain gaseous over all temperatures of significance; this removes the possibility of abrupt changes in the heat removal capacity of the coolant due to phase change. An additional advantage is that the small inertia of the coolant means possible rapid startup to the emergency circulation in an accident situation. In the event of loss of coolant, the gas-breeder design ensures, unlike LMFBR, little addition of reactivity to the core. The transparency of the gas coolant is an added advantage that fascilitates possible visual inspection of the reactor.

The above are all inherent safety features. In addition there are significant engineered safety features. A feature characteristic of gas cooled system is the use of a Prestressed Concrete Pressure Vessel (*PCPV*). A PCPV, due to structure redundancy and small penetration sizes, has a significant role in slowing down the depressurization rate in the event of a possible primary break. Natural circulation is guaranteed, in the event of forced circulation loss by the adoption of upward flow. A separate cooling loop is available to remove shutdown heat in the event of a depressurization accident. This forced cooling loop; the auxiliary core cooling sytem (*ACCS*) runs on independent deisel motors if required.

4.2.2 Drawbacks

The GCFR does have some undesirable features. These, however, are in no way any worse than, and should be less severe than aspects of other reactor systems. Poor heat transfer to the coolant implies high fuel temperatures and necessary limits on the fuel rating. This is an important consideration in accident situations, such as depressurization, since the clad temperature must not be allowed to rise too much in the quickly deteriorating heat transfer regime. The low heat transfer capacity of gas brings about the need for high pressure operation. This in turn enhances the potential severity of a depressurization event. It is claimed, however, that with CO_2 cooling instead of helium, more heat can be removed in a transient situation involving loss of forced circulation and natural circulation in the fully pressurized primary loop (see reference 2).

Due to the 'harder' core neutron spectrum of the GCFR, the vital Doppler coefficient of reactivity is somewhat lower than in LMFBR. Several prescriptions to alleviate this have been proposed in this work.

4.3 THE EXISTING TECHNOLOGY GAS BREEDER REACTOR (ETGBR)

General Description of ETGBR

The Existing Technology Gas Breeder Reactor (ETGBR) has been proposed as a possible way forward for gas cooled reactor technology. The concept has arisen from considerations of competing economic and safety issues (see for example references [2] and [3]). It is based on the adaptation of AGR technology to a fast reactor, with the minimum of associated investment in research and developement through, together with other aspects, the use of components, construction and operational technologies typified by AGR stations. Fuel element technology is related directly to that of LMFBR. A low rated, high inventory core is proposed, which would be appropriate where a large thermal reactor programme and a small proportion of capactiy represented by fast reactors is the case.

The lower fuel rating permits lower pressure operation compared with say GBR-4. The heat transfer characteristics of CO_2 also permit lower pressure operation than in helium cooled designs.

Compared with AGR, removal of the need for moderator cooling means that re-entrant flow is eliminated as is the need for coolant chemistry control. As in other fast reactors, the absence of moderator leads to a smaller core size. Figure (4.1) compares the ETGBR with an AGR of similar power and technology.

A relaxation of the AGR outlet temperature of $645°C$ was considered prudent due to the potentially higher damage rates in the core. An outlet temperature of $525°C$ was selected and this in turn allows the use of one material in the boiler. The core design of the ETGBR benefits from LMFBR designs and uses a similar hexagonal fuel subassembly. Fuel pins contain mixed oxide of typically 20% PuO_2. The initial choice of cladding is SS316 with later progress to 20/25 TiN or PE16 envisaged. The core of ETGBR as studied in the present work includes 397 core subassemblies each holding 168 fuel rods. The reduction in subassembly size chosen represents a step towards improved safety especially in anticipation of the so-called 'diluted' ETGBR designs to be introduced in chapter 5. Table (4.1) shows the main design features. Of interest is the large pin spacing which would tend to minimise the possibility of accidental flow blockage. It is already been noted that the ETGBR neutronics are not expected to be sensitive to pin spacing due to the low density of the coolant.

A significant difference between LMFBR and GCFR is the external pressure on the pin due to the GCFR gas coolant. With this load and without support for the clad from fuel there would be danger of creep collapse during operation. Sealed pin pre-pressurization is the preferred solution to this problem and pressurization with helium provides a predetermined net external pressure over life [4]. In contrast, in LMFBR there is significant internal pressure arising during irradiation. A roughened clad surface is used to enhance heat transfer (as in AGR).

To summarise; the ETGBR pin design is based on: (a) pre- pressurization to avoid creep collapse or the need for fuel support, (b) a sized plenum to accomodate

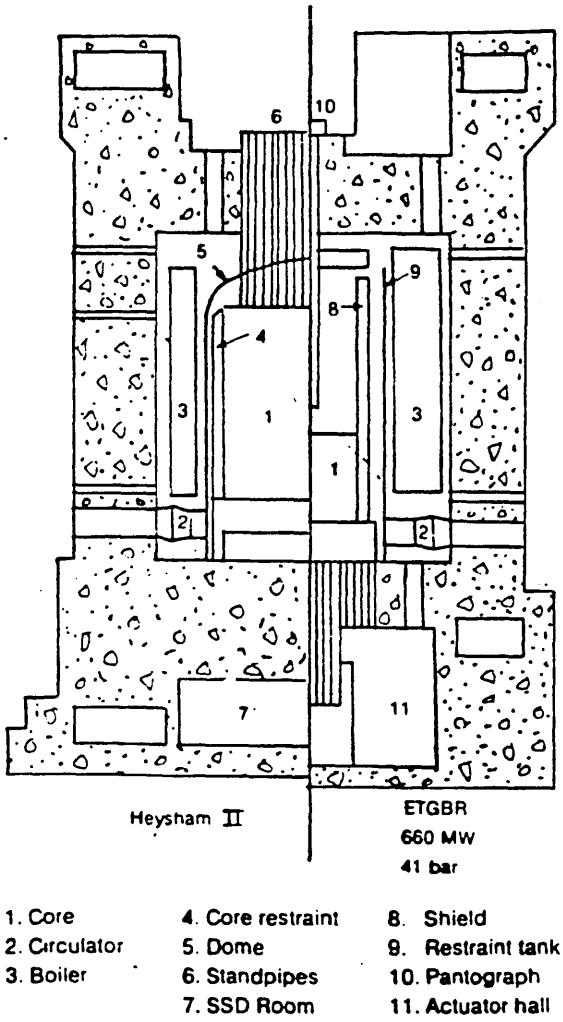

Figure 4.1. Comparison of ETGBR and AGR reactor elevations (from Kemmish, reference 3)

additional pressure due to fission gas and (c) a suitable clad thickness to give acceptable clad stress in the event of depressurization.

To take advantage of its high neutron leakage, the core in the ETGBR design is surrounded by radial breeder subassemblies containing larger natural uranium pins. Axially the fuel pins contain natural uranium, at the top and bottom, forming the axial breeders.

In common with other fast reactor designs, the ETGBR can operate over long burnups with little excess reactivity present at any time. This feature is due to the high conversion ratio of the core. It follows that control investment need not be as high as is the case in thermal reactors. A batch refuelling scheme would be used since the drop in reactivity is small and continuous refuelling is not warranted. The question of single-batch or multi-batch refuelling is still open. It is possible that a 2 batch fuel residence would be a reasonable compromise, offering minimum fuel disturbance and refuelling expenditure, while allowing a reasonable time before examination of the reactor, in its cold shutdown state, becomes necessary.

Table (4.1): ETGBR Design Features.

Fuel pin diameter(mm)	7.00
Clad thickness(mm)	0.35
Core length(m)	1.40
Assembly across flats(cm.)	15.74
Pitch/Diameter Ratio	1.49
Axial breeder height(m)	0.60
Plenum length(m)	0.70
No of subassemblies:	
zone C1	216
zone C2	180
zone RB	150
zone RR	84(or 174)
Enrichments(%Pu)	
zone C1	15.0
zone C2	21.0
Specific inventory(t/GWe)	7.0
Inlet temperature($^{\circ}C$)	252
Outlet temperature($^{\circ}C$)	525
Efficiency(%)	38.0
coolant pressure(bar)	42.0
Reactor power(MWh)	1680

4.4 ETGBR WHOLE REACTOR CALCULATIONS

4.4.1 Introduction to Reactor Calculations

An ETGBR variant of only one core zone can be studied using a 'lattice-cell' WIMS-D4 calculation. A fixed geometric bucklings is used to account for gross leakage. It is, however, not easy to represent a full reactor if there are to be several zones, including blankets, as in the case of the ETGBR. It is then neccesary to use a 2 or 3 dimensional model. The WIMS-E code incorporates approximate techniques in the form of the WSNAP diffusion theory module.

WIMS-D4 is extremely convenient to use for burnup and inventory studies in the leakage corrected lattice model. This is utilized in Chapter 5 for the standard ETGBR and its diluted variants. It suffices to say here that it may be desirable to study a one zone unreflected ETGBR (bare core) or else it becomes neccesary to use WIMS-E. A special design worth studying is a heterogeneous one zone ETGBR. This could be modelled using WIMS-D4 with its Multi-Cell mode in the first instance while a full reactor model could be performed later with WIMS-E. This is performed in Chapter 6.

4.4.2 Geometry and Specifications of Reflected Full Reactor

The detailed geometric features of the ETGBR are given in Table (4.2). It is probably coincidental, although possibly advantageous, that the 169 pin, 7.0 mm fuel rod diameter design, gives about the same fuel mass per subassembly as in a AGR channel. The ETGBR subassembly, with an across flats spacing (AF) of 15.74 cm., is significantly smaller than that of GBR-4 (21.5 cm. AF), and closer to LMFBR subassembly size (14.2 cm. AF). The smaller subassembly, it has already been suggested, may be advantageous with respect to transient safety. This is especially true in anticipation of diluted ETGBR designs incorporating ceramic block subassemblies that will be introduced in chapter 5. The ETGBR subassembly is shown in figure (4.2).

The standard axial size of the ETGBR core, blanket and reflector zones were taken from other GCFR designs (see AEEW-M1669 reference 5 for example). Radially, it was decided to attempt to match, as far as possible, the fuel masses

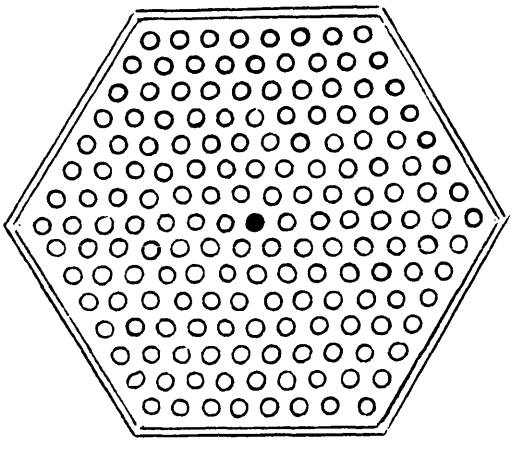

Figure 4.2. The standard 169 pin ETGBR subassembly

to those in reference 5. While this has been achieved, the radial dimensions of the reactor are as a result neccesarily altered from the reference values. Figure (4.3) shows the relative layouts of the two designs in R-Z geometry and shows that the present model a single AB zone.

Table (4.2): ETGBR geometrical specifications.

Zone	Number of subassemblies	Rings of rods	Zone radius (cm.)	Zone volume (cm^3)	U+Pu mass (tonne)
C1	217	1 to 8	121.73	46550	18.44
C2	180	9,10,11	164.65	38615	15.27
RB	150	12,13	193.26	32175	71.00
R	174	14,15	221.89	39900	-

The R-Z model has already been shown in figure (4.3b) with zone dimensions, while for the Hexagonal-Z model, the map of of the centre-line reactor is given in figure (4.4).

The ETGBR design used incorporates in the subassembly 164 fuel rods while the remaining 5 are taken to be steel 'hanger' rods. The subassembly fuel volume fraction is then 0.294 and the steel fraction 0.1707. With 7 control rod vacancies taken into account in zone C1, the fuel volume fraction is 0.280.

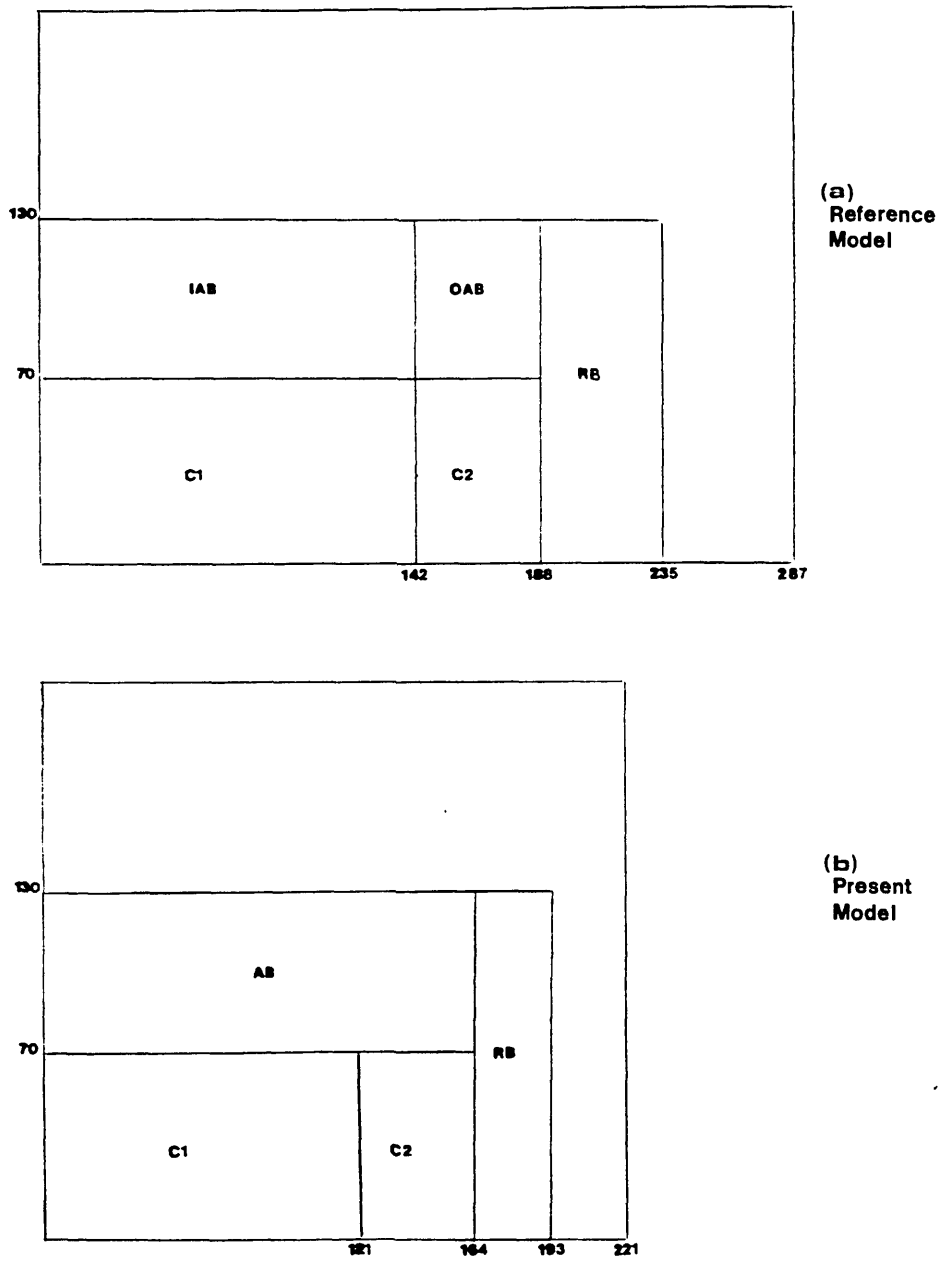

Figure 4.3. Comparison of the relative sizes of the reference and implemented R-Z models of the ETGBR

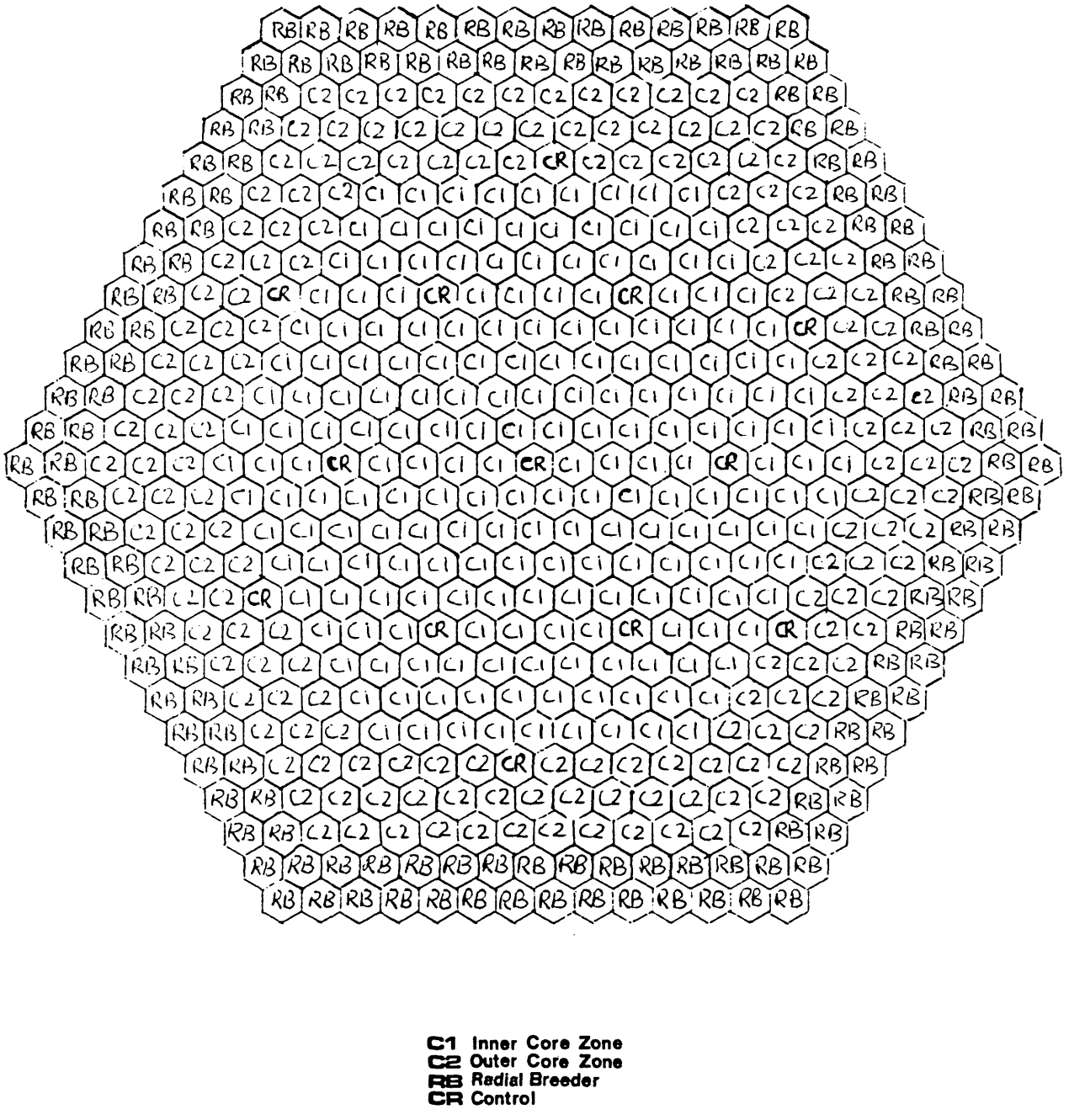

Figure 4.4. The centreline hexagonal map of the ETGBR

If the ETGBR studied here is compared with the design given by MacBean [5] some differences in dimensions and volume fractions are seen. This is in spite of the zone fuel masses being in reasonable agreement, as shown in table (4.3).

Table (4.3): Fuel masses comparison of present and reference ETGBR models.

	Fuel Masses,tonne(U+Pu)			
Model	Zone C1	Zone C2	Zone RB	Zone AB
ETGBR-IC	18.44	15.27	71.00	28.88
AEEW-M1669	17.49	14.31	69.96	29.15

4.4.3 Establishment of an ETGBR calculational procedure

Background

It has already been shown that predictions with WIMS-E agree reasonably well with those using COSMOS, for the freshly-fuelled, begining of life, GCFR design given in reference 5. Reactivity and reactions rates were shown to be comparable. Burnup prediction, however, produced a greater difference with WIMS-E seems to be predicting a somewhat longer life.

Local heterogeneity is not important in fast reactors; for this reason only energy self-shielding is normally treated in fast reactor physics codes. While the WIMS spatial self-shielding treatment may be regarded as a bonus, energy self-shielding treatment is deficient since resonances above about 10KeV are not represented explicitly and the energy group structure not fine enough. However, in intermediate spectrum systems considered in the thesis, the spatial self-shielding treatment will clearly be important. Due to the lack of importance of heterogeneity, a full reactor calculation in 2 or 3 dimensions can be carried out using diffusion theory (using WSNAP).

The method adopted in modelling ETGBR is one where lattice data is generated separately and is then used in the whole reactor calculation. The whole

reactor may be modelled, as in chapter 2, either with a WIMS-D4 cell calculation with a leakage correction, or with an explicit 2 or 3 dimensional diffusion calculation in R-Z or Hex-Z geometry using WIMS-E.

Calculation Route

Because of its simplicity and convenience, WIMS-D4 may be used to generate the lattice data in either pincell or cluster geometry. It has been shown that a smeared ring collision probability model of the cluster is adequate a 2 dimensional R-θ (PIJ) option, which accounts explicitly for the rods in the cluster is not neccesary. In cluster geometry WIMS-D4 is particularly simple to use [6]. Should this be required, a WIMS-E module WFORTE is provided to translate WIMS-D4 data into WIMS-E format for subsequent use. The overall WIMS-D4/WIMS-E calculational route is basically the same as that further expanded on later in chapter 5.

The wholly WIMS-E route is similar to that given in chapter 2 for the reference ETGBR calculation. The smearing volume fraction correction FACTORS in this section are those neccesary to convert the pin-cell values to those of the defined subassembly. The FACTORS are given in the table below.

Component	Pin-cell Volume fractions	FACTORS	Cluster Volume fractions
Fuel	0.352	0.835	0.294
Clad	0.074	2.309	0.171
Coolant	0.574	0.932	0.535

Using typical ETGBR materials and geometries (such as given in table (4.2)), a calculation can be performed for an ETGBR design made up of homogeneous zones. It is because of fast reactor insensitivity to local heterogeneity that the cluster can be modelled as a pin-cell, with subsequent smearing of the pin-cell including corrections to the fuel, can and coolant constituents. These correction factors force the pin-cell volume fractions to correspond with those of the cluster (ETGBR subassembly).

The Calculation

Both routes outlined above were used to study the ETGBR as specified in previous sections, in order to explore important sensitivities. Items likely to affect the results are discussed in the following pages and may be listed as follows:

1. Input data inconsistensy : enrichment or fuel volume fractions.
2. Data generation in infinite or leakage spectrum.
3. Dancoff factors for non-moderated cluster lattice.
4. Mesh or group structure.
5. Reflector data.
6. Fuel rating for burnup.
7. Nuclide Resonance tabulation in WIMS library.
8. Leakage treatment and spectrum recalculation frequency influence on burnup.

Reactivity and Reactivity-lifetime

Using the cluster design, fuel volume fractions, and calculational routes having been explained, ETGBR reactivity and reactivity-lifetime were studied taking into accont the above effects. Enrichments established using COSMOS for a GCFR were taken as a starting point, namely 15.17 and 21.41% Magnox Pu in core zones 1 and 2 respectively. The plutonium composition was typical of discharged Magnox reactor fuel and is given as: 80% Pu-239, 16.9% Pu-240, 2.7% Pu-241, and 0.4% Pu-242. This gives a core average enrichment of 17.99% Magnox Pu, which is roughly equivalent to 14.87% Fissile Pu (12.55%inner/17.70%outer)

Burnup of the 4 reactor zones was performed using both a WIMS-D4/WIMS-E method and a wholly WIMS-E method as already discussed. Power rating of the different zones were obtained using a single BOL reaction rate edit, for the whole reactor, given an inner core zone (C1) rating of 47.8 MW/t. This last figure was determined assuming a reactor power output of 1670 MW(th).

Data was generated in an infinite spectrum obtained with the aid of a 1-d collision probability option (PERSEUS). The collected BOL and EOL data, after homogenization, were fed to a 2-d R-Z diffusion theory option WSNAP, available in WIMS-E. The Hex-Z geometrical capability of WSNAP was used for some calculations. Data for the reflector was generated in a separate, but consistent,

1-d calculation using WIMS-E. Little change in effective reflector data ensues with burnup and BOL data was used for all cases.

Burnup was performed initially in the infinite spectrum, as mentioned previously. A period of 3.5 years in WIMS-E and 4 years in WIMS-D4 were the selected EOL targets times, both so as to be consistent with the reference COSMOS calculation and for convenience in WIMS-D4. The following table (4.4) shows the effective multiplication factor (k_{eff}) values at BOL and at EOL, using both WIMS methods for the base ETGBR case.

Table (4.4): k_{eff} by the two WIMS Routes.

	BOL	EOL
WIMS-E	1.153	1.118 (3.5 yrs.)
WIMS-D4/WIMS-E	1.154	1.130 (4.0 yrs.)

It is apparent that, although the BOL data correspond exactly, burnup data produces differences of over 1.2% dk between the two methods. The cause of this discrepancy was not clear, especially since comparative reaction rate edits seemed to show consistency for the two routes of calculation. In any event, the large value of EOL k_{eff} predicted is the concern of the study; both routes show this.

Leaving aside the burnup disagreement between the two method, the WIMS-E method is most useful for the present investigations; giving lower EOL k_{eff}, and being easier to use than the multi-step WIMS-D4/WIMS-E route.

Enrichment Search

An enrichment search was performed in order to investigate the reactivity-life behaviour of the ETGBR, as calculated by WIMS. Table (4.5) shows some of the cases tested while figure (4.5) highlights the 'flattening out' of burnup and the change in sensitivity to enrichment that is observed. The first effect is typical of a fast spectrum reactor where Pu is being produced and destroyed rapidly.

WIMS burnup treatment can then proceed in a leakage spectrum, or else in a calculated critical spectrum (where k_{eff} =1 by buckling adjustment). The

note: The above two lines should be on the next page just below the "Bucklings" table!

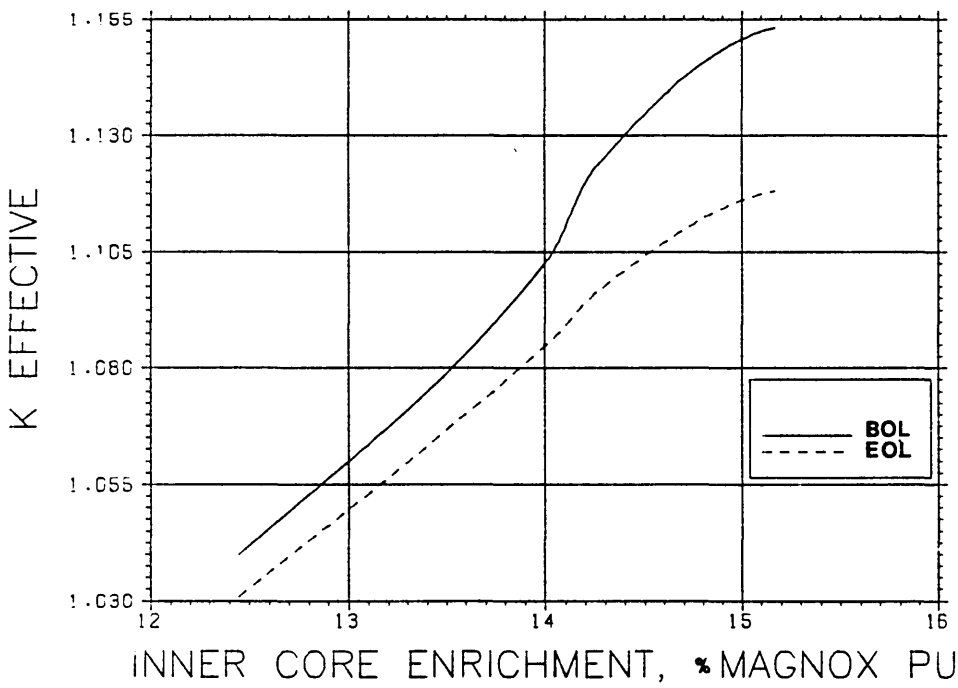

Figure 4.5. k_{eff} versus enrichment at BOL and EOL for standard ETGBR

Table (4.5): Enrichment search of base ETGBR calculated via WIMS-E/WSNAP(RZ) route (EOL is 3.5 years)

Enrichment %Magnox Pu zones C1/C2	k_{eff} (BOL)	k_{eff} (EOL)	dk(%)	dk/k(%)
15.17/21.41	1.153	1.118	3.50	3.03
14.75/20.81	1.144	1.111	3.30	2.88
14.25/20.09	1.123	1.096	2.60	2.31
14.01/19.77	1.103	1.085	1.78	1.61
12.45/17.57	1.040	1.031	0.91	0.87

Leakage Treatment

The first possible remedy for the shallow slope of the burnup (as shown in figure 4.5) is possibly the generation of the zonal data in suitably leakage-adjusted spectra. This was done by the inclusion of fixed geometrical bucklings into the spectrum calculations during burnup. For the ETGBR model used the following bucklings were applied:

Zone	Radial Buckling(cm^{-2})	Axial Buckling(cm^{-2})
C1	3.90×10^{-04}	5.03×10^{-04}
C2	4.70×10^{-04}	5.03×10^{-04}
AB	2.13×10^{-04}	2.74×10^{-03}
RB	5.60×10^{-04}	1.46×10^{-04}

two treatments produce only slightly different results since k_{eff} is never very far from unity anyhow. The effect on the reactivity-lifetime is shown in table (4.6) and figure (4.6) for the 15.17%/21.41% base case. Here the calculation is reported both for the WIMS-E and the WIMS-D4/WIMS-E methods. Although the difference in EOL k_{eff} is significant at just over 1%, the overwhelming observation is that,

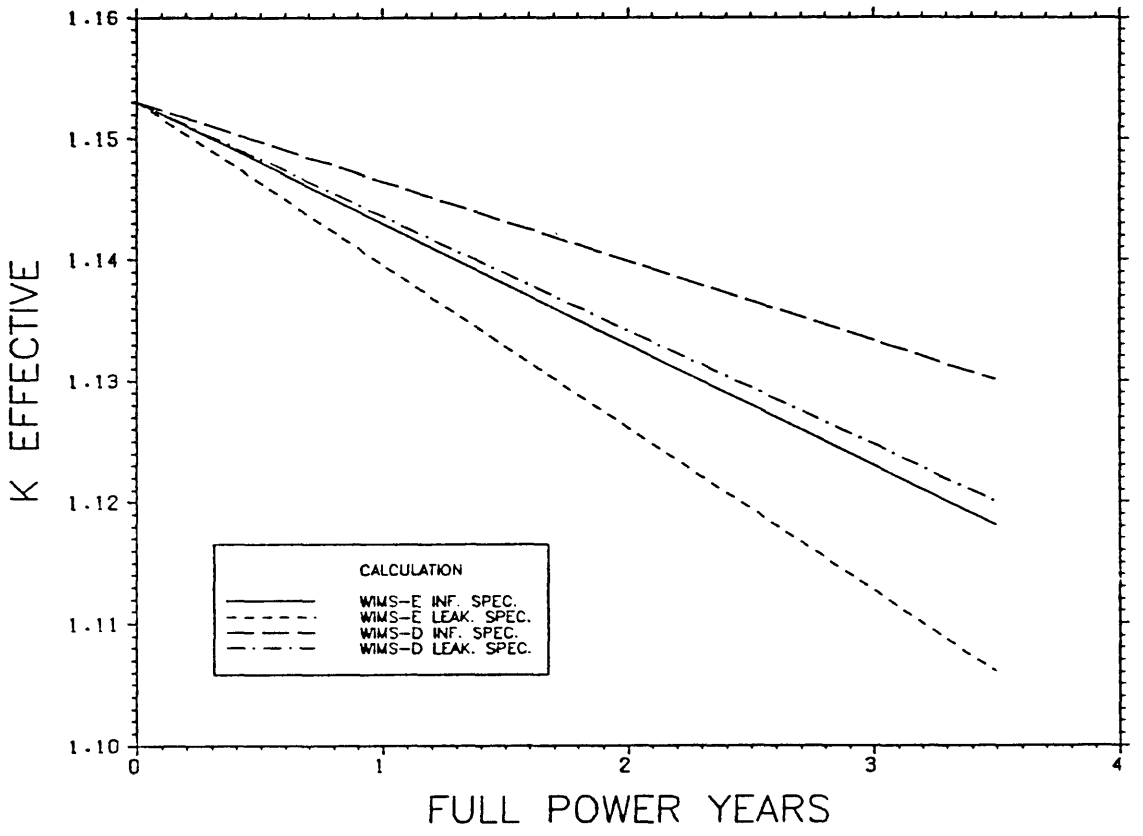

Figure 4.6. burnup of the ETGBR using either WIMS-D or WIMS-E together with either the infinite or leakage spectrum considered

even with leakage correction, the burnup of the ETGBR is still being overestimated using WIMS.

Table (4.6): Effect of leakage inclusion on burnup of 15.17/21.41% base ETGBR (k_{eff} (BOL) is 1.153)

Calculation method	k_{eff} (EOL)
Infinite spectrum:	
WIMS-E	1.118
WIMS-D4/WIMS-E	1.130
Leakage spectrum:	
WIMS-E	1.106
WIMS-D4/WIMS-E	1.120

Other Calculational Sensitivities

Concerning the other items affecting the calculation, the following observations can be listed:

(1) Reflector data:
Using reflector data generated and condensed with the radial breeder average flux spectrum gave results similar to those obtained when the flux from a 1-d centre-line core section was used. Additionally, the reflector data was seen to change little with burnup.

(2) Burnup power rating:
The effect on EOL k_{eff} was small for an arbitrary increase in the inner core zone power rating from 47.8 to 80 MW/t.

(3) Fuel density:
Reducing the fuel density from 11.0 to 9.9 gm/cm^3 resulted in a decrease in k_{eff} at EOL from 1.118 to 1.090 - a reduction of 2.5%dk/k. This, however, is not very significant in this context since the reactivity and dwell time are still overpredicted.

(4) Spatial meshing:
A considerable refinement of the meshing of the R-Z model of the ETGBR gave no change in k_{eff}, verifying the adequacy of the original meshing

(5) Dancoff factors:
Because, for the ETGBR, there is no intervening moderator between clusters (subassemblies), it is appropriate to substitute average pin-cell generated 'dancoff factors' for the default cluster values. No sensitivity to the substitution was found.

As a general conclusion for section 4.4 it may be stated that, using WIMS for the ETGBR with the fuel volume fraction as given (0.28-0.29), a long burnup prediction is obtained compared with values predicted using dedicated fast reactor codes (COSMOS). This has been verified by both WIMSD4/WIMSE and an even more consistent wholly WIMSE calculation with smearing volume correction. It may be judged, as has been previously suggested in chapter 2, that the calculation of ETGBR burnup with WIMS is not recommended although it is used of necessity throughout this work for scoping calculations.

4.5 AN UNDERLOADED-ETGBR MODEL

The underloaded-ETGBR (U-ETGBR) is defined as an ETGBR model with increased subassembly size and a resulting reduction in fuel volume fraction.

Subject, of course, to heat transfer related criteria, the ETGBR might be diluted by reducing the unit volume fuel loading; by increasing coolant volume fraction and by reducing the fuel volume fraction. To achieve this the pitch to diameter ratio is increased from the usual 1.45 to 1.77, thereby giving a larger subassembly. Table (4.7) gives a comparison of the underloaded ETGBR and the standard ETGBR both with 169 rods per subassembly.

Table (4.7): Comparison of ETGBR and U-ETGBR geometry, volume fractions, and masses.

	ETGBR	U-ETGBR
Fuel volume fraction	0.300	0.190
Coolant volume fraction	0.534	0.453
P/D ratio	1.45	1.77
Subassembly across flats (cm.)	15.74	19.79
Fuel(U+Pu) masses (t):		
Zone C1	18.44	-
Zone C2	15.27	-
zone RB	71.00	-

Whole Reactor Calculations of the Underloaded-ETGBR

The Calculational Model

The validity of WIMS and its library for the ETGBR was discussed in chapter 2; this was checked further by calculating ETGBR using a method wholly in WIMS-E. The agreement with the reference calculation was shown to be good in general, but to overestimate burnup. There are clearly limitations to the detailed leakage calculation and these may be accentuated in U-ETGBR.

The method of calculation adopted is again one based on a sequence of WIMS-D4 and WIMS-E runs. The treatment of the standard ETGBR whole reactor in 2 or 3 dimensional geometry has been discussed in the previous section. The fully reflected reactor could only be calculated in R-Z geometry, while Hex-Z geometry is limited to a configuration in which the reflectors are removed due to failure of WSNAP in Hex-Z mode to converge for large systems with too many energy groups [6]. However, with full blankets, the reflector worth is expected to be small. The energy structure employed all the fast groups available in the WIMS library leading to a 19 group case. In Hex-Z geometry, this necessitates the deletion of the reflectors or else the reduction in the number of groups to less than about 15; the first choice was opted for. In R-Z mode, no difficulty is encountered and an estimate of the reflector worth may be found.

It must be noted that, although from a homogenized lattice point of view, the neutronics of this concept are no different than those of the standard ETGBR, the reduced fuel volume fractions and increased pin spacing affect the lattice data generated prior to smearing.

Burnup of the base Underloaded ETGBR

The enrichment level of the 'base' U-ETGBR core zones is determined using the WIMS-D4/WIMS-E method previously outlined. The inner core zone (C1) is assigned a fixed rating of 47.8 MW/t and the rating of the other zones are found from a single BOL R-Z reaction rate edit. The enrichment ratio of zone C2 to that of zone C1 was maintained at or near 1.41 [5].

An enrichment search was performed using the fully reflected reactor in R-Z geometry. A case was sought with a core residence time in the range of 4 to 6 years to be consistent with ETGBR design considerations. To start with, the search considered single batch burnup. Table (4.8) shows the reactivity (k_{eff}) rundown for each enrichment set at several time intervals for the fully reflected reactor.

Table (4.8): Enrichment search for Underloaded ETGBR

Enrichment	Effective multiplication factor, k_{eff}			
%Magnox Pu C1/C2	BOL	2 years	4 years	6 years
17.00/23.97	1.1147	-	-	-
15.17/21.41	1.0398	1.0342	1.0251	1.0139
15.00/21.00	1.0313	1.0274	1.0194	1.0093
14.25/20.09	1.0125	-	-	-

As a check on the values obtained with the reflectors removed, Hex-Z calculations or, equivalently, an R-Z with no reflector regions, were performed. The 15.00/21.00 enrichment case gave the k_{eff} shown in table (4.9). Increased leakage from the blankets, due to fissile breeding, results in the increase in reflector worth with burnup. Table (4.10) shows the variation of internal conversion ratio and breeding ratio with burnup.

Table (4.9): Reflector worth of fully blanketted Underloaded ETGBR (15/21 case).

	BOL	2 years	4 years	6 years
unreflected k_{eff}	1.0268	1.0203	1.0104	0.9985
dk	0.0045	0.0071	0.0090	0.0108

Table (4.10): Variation of ICR and BR with full power time.

time (years)	ICR	BR
0	0.770	1.375
2	0.726	1.331
4	0.700	1.313
6	0.679	1.306

The reactivity rundown behaviour leads to the possible choice of 15.00/21.00 enrichment. This gives a single batch residence time of close to 7.0 years. The burnup of the underloaded ETGBR would be about 122 GWd/t. The choice of the enrichment level is based on an acceptable core residence time in addition to a reasonablly controllable excess reactivity. The BR for the base underloaded ETGBR is found to be high (1.375 at BOL) even though the ICR is lower than for a highly loaded ETGBR of the same enrichment. With the more open lattice there must be higher leakage, giving higher breeding in the external blankets.

Multi-batch Standard Underloaded-ETGBR

A single batch ETGBR of 15.00/21.00 gives a reactor residence time of 2555 days. An equivalent 3 batch refuelling scheme could produce the same burnup with a reduced initial reactivity. The k_{eff} of 1.0313 is reduced to 1.0156.

Axial Blanket Variation for the Underloaded-ETGBR

The BOL standard ETGBR is subjected to a final check, in R-Z geometry, to examine the effect of the variation of the blanket thickness on the reactivity and flux distribution. The axial blanket was studied, since it is the easiest to vary by simply varying the thickness of the depleted uranium in the pins, while keeping keeping the axial reflector thickness constant. Table (4.11) gives the results.

Table (4.11): Effect of axial blanket height on underloaded ETGBR breeding ratio.

AB Height (cm.)	k_{eff}	ICR	BR
60.00	1.03138	0.7701	1.3749
30.00	1.03175	0.7743	1.2597
1.000	1.03475	0.7495	1.0770

It is observed that a slight increase in reactivity ensues as the AB is reduced. This is due to increased reflection back into the core zones of neutrons that would have been captured in the AB. More importantly, the effect on breeding potential may be noted; as expected, the breeding ratio is reduced by decreasing the AB thickness. However, even with a near zero AB (1.0 cm.) the breeding ratio is still significantly. above 1.00.

In general the underloaded ETGBR has been presented as a possible concept fullfilling the aim of a lower fuel fraction in the ETGBR core. The high enrichments used create a difficulty in determining burnup due to, as already seen for the standard ETGBR, WIMS library inadequacy for fast systems.

4.6 CONCLUSIONS

The gas cooled fast reactor has been contrasted with LMFBR, bringing out some relative advantages and disadvantages. The ETGBR concept was introduced as a system appropriate to present day economic circumstances, with its direct use of established AGR and LMFBR technology. The ETGBR as studied in this thesis was defined, and its specifications set and compared to reference designs. Neutronic calculation techniques were outlined and whole reactor calculations of the ETGBR were described using both a combined WIMS-D4/WIMS-E route and a wholly WIMS-E route. Neutronic calculations were carried out in an attempt to establish where sensitivities in the calculation lay with respect to composition, geometry, or calculational assumptions.

The major result was that, with the given fuel loading and fuel volume fraction of 0.28 to 0.29, the burnup curve predicted with WIMS is very shallow leading to

long reactivity-lifetime. No calculation parameter was identified as a cause of this apparent overprediction of burnup, and the conclusions from chapter 2 regarding the deficiency in the WIMS library when applied to gas-cooled fast reactors were supported further.

As a possible solution to the high fuel loading problem, a reduced fuel volume fraction design was considered as a means of reducing the calculational difficulties with WIMS for the ETGBR. This led to the introduction of of the underloaded-ETGBR design which might be regarded as an additional way of diluting the ETGBR core (chapter 5 discusses the dilution of ETGBR). The neutronics of the underloaded ETGBR was studied briefly although other engineering factors in design optimisation were not considered.

REFERENCES

1. *The gas cooled breeder reactor - economic power with breeding*, Gas Breeder Reactor Association - Brussels, Nuclear Engineering International, p. 566, 1974

2. Gratton C. P. , *The gas-cooled fast reactor in 1981*, Nucl. Energy, Vol. 20, No. 4, pp. 287-295, August 1981

3. Kemmish W. B. , *Gas-cooled fast reactors*, Nucl. Energy, Vol. 21, No. 1, February 1982

4. Ibid. p. 85

5. MacBean I. J. , *A COSMOS calculation of the neutronics performance of a 1670 MW(th) GCFR with 7 mm. fuel pellets, and a comparison with results of CEGB calculations*, AEE-Winfrith report AEEW-M1669, April 1979

6. Askew J. R. , Roth M. J. , *WIMS-E, a scheme for neutronic calculations*, AEE-Winfrith report AEEW-R1315, June 1982

CHAPTER 5.

THE DILUTED ETGBR (DETGBR)

5.1 THE CONCEPT OF DILUTION

Features of both thermal and fast gas-cooled cores have been discussed in previous chapters. Limits of the thermal system have been pointed out and possible variants of 'intermediate' design presented in chapter 3. The idea was put forward that a fast system may be the way ahead but only if the maximum use could be made of present thermal reactor component technology. However, the negative aspects of moving from AGR to ETGBR must be noted and solutions be found.

The major difference between AGR and ETGBR core is the absence of moderator, leading to:

a) Loss of transient heat sink.
b) Less negative Doppler coefficient.

and, arising from the fast reactor characteristics:

c) Higher power density.
d) Higher burnups.

The safety-related features of AGR need to be retained where possible while, at the same time, the safety of the fully fast system needs to be augmented where appropriate. Some degree of 'dilution', leading to an increase in the core thermal inertia, is investigated in this chapter from the neutronics point of view. A diluent is a non-fuel material that need not be a moderator but is required to have good thermal and radiation stability.

It must be recognized that the amount of diluent allowed cannot be so high as to lead to significant departure from the desired fast neutron spectrum. Thus a 'sparingly diluted' ETGBR emerges with a neutron flux spectrum displaced only slightly into the resonance energy region (see η vs E graph shown in figure 1.1).

Diluent materials which might be considered include graphite, alumina (Al_2O_3), beryllia (BeO) and silicon carbide (SiC). Of these only graphite and alumina are studied, mainly because graphite is extensively used in thermal reactors and alumina is chemically inert up to very high temperatures, and has good mechanical and thermal properties (notably specific heat capacity at high temperatures). The way in which the diluents may be indroduced into the ETGBR core are various:

a) Block dilution: Building directly on the AGR concept of a fuel channel surrounded by a graphite block; the diluent is thus placed around the channel. The difference from AGR is that the fuel channel and the moderator block are integral, allowing them to be removed together at refuelling. In this the concept is similar to the 'integral AGR' design of chapter 3, introduced by Askew et al [1].

b) Heterogeneous ETGBR subassemblies: This concept is similar to the heterogeneous fast reactor design with in-core breeder subassemblies. The diluent is held in separate subassemblies. A very low overall dilution (moderation) could be achieved and a design could include both diluted and undiluted core zones. Clearly there will be greater local heterogeneity in power production than in type (a) dilution. Chapter 6 discusses this design in more detail.

c) Dispersion type fuel in rods: The idea of a dispersion of fuel in either metal or ceramic matrixes is one which has received some attention; for example the EBOR (experimental beryllium oxide reactor) design was helium cooled, used UO_2 dispersed in BeO and Hastelloy cladding [2]. For the relatively high temperatures and burnups envisaged in the ETGBR, fuel in a ceramic dispersion is envisaged. The enrichment requirement for this method of dilution is expected to be higher than for other dilution concepts.

d) Diluent rods in the subassembly: Separate diluent pins are placed among the fuel pins within the subassembly. This leads to a larger subassembly for a given output and hence a larger core. This concept may be of value if diluent blocks might suffer from thermal stress problems. Such an idea has been contemplated although with little detail being given [3]. Further consideration of this concept is given in chapter 6.

Only the block dilution, pin dilution, and the heterogeneous dilution are considered in this thesis; dispersion fuel is considered to involve a large departure from current fuel design.

5.2 BLOCK DILUTED ETGBR (THE DETGBR)

This concept involves effectively changing the wrapper zone of an ETGBR into a 'diluent', in a manner analogous to AGR and HTR concepts (see the Fort St. Vrain design for example [4]). The DETGBR subassembly is shown in figure (5.1). The fuel channel containing 169 rods is 15.69 cm. in diameter formed in an hexagonal diluent block. The block size and hence the core size depend on the diluent to fuel volume ratio considerd. The selection of 169 rods per channel was preffered, in this work, to the larger 371 rods per channel designs, in order to have a significant amount of diluent per fuel rod and to minimize the block mass. A first choice for the diluent material is graphite owing to experience with its irradiation properties and its availability. However, its possible exothermic burning in unforseen high temperature excursions with air ingress and its moderating properties make it less desirable for a gas-cooled fast reactor designs. As an alternative, alumina has a high volumetric thermal capacity; it is thus a candidate diluent for an increased thermal capacity ETGBR. Alumina is also an ineffective moderator (see chapter 7) and should allow a reasonably hard neutron spectrum. The efficiency of neutron usage in the alumina case is, however, a matter of concern since higher enrichments are probably required.

Section 5.3 presents lattice-cell calculations of the bare standard and diluted ETGBR's. Burnup is performed at the cell level in WIMS as in most thermal reactor codes. The cell burnup could be then followed by a whole reactor calculation. This calculation, may, or may not, include other reactor zones such as reflector. In section 5.4 whole reactor calculations of the ETGBR and its diluted variants are undertaken. Calculations of pin-diluted and heterogeneously diluted concepts are later given in chapter 6.

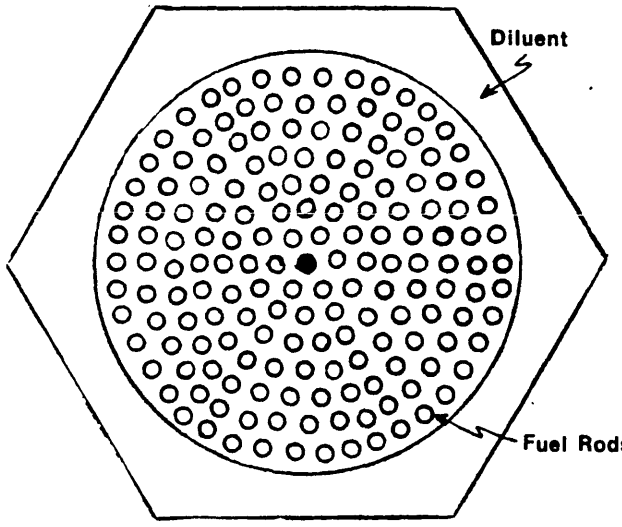

Figure 5.1. The DETGBR subassembly with a diluent to fuel volume ratio of 2.

5.3 BARE CORE LATTICE-CELL CALCULATIONS OF ETGBR AND DILUTED VARIANTS

For the purpose of comparative calculations, using the WIMS-D4 simple lattice- cell approximation of the bare core is both simple and direct. Firstly, it is useful to compare alumina with graphite for a range of diluent-to-fuel volume ratios (V_d/V_f) at several enrichments. The infinite multiplication factor (k_∞) is used to give an indication of the reactivity behaviour. Table (5.1) and Figure (5.2) show that, as expected, while graphite is an efficient moderator, alumina is more of an absorber. This is shown by the high k_∞ for high graphite-to-fuel ratios. The relative moderation (V_d/V_f) is only taken up to 5.0 since a requirement of this work is that the system be 'somewhat fast'.

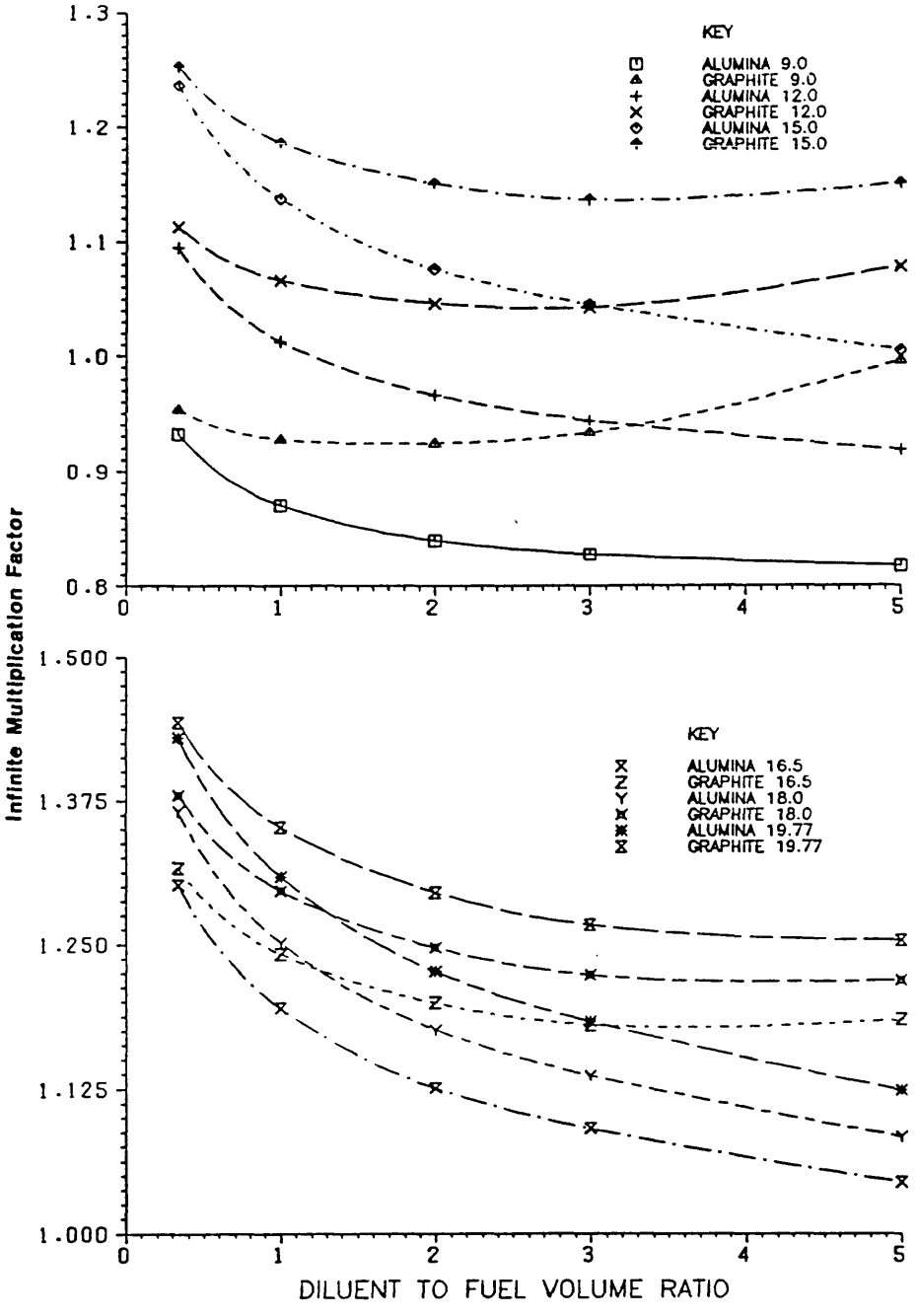

Figure 5.2. The variation of the infinite multiplication factor (k_∞) for the ETGBR and DETGBR's with a range of enrichments and dilution ratios (V_d/V_f).

Table (5.1): Infinite multiplication factor (k_∞) at BOL for graphite and alumina DETGBR's.

Diluent to Fuel Volume Ratio		Enrichment,% Magnox Pu 9	12	15	16.5	18	19.77
Base ETGBR		0.9410	1.1135	1.2631	1.3309	1.3982	1.4653
0.334	Graphite	0.9533	1.1130	1.2525	1.3160	1.3795	1.4426
	Alumina	0.9323	1.0946	1.2366	1.3013	1.3657	1.4299
1.00	Graphite	0.9273	1.0658	1.1865	1.2415	1.2966	1.3517
	Alumina	0.8703	1.0127	1.1375	1.1946	1.2515	1.3088
2.00	Graphite	0.9241	1.0458	1.1511	1.1991	1.2470	1.2951
	Alumina	0.8398	0.9657	1.0756	1.1258	1.1759	1.2263
3.00	Graphite	0.9333	1.0422	1.1367	1.1800	1.2231	1.2666
	Alumina	0.8279	0.9439	1.0446	1.0907	1.1365	1.1828
5.00	Graphite	0.9951	1.0776	1.1506	1.1843	1.2184	1.2528
	Alumina	0.8180	0.9177	1.0045	1.0442	1.0837	1.1239

Geometric bucklings are used to correct approximately for leakage effects. The system modelled would then be a one zone reactor, of one enrichment. As a later exercise this system may be reassessed with reflectors or even with multi-enrichments. The core height of all variants was kept at the ETGBR base value of 140 cm. The core radius was such that the amount of fuel was kept fixed (i.e. the same number of subassemblies for the different diluent to fuel volume ratios, V_d/V_f). For a 1670 MW core, with 396 subassemblies, the geometric bucklings are given in table (5.2).

Figure (5.3) shows the reactivity behaviour versus dilution with graphite or alumina for the finite block diluted ETGBR lattice. It is assumed that the BOL k_{eff} for an operable system is in the range of 1.04 to 1.07. This should give a reasonable control-margin. Table (5.3) is used to select possible enrichments and V_d/V_f ratios for the DETGBR's.

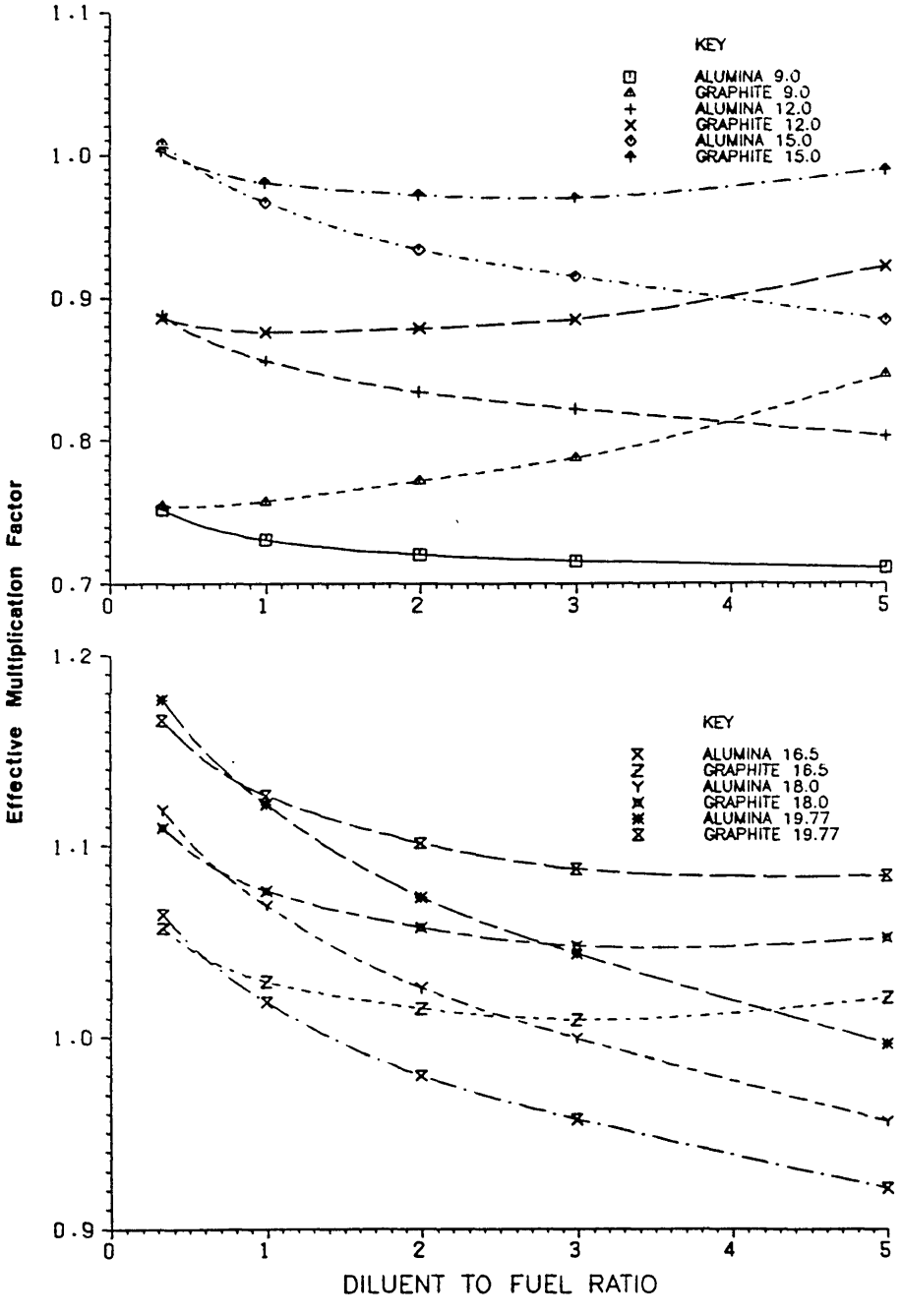

Figure 5.3. The effective multiplication factor (k_{eff}) for the ETGBR and DETGBRs with a range of enrichments and dilution ratios (V_d/V_f).

Table (5.2): The geometric sizes of The diluted ETGBR and the resulting geometrical bucklings for each V_d/V_f case.

V_d/V_f	Outer radius Cluster (cm)	Core zone radius (cm)	$B_r{}^2(cm^{-2})$
0.334	8.2635	164.44	2.13×10^{-4}
1.000	9.0612	180.31	1.77×10^{-4}
2.000	10.130	201.58	1.42×10^{-4}
3.000	11.090	220.70	1.185×10^{-4}
5.000	13.075	260.19	8.54×10^{-4}

Table (5.3): Effective multiplication factor (k_{eff}) at BOL for graphite and alumina DETGBR's.

Diluent to Fuel Volume Ratio		Enrichment, %Magnox Pu 9	12	15	16.5	18	19.77
Base ETGBR		0.7393	0.8776	1.0008	1.0577	1.1129	1.1720
0.334	Graphite	0.7548	0.8860	1.0029	1.0569	1.1096	1.1658
	Alumina	0.7520	0.8876	1.0085	1.0642	1.1188	1.1766
1.00	Graphite	0.7578	0.8760	0.9806	1.0289	1.0763	1.1263
	Alumina	0.7311	0.8559	0.9669	1.0182	1.0687	1.1217
2.00	Graphite	0.7721	0.8786	0.9719	1.0148	1.0571	1.1013
	Alumina	0.7205	0.8338	0.9338	0.9799	1.0255	1.0730
3.00	Graphite	0.7879	0.8848	0.9697	1.0088	1.0473	1.0876
	Alumina	0.7163	0.8218	0.9145	0.9571	0.9992	1.0431
5.00	Graphite	0.8455	0.9213	0.9887	1.0200	1.0512	1.0837
	Alumina	0.7113	0.8031	0.8839	0.9210	0.9558	0.9961

For comparative purposes the base (standard) ETGBR is taken to have a k_{eff} of 1.057 and initial conversion ratio (ICR) of 0.818 at an enrichment of 16.5 %Magnox Pu. The enrichments required to give the same BOL reactivity for the diluted cores are given in table (5.4).

Table (5.4): DETGBR enrichments for the low V_d/V_f ratios at k_{eff} =1.06.

	Diluent/Fuel Volume Ratio		
	1.0	2.0	3.0
graphite	17.48	18.12	18.56
alumina	17.74	19.28	19.77

From table (5.4) graphite shows an enrichment advantage over alumina. This is expected, due to its qualities of moderation and lower parasitic absorption. Figure (5.4) compares fission and capture rates in U-238 and Pu-239, and non-fuel captures for the graphite and alumina diluted DETGBR. More fissions in Pu-239 and less U-238 captures, and more U-238 fissions, characterize the graphite cases. The alumina diluted cases show increased non-fuel absorbtions, as V_d/V_f is increased, although below V_d/V_f of about 1.75 this is less than for the graphite diluted cases.

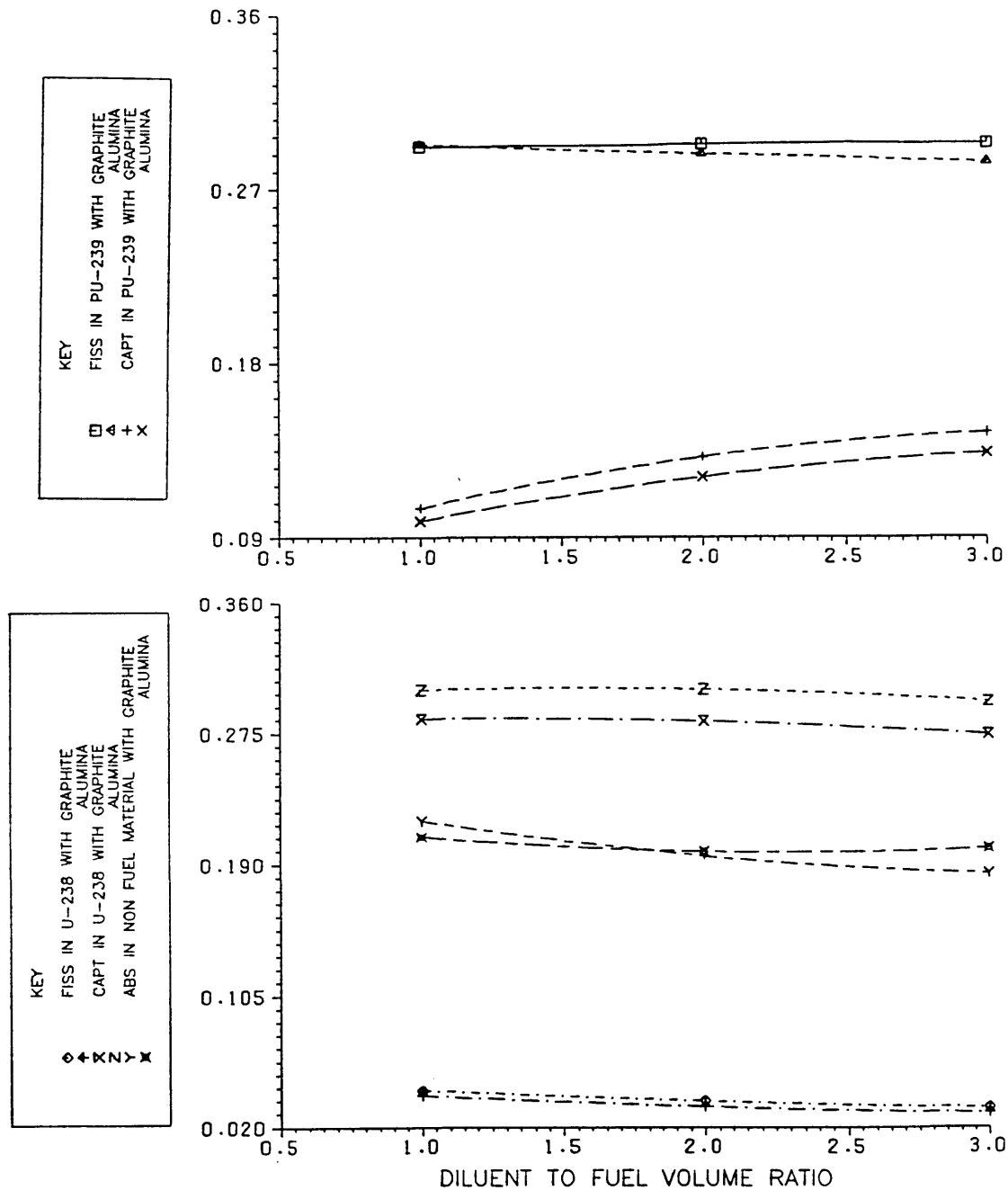

Figure 5.4.Cell average fission and capture reactions in U-238 and Pu-239, as well as captures in non-fuel material for a range of graphite and alumina DETGBR at 18.0 %Magnox Pu (total cell absorption of 1.0).

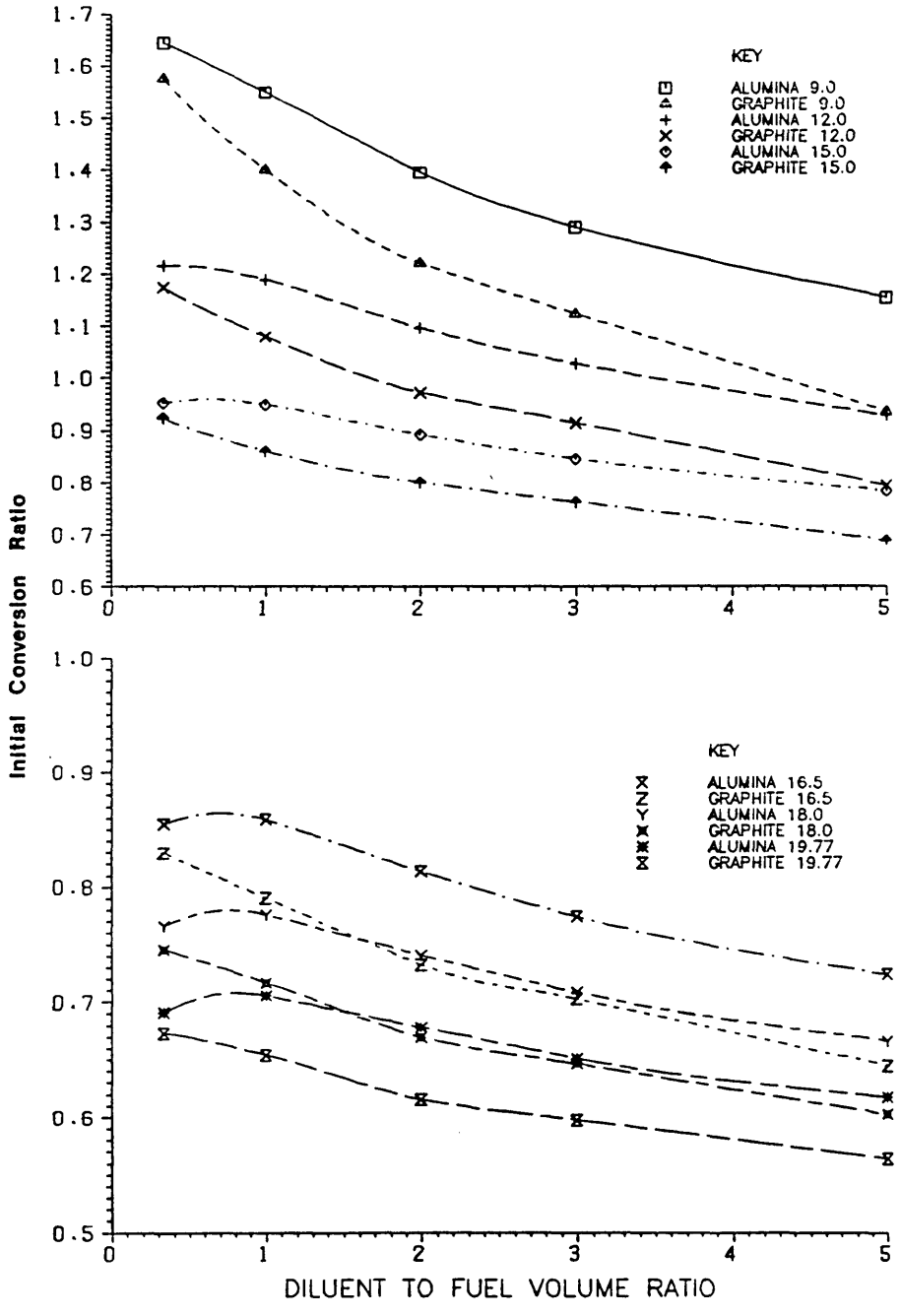

Figure 5.5. The initial conversion ratio (ICR) for the ETGBR and DETGBRs of a range of enrichments and dilution ratios (V_d/V_f).

Initial Conversion ratio (ICR) is another parameter of major importance in reactor performance. Table (5.5) and figure (5.5) give the ICR as a function of dilution, in the graphite and alumina variants, compared with the base ETGBR case.

Table (5.5) : Initial Conversion Ratios (ICR) for the ETGBR and DETGBR's in the lattice model (effective spectrum)

Diluent to Fuel Volume Ratio		Enrichment, %Magnox Pu 9	12	15	16.5	18	19.77
Base ETGBR		1.5988	1.1741	0.9138	0.8180	0.7316	0.6584
0.334	Graphite	1.5762	1.1739	0.9228	0.8298	0.7452	0.6732
	Alumina	1.6444	1.2162	0.9521	0.8546	0.7662	0.6910
1.00	Graphite	1.4012	1.0796	0.8603	0.7907	0.7170	0.6544
	Alumina	1.5500	1.1889	0.9489	0.8587	0.7761	0.7056
2.00	Graphite	1.2213	0.9722	0.7995	0.7324	0.6698	0.6156
	Alumina	1.3962	1.0965	0.8919	0.8138	0.7408	0.6784
3.00	Graphite	1.1239	0.9141	0.7624	0.7026	0.6464	0.5973
	Alumina	1.2908	1.0276	0.8449	0.7741	0.7082	0.6512
5.00	Graphite	0.9358	0.7945	0.6885	0.6446	0.6021	0.5640
	Alumina	1.1548	0.9277	0.7832	0.7231	0.6665	0.6172

In Figure (5.6) the reactivity and ICR are plotted together versus enrichment. Reactivity rises and conversion falls with increasing enrichment. The diluted cases shown are for V_d/V_f of 2.0 and, interestingly, alumina shows a superior ICR to even the undiluted standard ETGBR of the same enrichment (considering alumina to require enrichments of at least about 17% to have a k_{eff} of 1.0), for small V_d/V_f values up to 2.0 (also refer back to table 5.5).

In a similar manner as table (5.4) the selected DETGBR variants have been contrasted based on their ICR's. This is shown in table (5.6); it appears that alumina has a small advantage over graphite in this respect.

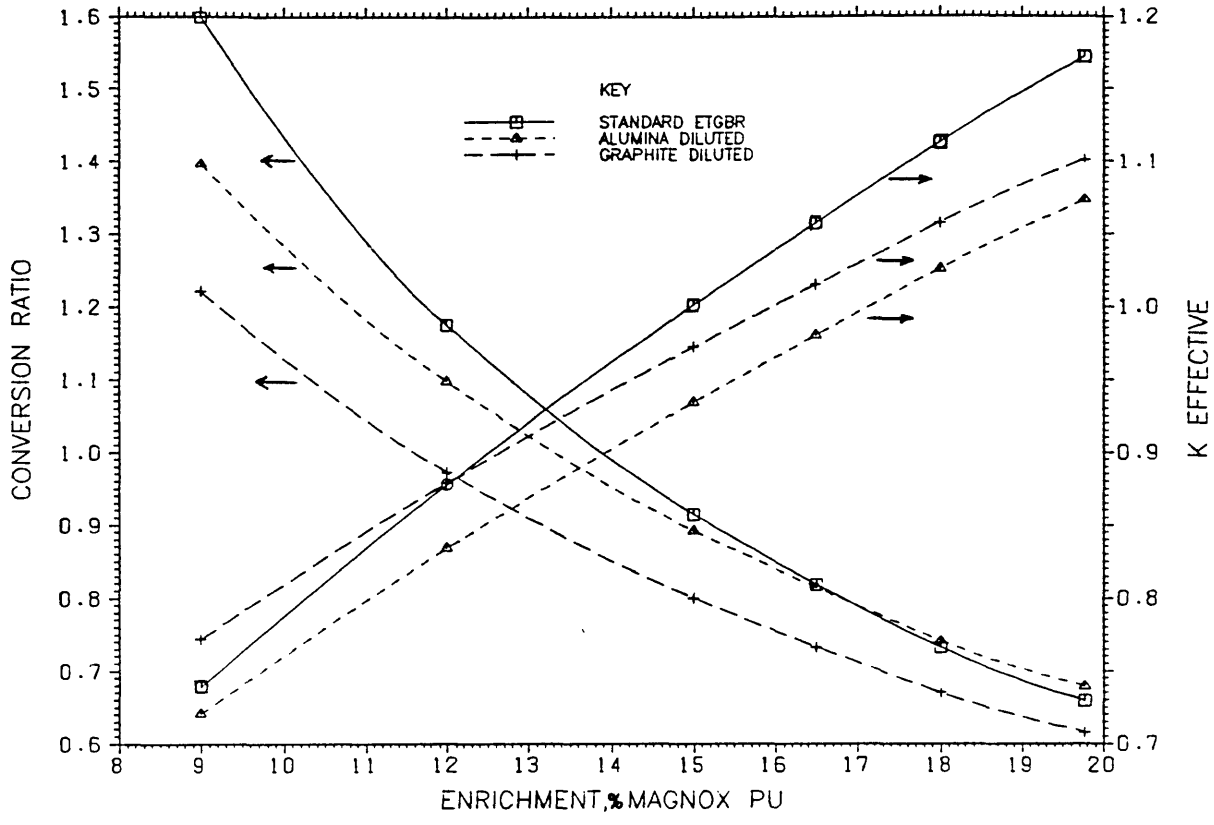

Figure 5.6. BOL DETGBR k_{eff} and ICR variation with enrichment

Figure (5.7) shows the neutron flux spectrum of the average subassembly for two values of V_d/V_f (1.0 and 2.0) for graphite and alumina DETGBR's, and with the high energy part enlarged in figure (5.8). As expected, alumina causes less softening of the neutron spectrum than does graphite.

When moderating anulli separate the subassemblies in thermal systems, it is expected that flux peaking will exist within the subassembly. In a fast system this should not be of significance due to the lack of moderator. Table (5.7) shows the outer ring peaking factors at BOL for the ETGBR and the major diluted variants. The alumina DETGBR shows less flux peaking than the graphite case.

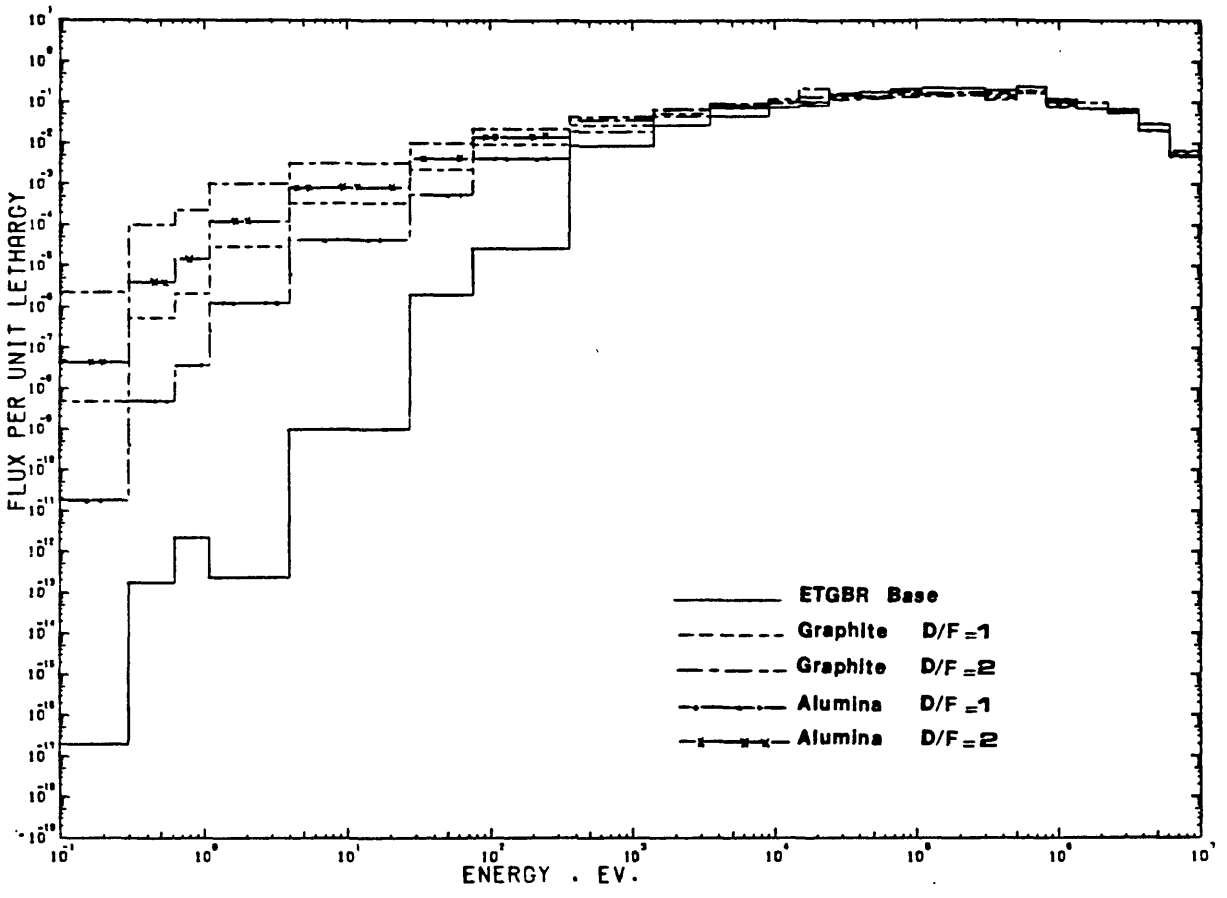

Figure 5.7. Flux spectrum of average core ETGBR and DETGBRs (normalized to a total flux of 1.0)

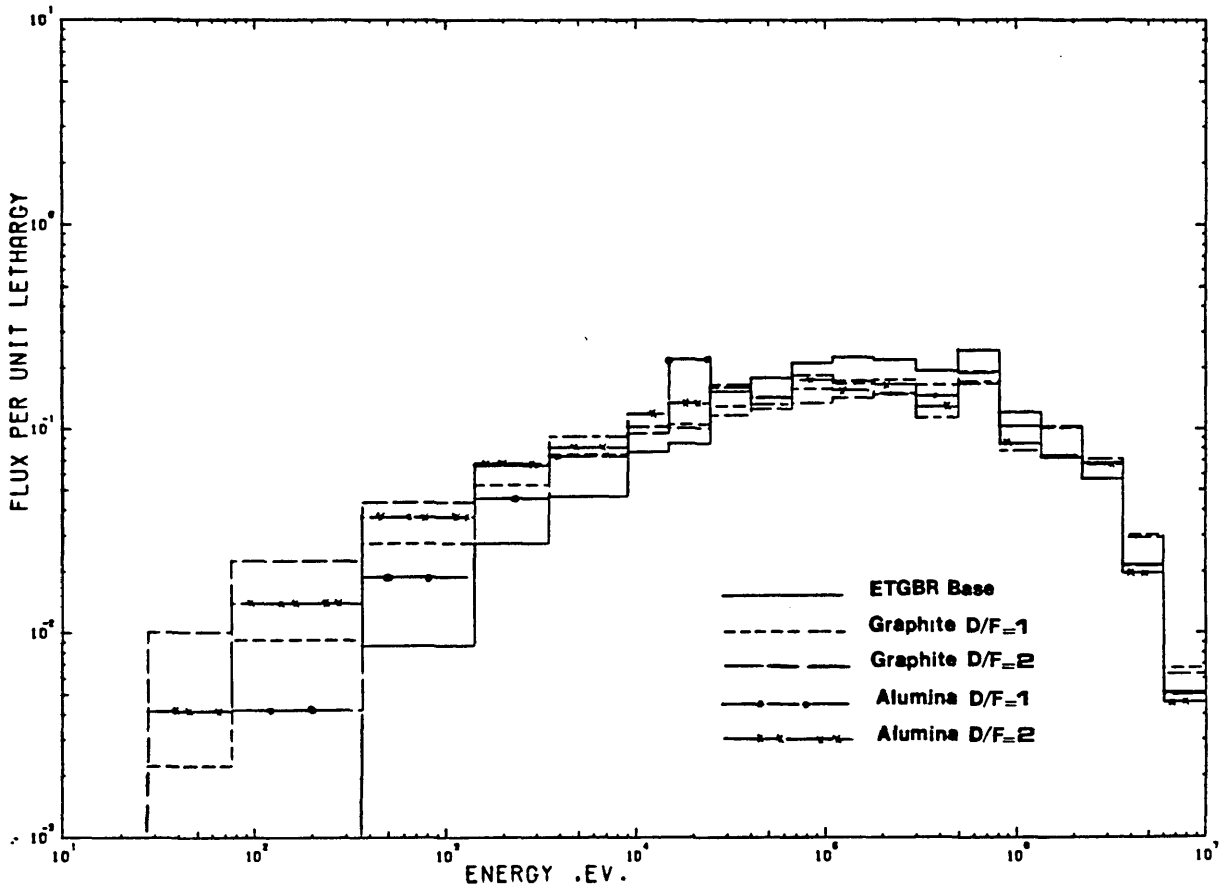

Figure 5.8. High energy section of flux spectrum for ETGBR and DETGBRs (normalized to a total flux of 1.0)

Table (5.6): DETGBR of the low V_d/V_f ratios contrasted based on ICR.

	Diluent/Fuel Volume Ratio		
	1.0	2.0	3.0
Graphite	0.790-0.717	0.669	0.646-0.597
Alumina	0.776	0.741-0.678	0.651

Table (5.7): Outer ring peaking factor (BOL).

System	Peaking Factor	Fraction of Power in outer ring(%)
ETGBR	1.003	25.6
Graphite V_d/V_f =2,E=19.77%	1.116	28.6
Alumina V_d/V_f =2,E=19.77%	1.061	27.2

Burnup and Fuel Usage

Core life and hence burnup need to be maximized, without violating materials constraints. A feature of fast reactors is high conversion ratios and thus low rates of fall of k_{eff} with time. High fuel ratings are, naturally, associated with high burnups. The standard ETGBR single batch fuel life is quoted at about 3.5 years [5]. The ETGBR used in these calculations is rated at 1670 MW_t overall and contains 34.9 tonnes of heavy metal, giving a fuel rating of 47.8 MW/t. As a first indication of core life, burnups of the base ETGBR and both graphite and alumina DETGBR cores were carried out. A better treatment of asymetric neutron diffusion was included via the WIMS Benoist option. Table (5.8) gives selected core lifetimes.

Table (5.8) is used to select cases with acceptable single batch dwell times in the range of 3 to 4 years. The possible DETGBR's and their burnups are shown in the table (5.9) with the terminal irradition obtained, if neccesary, by extra interpolation in figures (5.9a) and (5.9b).

It is apparent that with a V_d/V_f of 2.0 the achievable burnups are reduced to values in the range of 50 to 60 GWd/t with core dwell times of no more than 3.2

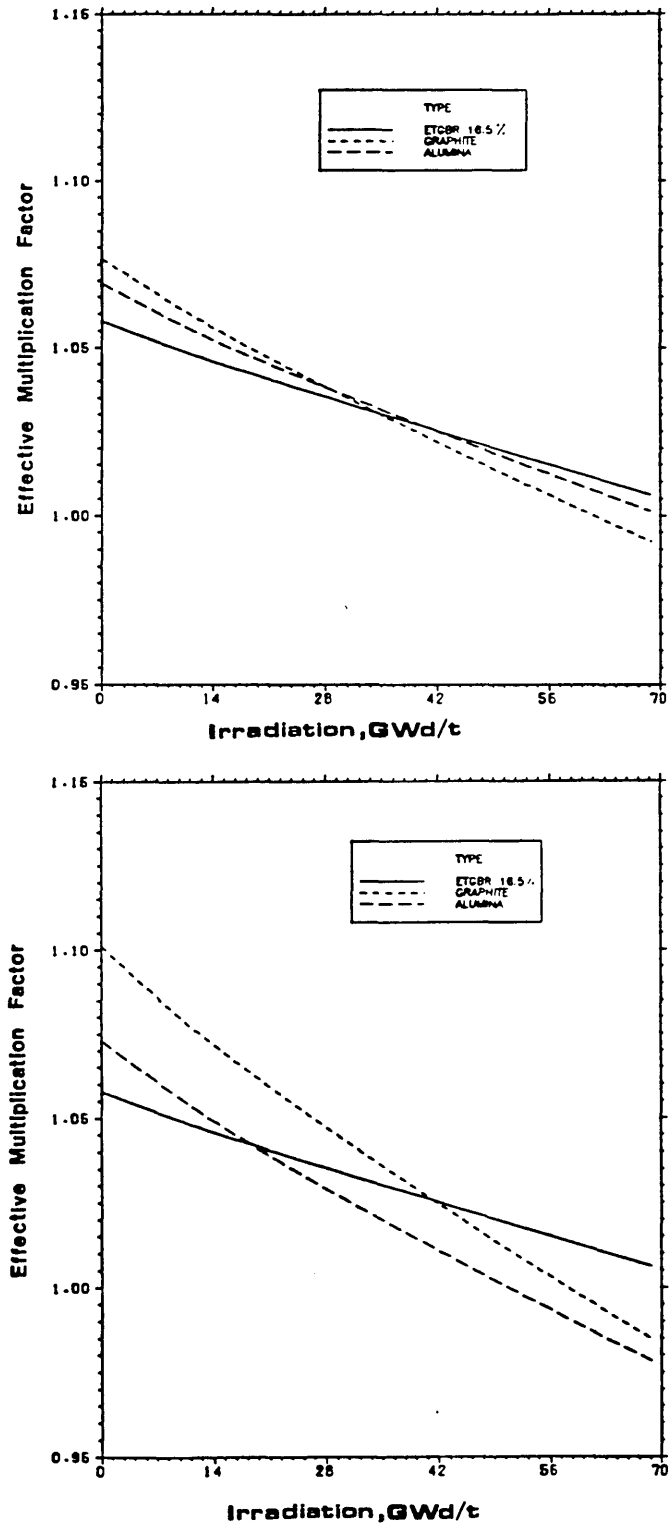

Figure 5.9. Burnup of ETGBR compared to DETGBRs at (a)V_d/V_f =1 and 18.0% enrichment (b)V_d/V_f =2 and 19.77% enrichment

Table (5.8): k_{eff} change with Burnup of ETGBR and DETGBR's of different Enrichment and V_d/V_f Ratio

Case	Diluent to Fuel ratio	Enrichment %Magnox Pu	Time, years 0.0	1.0	2.0	3.0	4.0
Base ETBGR	0.0	16.0	1.0389	1.0266	1.0158	1.0052	0.9944
Base ETGBR	0.0	16.5	1.0578	1.0434	1.0307	1.0183	1.0061
	1.0	18.0	1.0766	1.0517	1.0307	1.0110	0.9923
Graphite	2.0	18.0	1.0568	1.0252	0.9992	0.9751	0.9526
D-ETGBR	2.0	19.77	1.1011	1.0660	1.0368	1.0098	0.9847
	3.0	19.77	1.0871	1.0462	1.0134	0.9835	0.9559
	1.0	17.0	1.0409	1.0240	1.0103	0.9973	0.9846
Alumina	1.0	18.0	1.0691	1.0488	1.0321	1.0163	1.0013
D-ETGBR	2.0	18.0	1.0255	1.0015	0.9816	0.9632	-
	2.0	19.77	1.0730	1.0445	1.0207	0.9988	0.9782
	3.0	19.77	1.0427	1.0108	0.9845	0.9604	0.9380

Table (5.9): Burnup of ETGBR and DETGBR unreflected leakage corrected bare cores.

Core Type	Enrichment (%)	Burnup (MWd/t)	Initial %dk/year
ETGBR	16.5	78400	1.44(1.36)
Graphite DETGBR V_d/V_f =1	18.0	63000	2.49(2.31)
Alumina DETGBR V_d/V_f =1	18.0	70000	1.69(1.62)
Graphite DETGBR V_d/V_f =2	19.77	58400	3.51(3.18)
Alumina DETGBR V_d/V_f =2	19.77	51000	2.85(2.65)

years. The %dk per year are much larger than in the base ETGBR. It must be noted that these burnups are based on a single zone unreflected core; full burnup performance is investigated later, in 2-d and 3-d geometry with reflectors and optional blankets represented.

To show the variation of the fuel usage with irradiation, figure (5.10) gives conversion ratio as a function of time. The single most striking result is that the alumina DETGBR conversion ratio, with leakage included, exceeds that of the graphite case, of the same enrichment, throughout burnup. Greater neutron

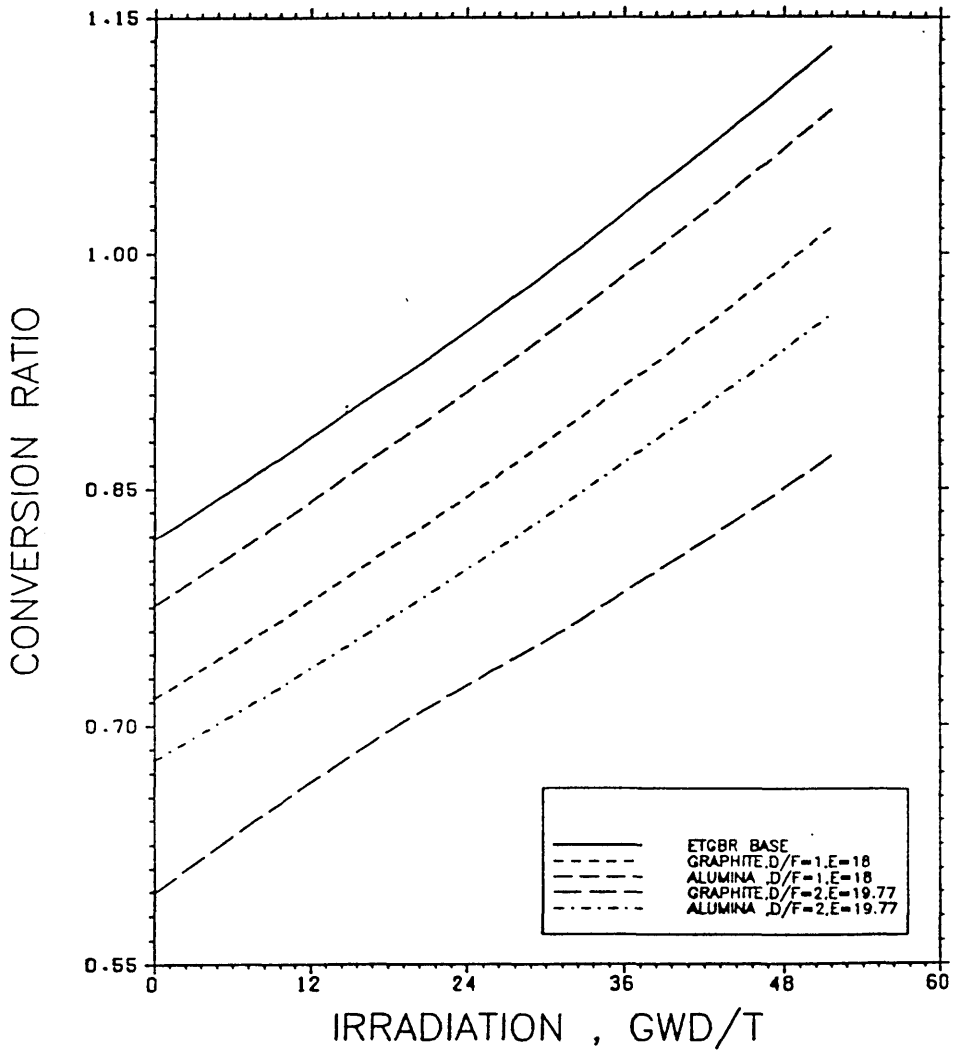

Figure 5.10. Conversion ratio versus time for ETGBR and DETGBRs

capture in U-238 giving more Pu throughout core life being the case with alumina dilution.

With regards to fissile inventory change over life, figures (5.11) and (5.12) show U-238, Pu-239, and Pu-240 isotope content of the ETGBR base case compared with the principal variants. Fissile utilization of the variants is shown in table (5.10). It is apparent that, with these fast systems, the end of life fissile content is too high to reprocess in a plant like THORP [6]. None of the fast systems studied conform to an end of life fissile enrichment of up to 5% and a dedicated fast reactor reprocessing plant is required (although blankets may be reprocessed in THORP). A low feed enrichment of about 7% may be the solution, but at that level, for a critical system, it is necessary to use graphite and to reject alumina. A V_m/V_f of about 20 may be required leading to a core more similar to an HTR.

Table (5.10): Fissile utilization of ETGBR and DETGBR unreflected leakage corrected bare core.

		Graphite		Alumina	
	Standard 16.5%	E=18.0% V_d/V_f =1	E=19.77% V_d/V_f =2	E=18.0% V_d/V_f =1	E=19.77% V_d/V_f =2
Feed Fissile	0.0842	0.0911	0.1008	0.0911	0.1008
Feed U+Pu	0.6132	0.6088	0.6133	0.6088	0.6133
Disch Fissile	0.0754	0.0798	0.0843	0.0811	0.0887
Disch U+Pu	0.5861	0.5867	0.5925	0.5842	0.5954
Feed kg/GWd	1.7510	2.3760	2.8130	2.1380	3.215
Feed kg/GW-yr	639.00	867.20	1026.8	780.40	1173.5
Disch kg/GWd	1.6403	2.1580	2.4360	1.9830	2.915
Disch kg/GW-yr	598.00	788.30	889.20	723.90	1063.9
consumption (kg/GW-yr)	41	78.9	137.6	56.5	109.5
(consump/Feed)	(6.41%)	(9.11%)	(13.4%)	(7.2%)	(9.3%)

Fissile contents throughout core life are shown in table (5.11); EOL fissile content for diluted cases are seen to be somewhat greater than for the standard ETGBR.

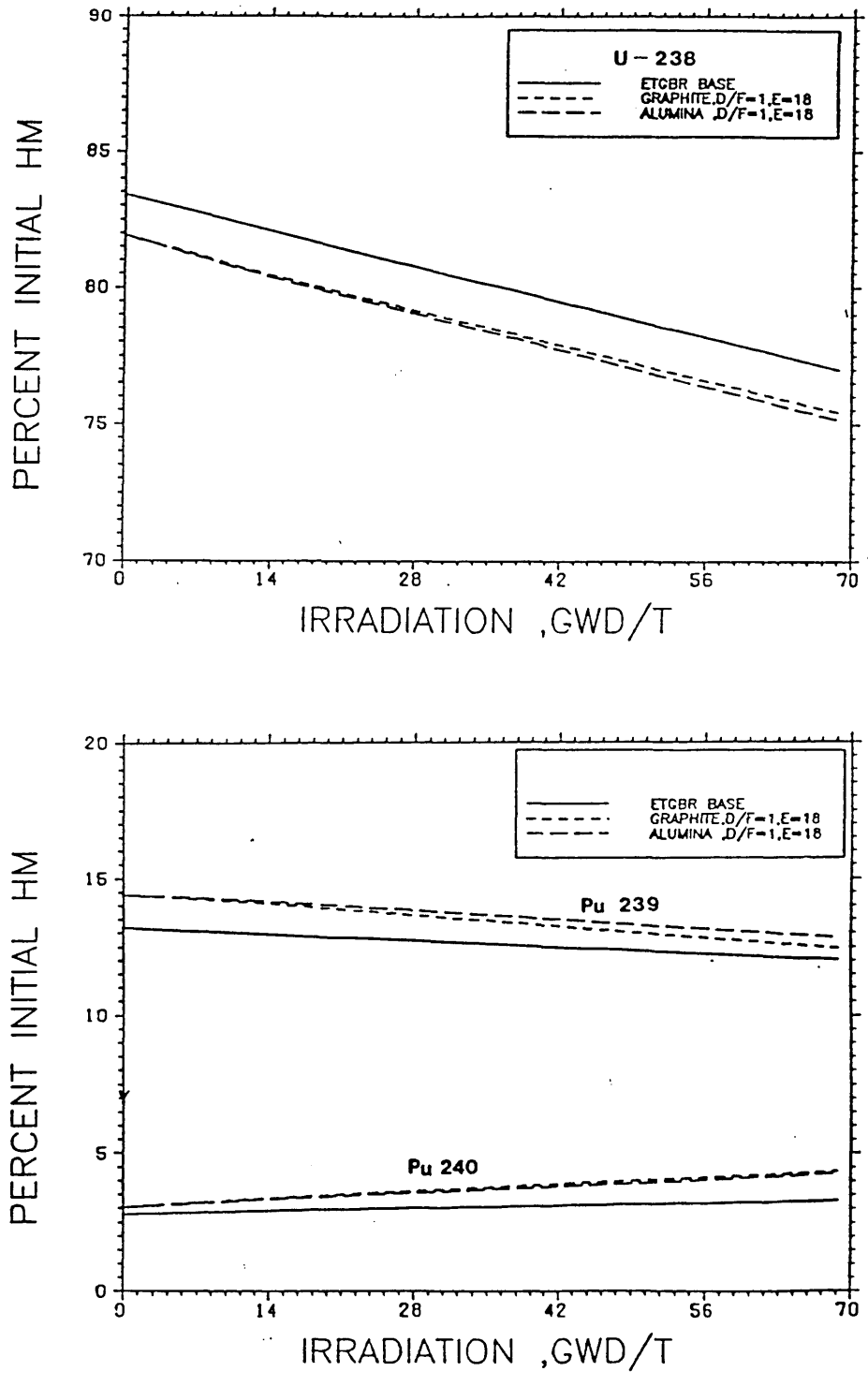

Figure 5.11. Major isotopic change versus time for ETGBR and for DETGBRs with V_d/V_f =1 and 18.0% enrichment

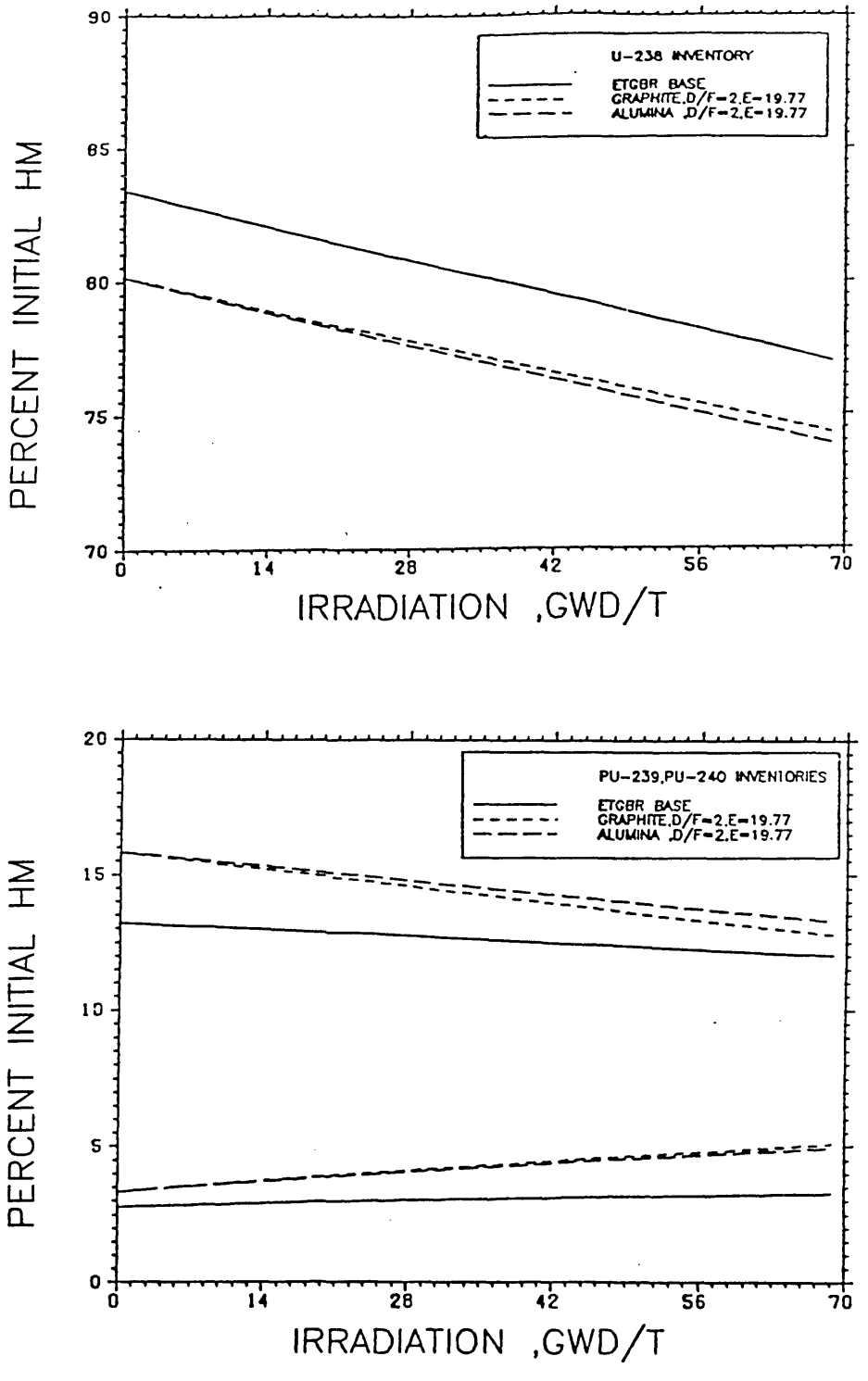

Figure 5.12. Major isotopic change versus time for ETGBR and for DETGBRs with V_d/V_f =2 and 19.77% enrichment

Table (5.11): Fissile content variation (%Fissile(239+241) in U+Pu) of ETBGR and DETGBR's.

	16.5%	18%		19.77%	
time (yrs.)	ETGBR	Graphite	Alumina	Graphite	Alumina
0	13.645	14.886	14.886	16.349	16.349
1	13.355	14.468	14.582	15.560	15.697
2	13.034	13.920	14.141	14.755	15.028
3	12.720	13.397	13.717	13.991	14.394
4	12.414	12.900	13.307	13.266	13.792
EOL	12.297	13.069	13.282	13.700	14.412
Dwell Time(days)	1641	1317	1464	1222	1069

Doppler Coefficient

The selected DETGBR variants were inspected to determine their Doppler coefficients of reactivity. This was accomplished by repeating the calculations at three different fuel temperatures. Table (5.12) shows the change in k_{eff} with temperature for the DETGBR variants compared with that of the base ETGBR while table (5.13) gives the derived coefficients of reactivity. The advantage that the softer spectrum of the DETGBRs gives in doppler coefficient is apparent. In the 1000-1500°K range, for example, the alumina DETGBR (19.77% enrichment, V_d/V_f =2) has a coefficient nearly 6 times greater than that of the standard ETGBR (of 16.5% enrichment). The Doppler coefficients of the DETGBRs resemble more those of a thermal reactor.

Table (5.12): Varition of k_{eff} with fuel temperature for the ETGBR and the major DETGBR variants.

	V_d/V_f	Enrichment (%Magnox)	Fuel Temperature(K) 500	1000	1500
Standard	-	16.5	1.0610	1.0577	1.0555
Graphite DETGBR	1.0	18.0	1.0866	1.0763	1.0693
Graphite DETGBR	2.0	19.77	1.1132	1.1013	1.0931
Alumina DETGBR	1.0	18.0	1.0773	1.0687	1.0630
Alumina DETGBR	2.0	19.77	1.0837	1.0731	1.0657

Table (5.13): Doppler coefficients of reactivity for ETGBR and DETGBRs ($T\frac{dk}{dT}$).

	V_d/V_f	Enrichment (%Magnox)	Doppler Coefficient (K^{-1}) 500-1000(K)	1000-1500(K)
Standard	-	16.5	-4.76×10^{-3}	-5.42×10^{-3}
Graphite DETGBR	1.0	18.0	-1.48×10^{-2}	-3.65×10^{-2}
Graphite DETGBR	2.0	19.77	-1.71×10^{-2}	-4.21×10^{-2}
Alumina DETGBR	1.0	18.0	-1.24×10^{-2}	-3.06×10^{-2}
Alumina DETGBR	2.0	19.77	-1.52×10^{-2}	-3.75×10^{-2}

5.4 VARIATIONS ON THE WHOLE REACTOR ETGBR AND DILUTED VARIANTS - 2 and 3 DIMENSIONAL STUDIES.

Dilution of core zones has already been discussed in the lattice-cell approximation. Enrichments selected were relatively high, since the cores were unreflected. In this section detailed spatial studies of the cores are reported, using WIMS-E/WSNAP; this gives the ability to vary reactor geometry.

The strategy is to first simplify a full ETGBR to study the effect of the different zones on the main neutronic indicators. The emergent geometries are shown in figure (5.13) and listed below.

(i) Core only with or without reflector.
(ii) Core with Radial Breeder.
(iii) Core with Axial Breeder.
(iv) Core with Axial and Radial Breeder.
(v) Two core zones with Axial and Radial Breeder.

5.4.1 The single zone reflected ETGBR

In this case, the cores are surrounded by an iron reflector; the thickness is fixed normally at that of a single ring of subassemblies. This case, with no breeder and high neutron leakage, could only be justified on grounds of high coversion ratio (CR) and long reactivity-life. However, this case represents a possible interesting comparison with internal breeder designs reported in chapter 6.

As before, the core contains 397 subassemblies of 169 rods each; control channels are not considered in the R-Z model, although in principle, they could be modelled in Hex-Z a geometry which has been used in some cases.

Data are generated as before using WIMS-D4 with leakage correction alone, or followed by the use of the whole reactor capability of WIMS-E, with the module WFORTE providing the link between the two codes (see chapters 2 and 4). Table (5.14) shows the consistency between the calculation of the bare core by the two WIMS methods. The reflector data were, generated using radial and axial slice's of the reactor wholly within WIMS-E.

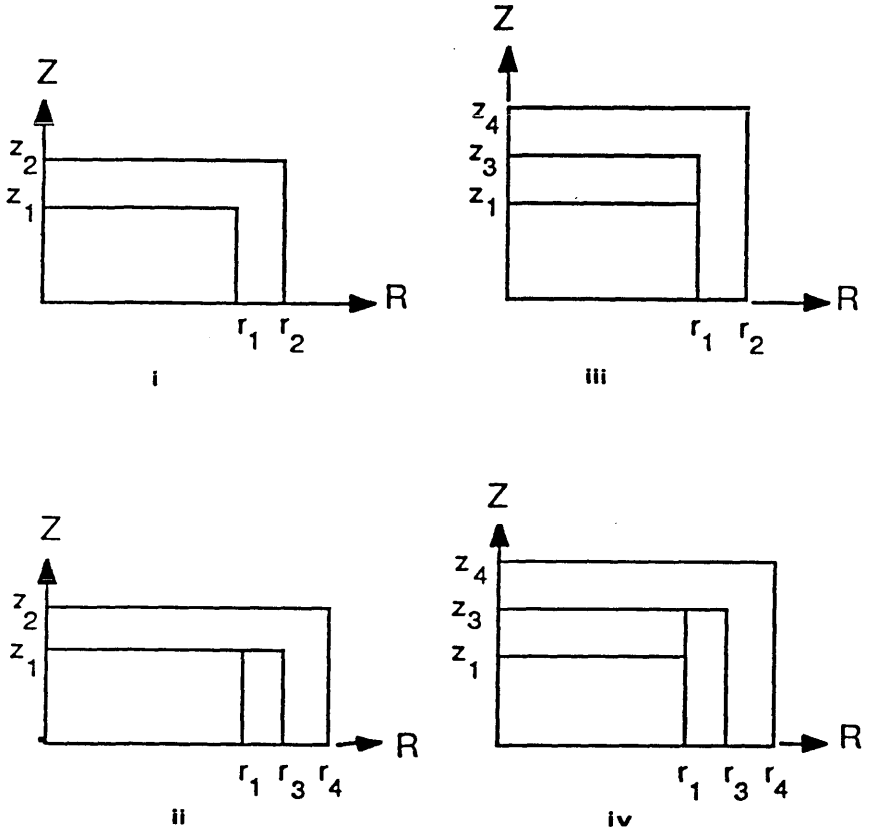

	Dimensions (cm.)	
	Standard	Diluted (D/F=2)
r_1	164.45	201.58
r_2	178.77	215.90
r_3	193.09	236.70
r_4	207.41	251.00
z_1	70.00	70.00
z_2	84.32	84.32
z_3	98.64	98.64
z_4	112.96	112.96

Figure 5.13. The RZ models and dimensions of the ETGBR and DETGBRs with no, partial, or full blankets

Table (5.14): BOL reactivity and conversion ratio of unreflected ETGBR core at 16.5 % Magnox Pu enrichment calculated by WIMS-D4 or WIMS-D4/WIMS-E routes. The reflected ETGBR is calculated by the WIMS-D4/WIMS-E route.

	unreflected		reflected	
	k_{eff} (BOL)	ICR	k_{eff} (BOL)	ICR
WIMS-D4 with leakage corrected lattice	1.0577	0.8180	-	-
WIMS-D4/WIMS-E	1.0611	0.8198	1.1437	0.8322

It is apparent that the lattice-cell model is adequate as far as reactivity and reaction rates are concerned for the unreflected ETGBR. A difference of 0.4%dk in reactivity and 0.2% in conversion ratio are found between the two routes.

The inclusion of a reflector, in this case a single ring of subassemblies of pure Iron, is seen to increase reactivity quite significantly, with a reflector worth of some 8%. A neutron balance performed on the reflected and on the unreflected core shows, as expected, leakage from the reactor to be reduced by adding the reflector, together with an increase in absorption in the core itself. The latter feature is due to reflected neutrons appearing in the core at lower energy. Table (5.15) shows the neutron balance.

Table (5.15): Neutron Balance of 16.5% standard ETGBR core. (normalized to 100 neutron's produced in system).

	Unreflected	Reflected
Neutron Produced	100.0	100.0
Neutrons Absorbed:		
In core	71.1	72.6
In Reflector	-	1.4
Neutrons Leaking	28.9	26.0

For the single core zone, 16.5% enrichment standard ETGBR, a reaction edit is shown in table (5.16). It is apparent that the inclusion of a reflector changes the reactions in such a way that the conversion ratio increases by some 2%. An increase in fertile capture is the main cause.

Table (5.16): Reaction rate edit of 16.5% standard ETGBR core.

	Reactions in Core Zone	
	Unreflected	Reflected
Absorbtions 238	6.56E04	1.28E05
Fissions 238	1.00E04	1.79E04
Absorbtions 239	6.83E04	1.33E05
Fissions 239	5.64E04	1.09E05
Absorbtions 240	6.09E03	1.16E04
Fissions 240	2.70E03	4.93E03
Absorbtions 241	3.65E03	7.19E03
Fissions 241	3.23E03	6.34E03
ICR	0.9823	1.0050

Adding a reflector to the standard ETGBR (16.5% Magnox Pu) is found to give excessive BOL reactivity (table 5.14), and it is necessary to re-investigate the enrichment required. Table (5.17) gives the results of the enrichment search and shows WIMS-E/WSNAP results for the single core zone ETGBR at different enrichment levels with and without reflectors. As before a choice of BOL k_{eff} of around 1.06 is considered reasonable; this gives a choice of 14.50% Magnox Pu for the core of the 'standard reflected' ETGBR. Reactivity of the reactor has been broken down further in order to investigate reactivity worths of the reflector

Table (5.17): Enrichment Search for Single-core zone standard ETGBR with no blankets- with and without reflector at BOL.

Enrichment	Effective multiplication factor, k_{eff}	
(%Magnox Pu)	unreflected	reflected
12.0	0.88088	0.94919
12.5	0.90237	0.97216
13.0	0.92346	0.99467
13.5	0.94417	1.01674
14.0	0.96450	1.03839
14.5	0.98446	1.05963

Table (5.18): Single core zone ETGBR (BOL) k_{eff} with partial and full reflectors.

	14.5%	14.25%
unreflected	0.9872	0.9771
radially ref.	0.9999	0.9898
axially ref.	1.0461	-
fully ref.	1.0603	1.0496

Table (5.19): Reflector reactivity worth of 14.5% standard ETGBR core at BOL.

	reactivity worth(dk%)
radial	1.27
axial	5.88
radial + axial	7.30

in both the radial and axial directions and the results are given in table (5.18); corresponding reactivity worths of the reflectors are also shown in table (5.19).

Burnup of Single Zone Reactors (whole reactor calculations)

Three single zone cases, one a standard ETGBR and two diluted (DETGBR) variants were studied in more detail; with and without reflectors. The burnup

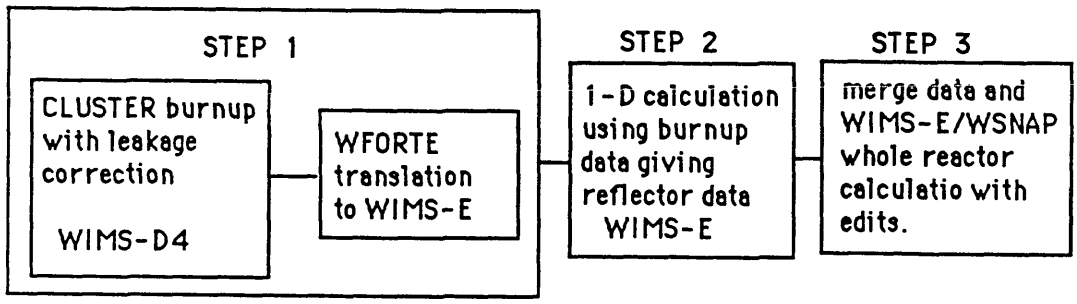

Figure (5.14): General burnup route followed for ETGBR and DETGBR whole reactors.

route followed for this and all following cases in this section is shown in figure (5.14).

Burnup was performed at a fixed core rating of 47.8 MW/t. The frequency of spectrum recalculation was increased as necessary to minimize the change in k_{eff} at each particular time (and within practical computer-time limitations). Normally, spectrum recalculations every 180 days were sufficient; one year intervals with longer dwell times gave closely similar results.

However, burnup at the selected 14.5% enrichment level gave a reactivity-life of a little over 8 years resulted and so some lower enrichments were also assessed.

It is seen from figure (5.15) and table (5.20) that k_{eff}, for less than about 14.0% initial enrichment, rises and then falls giving an extended reactivity-life. Burnup curves show little change between 13.75 and 14.50% enrichment as far as the reactivity-life is concerned (while 13.75 gives exactly 8 years, 14.50% gives about 9 years). The likely limitations in the WIMS methodology for fully fast systems should be noted.

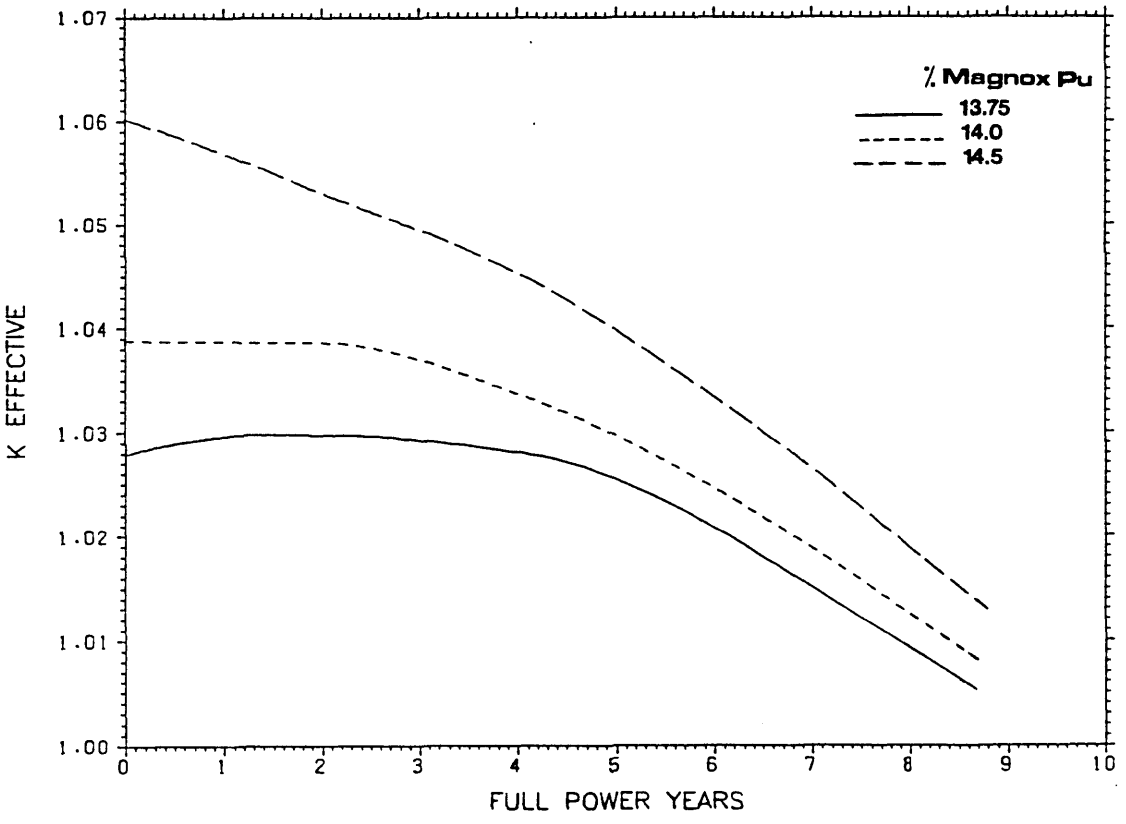

Figure 5.15. The burnup of the standard ETGBR at 3 enrichment levels

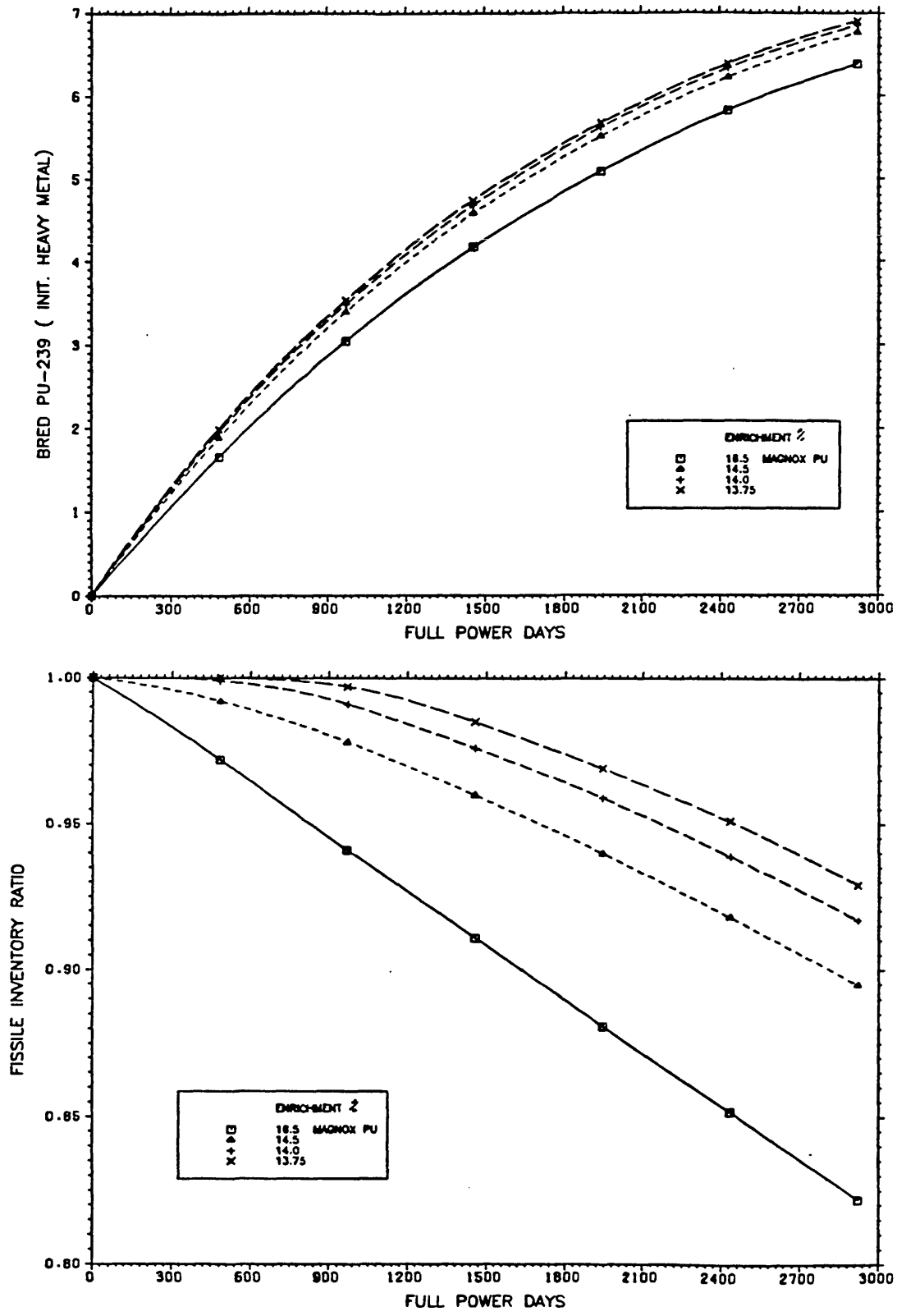

Figure 5.16.(a) The breeding of Pu-239 in the standard ETGBR at several enrichments.(b) The fissile inventory ratio for the same cases as in (a).

If the 'bred' Pu-239 inventory change is considered (figure (5.16a) and table (5.22)), it is clear that, at the lower enrichments, increased breeding results from greater absorption in U-238, in a 'softer' spectrum. Figure (5.16b) shows the corresponding fissile inventory ratio for the same enrichments; the same conclusions may be drawn.

Table (5.20):Reactivity rundown (k_{eff}) of Reflected Standard 14.5% ETGBR.

time(yrs.)	Enrichment (%Magnox Pu) 13.75	14.0	14.5
0	1.0279	1.0388	1.0602
1	1.0296	1.0387	1.0569
2	-	1.0386	-
3	-	-	-
4	1.0281	1.0337	1.0453
5	-	-	-
6	-	1.0246	1.0334
7	-	-	-
8	1.0093	1.0124	1.0188

Table (5.21): Reflector reactivity worth of standard 14.5% ETGBR

time(yrs)	Enrichment (%Magnox Pu) 13.75	14.0	14.5
0	7.11	7.18	7.30
1	7.21	7.27	7.38
2	-	7.37	-
3	-	-	-
4	7.51	7.54	7.61
5	-	-	-
6	-	7.71	7.76
7	-	-	-
8	7.84	7.86	7.90

Table (5.22): Pu-239 Bred in core for standard ETGBR at different enrichment as a function of irradiation time (% Initial Heavy Metal).

time (days)	Enrichment (%Magnox Pu) 16.5	14.5	14.0	13.75
0.0	0	0	0	0
487	1.66	1.89	1.96	1.99
974	3.05	3.40	3.49	3.54
1461	4.18	4.59	4.69	4.75
1948	5.09	5.51	5.62	5.67
2435	5.82	6.22	6.33	6.38
2922	6.38	6.76	6.85	6.90

It also appears that the reactivity-life of the fully reflected ETGBR and variants is influenced by the reflector. Referring to table (5.21), the reflector reactivity worth for the single zone standard ETGBR was shown to be 7.3% at BOL for the 14.5% enrichment case. However, should blankets be used in the normal way, the reflector worth would be reduced, due to the much reduced fluxes at the blanket outer edges.

It becomes worthwhile, in this context to repeat, for a select few ETGBR and DETGBR variants, a calculation of reactivity-lifetime and performance indicators. The lattice-cell calculations are taken as a first-hand guide keeping in mind a figure of some 8% reactivity-worth for the reflector.

5.4.2 The Single zone diluted variants

It was seen that the purely fast standard ETGBR had quite considerable leakage. This is both a waste of neutron economy even at the reasonably low 14.5% enrichment, and implies the need for more than the single row of steel reflector subassemblies considered. The very high reflector worth of the 'single-zone' ETGBR has been noted. It is of interest to examine reflector worth and burnup details for 'single zone' (no blanket) diluted cases (DETGBR). As before graphite and alumina are considered as diluents.

As for the standard ETGBR cases, the initial enrichment was varied until a value for k_{eff} (BOL) of about 1.06 was obtained. Table (5.23) shows that the resulting enrichments were 16.25% Magnox Pu for the graphite diluted ETGBR and 18.0% Magnox Pu for the alumina diluted ETGBR.

Table (5.23): BOL reactivity (k_{eff}) for the two diluted ETGBR's.

	k_{eff} (BOL)		
ETGBR Variant	Unreflected	Reflected	Ref worth(%)
Graphite(16.25%)	1.0047	1.0551	5.04
Alumina (18.0%)	1.0152	1.0508	3.56

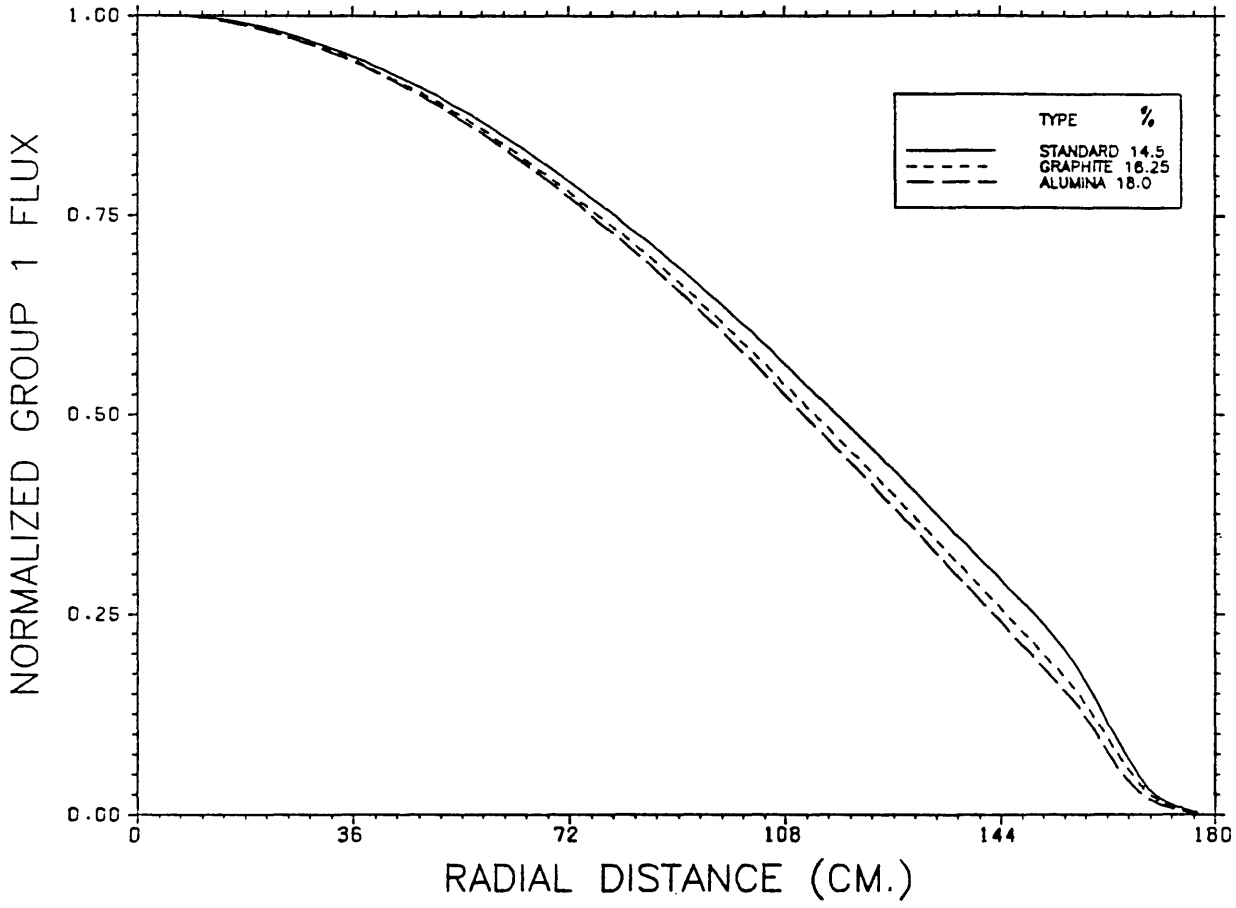

Figure 5.17. The radial flux profile (group 1) for the ETGBR and DETGBRs (normalized to mid-core value of 1.0)

It is clear (from table (5.23)) that reflector worth is much reduced in the diluted ETGBR cases. This is especially the case for alumina dilution; due to changes in neutron transport (greater loss of neutrons by non-fuel absorption in the core). Additionally, figure (5.17) shows the reactor midplane radial flux profile for the three variants. Changes in flux and flux gradient are apparent near the reflector of the diluted variants.

Calculated burnup behaviour differs substantailly from that of the standard ETGBR. From the small change in dilution introduced ($V_d/V_f = 2.0$), a large reduction in reactivity-life results compared with the standard cases (about which there are some reservations on the validity using WIMS). Table (5.24) shows the burnup of both the graphite-diluted-ETGBR at 16.25% enrichment and the alumina-diluted-ETGBR at 18.0% enrichment.

Table (5.24): Reactivity rundown of diluted ETGBR variants at $V_d/V_f = 2$ (WIMS Benoist leakage treatment)

	Effective multiplication factor, k_{eff}			
	Graphite		Alumina	
time(yrs)	unreflected	reflected	unreflected	reflected
0	1.0047	1.0551	1.0152	1.0508
1	0.9785	1.0279	0.9924	1.0273
2	0.9574	1.0060	0.9738	1.0081

Reactivity-lives of about two years are suggested for both fully reflected diluted concepts, corresponding to around 35 GWd/t burnup at a power rating of 47.8 MW/t.

The fissile usage was considered briefly for each of the whole cores. Figure (5.18) shows the fissile-inventory-ratio change over one year of life for the 14% standard ETGBR compared with the 16.25% graphite and 18% alumina diluted ETGBR cores (at V_d/V_f =2). The same information is contained in table (5.25).

It is apparent that the more downgraded the fast spectrum, the higher the net consumption of fissile material. With the graphite case, in fact, some 30% of

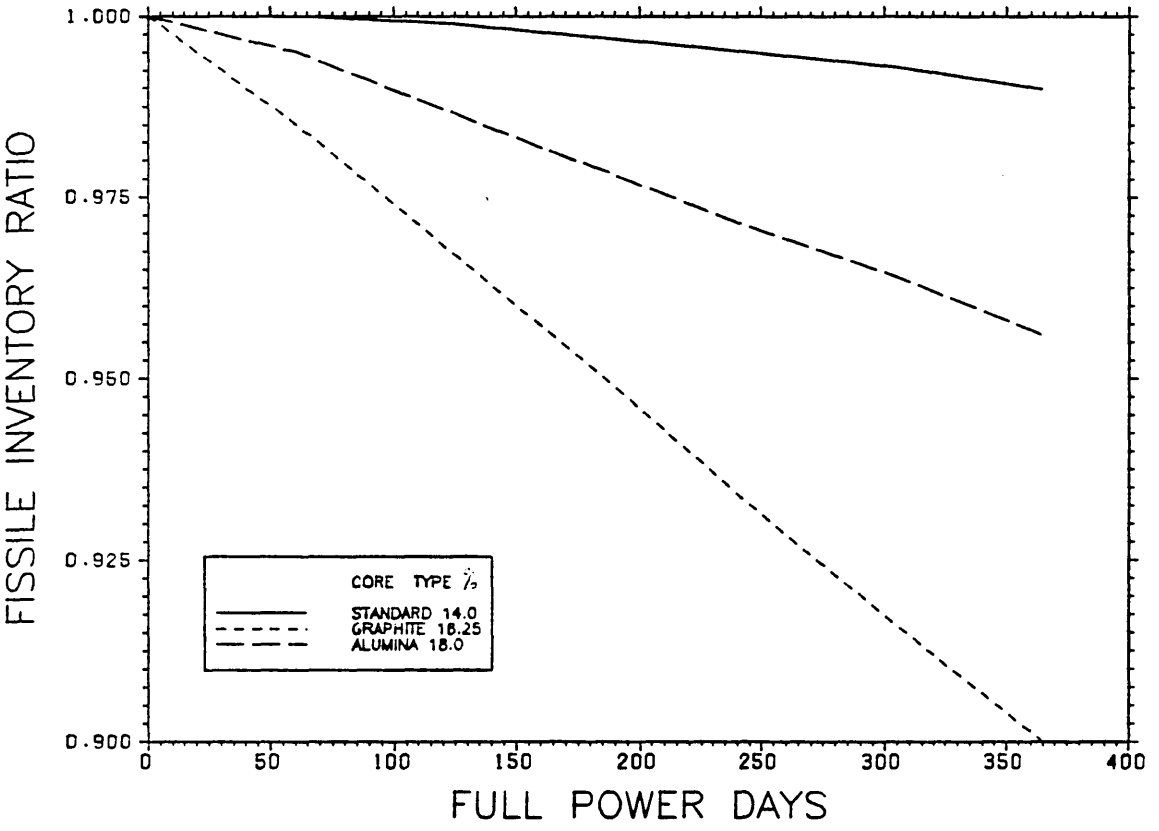

Figure 5.18. The fissile inventory ratio versus time for the ETGBR and DETGBRs.

Table (5.25): Fissile inventory ratio (FIR) variation through one year for the ETGBR and DETGBR variants.

	Fissile Inventory Ratio		
time(days)	Standard 14.0%	Graphite 16.25%	Alumina 18.0%
0	1.0	1.0	1.0
60.83	1.0007	0.9854	0.9949
121.66	0.9989	0.9680	0.9871
182.49	0.9969	0.9507	0.9794
243.32	0.9947	0.9335	0.9716
304.15	0.9926	0.9164	0.9639
365	0.9903	0.8996	0.9563

the original Pu-239 is consumed with bred isotopes making up about 23% of the fissile at 1 year. For both the standard ETGBR (14.0%) and the Alumina (18.0%) case, only 15.0% of the original Pu-239 is used and the year old fissile material contains 16.0% and 13.0% bred Pu-239 and Pu-241 respectively.

5.4.3 Partially and Fully Blanketted ETGBR and its Diluted Variants

Leakage is quite high in the ETGBR fast-spectrum core. The reflected reactor has a high value of reactivity due to the neutrons being reflected back into the core. It is not desirable, for safety reasons, to work with a fast reactor of such a high reactivity. The more practical and usual method of utilizing the high leakage is to introduce breeder zones; as a first step surrounding the core. Of course, this has the inherent advantage of free breeding of fissile fuel. Partial Blanketting is considered on the economic supposition that only a small amount of breeder will be required. The choice of radial or axial partial blankets may be a neutronic issue, as well as a reactor engineering and economic issue.

Radially-Blanketted ETGBR and Diluted Variants

A partially blanketted ETGBR may be the answer to the economic problems that seems to confront full-fledged breeders. A reduction in the bred fissile material results and this is in-line with the present excess of fissile material worldwide.

A radially-blanketted core has the advantage of seperate subassemblies for the breeders allowing them to have their independent in-core dwell period in addition to individual access. On the other hand, the unblanketted axial direction may be a wastefull design allowing too much unused leakage neutrons. In any event it is worth studying the radially-partially-blanketted ETGBR and to note the effect of core dilution on the reactor performance.

Two possible designs were studied, one with a single-core zone, and a two core zone case. The second case may be neccessary for power flattening.

The thickness of reflector used is kept, as in all cases, at 14.32 cm., equivalent to one ring of subassemblies radially. The size of the reactor depends on whether it is standard or diluted as shown in table (5.26).

Table (5.26): Radial size (cm.) of standard ETGBR and diluted DETGBR.

Radius of :	Standard	Diluted(V_d/V_f =2)
core zone 1	121.78	149.22
core zone 2	164.45	201.58
Rad. Blanket	193.09	236.70
Rad. Reflector	207.41	251.0

Most of the neutronic edits are performed using an R-Z model of the reactor. For the power distribution, however, it is convenient to use a Hex-Z model.

In figure (5.19) the power maps of the reflected single core zone ETGBRs and DETGBRs are shown (BOL) at 1670 MW(t). The power maps of the radially-blanketted ETGBRs are shown in figure (5.20) for the same three cases and it is shown that the radial power peaking factors are reduced from 1.897 to 1.734, from 1.939 to 1.719, and from 1.995 to 1.737 for the standard, graphite and alumina cases respectively. It appears that the inclusion of a radial blanket gives rise to some measure of power flattening. Figure (5.21) shows the power maps for radially-blanketted two core zone cases. The radial power peaking factors are shown to be further reduced, and are 1.527, 1.633, and 1.649 for the three cases. A further

note that must be made is that the subassembly powers shown do not differ greatly between graphite and alumina cases due to their similar fission rate distributions.

The burnup behaviour for the radially blanketted ETGBR is not significantly different from the single zone core unblanketted ETGBR. In both cases a lengthy single batch reactivity-lifetime of over 10 years is indicated; a small difference results from an increase in the neutrons being reflected back into the core. Table (5.27) shows the reactivity rundown of the standard ETGBR with and without a radial blanket.

Table (5.27): Reactivity rundown of standard 14.5% ETGBR core with and without a radial blanket.

	Effective multiplication factor, k_{eff}	
time(years)	Core only	Core plus Radial Blanket
0	1.0602	1.0621
1	1.0569	-
2	-	1.0571
4	1.0453	1.0489
6	1.0334	1.0377
8	1.0188	1.0240

In the case of diluted ETGBR variants, with a radial blanket only, once again the burnup behaviour does not differ significantly from the core-only cases. This is shown in table (5.28) where reactivity-lifetimes of some 2 years are indicated.

Use of a radial blanket only implies increased leakage in the axial direction. Accordingly, a calculation was performed with the axial reflector thickness increased from 14.32 to 28.64 cm. in order to assess the effect on reactivity and fluxes. The alumina diluted core was considered, and a change of k_{eff} from 1.0512 to 1.0601 was observed; a significant but not a major change in the context of these survey calculations. Fluxes in the axial direction are shown in figure (5.22). It is seen that, for a doubling of the axial reflector thickness, group 1 neutron flux

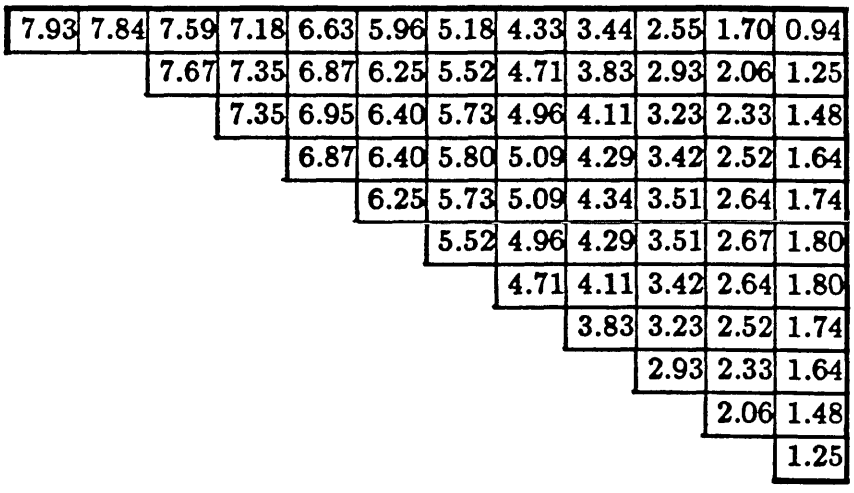

7.93	7.84	7.59	7.18	6.63	5.96	5.18	4.33	3.44	2.55	1.70	0.94
		7.67	7.35	6.87	6.25	5.52	4.71	3.83	2.93	2.06	1.25
			7.35	6.95	6.40	5.73	4.96	4.11	3.23	2.33	1.48
				6.87	6.40	5.80	5.09	4.29	3.42	2.52	1.64
					6.25	5.73	5.09	4.34	3.51	2.64	1.74
						5.52	4.96	4.29	3.51	2.67	1.80
							4.71	4.11	3.42	2.64	1.80
								3.83	3.23	2.52	1.74
									2.93	2.33	1.64
										2.06	1.48
											1.25

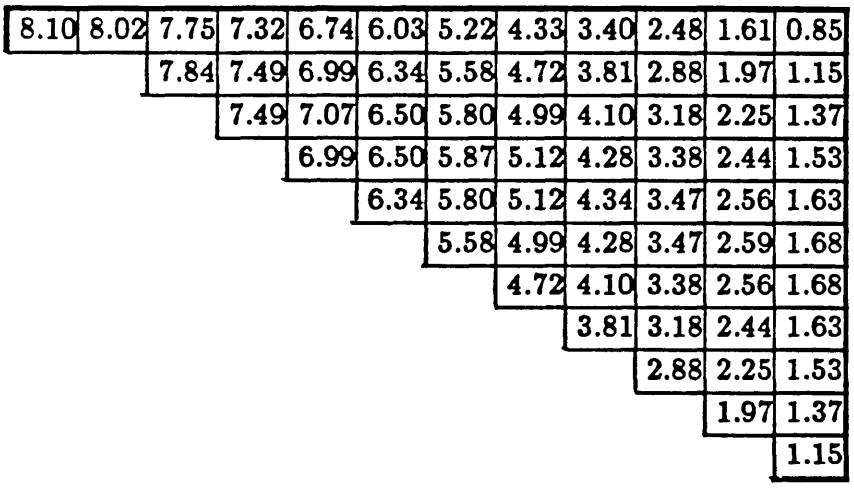

8.10	8.02	7.75	7.32	6.74	6.03	5.22	4.33	3.40	2.48	1.61	0.85
		7.84	7.49	6.99	6.34	5.58	4.72	3.81	2.88	1.97	1.15
			7.49	7.07	6.50	5.80	4.99	4.10	3.18	2.25	1.37
				6.99	6.50	5.87	5.12	4.28	3.38	2.44	1.53
					6.34	5.80	5.12	4.34	3.47	2.56	1.63
						5.58	4.99	4.28	3.47	2.59	1.68
							4.72	4.10	3.38	2.56	1.68
								3.81	3.18	2.44	1.63
									2.88	2.25	1.53
										1.97	1.37
											1.15

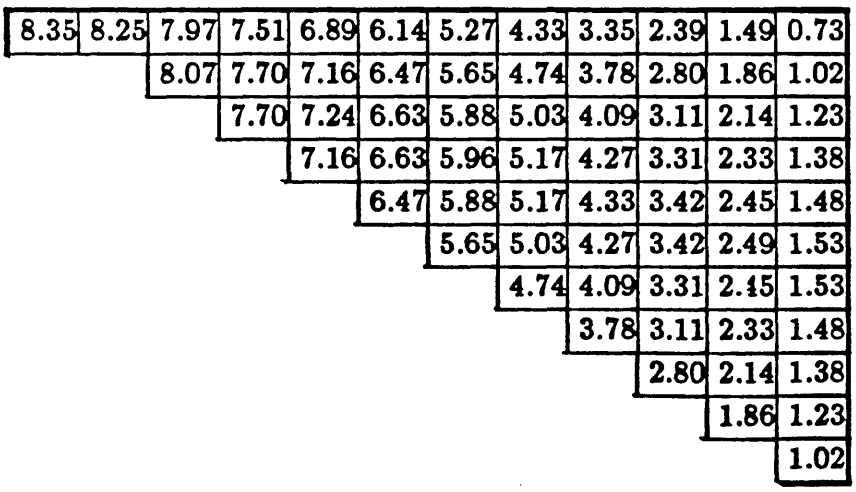

8.35	8.25	7.97	7.51	6.89	6.14	5.27	4.33	3.35	2.39	1.49	0.73
		8.07	7.70	7.16	6.47	5.65	4.74	3.78	2.80	1.86	1.02
			7.70	7.24	6.63	5.88	5.03	4.09	3.11	2.14	1.23
				7.16	6.63	5.96	5.17	4.27	3.31	2.33	1.38
					6.47	5.88	5.17	4.33	3.42	2.45	1.48
						5.65	5.03	4.27	3.42	2.49	1.53
							4.74	4.09	3.31	2.45	1.53
								3.78	3.11	2.33	1.48
									2.80	2.14	1.38
										1.86	1.23
											1.02

Figure 5.19. Power maps of single zone core reflected: Standard ETGBR, graphite DETGBR, and alumina DETGBR. (MW)

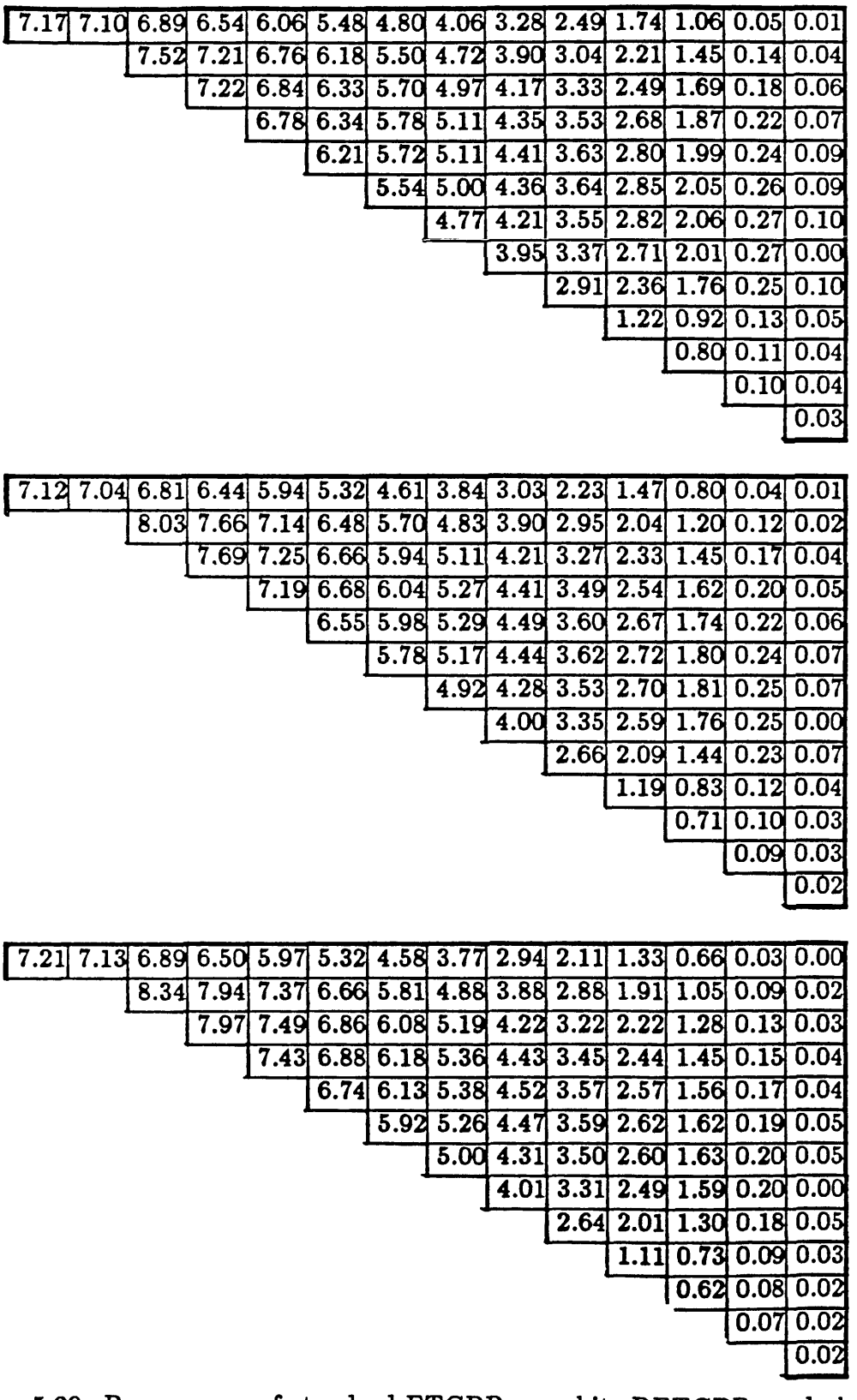

7.17	7.10	6.89	6.54	6.06	5.48	4.80	4.06	3.28	2.49	1.74	1.06	0.05	0.01
		7.52	7.21	6.76	6.18	5.50	4.72	3.90	3.04	2.21	1.45	0.14	0.04
			7.22	6.84	6.33	5.70	4.97	4.17	3.33	2.49	1.69	0.18	0.06
				6.78	6.34	5.78	5.11	4.35	3.53	2.68	1.87	0.22	0.07
					6.21	5.72	5.11	4.41	3.63	2.80	1.99	0.24	0.09
						5.54	5.00	4.36	3.64	2.85	2.05	0.26	0.09
							4.77	4.21	3.55	2.82	2.06	0.27	0.10
								3.95	3.37	2.71	2.01	0.27	0.00
									2.91	2.36	1.76	0.25	0.10
										1.22	0.92	0.13	0.05
											0.80	0.11	0.04
												0.10	0.04
													0.03

7.12	7.04	6.81	6.44	5.94	5.32	4.61	3.84	3.03	2.23	1.47	0.80	0.04	0.01
		8.03	7.66	7.14	6.48	5.70	4.83	3.90	2.95	2.04	1.20	0.12	0.02
			7.69	7.25	6.66	5.94	5.11	4.21	3.27	2.33	1.45	0.17	0.04
				7.19	6.68	6.04	5.27	4.41	3.49	2.54	1.62	0.20	0.05
					6.55	5.98	5.29	4.49	3.60	2.67	1.74	0.22	0.06
						5.78	5.17	4.44	3.62	2.72	1.80	0.24	0.07
							4.92	4.28	3.53	2.70	1.81	0.25	0.07
								4.00	3.35	2.59	1.76	0.25	0.00
									2.66	2.09	1.44	0.23	0.07
										1.19	0.83	0.12	0.04
											0.71	0.10	0.03
												0.09	0.03
													0.02

7.21	7.13	6.89	6.50	5.97	5.32	4.58	3.77	2.94	2.11	1.33	0.66	0.03	0.00
		8.34	7.94	7.37	6.66	5.81	4.88	3.88	2.88	1.91	1.05	0.09	0.02
			7.97	7.49	6.86	6.08	5.19	4.22	3.22	2.22	1.28	0.13	0.03
				7.43	6.88	6.18	5.36	4.43	3.45	2.44	1.45	0.15	0.04
					6.74	6.13	5.38	4.52	3.57	2.57	1.56	0.17	0.04
						5.92	5.26	4.47	3.59	2.62	1.62	0.19	0.05
							5.00	4.31	3.50	2.60	1.63	0.20	0.05
								4.01	3.31	2.49	1.59	0.20	0.00
									2.64	2.01	1.30	0.18	0.05
										1.11	0.73	0.09	0.03
											0.62	0.08	0.02
												0.07	0.02
													0.02

Figure 5.20. Power maps of standard ETGBR, graphite DETGBR, and alumina DETGBR fully reflected single zone cores with radial blanket. (MW)

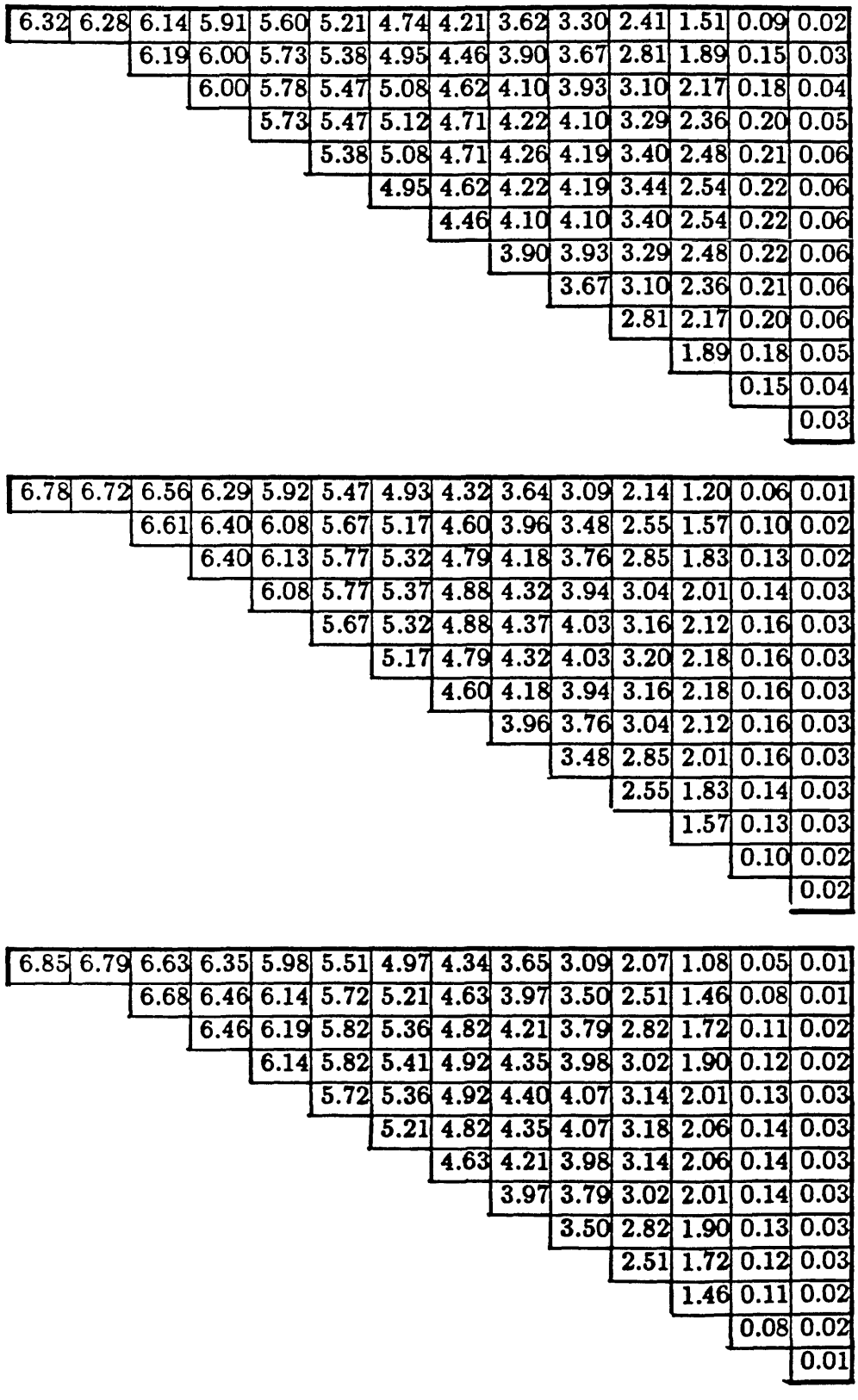

Figure 5.21. Power maps of standard ETGBR, graphite DETGBR, and alumina DETGBR fully reflected two zone cores with radial blanket. (MW)

Table (5.28): Reactivity rundown of Diluted ETGBR variant cores with and without radial blankets (16.25% for graphite and 18% enrichment for alumina.

	Effective multiplication factor, k_{eff}			
	Core only		With Radial blanket	
time(years)	Graphite	Alumina	Graphite	Alumina
0	1.0551	1.0508	1.0552	1.0512
1	1.0279	1.0273	-	-
2	1.0060	1.0081	1.0071	1.0086
4	-	-	-	0.9739

is reduced in the outermost regions of the core and increases in the inner regions. This indicates the need for a thicker reflector.

From the engineering standpoint a stainless-steel restraint may be required if upward flow, with its safety advantages, is to be adopted and possible core levitation problems eased.

Axially Blanketted ETGBR and Diluted Variants

An ETGBR with an axial blanket only will also provide partial breeding. In such a design, however, core and blanket pellets are contained in the same pins and are discharged together in the whole subassembly. An axial blanket has the advantage of design flexibility; being as thin or thick as required above and below the core pellets. The issue of core levitation, although beyond the scope of this thesis, may be assumed to be eased by the heavier axial subassemblies.

It does also add on further power to the output of each subassembly. This is shown by the power maps of the axially blanketted ETGBR and its two diluted variants in figure (5.23) (note the central subassembly power rose to 9.39 MW from a value of 7.93 for the standard reflected ETGBR).

With an axial breeder there is (table (5.29)) a small gain in of reactivity, leading to a slightly greater reactivity-life compared with core only or core with axial breeder cases. Reactivity worth of the axial breeder was shown to be greatest (refer back to table 5.19 for example), accounting for the observed behaviour.

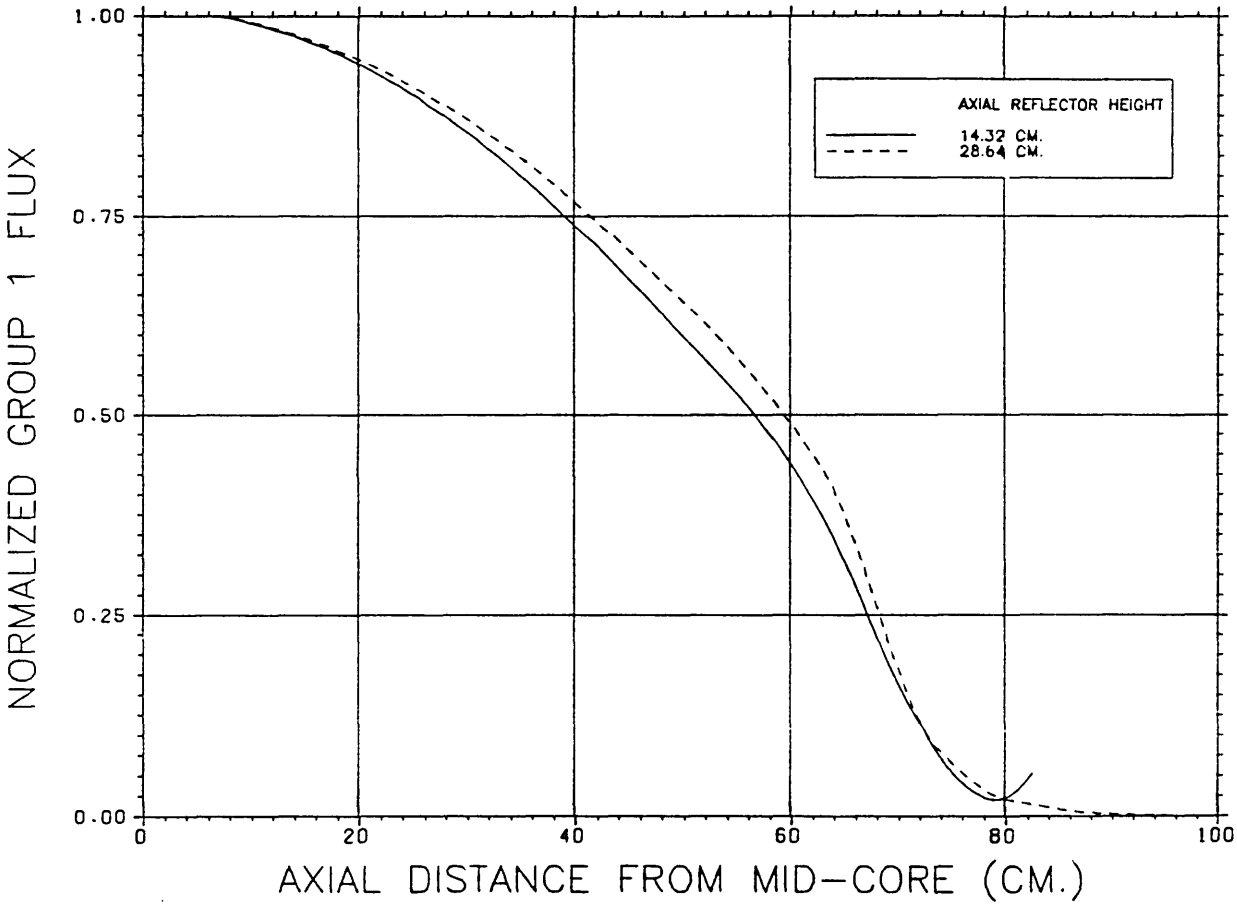

Figure 5.22. Dependence of the ETGBR axial flux profile on axial reflector thickness (normalized group 1 flux of 1.0 at centre).

Table (5.29): Reactivity rundown of axially blanketted standard ETGBR core versus unblanketted same core.

time(years)	core only	core + AB
0	1.0602	1.0648
1	1.0569	-
2	-	1.0594
4	1.0453	1.0512
6	1.0334	1.0399
8	1.0188	1.0262

For the diluted cases also, an axial breeder slightly increases the reactivity-life compared with core only or core with radial breeder, as shown in table (5.30).

Table (5.30): Reactivity rundown of axially blanketted diluted ETGBR cores versus unblanketted same cores.

	core only		core + AB	
time(yrs)	Graphite	Alumina	Graphite	Alumina
0	1.0551	1.0508	1.0570	1.0461
1	1.0279	1.0230	-	-
2	1.0060	1.0081	1.0095	1.0100
4	-	-	0.9683	0.9755

Figure (5.23) shows power maps of the axially-blanketted ETGBR and its diluted variants. There is increased power output, compared with unblanketted cores or cores with radial blankets, for the inner subassemblies due to the presence of the axial blanket leading to increased neutron reflection (up to 30% increase for the highest rated centre subassembly for the same total power). The radial power peaking factors are 2.246, 2.120, 2.187 for the 14.5% standard, 16.25% graphite, and 18% alumina ETGBRs respectively (compared to 1.734, 1.719, and 1.737 for the same three cases with radial blankets).

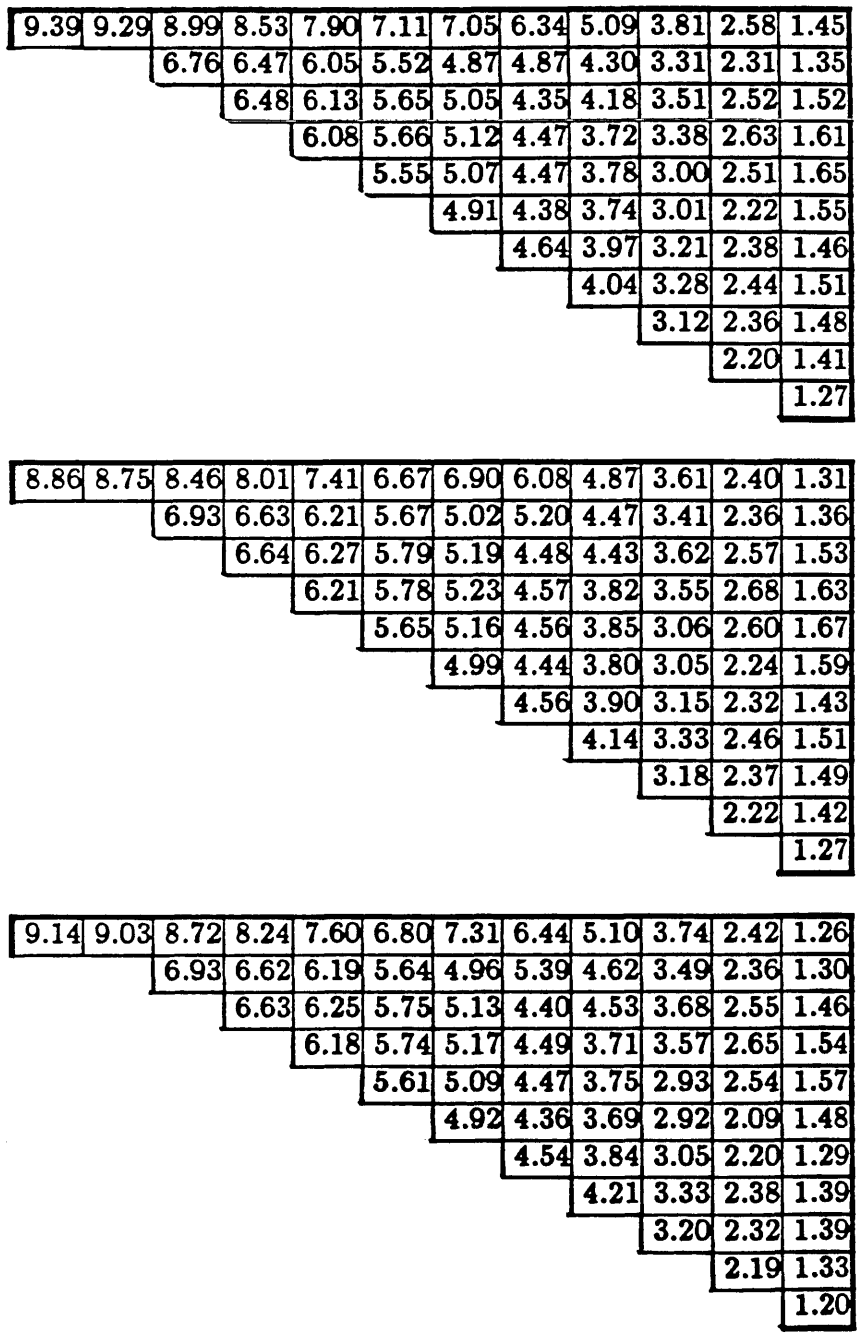

9.39	9.29	8.99	8.53	7.90	7.11	7.05	6.34	5.09	3.81	2.58	1.45
		6.76	6.47	6.05	5.52	4.87	4.87	4.30	3.31	2.31	1.35
			6.48	6.13	5.65	5.05	4.35	4.18	3.51	2.52	1.52
				6.08	5.66	5.12	4.47	3.72	3.38	2.63	1.61
					5.55	5.07	4.47	3.78	3.00	2.51	1.65
						4.91	4.38	3.74	3.01	2.22	1.55
							4.64	3.97	3.21	2.38	1.46
								4.04	3.28	2.44	1.51
									3.12	2.36	1.48
										2.20	1.41
											1.27

8.86	8.75	8.46	8.01	7.41	6.67	6.90	6.08	4.87	3.61	2.40	1.31
		6.93	6.63	6.21	5.67	5.02	5.20	4.47	3.41	2.36	1.36
			6.64	6.27	5.79	5.19	4.48	4.43	3.62	2.57	1.53
				6.21	5.78	5.23	4.57	3.82	3.55	2.68	1.63
					5.65	5.16	4.56	3.85	3.06	2.60	1.67
						4.99	4.44	3.80	3.05	2.24	1.59
							4.56	3.90	3.15	2.32	1.43
								4.14	3.33	2.46	1.51
									3.18	2.37	1.49
										2.22	1.42
											1.27

9.14	9.03	8.72	8.24	7.60	6.80	7.31	6.44	5.10	3.74	2.42	1.26
		6.93	6.62	6.19	5.64	4.96	5.39	4.62	3.49	2.36	1.30
			6.63	6.25	5.75	5.13	4.40	4.53	3.68	2.55	1.46
				6.18	5.74	5.17	4.49	3.71	3.57	2.65	1.54
					5.61	5.09	4.47	3.75	2.93	2.54	1.57
						4.92	4.36	3.69	2.92	2.09	1.48
							4.54	3.84	3.05	2.20	1.29
								4.21	3.33	2.38	1.39
									3.20	2.32	1.39
										2.19	1.33
											1.20

Figure 5.23. Power maps of axially-blanketted (a) standard 14.5% ETGBR, (b) 16.25% graphite DETGBR, and (c) 18% alumina DETGBR. (MW)

The Fully Blanketted ETGBR and Diluted Variants

A fully blanketted ETGBR is the next logical step from the partial blanketted cases studied. Increased breeding ratios and reduced total reflector worths are apparent benefits. If fissile demand justifies it, then a fully blanketted ETGBR might be warranted.

For simplicity a single zone core is considered first. Power maps of the fully blanketted standard and diluted ETGBR variants are shown in figure (5.24). Radial power peaking factors of 1.828 for the standard, 1.922 for the graphite, and 1.976 for the alumina variants were calculated. Further power flattening, by better zone enrichment selection, may be required and is especially apparent for the diluted core cases.

In figure (5.25) the introduction of a second core zone is shown to reduce radial peaking. For the graphite diluted core, with blankets, an enrichment of 18.0% Magnox Pu was adopted for the outer core, and 19% for the alumina diluted core. Resultant radial power peaking factors were 1.315, 1.634, and 1.650 for the three cases shown in the figure; a measure of power flattening has been accomplished.

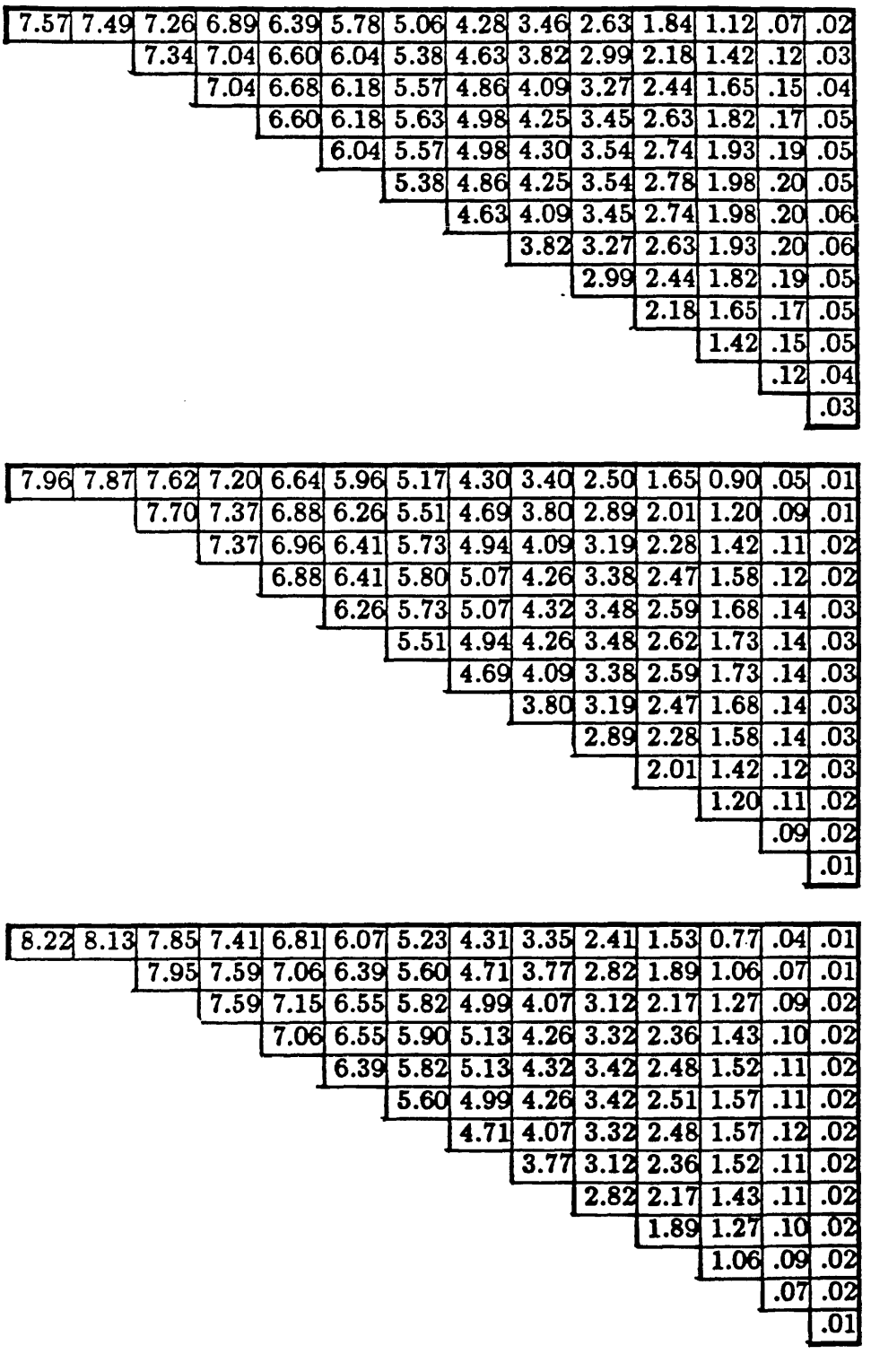

7.57	7.49	7.26	6.89	6.39	5.78	5.06	4.28	3.46	2.63	1.84	1.12	.07	.02
		7.34	7.04	6.60	6.04	5.38	4.63	3.82	2.99	2.18	1.42	.12	.03
			7.04	6.68	6.18	5.57	4.86	4.09	3.27	2.44	1.65	.15	.04
				6.60	6.18	5.63	4.98	4.25	3.45	2.63	1.82	.17	.05
					6.04	5.57	4.98	4.30	3.54	2.74	1.93	.19	.05
						5.38	4.86	4.25	3.54	2.78	1.98	.20	.05
							4.63	4.09	3.45	2.74	1.98	.20	.06
								3.82	3.27	2.63	1.93	.20	.06
									2.99	2.44	1.82	.19	.05
										2.18	1.65	.17	.05
											1.42	.15	.05
												.12	.04
													.03

7.96	7.87	7.62	7.20	6.64	5.96	5.17	4.30	3.40	2.50	1.65	0.90	.05	.01
		7.70	7.37	6.88	6.26	5.51	4.69	3.80	2.89	2.01	1.20	.09	.01
			7.37	6.96	6.41	5.73	4.94	4.09	3.19	2.28	1.42	.11	.02
				6.88	6.41	5.80	5.07	4.26	3.38	2.47	1.58	.12	.02
					6.26	5.73	5.07	4.32	3.48	2.59	1.68	.14	.03
						5.51	4.94	4.26	3.48	2.62	1.73	.14	.03
							4.69	4.09	3.38	2.59	1.73	.14	.03
								3.80	3.19	2.47	1.68	.14	.03
									2.89	2.28	1.58	.14	.03
										2.01	1.42	.12	.03
											1.20	.11	.02
												.09	.02
													.01

8.22	8.13	7.85	7.41	6.81	6.07	5.23	4.31	3.35	2.41	1.53	0.77	.04	.01
		7.95	7.59	7.06	6.39	5.60	4.71	3.77	2.82	1.89	1.06	.07	.01
			7.59	7.15	6.55	5.82	4.99	4.07	3.12	2.17	1.27	.09	.02
				7.06	6.55	5.90	5.13	4.26	3.32	2.36	1.43	.10	.02
					6.39	5.82	5.13	4.32	3.42	2.48	1.52	.11	.02
						5.60	4.99	4.26	3.42	2.51	1.57	.11	.02
							4.71	4.07	3.32	2.48	1.57	.12	.02
								3.77	3.12	2.36	1.52	.11	.02
									2.82	2.17	1.43	.11	.02
										1.89	1.27	.10	.02
											1.06	.09	.02
												.07	.02
													.01

Figure 5.24. Power maps of fully-blanketted single zone cores. (a) standard 14.5% (k_{eff} =1.069), (b) graphite 16.25% (k_{eff} =1.060), and (c) alumina 18% (k_{eff} =1.055). (MW)

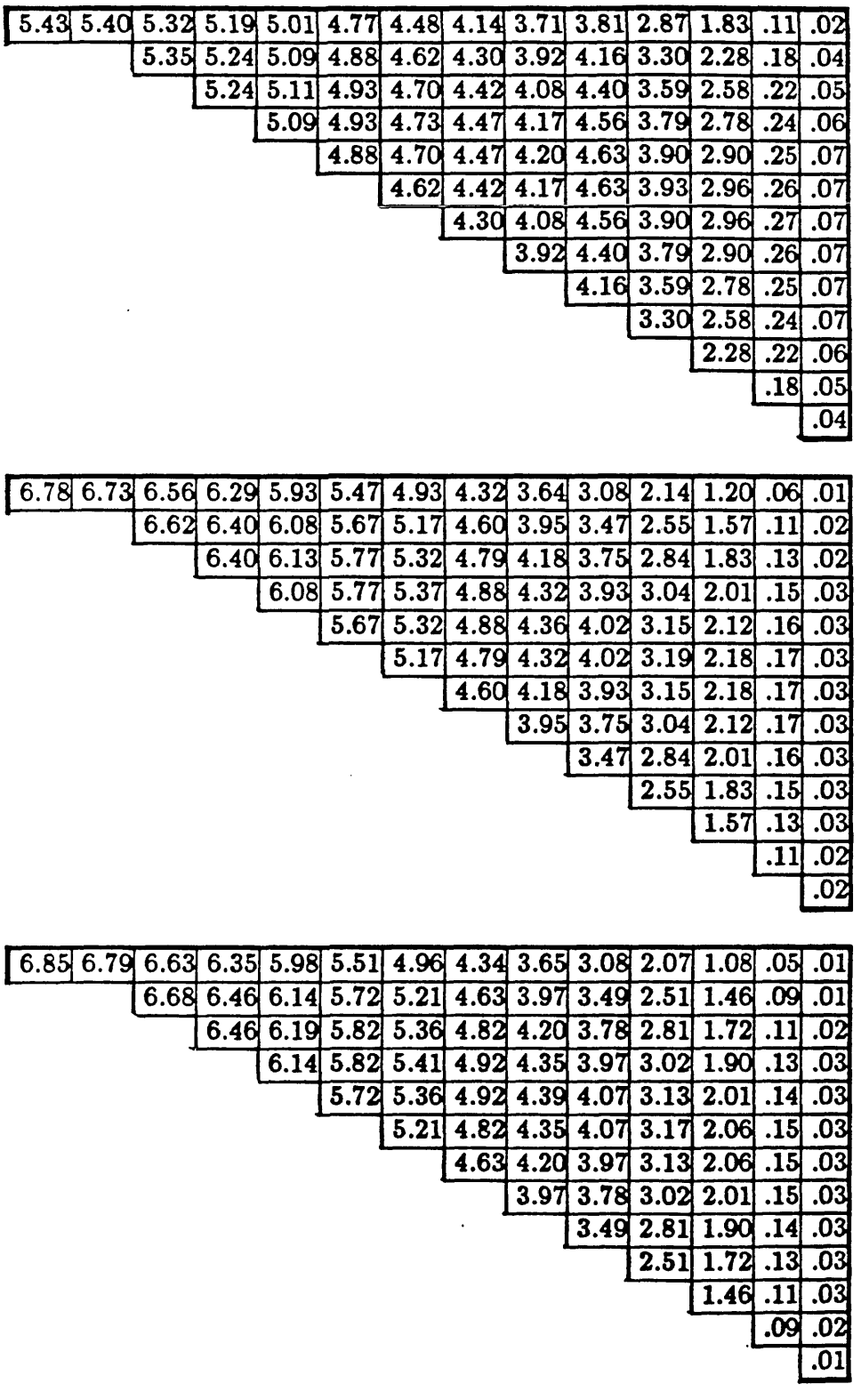

5.43	5.40	5.32	5.19	5.01	4.77	4.48	4.14	3.71	3.81	2.87	1.83	.11	.02
		5.35	5.24	5.09	4.88	4.62	4.30	3.92	4.16	3.30	2.28	.18	.04
			5.24	5.11	4.93	4.70	4.42	4.08	4.40	3.59	2.58	.22	.05
				5.09	4.93	4.73	4.47	4.17	4.56	3.79	2.78	.24	.06
					4.88	4.70	4.47	4.20	4.63	3.90	2.90	.25	.07
						4.62	4.42	4.17	4.63	3.93	2.96	.26	.07
							4.30	4.08	4.56	3.90	2.96	.27	.07
								3.92	4.40	3.79	2.90	.26	.07
									4.16	3.59	2.78	.25	.07
										3.30	2.58	.24	.07
											2.28	.22	.06
												.18	.05
													.04

6.78	6.73	6.56	6.29	5.93	5.47	4.93	4.32	3.64	3.08	2.14	1.20	.06	.01
		6.62	6.40	6.08	5.67	5.17	4.60	3.95	3.47	2.55	1.57	.11	.02
			6.40	6.13	5.77	5.32	4.79	4.18	3.75	2.84	1.83	.13	.02
				6.08	5.77	5.37	4.88	4.32	3.93	3.04	2.01	.15	.03
					5.67	5.32	4.88	4.36	4.02	3.15	2.12	.16	.03
						5.17	4.79	4.32	4.02	3.19	2.18	.17	.03
							4.60	4.18	3.93	3.15	2.18	.17	.03
								3.95	3.75	3.04	2.12	.17	.03
									3.47	2.84	2.01	.16	.03
										2.55	1.83	.15	.03
											1.57	.13	.03
												.11	.02
													.02

6.85	6.79	6.63	6.35	5.98	5.51	4.96	4.34	3.65	3.08	2.07	1.08	.05	.01
		6.68	6.46	6.14	5.72	5.21	4.63	3.97	3.49	2.51	1.46	.09	.01
			6.46	6.19	5.82	5.36	4.82	4.20	3.78	2.81	1.72	.11	.02
				6.14	5.82	5.41	4.92	4.35	3.97	3.02	1.90	.13	.03
					5.72	5.36	4.92	4.39	4.07	3.13	2.01	.14	.03
						5.21	4.82	4.35	4.07	3.17	2.06	.15	.03
							4.63	4.20	3.97	3.13	2.06	.15	.03
								3.97	3.78	3.02	2.01	.15	.03
									3.49	2.81	1.90	.14	.03
										2.51	1.72	.13	.03
											1.46	.11	.03
												.09	.02
													.01

Figure 5.25. Power maps of fully-blanketted two zone cores. (a) standard 14.5%/18%, (b) graphite 16.25%/18%, and (c) alumina 17.25%/19%. (MW)

The fully blanketted standard ETGBR has an even longer reactivity-life than the partially blanketted cases. Table (5.31) shows the large increase in reactivity-life resultant from adding blankets and including a second core zone of higher enrichment.

Table (5.31): Reactivity-life (burnup) of standard ETGBR with blanket addition and core subdivision.

	Effective multiplication factor, k_{eff}			
time(yrs.)	core + RB	core + AB	core +AB +RB	C1/C2 +AB +RB
0	1.0621	1.0648	1.0667	1.0945
6	1.0377	1.0399	-	1.0619
8	1.0240	1.0262	1.0318	-

Diluted variant reactivity-lives are somewhat greater than those for the core or partially blanketted core cases. Table (5.32) shows the burnup of the fully blanketted single core zone DETGBRs.

Table (5.32): Burnup of fully-blanketted single core zone DETGBRs.(k_{eff})

	Core +AB +RB	
time	Graphite (16.25%)	Alumina (18.0%)
0	1.0579	1.0526
2	1.0197	1.0110
4	0.9702	0.9766

An Overall Comparision of the Partially and Fully Blanketted ETGBR's and its Diluted Variants

The following points represent a summary of the partial and full blanket study of the ETGBR and DETGBR. Table (5.33) is used as a guide to the conclusions.

Table (5.33): Overall comparison of BOL neutronic parameters of ETGBR and DETGBRs.

	unreflected			reflected		
	k_{eff}	ICR	BR	k_{eff}	ICR	BR
Core only:						
Stnd ETGBR	0.987	0.963	0.963	1.060	0.979	0.979
Graph ETGBR	1.005	0.748	0.748	1.055	0.749	0.749
Alumina ETGBR	1.015	0.754	0.754	1.050	0.753	0.753
Core and axial blanket:						
Stnd ETGBR	1.046	0.978	1.117	1.065	0.983	1.163
Graph ETGBR	1.048	0.750	0.838	1.057	0.751	0.870
Alumina ETGBR	1.046	0.754	0.841	1.052	0.754	0.869
Core and Radial blanket:						
Stnd ETGBR	1.001	0.968	1.078	1.062	0.980	1.105
Graph ETGBR	1.010	0.749	0.798	1.055	0.750	0.804
Alumina ETGBR	1.019	0.754	0.798	1.051	0.753	0.801
Core+AB+RB:						
Stnd	1.062	0.983	1.229	1.066	0.984	1.306
Graph	1.054	0.751	0.897	1.057	0.751	0.934
Alumina	1.050	0.754	0.894	1.052	0.754	0.926
Core1+Core2+AB+RB:						
Stnd 14.50/18.0	1.090	0.897	1.166	1.094	0.898	1.244
Alumina 17.25/Alumina 19.0+RB	-	-	-	1.036	0.762	0.828
Graphite 16.25/Graphite 18.0+RB	-	-	-	1.062	0.729	0.798
Alumina 17.25/Alumina 19.0+AB+RB	-	-	-	1.040	0.788	0.949

1. Reactivity:

There is an enrichment penalty in achieving reasonable reactivity values for the diluted ETGBR. A 2 year batch life requires 16.25% for graphite and 18.0% for alumina. The resulting BOL reactivities are 1.055 and 1.050. For burnup, there is a small difference between core only and fully blanketted cases. For the alumina diluted ETGBR (V_d/V_f =2 and 18% enrichment), theoretical burnups, limited by

reactivity considerations, are 40.9, 41.6, 43.7, and 44.2 GWd/t for the core only, radially-blanketted, axially-blanketted, and fully-blanketted cases respectively.

2. Conversion Ratio:

With dilution (moderation), we cannot approach the high ICR (0.979) of the standard ETGBR. However, ICRs are relatively high at 0.749 and 0.753 for graphite and alumina diluted ETGBRs respectively and represent a near 50% increase over thermal cores.

3. Breeding using external blankets:

It appears that for the radially or axially partially blanketted diluted designs, breeding ratios (BR) are somewhat below 0.9 and are a function of geometry. For a fully blanketted design, BR values are 0.934 and 0.926 for graphite and alumina dilution. With an alumina diluted two zone core of average enrichment of 18.04% (17.25% inner/19.0% outer), full blanketting yields a BR of about 0.95. This reactor has a BOL k_{eff} of 1.0396 compared to 1.050 for the single zone 18% alumina DETGBR. A relatively high ICR of 0.79 compared to 0.75 for the single zone 18% alumina DETGBR is the case. Without the axial blanket, this same reactor has a k_{eff} (BOL) of 1.0365, a BR of 0.83 and an ICR of 0.76. It may be simply a matter of adding an axial blanket of the desired thickness to arrive at the BR desired. Figure (5.26) shows BR as a function of AB thickness for this reactor (keeping RB thickness fixed at 2 rows of subassemblies). It becomes apparent from the figure that, while the internal conversion ratio barely changes, the overall CR (or BR) increases but only approaches 1.0 at large axial blanket thicknesses. The thickness of the axial reflector has little effect on CR.

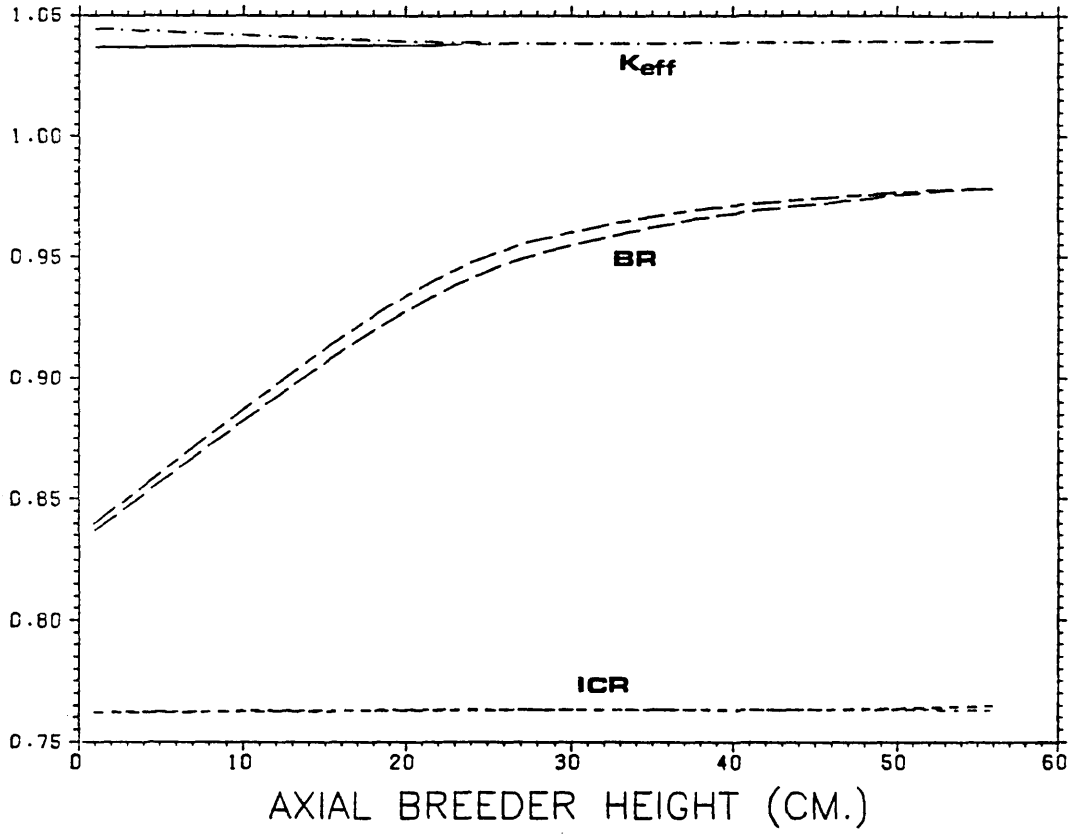

Figure 5.26. Effect of axial blanket thickness on Breeding Ratio of fully blanketted alumina DETGBR

5.5 CONCLUSIONS

The concept of 'dilution' of the ETGBR has been introduced. The method of core dilution recommended and studied in this chapter was the block dilution concept involving an integral block of diluent with a drilled circular channel containing the fuel rods; based largely on AGR and HTR design. The neutronics of using graphite or alumina dilution were considered and compared as far as possible with the standard ETGBR.

A plot of reactivity (k_∞ or k_{eff}) versus diluent to fuel ratio showed values for alumina dilution to fall for all enrichments considered. For the graphite case the reactivity was shown to go through a minimum before rising with increasing dilution, although above about 16.5% Magnox Pu enrichment behaves like the alumina cases and falls monotonically.

To obtain the same k_{eff}, the alumina diluted ETGBR (DETGBR) would require higher enrichment than a graphite DETGBR. For V_d/V_f =2, alumina requires 19.28% Magnox Pu initial enrichment while graphite requires 18.12%. for a BOL k_{eff} of 1.060. More resonance absorbtion, especially in U-238, characterizes the alumina DETGBR and, while this creates the need for the higher enrichment, it also results in a higher core conversion ratio and nearly as long a burnup as the graphite DETGBR.

Fissile utilization of the alumina DETGBR is a little less than for the graphite DETGBR (V_d/V_f =2) since it requires a larger fissile feed mass per GW-yr of energy extracted from its burnup. The fissile feed consumption is less and higher content of fissile is discharged (14.4% vs. 13.3% for graphite).

The standard ETGBR core, at 16.5% Magnox Pu enrichment, calculated in 2-dimensional R-Z geometry with reflectors added, showed an 8% increase in reactivity over the bare core. Also, the core conversion factor increased by some 2% with reflectors added. With the reactivity of the 16.5% standard reflected ETGBR considered high at 1.143, it was decided to search for a lower value giving a BOL k_{eff} of about 1.060. This resulted in the selection of 14.5% initial enrichment.

Even with enrichment adjusted to reduce the BOL k_{eff}, the burnup of the reflected ETGBR showed very long reactivity-lifetimes in the range of 8 to 10 years for enrichments of 13.75 to 14.5% Magnox Pu.

With the diluted ETGBR cores, reflector reactivity worth is reduced considerably; the 18% enriched alumina DETGBR core only (V_d/V_f =2) case had a reflector worth of 3.65%dk compared with 7.3%dk for the standard ETGBR. The problem of over-prediction of reactivity-lifetime did not appear significant for the V_d/V_f =2 DETGBR reflected cores. Burnups of about 35 GWd/t wer found.

With the present economic circumstances in mind, partial blankets: radial or axial were considered. With only a radial blanket or only an axial blanket, the burnup of the diluted ETGBR was shown not to be very different from the core alone cases, achieving a reactivity-lifetime of a little over 2 years. At the enrichments required for the alumina DETGBR an ICR of about 0.75 results. If a two zone differentially enriched core is used, the ICR rises to 0.76 for a radially blanketted case and to 0.79 for a fully blanketted case.

Overall breeding ratio (BR) was shown to be variable and to depend on the 'blanketting' adopted. For the alumina DETGBR, breeding ratios of 0.80, 0.87, and 0.92 werefound for the radially, axially, and fully blanketted cases respectively. With a two zone core and full blankets the BR for the alumina DETGBR reaches 0.95, just short of being a true breeder. This last condition applied at the enrichments required for the DETGBRs studied at V_d/V_f =2. As conversion falls with increasing enrichment, it may be possible to obtain a DETGBR with BR=1.0 and maintain the 18% enrichment and 2 year dwell time if a reduced V_d/V_f of around 1.75 is used.

REFERENCES

[1] Askew J. R. , Thorpe G. , *Possible developments from the AGR*, Nuclear Energy, Vol. 25, No. 1, pp. 41-46, February 1986

[2] Stewart H. B. , Rickard C. L. , and Melese G. B. , *Gas-Cooled Reactor Technology*, Advances in Nuclear science and Technology, Vol. 4, p. 36, 1968

[3] Cohen K. P. , O'Neil G. L. , *Safety and Economic Characteristics of a 1000 MW_e Fast Sodium-Cooled Reactor Design*, Advances in Nuclear Science and Technology, Vol. 4, p. 67, 1968

[4] Marshall W. , *Nuclear Power Technology - Vol. 1*, pp. 186-195, Clarendon Press, Oxford, 1983

[5] MacBean I. J. , *A COSMOS Calculation of the Neutronics of a 1670 MW_h GCFR with 7 mm. Fuel Pellets, and a Comparison with Results of CEGB Calculations*, AEE-Winfrith report AEEW-M1669, April 1979

[6] Gratton C. P. , Askew J. R. , Personal Communication, AEE-Winfrith, 1984

CHAPTER 6.

OTHER DILUTED ETGBR VARIANTS

6.1 A MIXED FUEL/DILUENT PIN ETGBR VARIANT

6.1.1 Introduction to Concept

The main reason for this design is the need to locate diluent as close as possible to the fuel rods. This is to say, that the heat source (the fuel rods) are in close proximity to non-fuel heat sinks; diluent rods thus provide an additional heat sink in unforseen temperature transients. Benefits of this concept will be clarified further in Chapter 7.

The neutronic behaviour of cores with this method of dilution is the main concern of this section; differences between this and other methods of dilution are highlighted.

6.1.2 Design and Geometry

It is assumed that diluent rods can be accomodated in a subassembly of the same size as that of a standard ETGBR.

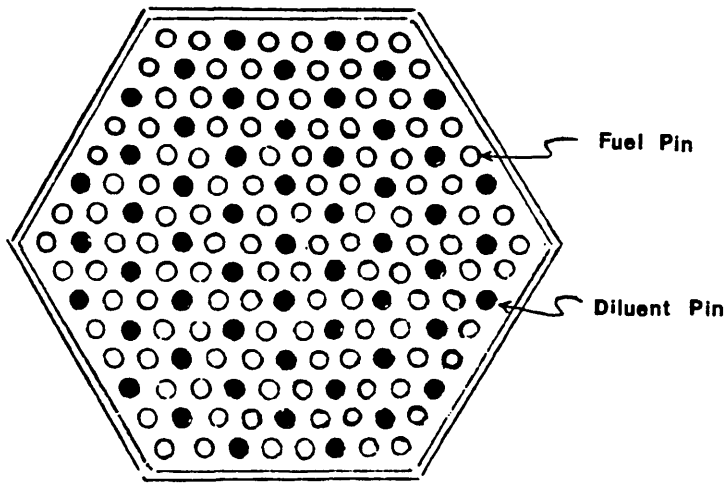

Figure 6.1. The mixed pin diluted ETGBR subassembly.

In the outline design shown in figure (6.1) every group of six fuel pins has a diluent pin at its center; corresponding to a number ratio of 0.473 diluent pins to fuel pins. This is equivalent to a volume ratio of diluent-to-fuel of 0.573, if the diluent pins are taken to have a diameter of 7.0 mm (the same as the outer radius of the fuel pin). The fuel volume fraction of the whole subassembly is 0.2045,

compared with 0.290 for the standard ETGBR. The subassembly is 15.74 cm. across flats and therefore retains the same size as the standard ETGBR.

With a relatively low fuel loading, the core size for a power output similar to the standard ETGBR would be greater. Alternatively, a higher power rating might be adopted with different coolant conditions.

The use of moderator pins in a fast reactor subassembly has been proposed previously [1]. The idea, there, was to improve on the Doppler coefficient and the void reactivity change for an LMFBR. Beryllia was considered as the diluent, a choice based solely on neutronic properties. In this section the diluent materials selected for this thesis are considered: graphite and alumina.

6.1.3 Bare Reactor Calculation

Inspection of the fuel (inner ring) flux spectrum (normalized to the same total flux) shows this design to have a large fraction of fast neutrons greater even than for the standard 14.5% ETGBR. The thermal component of the spectrum is only slightly greater than that of the standard 14.5% ETGBR. The mixed pin design may thus be a means of introducing a diluent heat sink, improve the Doppler coefficient, and at the same time retain a large contribution of fast neutrons (a benefit in fissile breeding and burnup).

Compared with the 'diluted block' designs, which have V_d/V_f of 2.0, as opposed to the mixed pin design value of 0.6, the neutron spectra are seen to be far less shifted towards thermal and hence are much more typical of a 'real' fast reactor. Table (6.1) below shows the median and the mean energies for the neutron spectra of the present 'pin diluted' and 'block diluted' concepts, while figure (6.2) shows the spectra in the inner fuel ring of the subassembly.

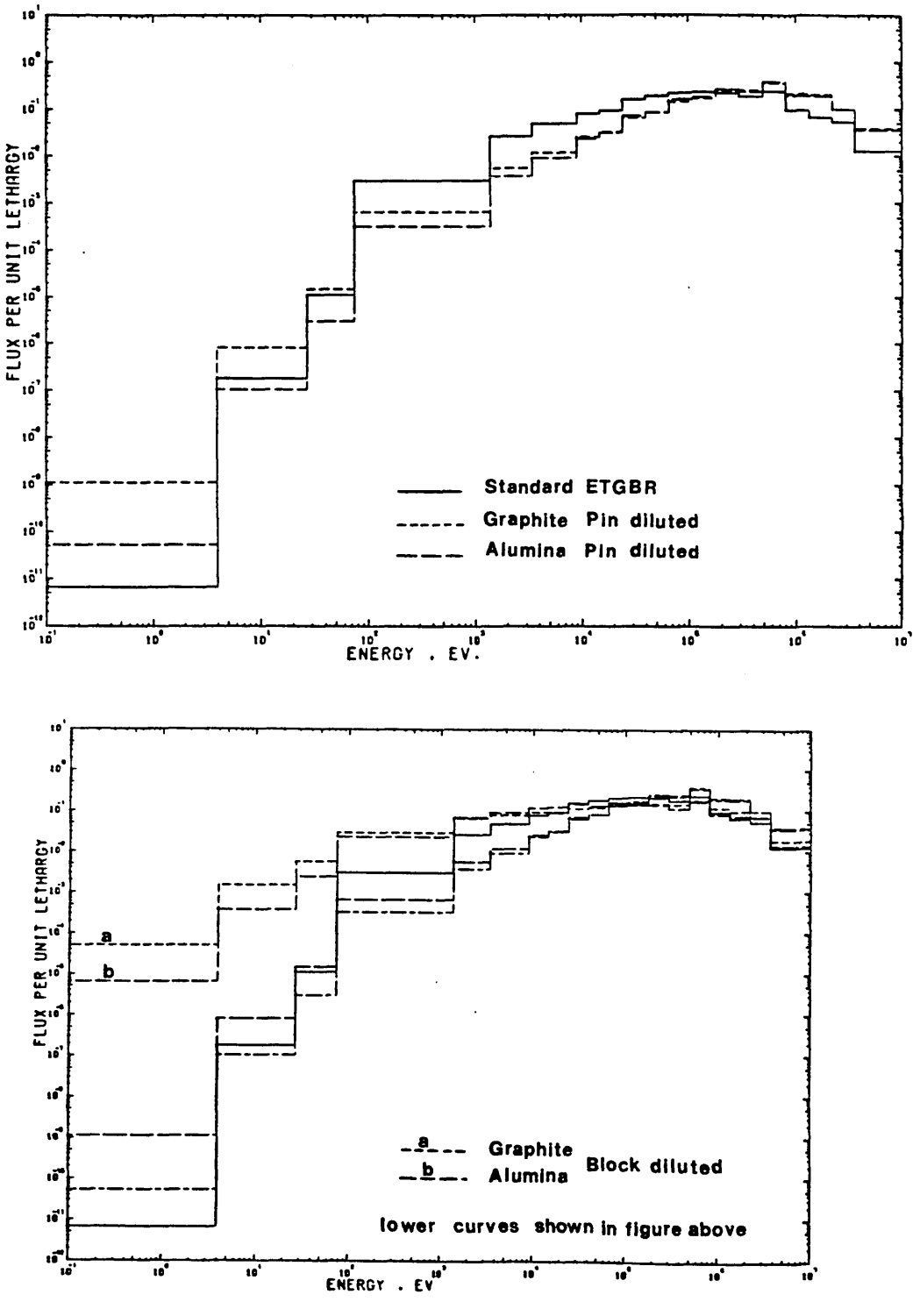

Figure 6.2. The neutron spectra in inner fuel region of the block diluted ETGBR and the pin diluted ETGBR.

Table (6.1): Comparison of median and mean energies of pin-diluted and block-diluted ETGBR's.

	Median Energy(keV)	Mean energy(keV)
Standard 14.50%	144.4	52.7
Graphite 16.25%	99.5	116.6
Alumina 18.00%	71.4	87.7
Mixed Pin Graphite 16.25%	454.1	443.9
Mixed Pin Alumina 16.25%	438.2	414.7

This concept has merit because the neutron environment is still close to that of a 'true' fast reactor and because the subassembly design and dimensions are the same as for the basic fast reactor. It also becomes possible to have a reactor core incorporating zones of mixed pin diluted subassemblies and zones of standard fast subassemblies.

Initially, it is again straight forward to study a bare core, with no reflector using WIMS-D4, leakage-corrected lattice-cell model. Table (6.2) below shows the results of an enrichment search, for the diluted ETGBR lattices, at begining of life.

Table (6.2): BOL enrichment search for pin diluted ETGBR

Enrichment	Graphite		Alumina	
(%Magnox Pu)	k_∞	k_{eff}	k_∞	k_{eff}
18.0	1.2571	0.9689	1.2390	0.9759
19.0	1.2926	0.9985	1.2753	1.0067
19.77	-	1.0210	-	1.0301
21.0	1.3602	1.0552	1.3442	1.0657

At these high enrichments, alumina is seen to have a higher k_{eff} ; inspection of k_{∞} values shows that reduced leakage gives this advantage. Alumina is also seen to produce a longer burnup at 21% enrichment as shown in table (6.3) which gives the reactivity rundown of the two diluted lattices (unreflected cores) over two years.

Table (6.3): Burnup of mixed-pin diluted ETGBR at 21% Magnox Pu Enrichment

time(days)	Graphite	Alumina
0	1.0551	1.0656
182.5	1.0406	1.0519
365.0	1.0280	1.0401
547.5	1.0159	1.0286
730.0	1.0040	1.0176
912.5	0.9924	1.0067

Before moving to the fully reflected cases, it is worth noting the fissile utilization of the pin-diluted ETGBR lattice. Table (6.4) shows this data for the pin-diluted cases compared with the (V_d/V_f =2) block diluted cases (of chapter 5). Comparisons are shown for 19.77 % Magnox Pu enrichment for both graphite and alumina.

Table(6.4): Comparison of fissile fuel utilization of block and pin diluted ETGBRs

	Block DETGBR		Pin DETGBR		Pin DETGBR
	Alumina V_d/V_f =2 19.77%	Graphite V_d/V_f =2 19.77%	Alumina 19.77%	Graphite 19.77%	Alumina 21.0%
Burnup (GWd/t)	33.10	47.10	21.5	13.0	47.3
Feed:(kg/cm)					
Fissile	0.1011	0.1101	0.0703	0.0703	0.0746
U+Pu	0.6133	0.6133	0.4263	0.4263	0.4260
Discharge:(kg/cm)					
Fissile	0.0929	0.0874	0.0671	0.0682	0.0668
U+Pu	0.6019	0.0597	0.4213	0.4233	0.4147
Usage: (kg/GW-yr)					
Feed(F)	1818	1391	2799	4629	1351
Discharge(D)	1702	1135	2703	4520	1243
Consumption(C=F-D)	116	256	96	251	108
C/F(%)	6.38	18.40	3.42	5.42	7.99

From table (6.4) it is seen that burnups of the block diluted cases are significantly longer and this alone leads to higher fuel utilization. With pin-diluted cases, alumina gives a longer burnup than graphite and this significantly reduces the magnitude of the fuel utilization. The alumina pin-diluted ETGBR, however, gives a lower C/F ratio (possibly due to greater fissile breeding in the core (a 'harder' spectrum). Only at an enrichment of 21% does the alumina pin-diluted ETGBR give increased fuel utilization comparable to block diluted ETGBR values.

6.1.4 Pin Diluted ETGBR Whole Reactor Calculations

The calculational route adopted for whole reactor calculations is the same as that described already for the block diluted ETGBR of chapter 5. Only the geometry at the subassembly level differs from that of the block diluted ETGBR.

As was the case in chapter 5 (section 5.4.1), it was expected here that enrichment levels required for reasonable (i.e. not excessively long) reactivity-lifetimes, would have to be reduced. This gave one incentive to proceed to whole reactor calculations for the pin-diluted cases. The second advantage is the ability to generate full core power maps based on total reactor output.

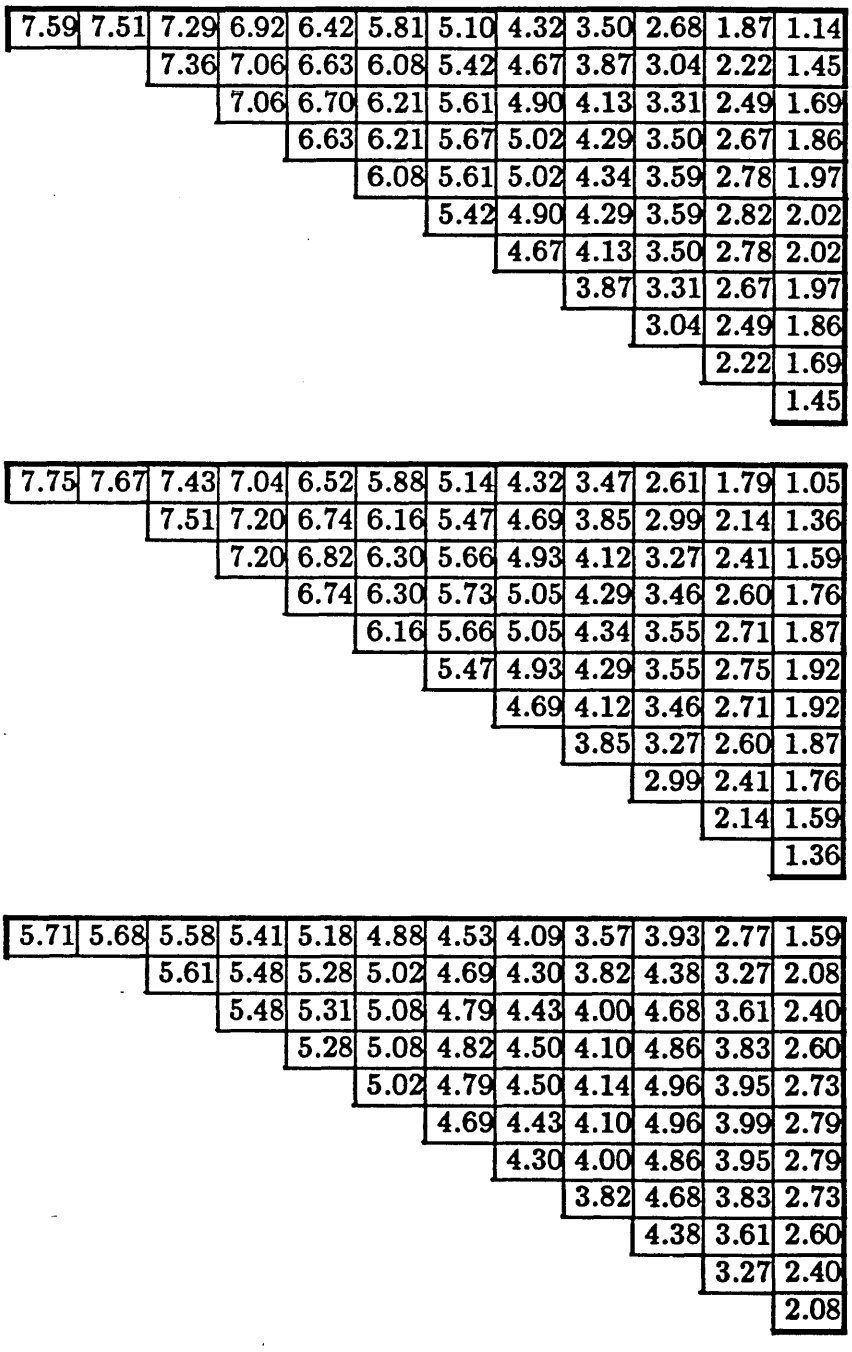

7.59	7.51	7.29	6.92	6.42	5.81	5.10	4.32	3.50	2.68	1.87	1.14
		7.36	7.06	6.63	6.08	5.42	4.67	3.87	3.04	2.22	1.45
			7.06	6.70	6.21	5.61	4.90	4.13	3.31	2.49	1.69
				6.63	6.21	5.67	5.02	4.29	3.50	2.67	1.86
					6.08	5.61	5.02	4.34	3.59	2.78	1.97
						5.42	4.90	4.29	3.59	2.82	2.02
							4.67	4.13	3.50	2.78	2.02
								3.87	3.31	2.67	1.97
									3.04	2.49	1.86
										2.22	1.69
											1.45

7.75	7.67	7.43	7.04	6.52	5.88	5.14	4.32	3.47	2.61	1.79	1.05
		7.51	7.20	6.74	6.16	5.47	4.69	3.85	2.99	2.14	1.36
			7.20	6.82	6.30	5.66	4.93	4.12	3.27	2.41	1.59
				6.74	6.30	5.73	5.05	4.29	3.46	2.60	1.76
					6.16	5.66	5.05	4.34	3.55	2.71	1.87
						5.47	4.93	4.29	3.55	2.75	1.92
							4.69	4.12	3.46	2.71	1.92
								3.85	3.27	2.60	1.87
									2.99	2.41	1.76
										2.14	1.59
											1.36

5.71	5.68	5.58	5.41	5.18	4.88	4.53	4.09	3.57	3.93	2.77	1.59
		5.61	5.48	5.28	5.02	4.69	4.30	3.82	4.38	3.27	2.08
			5.48	5.31	5.08	4.79	4.43	4.00	4.68	3.61	2.40
				5.28	5.08	4.82	4.50	4.10	4.86	3.83	2.60
					5.02	4.79	4.50	4.14	4.96	3.95	2.73
						4.69	4.43	4.10	4.96	3.99	2.79
							4.30	4.00	4.86	3.95	2.79
								3.82	4.68	3.83	2.73
									4.38	3.61	2.60
										3.27	2.40
											2.08

Figure 6.3. Power maps of (a) reflected graphite pin diluted core at 16.25% enrichment, (b) reflected alumina pin diluted core at 16.25% enrichment, and (c) reflected alumina 16.25% pin diluted inner and standard 18% outer.

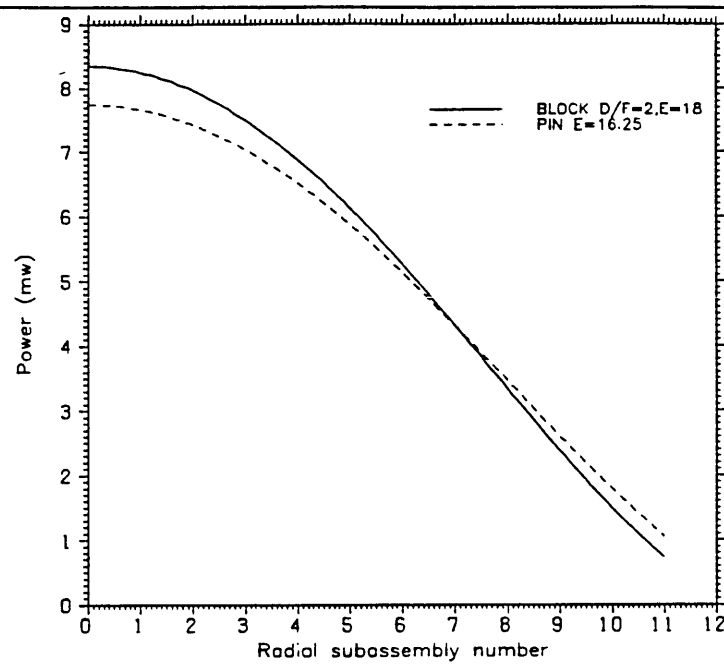

Figure 6.4. Comparison of radial power profile of block and pin diluted ETGBRs.

The mixed pin design, with its relatively fast spectrum, has a power map more similar to the fully fast ETGBR (compare to figure 5.19). The power maps of the two diluted variants are shown in figures (6.3 a and b). Radial power peaking factors are calculated to be 1.816 and 1.854 for the two cases respectively. The power profile of the pin diluted design is compared to that of the block diluted case (alumina dilution) in figure (6.4) and shows an improved 'flattening' typified by reduced central subassembly power and increased peripheral subassembly power.

The ability to admit subassemblies of similar size (whether pin-diluted or standard) into the core, is a feature of the pin-diluted concept. Power flattening is shown in figure (6.3c) where the core map of a two core zone reactor is shown. Here a purely fast 18.0% outer core zone is used to flatten a 16.25% alumina pin-diluted inner core. The radial power peaking factor for this case was found to be 1.366. The 18.0% outer enrichment was selected in order to produce significant flattening and this is indeed shown by the low peaking factor.

Burnup of the mixed pin diluted designs show significantly longer reactivity-lifes than for the block diluted ETGBR's, due to the 'harder' spectrum. Table (6.5) shows the reactivity rundown of the single batch mixed pin design for both

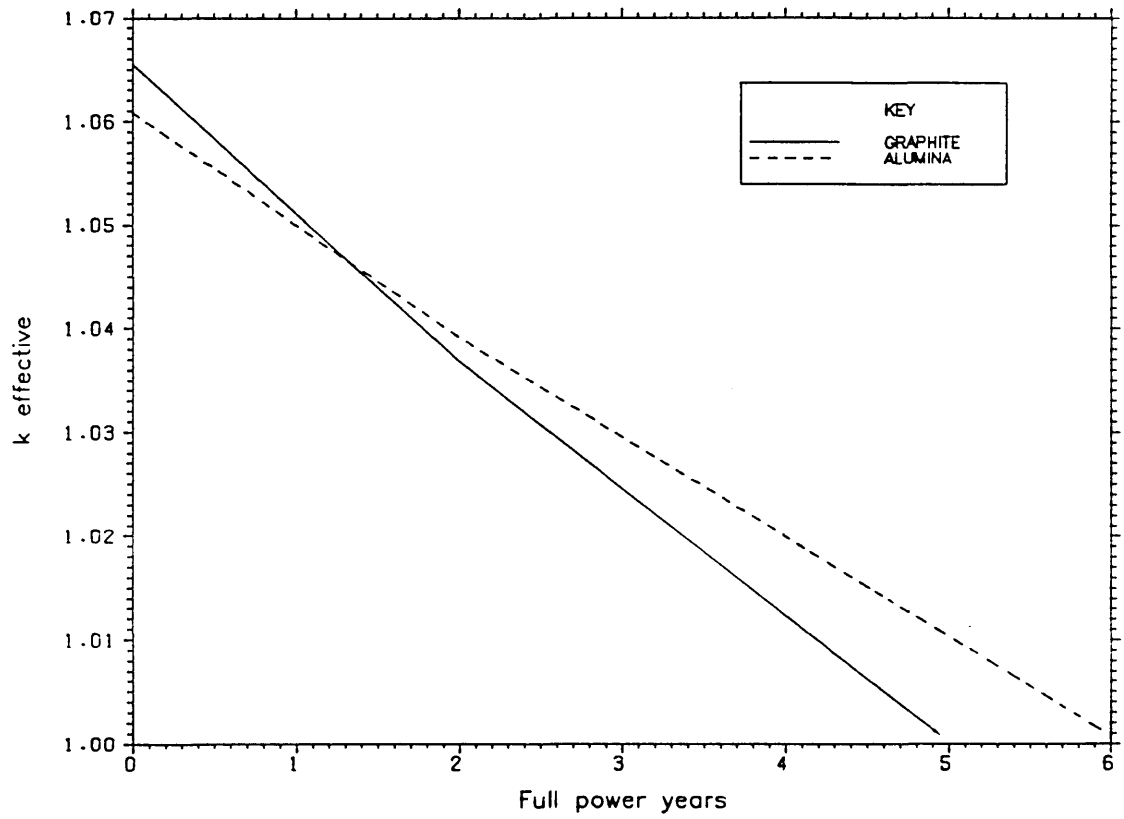

Figure 6.5. Burnup of pin diluted ETGBR lone reflected cores. Alumina and graphite dilution at 16.25% enrichment.

the bare core and the reflected one. A reactivity-life of about 5 years is indicated for graphite and 6 years for alumina (taking k_{datum}=1.00 and extrapolating). This is illustrated in figure (6.5). With a shutdown margin of, say, 0.5% in k_{eff}, the discharge burnups are about 78.5 GWd/t for the graphite variant and 92.5 GWd/t for the alumina variant (single batch burnup). It appears that the 16.25% enrichment pin-diluted variants, with reflectors, give burnups roughly twice those of the 21% leakage corrected lattice cell model of the same core (refer back to table 6.4 for burnup values). It is of interest to note from table (6.5) that reflector reactivity worth for the 16.25% enriched pin-diluted cases is about 9%dk; an indication of the high neutron leakage from these 'hard' spectrum cores.

It must be pointed out, at this stage, that some difference was noted in values of BOL k_{eff} for the leakage corrected lattice-cell and the unreflected whole reactor pin-diluted calculation of the same enrichment. In fact, for an 18% graphite pin-diluted case, the difference was 3.5%dk. It remains difficult to say if the differences between the lattice cell (leakage corrected), and the whole reactor models are not due to WIMS presently being inadequate for 'harder' systems.

Table (6.5): Reactivity rundown of 16.25% enrichment mixed pin diluted ETGBR's (WIMS-E)

	Effective multiplication factor, k_{eff}			
	Unreflected		Reflected	
time(years)	Graphite	Alumina	Graphite	Alumina
0.0	0.95020	0.96360	1.06550	1.06090
2.0	0.92229	0.94212	1.03698	1.03920
4.0	0.89780	0.92261	1.01247	1.02000

Conversion and breeding have also been calculated for fully and partially blanketted cores. Table (6.6) shows the internal core conversion (ICR), overall conversion ratio (or BR), and k_{eff} for the mixed pin-diluted ETGBRs using alumina and graphite. Results are shown for the single zone core, the radially-blanketted single core, the fully blanketted single core, and a two region core fully blanketted case.

As blankets are added on, the overall BR increases as expected while a smaller but definite increase in the internal core conversion ratio also takes place. The last entry in table (6.6) shows a case where the outer zone consisted of standard ETGBR fast subassemblies; with the enrichments used results similar to the single zone core were found.

Table (6.6): Mixed pin-diluted ETGBR, V_d/V_f =0.57, 16.25% enrichment (fully reflected)

	Graphite			Alumina		
	k_{eff}	ICR	BR	k_{eff}	ICR	BR
Core only	1.0655	0.8359	0.8359	1.0609	0.8701	0.8701
Single core +RB	1.0689	0.8571	1.0065	1.0637	0.8754	1.0169
Single core +RB+AB	1.0765	0.8458	1.2140	1.0700	0.8792	1.2408
16.25 mixed pin inner 14.5 standard outer +RB+AB	1.0791	0.8853	1.2254	1.0712	0.9105	1.2517

Breeding ratios just over 1.00 are the case for the radially-blanketted pin-diluted variants and may thus be considered if "just-breeding" conditions were desired. Although the economic arguments are far more involved, it is justifiable to say that with the present surplus of fissile material in the world market, "just-breeders" may be feasible.

The radially-blanketted pin-diluted ETGBR has a reactivity-life that is somewhat longer than the unblanketted diluted core. Figure (6.6) compares the burnup of the alumina mixed pin diluted core with and without the radial blanket (with full reflectors). A reactivity-lifetime of 7 years, rather than 6 years for the single zone case, emerges with a radial blanket added.

The single-core zone, radially-blanketted, pin-diluted ETGBR, if selected, would required some measure of power flattening as a large gradient in power production exists between the inner and peripheral subassemblies. Figures (6.7) show the power maps for the cases where the outer core zone subassemblies (180/397) are taken as 16.5% standard ETGBR ones. The improved power profile is evident (compared to those of figure 6.3) and the radial power peaking factors are reduced

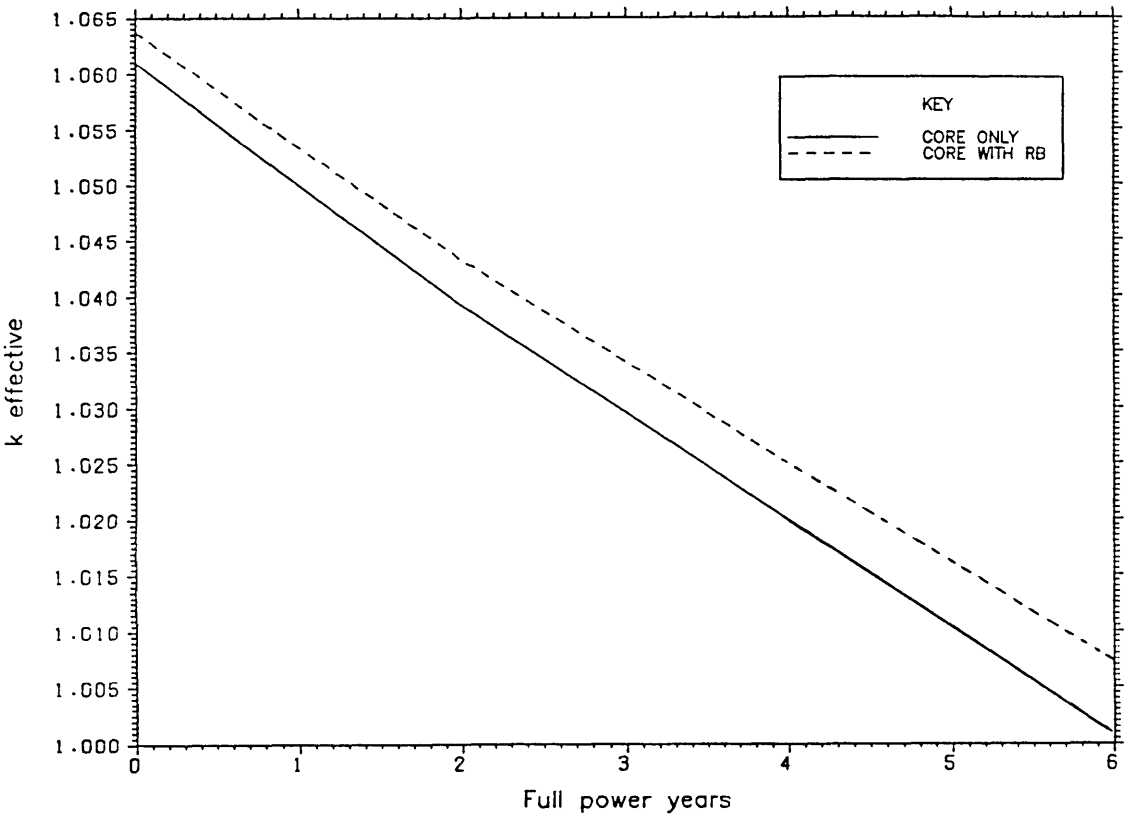

Figure 6.6. Burnup of alumina pin diluted ETGBR with and without radial blanket.

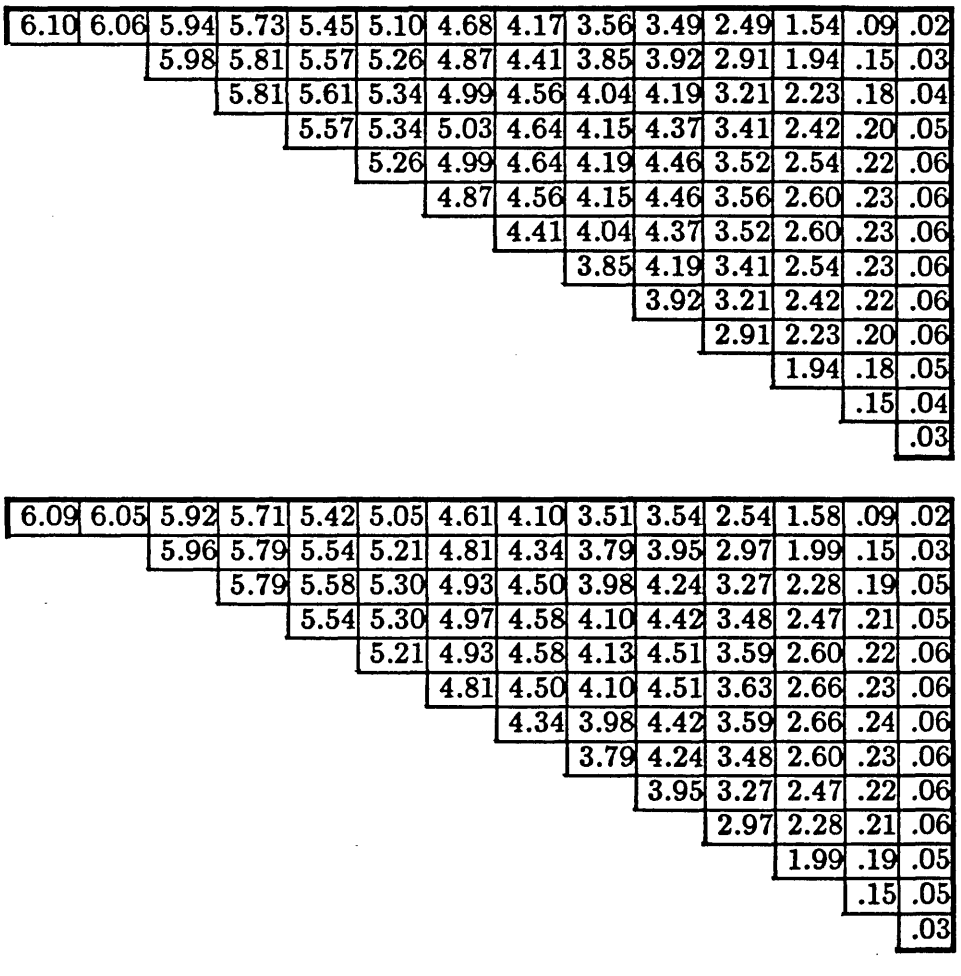

6.10	6.06	5.94	5.73	5.45	5.10	4.68	4.17	3.56	3.49	2.49	1.54	.09	.02
		5.98	5.81	5.57	5.26	4.87	4.41	3.85	3.92	2.91	1.94	.15	.03
			5.81	5.61	5.34	4.99	4.56	4.04	4.19	3.21	2.23	.18	.04
				5.57	5.34	5.03	4.64	4.15	4.37	3.41	2.42	.20	.05
					5.26	4.99	4.64	4.19	4.46	3.52	2.54	.22	.06
						4.87	4.56	4.15	4.46	3.56	2.60	.23	.06
							4.41	4.04	4.37	3.52	2.60	.23	.06
								3.85	4.19	3.41	2.54	.23	.06
									3.92	3.21	2.42	.22	.06
										2.91	2.23	.20	.06
											1.94	.18	.05
												.15	.04
													.03

6.09	6.05	5.92	5.71	5.42	5.05	4.61	4.10	3.51	3.54	2.54	1.58	.09	.02
		5.96	5.79	5.54	5.21	4.81	4.34	3.79	3.95	2.97	1.99	.15	.03
			5.79	5.58	5.30	4.93	4.50	3.98	4.24	3.27	2.28	.19	.05
				5.54	5.30	4.97	4.58	4.10	4.42	3.48	2.47	.21	.05
					5.21	4.93	4.58	4.13	4.51	3.59	2.60	.22	.06
						4.81	4.50	4.10	4.51	3.63	2.66	.23	.06
							4.34	3.98	4.42	3.59	2.66	.24	.06
								3.79	4.24	3.48	2.60	.23	.06
									3.95	3.27	2.47	.22	.06
										2.97	2.28	.21	.06
											1.99	.19	.05
												.15	.05
													.03

Figure 6.7. Power maps of pin-diluted, two zone cores of radially-blanketted ET-GBRs. (a) graphite 16.25% inner, standard 16.5% outer (k_{eff} =1.090), and (b) alumina 16.25% inner, standard 16.5% outer (k_{eff} = 1.083). (MW)

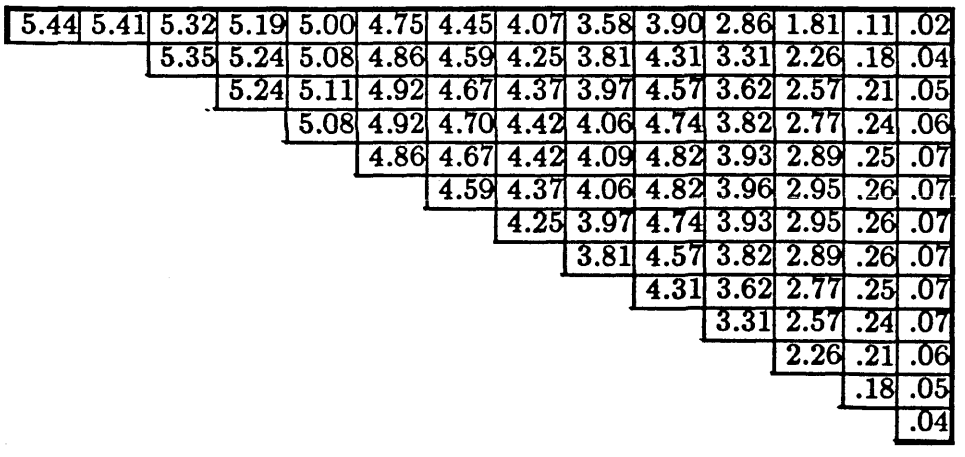

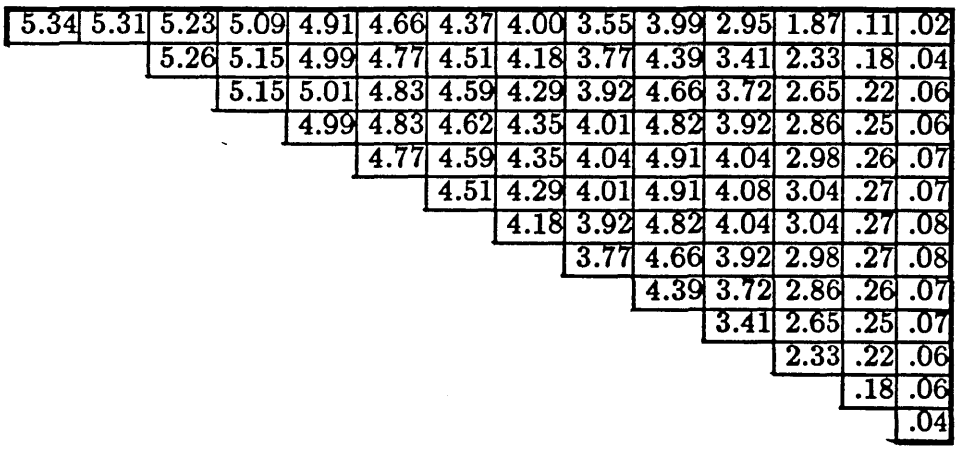

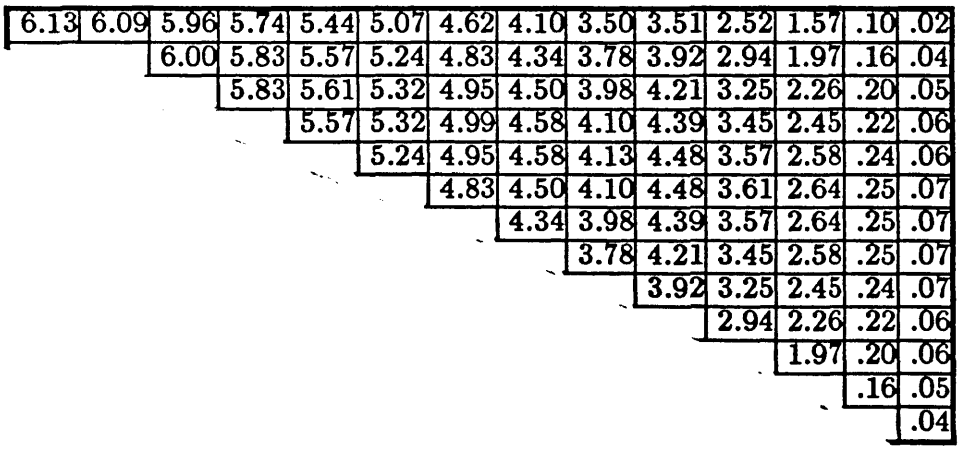

Figure 6.8. Power maps of pin-diluted two zone cores of fully-blanketted ETGBRs. (a) graphite 16.25% inner, standard 18% outer (k_{eff} =1.112), (b) alumina 16.25% inner, standard 18% outer (k_{eff} =1.105), and (c) alumnia 16.25% inner, standard 16.5% outer (k_{eff} =1.090). (MW)

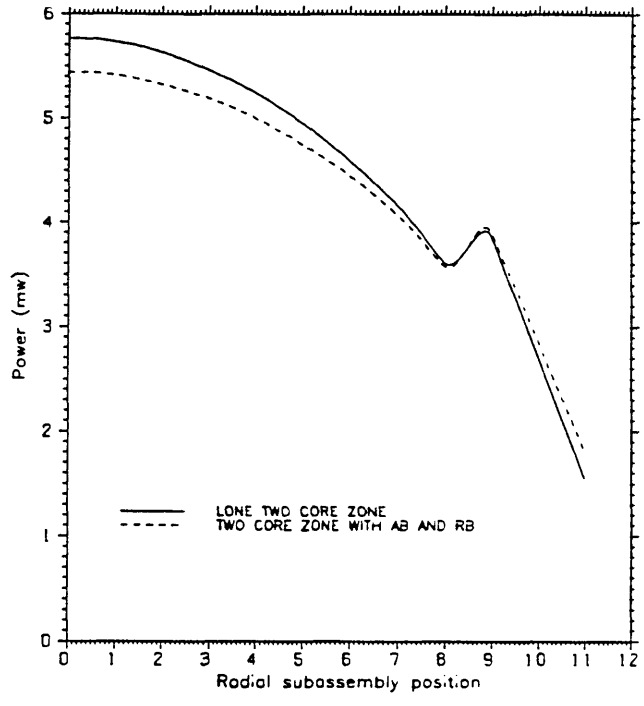

Figure 6.9. Radial power profile of graphite pin diluted ETGBR with and without full blankets (normalized to total core power of 1670 MW_t).

to 1.425 and 1.473 for the graphite and alumina cases respectively (compared to 1.816 and 1.854 in single zone core cases).

In figures (6.8) the power maps of fully(axially and radially)-blanketted mixed-pin diluted ETGBR's are shown. The power flattening arising from the use of a 18% enriched standard outer core is typified by the reduced radial power factors: 1.317 for the graphite and 1.294 for the alumina case. Although, with 18.0% enrichment standard outer core, the power profile is greatly improved, the resultant excess reactivity in the reactor is high and a 16.5% standard fast outer core is taken as a compromise. Figure (6.9) shows that the inclusion of the blankets does, in fact, slightly improve the power profile.

As mentioned before the radially-blanketted pin-diluted core of the given enrichment is a net producer of fissile material as shown by BR being greater than 1.0, and is has a long reactivity-lifetime as a result of its high internal conversion ratio. In figure (6.10) the variation of conversion ratios are shown, together with that of the block diluted ETGBR ($V_d/V_f = 2$) from the previous chapter. It

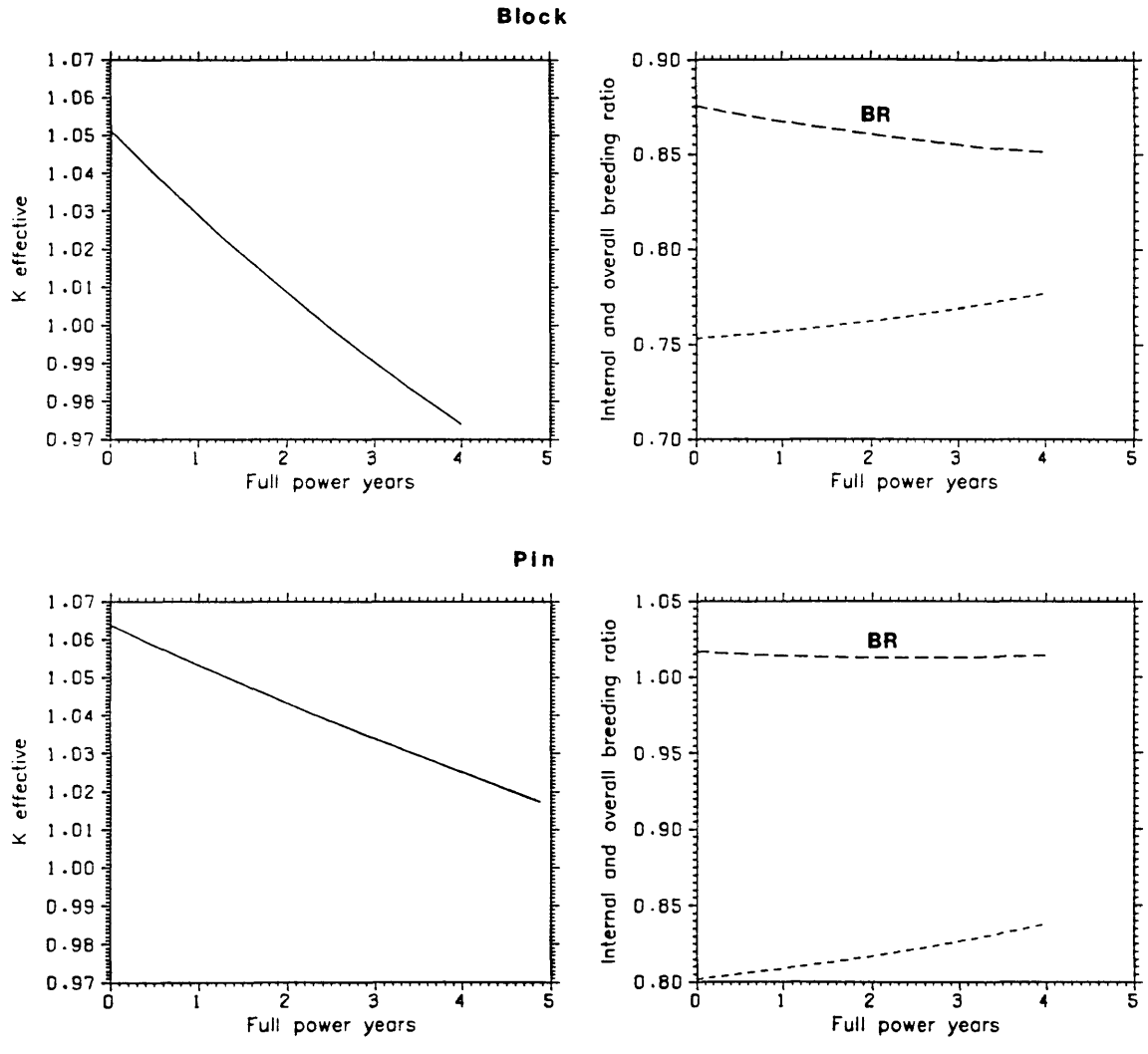

Figure 6.10. Comparison of k_{eff}, ICR, and BR variation with burnup for 18% block and 16.25% pin alumina diluted ETGBRs with radial blankets.

should be noted that the mixed pin design, although having lower enrichment, has a 'harder' spectrum due to its low V_d/V_f value. The difference in ICR is apparent, while the overall BR for the mixed-pin case dips slightly but recovers again soon after 2 years. The conversion ratios are higher than for the block diluted ETGBR. The radially-blanketted mixed pin design gives a core life of about 6 years.

6.2 HETEROGENEOUSLY DILUTED ETGBR DESIGN

Heterogeneous fast breeder reactors have been studied extensively; the present work extends the concept of dilution of the ETGBR core to designs of this type [2]. A heterogeneously diluted design has the additional possibility of internal diluent subassemblies within the core; these might be in addition to internal breeder subassemblies. Possible advantages of heterogeneous breeders may include:

(a) Single enrichment possibilty. (b) Simpler inclusion of diluent as separate subassemblies. (c) More negative predicted doppler coefficients of reactivity for fully fast systems.

6.2.1 Geometry

The geometry selected is one that brings every fuel subassembly close to a diluent subassembly. A diluent subassembly surrounded by six fuel subassemblies corresponds to V_d/V_f of 0.755, and to a 2:1 ratio of fuel to diluent subassemblies. A diluent subassembly is taken to resemble core subassemblies, but with the diluent rods larger, 0.43 cm. in radius, and unclad. Figure (6.11) shows the core map of the heterogeneous reactor with associated radial breeder and reflector subassemblies.

A heterogenously diluted ETGBR core may use either a diluent block with drilled coolant holes or a subassembly of diluent rods. The first option provides ,in principle, a greater amount of diluent and hence a greater thermal capacity. The second option, has the advantage of ease of cooling of diluent rods and also the possibility of reduced thermal stress. In this work the rod type diluent subassembly was chosen.

In this study, depleted uranium is considered as a diluent (or breeder).This clearly must be clad.

6.2.2 The Multi-Cell Approximation of a Heterogeneous Core

WIMS offers a unique feature in taking account of the effect of the surrounding environment upon the neutron spectrum of a cell. Geometry is expressed in terms of the 'frequency' in the system, where cells are combined in a collision probability

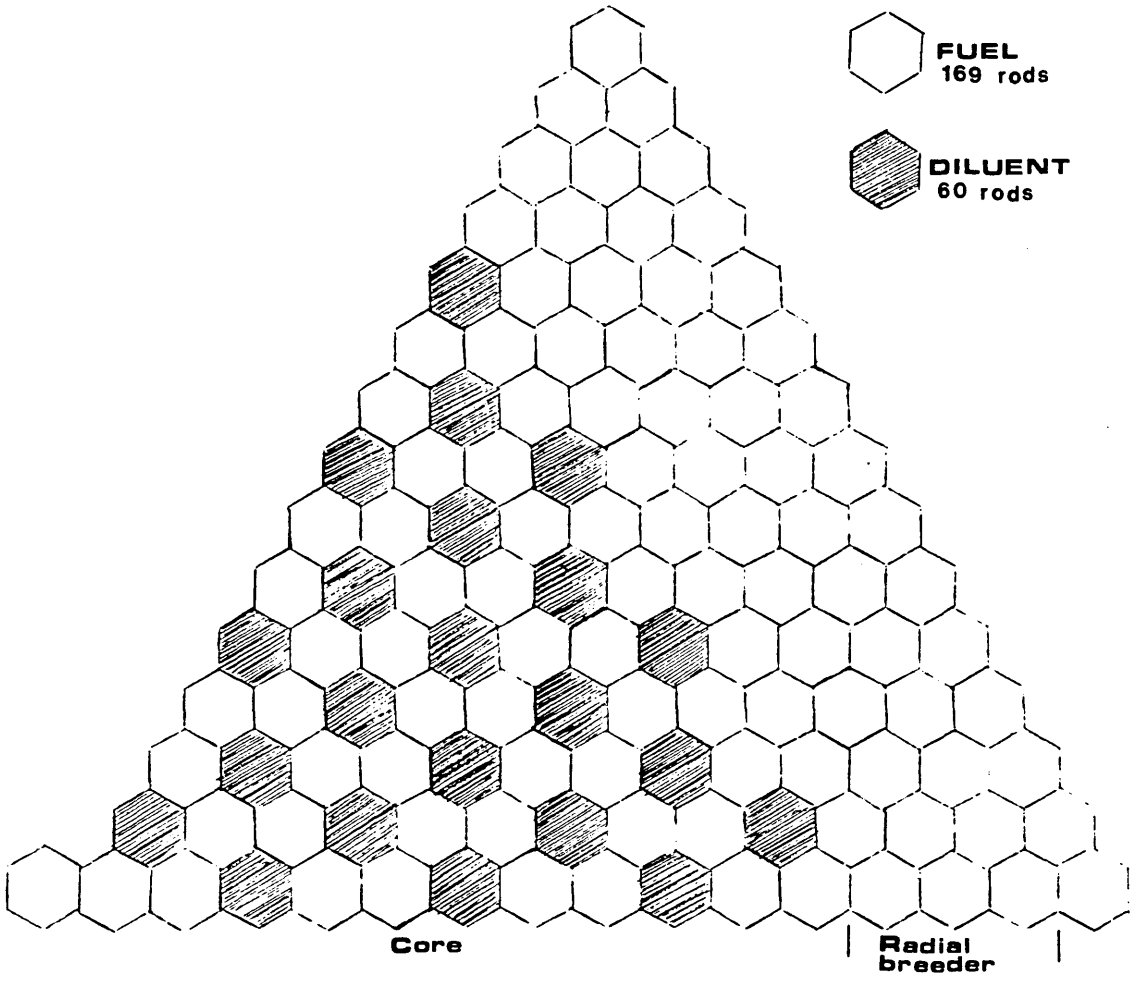

Figure 6.11. A sextant of the heterogeously diluted ETGBR core.

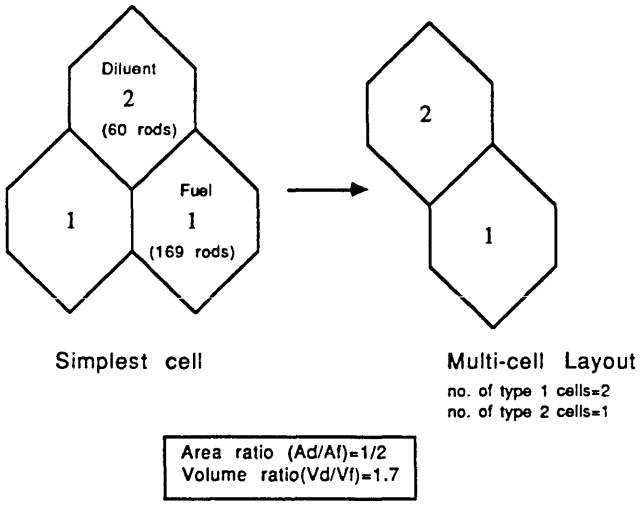

Figure 6.12. The Multi-Cell unit used in WIMS

solution in WIMS-D4/MULTICELL by specifying the probabilities that a neutron leaving each cell type will enter a cell of the same or another type [3].

The recomended [4] and simplest assumption is that the probabilities are directly proportional to the "contiguous" surface between the cells. For the geometry in question here, figure (6.12) shows the multi-cell unit of fuel and a diluent subassembly.

The probabilities based on a six sided hexagon thus become:

$$\begin{pmatrix} P_{11} & P_{12} \\ P_{21} & P_{22} \end{pmatrix}$$

and is equal to

$$\begin{pmatrix} 3/6 & 3/6 \\ 1 & 0 \end{pmatrix}$$

where P_{ij} is the probability that a neutron born in region i enters j. A WIMS-D4/MULTICELL input listing for a heterogeneously diluted ETGBR core is shown in Appendix (3).

The BOL heterogeneous models studied in this section:

(1) fuel + graphite
(2) fuel + alumina
(3) fuel + depleted uranium
(4) fuel + graphite + depleted uranium
(5) fuel + alumina + depleted uranium

Where, for (4) and (5), the model has graphite or alumina in the inner core zone and depleted uranium (depleted U) in the outer.

6.2.3 Bare Lattice Cell Calculation

This is the simplest possible calculation and is performed wholly and consistently with WIMS-D4. As before the geometry is one without any region other than the heterogeneously diluted core. This, then, is a calculation of a non-externally blanketted or non-reflected core. Leakage is approximated by the use of geometrical bucklings obtained using the dimensions of the bare core zone standard ETGBR. Hence, the bare radius is 164.45 cm and the bare height is 140.0 cm giving $B_r{}^2 = 2.13 \times 10^{-4}$ and $B_z{}^2 = 5.03 \times 10^{-4}$ (cm^{-2}).

Both BOL calculations and burnup are performed using the WIMS-D4 lattice model,where data for the diluent subassemblies and for the fuel subassemblies are smeared and catalogued in WIMS-E format as usual. Data is subsequently available for WIMS-E/WSNAP whole reactor models.

Table (6.7) shows the change in k_{eff} with time for the diluted heterogeneous lattices. The similarity to the k_{eff} values of the pin-diluted cases of the previous section is apparent; and aa enrichment of 21% is required for a reasonable reactivity-lifetime.

Table (6.7): Bare lattice reactivity rundown of heterogeneously diluted cores

	k_{eff}			
	Graphite		Alumina	
time(yrs)	18%	21%	18%	21%
0	0.9678	1.0521	0.9793	1.0676
0.5	0.9512	1.0317	0.9643	1.0487
1	0.9446	1.0221	0.9595	1.0402
1.5	0.9304	1.0044	0.9468	1.0239
2	0.9248	0.9959	0.9426	1.0161

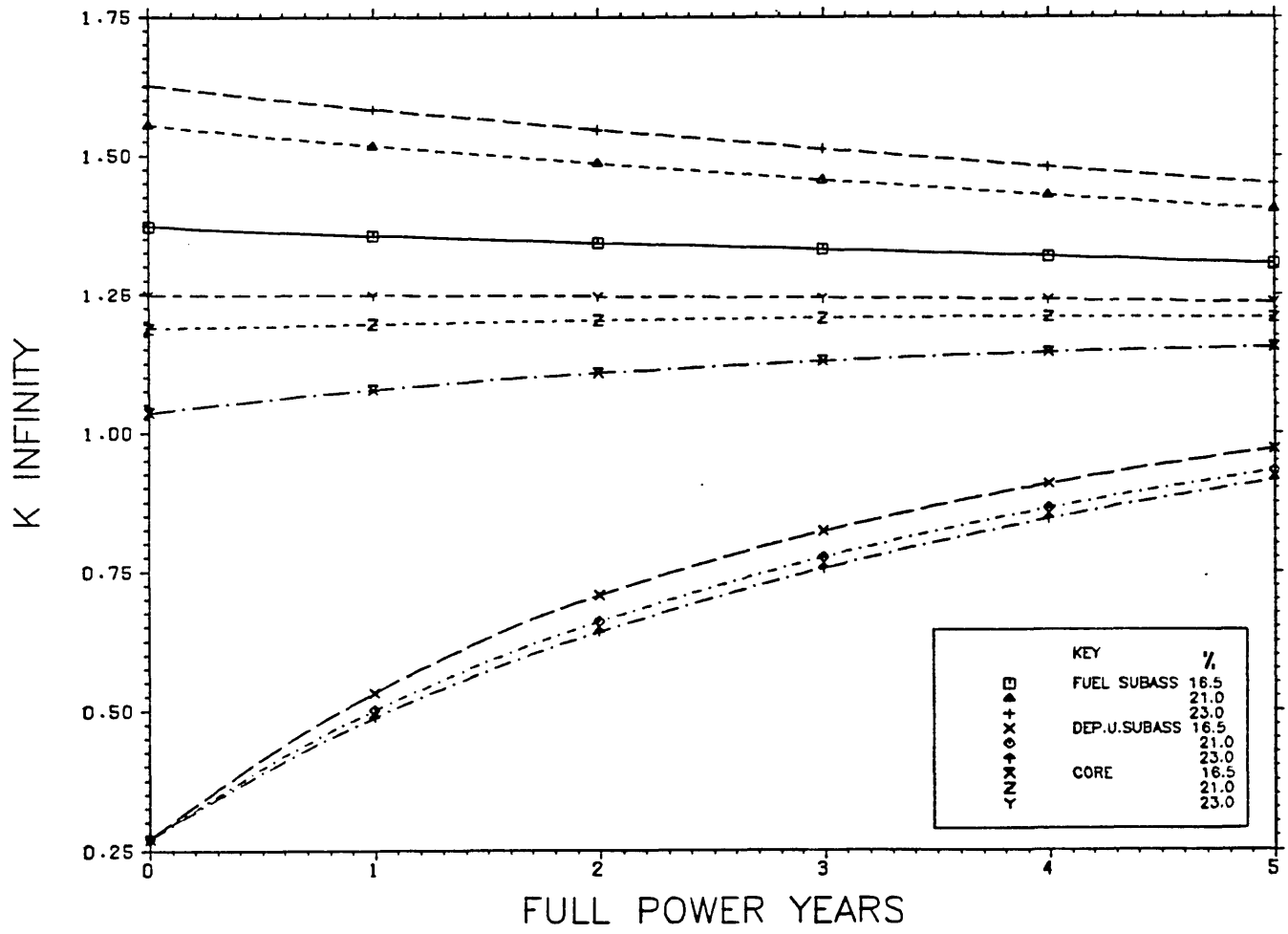

Figure 6.13. k_∞ versus time for the heterogeneous breeder at three enrichments. Shown is the partial k_∞ for fuel subassemblies, the depleted U subassemblies, and the overall core.

The heterogeneous core with depleted uranium dilution shows a different behaviour of reactivity with time as shown in table (6.8) for several enrichments. Figure (6.13) further clarifies this by showing that the k_∞ of the internal breeder to rise with time and to approach 1.0.

Table (6.8): Depleted uranium heterogeneous lattice reactivity rundown.

	k_{eff}		
time(yrs)	18%	21%	23%
0	0.8845	0.9676	1.0195
1	0.9051	0.9714	1.0151
2	0.9203	0.9743	1.0111
3	0.9304	0.9749	1.0062
4	0.9369	0.9739	1.0006
5	0.9403	0.9716	0.9944

Using this lattice-cell approximation, reactivity-liftimes (single-batch) of 1.6 years for graphite and 2.2 years for alumina cases were predicted. The corresponding initial enrichment for these cases was 21% Magnox Pu. For the depleted uranium heterogeneous core, at an initial enrichment of 23.0% Magnox Pu, a reactivity-lifetime of some 3.2 years is noted with an extremely shallow burnup drop.

The time variation of k_{eff} for the 396 subassembly reactor has been discussed up to this stage. To study the possibility of designing a heterogeneously blanketted core that is critical at lower enrichment, the size of the core was varied using WIMS-D4 with appropriate geometric bucklings. The height of the core was such that the ratio of core height to diameter remained at 0.425.

Table (6.9): Dependence of k_{eff} on reactor lattice size for (depleted uranium heterogeneous core)

No. of subassemblies	Radius(cm.)	Height(cm.)	k_{eff} (BOL)
396	164.45	140.00	0.8845
546	193.27	164.45	0.9338
630	207.41	176.55	0.9519
918	250.37	213.12	0.9916

Table (6.9) shows that a very large core is required to approach criticality at BOL. Burnup of such an enlarged core, with 630 subassemblies, is shown in figure (6.14). It shows the difficulty of designing a reactor, with sufficient reactivity, which also produces a reasonable reactivity-life. A reactivity-life of some 10 years is noted. An enrichment of at least some 20% is required to have a system with just enough reactivity from the onset of core burnup. Lower initial enrichments (16.5 to 19%) all lead to roughly the same discharge burnup levels, but have initial periods of subcriticality of about 4 years for the lower enrichments down to about 1 year for the 19% case.

6.2.4 Fully Reflected Heterogeneous Cores

In order to study the more realistic, reflected (or blanketted) reactor, the WIMS-E WSNAP/Hex-Z capability was used. The reflector, as before is taken to be pure iron. First, as a check on the calculation, the leakage-corrected lattice data was used in WIMS-D4 and WIMS-E to calculate the finite bare heterogeneous lattice cases. Table (6.10) compares the BOL k_{eff} of the heterogeneous cases as computed by the WIMS-D4/PERSEUS cluster option and the WIMS-E/WSNAP Hex-Z diffusion theory calculation.

Agreement for the diluted cases is reasonable at 1.3%dk for graphite and 0.9%dk for alumina heterogeneous dilution. For the depleted uranium case at 18% enrichment the discrepancy is greater at 3.24%dk.

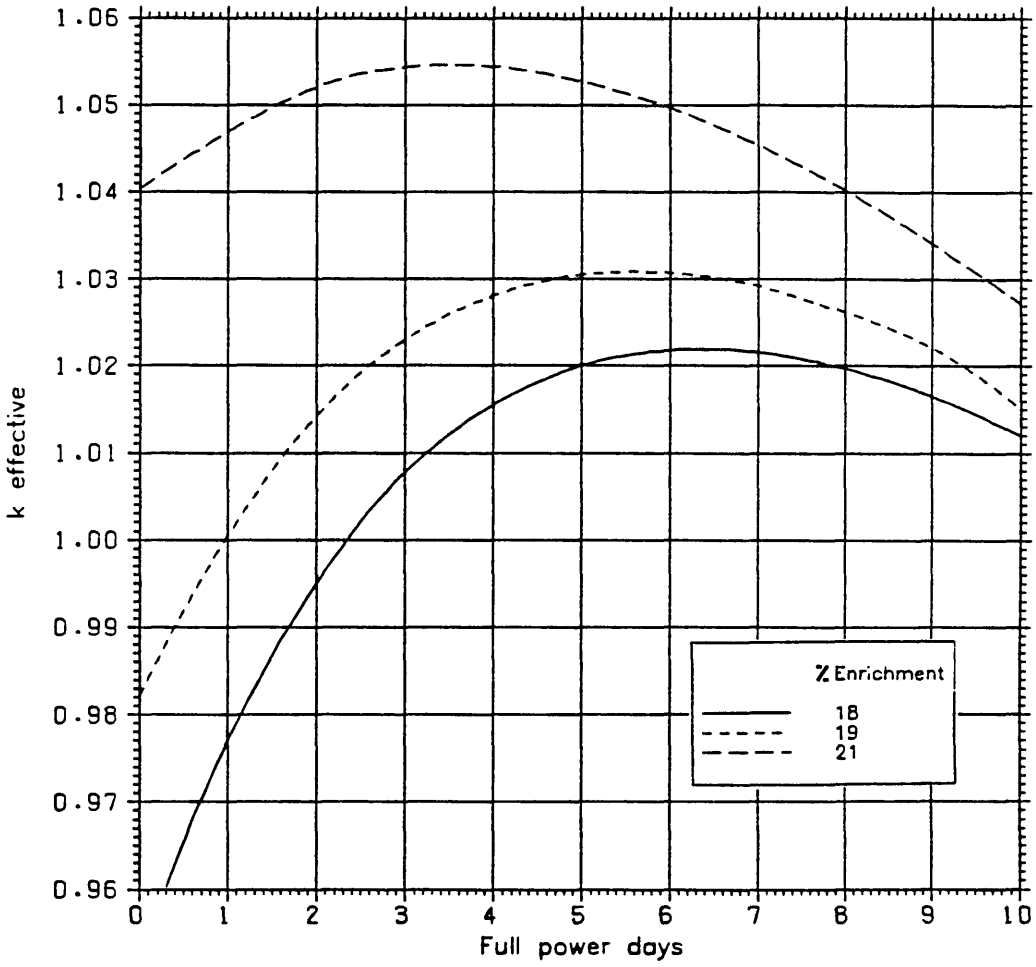

Figure 6.14. Burnup of large heterogeneous breeder core. (depleted uranium breeder/diluent)

Table (6.10): Bare heterogeneous core k_{eff} as computed by either WIMS-D4 or WIMS-E routes

	k_{eff}		% Discrepancy
	WIMS-D4	WIMS-E	
Graphite, 18%	0.9678	0.9550	1.3
Alumina, 18%	0.9793	0.9701	0.9
Depleted U, 18%	0.8845	0.9169	3.20
Depleted U, 23%	1.0195	-	-

The single region fully reflected heterogeneous core was then subjected to burnup in order to determine reactivity-lifetimes. Table (6.11) shows that, for the 18% enrichment heterogeneous core, graphite dilution gives a reactivity-lifetime of somewhat less than 2 years, while the alumina diluted case gives about 2 years.

Table (6.11): Burnup of 18% enriched fully reflected heterogeneously diluted cores (single regions).

	Graphite		Alumina	
time(yrs.)	unreflected	reflected	unreflected	reflected
0	0.9550	1.0313	0.9701	1.0387
1	0.9316	1.0065	0.9499	1.0175
2	0.9116	0.9856	0.9326	0.9997

The heterogeneously blanketted depleted uranium core shows the different behaviour already shown in figure (6.14) for the bare core. Here, with reflectors included, the burnup behaviour is even more difficult to determine due to the rapidly rising values of k_{eff} that appears to be a feature of this type of core (Table (6.12)).

Table (6.12): Burnup of 18% enriched hetergeneous breeder with reflectors.

time (years)	unreflected	reflected
0	0.9169	0.9806
1	-	1.0143
2	-	1.0348

6.2.5 The Alumina Heterogeneously Diluted ETGBR

Alumina, the candidate diluent of this work, was given further assessment. Results given in this section show alumina to have some neutronic advantages over graphite.

An 18% initial enrichment for the core fuel subassemblies was adopted and the core zone kept at the size given previously. Whole reactor calculations are performed to determine the relative reactivity worths of the different zones as they are added to the core. Table (6.13) shows the results.

Table (6.13): Break down of the reactivity of the 18% alumina heterogeneously diluted ETGBR. (reactivity worth above bare core value).

Zone	k_{eff}	%Reactivity Worth
Bare Core	0.9701	-
Radial Reflector	0.9819	1.18
Axial Reflector	1.0257	5.56
Radial and Axial Reflector	1.0387	6.85
Radial Breeder	0.9839	1.38
Axial Breeder	1.0278	5.76
Radial and Axial Breeder(*)	1.0439	7.38

(**AR had to be removed but accounted for little worth anyhow*)

A large axial reactivity worth component is noted (some 80% of the total). This confirms the significance of the axial leakage.

To have

A single region is expected a large power gradient and for this reason a two core zone design was assessed. A two zone core was studied with an inner enrichment of 17.0% and an outer enrichment of 19.0%, giving an average enrichment of 17.91% (for 217 inner and 180 outer subassemblies). The reflected core gives k_{eff} of 1.0146 while the reflected radially-blanketted core has k_{eff} of 1.0381.

Initial internal and overall fuel conversion ratios of selected cases are shown in table (6.14); alumina cases are compared with other heterogeneous cases. The alumina diluted two zone core is seen from the table to have higher conversion ratio, while having a lower k_{eff} than the single zone core of the same effective enrichment. Greater leakage from the higher enrichment outer zone is the apparent reason.

Table (6.14): Conversion ratios for reflected heterogeneous cores (axial reflector thickness is 14.32 cm. except in the last two entries where it is 42.96 cm.)

Case	k_{eff}	ICR	CR(or BR)
Graphite 18%	1.0312	-	0.7128
Alumina 18%	1.0387	-	0.7482
Depleted U 18%	0.9806	0.7457	1.1632
Alumina 18% + RB	1.0411	0.7536	0.8643
Alumina 18% + RB + AB	1.0439	0.7444	0.9447
Depleted U 18% inner, Alumina 18% outer,	1.0070	-	0.9706
Alumina 18% + RB	1.0631	0.7560	0.8671
Alumina 17% inner, Alumina 19% outer + RB	1.0381	0.7754	0.9084

Burnup behaviour of the alumina heterogeneous reactor, with a radial blanket, differs little from that of the alumina core alone. However, table (6.15) shows that the axial reflector height is small enough to influence the reactivity magnitude due to less neutrons being lost by leakage. A three fold increase in the thickness of the

axial reflector leads to a 2% increase in k_{eff}. This, in turn, leads roughly to the extending of the core life from 2 to about 3 years.

Table (6.15): Effect of axial reflector height on reactivity of alumina heterogeneously diluted ETGBR (18 %).

	effective multiplication factor, k_{eff}	
time(yrs)	AR height=14.32cm	AR height=42.96cm
0	1.0411	1.0613
2	1.0030	1.0226

(note: AR denotes axial reflector)

The influence of axial reflector height upon reactivity is further shown in table (6.16) for the heterogeneous alumina with two core zones and radial blanket.

Table (6.16): Effect of axial reflector height on reactivity of alumina heterogeneous core with radial blanket

Axial reflector height(cm.)	k_{eff} (BOL)
14.32	1.01824
21.48	1.02781
42.96	1.03810
57.28	1.03860

Setting aside the issue of fuel cost, it is possible to provide some saving on enrichment by enlarging the size of the core. An enlarged core lattice is compared with the standard core in table (6.17). Both the height and the radial number of subassemblies has been increased while maintaining the height-to-diameter ratio fixed close to 0.5.

Table (6.17): Alumina heterogeneous ETGBR specifications for small and large core cases.

	Base	Large
Subassemblies	397	547
Radius (cm.)	164.45	193.27
Height (cm.)	140.0	164.5
B_r^2	2.13×10^{-4}	1.548×10^{-4}
B_z^2	5.035×10^{-4}	3.647×10^{-4}
L/D	0.4256	0.4256
Rating (¡MW/t)	47.8	47.8

The effect of this change on reactivity rundown is shown in table (6.18). The increased reactivity of the larger lattice is apparent. k_{eff} is larger by 5 to 6 % for the 18% to 21% enrichment cases. A reasonable reactivity- lifetime ensues for the 'large' 18% enriched alumina heterogeneous ETGBR: about 2 years.

Table (6.18): Reactivity rundown for alumina heterogeneous ETGBR small and large core cases.- k_{eff} values

	18%		19%	21%	
time(years)	Base	Large	Large	Base	Large
0	0.9793	1.0375	1.06911	1.0676	1.1293
1	0.9595	1.0123	1.0407	1.0362	1.0960
2	0.9426	0.9949	1.0204	1.0122	1.0710

(*note: Magnox discharged plutonium enrichment*)

Tables (6.19) and (6.20) show fissile utilization of the heterogeneously diluted variants. Fissile usage is typical of a fast core showing a small consumption figure (and hence consumption per feed). The discharge enrichment is quite high (about 80-90% of feed enrichment). With a larger core, although the fissile usage is not very different from the smaller core, the reduction in enrichment is clear. As

already noted, the high breeding of fissile material in such fast cores leads to the low net consumption of fuel and high fissile discharge.

Table (6.19): Small core fissile usage at 21% Magnox Pu, (kg/GW-yr)

	Graphite	Alumina
Feed (F)	2288	1465
Discharge (D)	2071	1348
Consumption (C)	217	117
C/F (%)	9.5	8.0
D.I.(GWd/t)	29.02	45.32
Discharge fissile enrichment(%)	15.91	15.33 (BOL=17.51)

Table (6.20): Large core fissile usage at two Magnox Pu enrichment levels, (kg/GW-yr)

	18%	19%	
	Alumina	Graphite	Alumina
Feed (F)	2618	1450	1143
Disharge (D)	2541	1347	1052
Consumption (C)	77	102	91
C/F (%)	3	7	8
D.T.(days)	438	803	1058
Fissile Enrichment% :			
Feed	15.02	15.85	15.85
Discharge	14.24	14.10	13.74

Doppler Coefficient of Reactivity for Heterogeneous Lattices

A calculation of the temperature coefficient of reactivity for the three types of heterogeneously diluted ETGBRs was performed using the temperature states given in table (6.21). Changes in k_{∞} and k_{eff} with temperature are presented in table (6.22). Based on these calculations, the Doppler coefficients of reactivity are estimated as -8.77×10^{-3} for the graphite heterogeneous ETGBR, -8.22×10^{-3} for the alumina heterogeneous ETGBR, and -7.67×10^{-3} for the depleted uranium heterogeneous ETGBR in the $1000 to 1200°C$ range. Although the dopplers are comparable, the lower value for the depleted uranium core is apparent. The Doppler coefficients for the heterogeneous ETGBRs appear to be less negative than for the block diluted ETGBRs of chapter 5 (greater by close to a factor of 5).

Table (6.21): The temperatures of the components of the heterogeneous ETGBRs at the three temperature states assumed.

Temperature	Temperature State (*)		
(C)	(1)	(2)	(3)
Fuel	1000	1200	800
Clad	850	1050	650
Coolant	750	950	550
Diluent	750	950	550
Dep.U	850	1050	650

** Note: State 1 is base, State 2 is base + 200°, State 3 is base - 200°*

Table (6.22): The variation of k_{∞} and k_{eff} for the heterogeneous ETGBRs with temperature.

	Graphite 18%		Alumina 18%		Dep. U 18%	
State	k_{∞}	k_{eff}	k_{∞}	k_{eff}	k_{∞}	k_{eff}
1	1.2305	0.9678	1.2207	0.9793	1.0726	0.8775
2	1.2279	0.9662	1.2182	0.9778	1.0705	0.8761
3	1.2335	0.9697	1.2235	0.9811	1.0751	0.8790

6.3 CONCLUSIONS

Two additional methods, mixed pin and heterogeneously block diluted, other than that studied in chapter 5, for introducing diluent into an ETGBR core have been presented. As in the previous chapter graphite and alumina dilution were considered. In the heterogeneously diluted concept, depleted uranium was a further dilution consideration. The mixed pin diluted subassembly was shown to be a method offering close proximity of fuel and diluent, while preserving a fast neutron spectrum closer to that of the standard fast ETGBR and therefore giving higher conversion ratios. The more homogeneous nature of the fuel design compared with the block diluted methods, leads to more captures in the diluent and shorter burnups for a given enrichment. Increased reflector worth for the pin diluted cores, with their 'harder' neutron spectra, leads to greater reactivity than for the block diluted cases. Interestingly, alumina shows a burnup advantage over graphite for a 19.77% enriched mixed pin diluted ETGBR.

Reactivity and burnups obtained when using 2/3 dimensional models of the mixed pin diluted ETGBR were shown to be different from those of the lattice calculation. For the 18% enriched graphite pin diluted ETGBR, the difference between the two models was about 3.5%dk at BOL. For the heterogeneously diluted ETGBRs, a similar problem exists but is far less significant (less than 1%dk), except in the depleted uranium case where it is the difference is again above 3%dk. It is of interest to note that the neutron spectrum of these cores are quite 'hard' due to the lower dilution (especially compared to the block diluted cores of chapter 5).

REFERENCES

1. Cohen K. P. , O'Neil G. L. ,*Safety and economic charachteristics of a 1000 MW_e fast sodium-cooled reactor design*, Advances in Nuclear Science and Technology, vol. 4, p. 67, 1968

2. Dickson P. W. , *Engineering aspects of heterogeneous and homogeneous reactors*, BNES conference on optimization of sodium-cooled fast reactors, p. 269, London 1977

3. Massimo L. , *Physics of high-temperature reactors*, Pergamon Press, p. 88, 1976

4. Roth M. J. , Macdougal J. D. , and Kemshell P. B. , *The preparation of input data for WIMS*, AEEW-R538, 1967

CHAPTER 7.

THERMAL AND MATERIAL ASPECTS

7.1 GAS-COOLED REACTOR SAFETY - A GENERAL INTRODUCTION

Hypothetical accidents may be classified by the mismatch between energy production and removal, for example reactivity insertions causing excessive power production, and on the other hand, failure of the heat transport system hindering heat removal. Accidents may be clasified very broadly as 'unprotected' or 'protected' where the term 'protected' implies succesful operation of the Plant Protection System (PPS) [1].

Unprotected transients can be classed as either Transient Over Power (TOP), or Transient Undercooling (TUC). The first occurs when reactivity is inserted into the system at full power, while the second occurs where the power remains constant, but the coolant flow is lost. In both unprotected transients, the primary and secondary reactor shutdown systems are assumed to be unavailable. A third unprotected type of transient is the so-called 'Loss of Shutdown Cooling' (LOSC). Here, a total loss of core cooling occurs for an extended period following reactor shutdown. Unprotected transients may also be termed 'Beyond Design Basis Accidents' (BDBA) because a multitude of engineered safeguards are postulated to fail.

A selection of protected transients initiators may be listed as follows [2]:

1. Breaks in feedwater system piping.
2. Increase/decrease in core heat removal.
3. Reactivity and power distribution anomalies.
4. Moisture ingress into primary coolant system.
5. Decrease in reactor coolant inventory.
6. Failure of normally operating auxiliary systems.

For gas-cooled reactors and GCFR in particular, initiators (3) and (5) in the above list are of significance. In the particular case of the initiator: 'decrease in reactor coolant inventory', the design basis depressurization accident (DBDA) is of major importance since this will lead to raised temperatures. Due to the features of gas cooled reactors, covering both inherent and engineered safeguards,

it is possible to limit the discussion of this accident to a few issues. Of primary importance for a gas-cooled reactor is the ability to cope with a depressurization event. Due to designsimplicity, the design basis accident (DBA) for these reactors has been termed a 'Maximum Credible Depressurization Accident'.

As is the practice with the AGR, the ETGBR DBA may be taken to be a breached vessel with the pressure falling in an exponential manner with time. The time constant depends on the hole size, the volume of the vessel, and the physical properties of the gas. A simple equation to determine the depressurization time constant is as follows [3]:

$$\tau = K \times V/A\sqrt{T}$$

where:

K is 0.3 for Helium and 1.05 for Carbon Dioxide.
V (liters) is the core cavity volume.
A (cm^2) is the rupture hole area.
T (K) is the average (initial) gas temperature.

With roughly the same core cavity volume of 6.45×10^6 liters, ETGBR and AGR depressurization time constants would basically differ as a result of differing average coolant temperatures: $742°K$ for AGR and $661°K$ for ETGBR. For a breached gas-circulator penetration of 325 cm^2, considered as the worst case [4], the depressurization time constants (τ) obtained using the above equation are 765 and 810 seconds for AGR and ETGBR respectively. Kemmish [5] adopts a depressurization time constant of 900 seconds for ETGBR and argues that this value is conservative. It is clearly an improvement over the GBR-4 value of 200 seconds. The role of the depressurization time constant in limiting excessive temperatures will become more apparent in section (7.4).

7.2 THE THERMAL IMPLICATIONS OF ETGBR CORE DILUTION

The motive for much of the work in this thesis is the provision of a material heat sink inside the core zone of the ETGBR. The ETGBR core is mainly composed of fuel (30%) and coolant (55%) with the remainder being cladding and structural stainless steel. The thermal capacity is low especially since the gas coolant, the largest component by volume, has very little thermal inertia.

The additional heat sink (or diluent) considered is in the form of a material with a high specific heat (C_p). Two materials stand out on this basis and on the basis of good structural integrity in the high-temperature, high irradiation field of the reactor. These are graphite and alumina which also have the advantage of being commonly available [6]. Although graphite would absorb fewer of the available neutrons than would alumina, it is a more effective moderator, and would lead to a softer spectrum. This becomes an important feature if a breeding design is required.

Clearly, the diluent should be close to the heat source (fuel-rod) for good heat removal, a homogeneous fuel-diluent fuel rod would be ideal, however, this idea would give design complications with respect to neutronics and material aspects [7].

A second means of introducing diluent into the core is a subassembly made of alternating and seperate pins of fuel and diluent. It is presumed here that both graphite or alumina could easily and cheaply be worked into rods of radius around 0.35 to 0.5 cm. (so as to fit in a subassembly correctly). in this case, heat must be transferred between fuel and diluent by convection or radiation mechanisms. If only radiation transport is available, then this geometry gives good transfer interfaces.

A third alternative would build on the AGR design, giving a diluent block, of hexagonal shape with a fuelled coolant channel in the centre, much like the integral HTR design. The forming of such blocks is likely to be feasible with either graphite or alumina but clearly depends on diluent annulus thickness This design has a good portion of diluent in a location reasonably close to fuel rods,

but radiation heat transport is obviously not as good as in the mixed diluent/fuel rod design. Only the outer rings of fuel rods view the cooler diluent surface.

Diluent inclusion in the core may be of benefit in both DBA and BDBA accident situations (review sec. 7.1). In the case of DBA, the diluent provides, as described above, an additional heat sink for the increasingly hot coolant in a situation where flow is rapidly falling. Although of very small probability of occurence, a particular BDBA case is the loss of shutdown cooling (LOSC) event. With total loss of the cooling system (the main heat sinks which are the boilers), and the system shutdown at full pressure, any heat transport takes place within the core and reflector regions only. Diluent material inclusion would slow down core heat-up.

7.3 THERMAL CAPACITY CONSIDERATIONS

A review of AGR literature will show that temperature transients are said to be slow due to the large heat sink in the core: the Graphite moderation [8].

The safety benefits from a diluent would depend on the diluent quantity; this will depend on whether a fast or thermal system is required. alumina and graphite have been identified as candidate materials. Graphite, which is an excellent moderator and Alumina which has a larger specific heat per unit volume than Graphite. Table (7.1) shows the main thermal properties of these materials. It is apparent from table (7.2) that alumina is an inefficient moderator.

In a full assessment, thermal conductivity, ρC_p, and fire behaviour all need to be considered. For example, with graphite the possibility of igniting exists while alumina does not ignite, at least up to very high temperatures. Furthermore, if temperatures are raised, graphite reacts with the CO_2 coolant.

If the specific heat capacity (joules /gram non-fuel /degree) is calculated for the AGR and compared with that for the ETGBR, it is apparent that it has about ten times the thermal capacity. However, in this work the aim is to increase the heat capacity of ETGBR somewhat, without departing substantially from a

Table (7.1): Thermal properties for pertinent materials

Material	Density $(\rho)(Kg/m^3)$	Thermal conductivity (k) $(W/m.K)$	Heat capacity (C_p) $(KJ/Kg.K)$	(ρC_p) $(KJ/m^3.K)$
UO_2	10500	2.50	0.325	3412
Steel	7960	25.0	0.500	3980
Graphite	1700	83.5	1.835	3119
Alumina	3700	7.0	1.282	4743
CO_2	35	-	1.088	40

Table (7.2): Moderating properties of some materials of interest

	$\xi\Sigma_s$	$\xi\Sigma_s/\Sigma_a$
Water	1.380	62
Graphite	0.066	227
Alumina	0.035	4

Table (7.3): Heat capacities of pertinent reactor cores

	Total J/deg.	Total J/deg./gm.	Non-fuel J/deg./gm.
AGR	1.41×10^6	1.485	1.414
ETGBR	1.43×10^5	0.375	0.145
DETGBR V_d/V_f =2.0 graphite	2.69×10^5	0.672	0.452
DETGBR V_d/V_f =2.0 Alumina	3.55×10^5	0.703	0.529

fast spectrum reactor. In table (7.3) the AGR, ETGBR, and the 'mildly' diluted ETGBR cases (chapter 5) are compared in terms of heat capacity per unit height of core.

It may be seen that a relatively small dilution of ETGBR cores can increase the thermal capacity available in non fuel components of the core by some 300%

and bring the core to above one third of the AGR thermal capacity (if Alumina is used). In fact, figure (7.1) shows that for the lower diluent to fuel volume ratios, alumina cores have a higher thermal capacity than graphite cores. It is not until a V_d/V_f ratio of about 5.0 is reached that graphite shows an advantage. This is due to the greater heat capacity of graphite per unit mass, when larger masses begin to dominate.

To make a link with neutronics, if the non-fuel specific heat capacity of the diluted lattices are plotted against conversion ratio, figure (7.2) results. An inverse relationship is apparent. For a given conversion ratio, alumina gives in general a higher specific heat capacity. Reactivity must, however, be taken into account. It can be seen from the figure that, for 18.0% enrichment, for the same conversion ratio, only a small margin exists for an alumina diluted core and then only at small dilution ratio's. Hence, there is, as previously noted in chapter 5, an enrichment benefit favouring graphite and yielding longer burnups. Alumina, however, with 18.0 % enrichment and V_d/V_f =2 may be a desirable possibility and gives superior specific heat capacity to graphite at the same neutronic conditions.

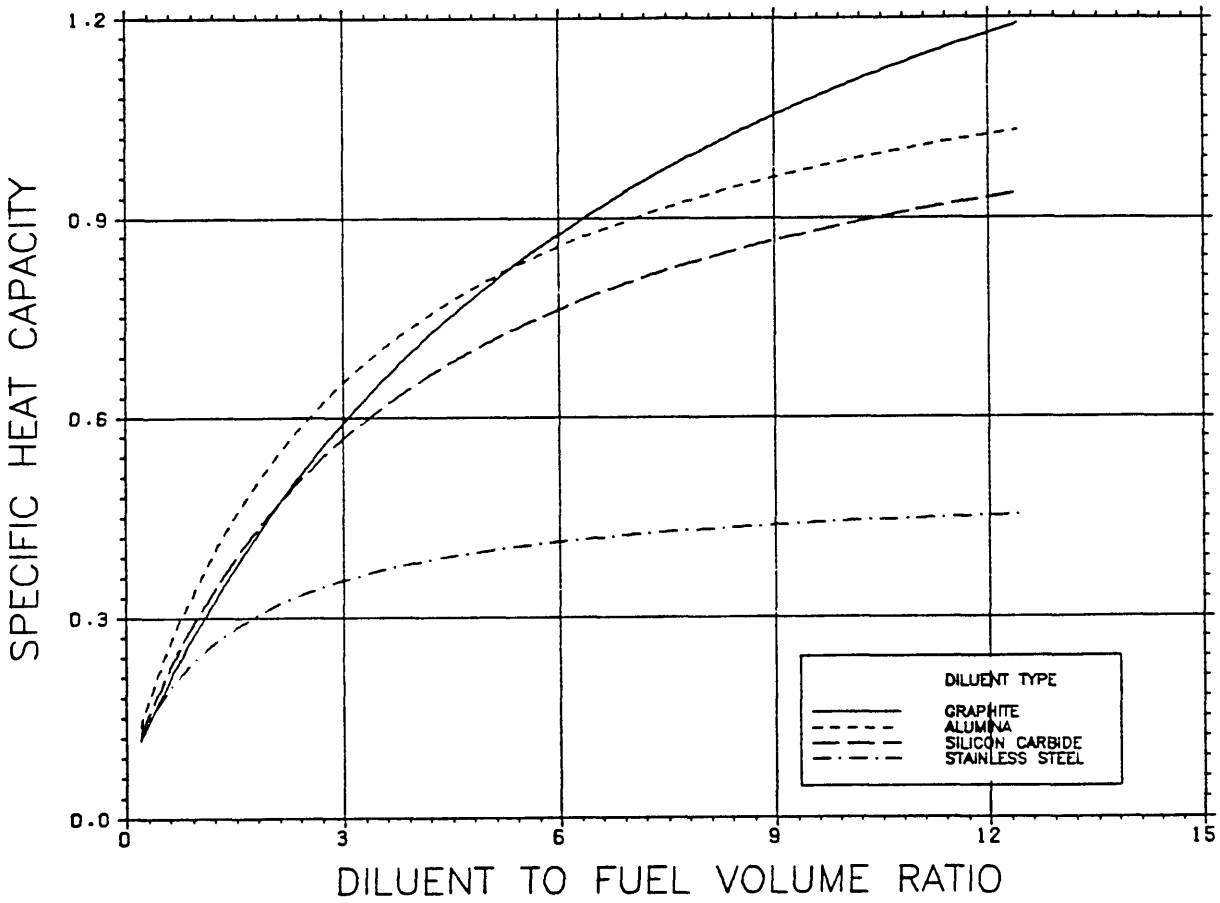

Figure 7.1. Heat capacity in non-fuel materials per unit mass of all components of cluster lattices with different diluents.

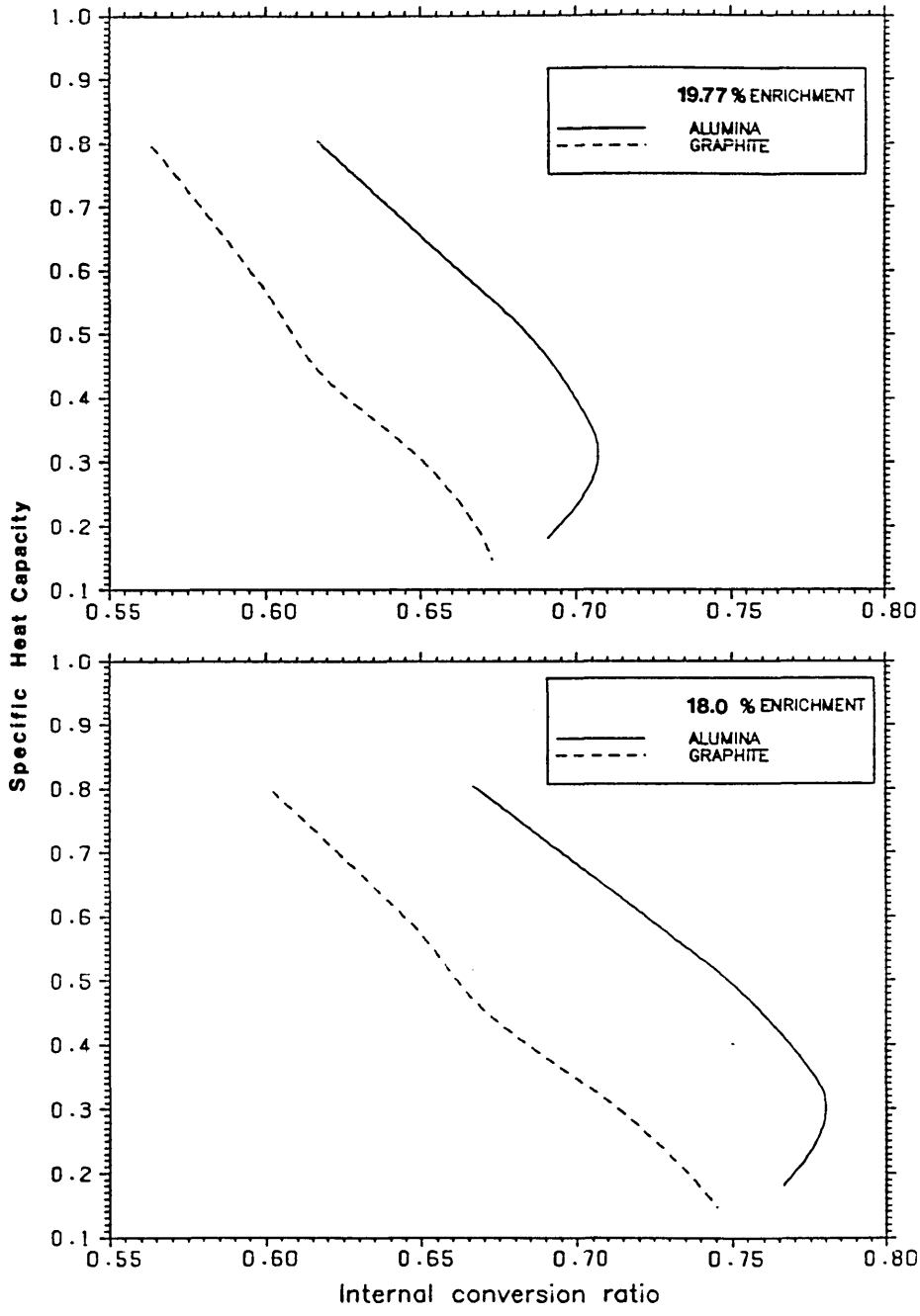

Figure 7.2. Specific heat capacity versus coversion ratio for DETGBR cases studied.

7.4 A REACTOR PRIMARY CIRCUIT DEPRESSURIZATION TRANSIENT

The value of diluent in the event of a depressurization has been studied in a simple manner. The calculation employed only a few parameters, such as the depressurization time constant and the time at which the reactor trips from full power to decay heat level.

By necessity some assumptions had to be made about the reactor and the associated boiler(s) in order to keep the calculation simple as well as consistent and realistic. Table (7.4) gives the major characteristics of the ETGBR as assumed in the depressurization study.

Table (7.4): Assumed ETGBR characteristics.

Power Output	1680 MW(h)
Total Mass Flow Rate	5750 kg/s.
Subassemblies	397
Rods Per Subassembly	169
Coolant Density	31 kg/m^3
Coolant Pressure	40 bar

These specifications lead to the following values :

Power per rod	25 kW
Coolant Flow Area per Rod	6.77×10^{-5} m^2
Mass Flow per rod	1265 $kg/s.m^2$
Coolant Velocity	41 m/s.

The main assumptions adopted in this study were as follows:

1. The fuel channel is an average channel, generating an average power given by the total output and the number of fuel rods.

2. Power rating of the fuel rod is axially flat so that only the total rod output is used. Additionally, the maximum temperature occurs at the core top.

3. The boiler has a fixed steam side temperature, given as the saturation temperature at the initial pressure conditions. Also, the boiler behaves as a simple single heat exchanger of a given area.

4. There is no heat loss between core and boiler.

5. The pressure during the depressurization transient behaves in an exponential fashion as:

$$P = P_0 \times exp(-t/\tau)$$

where τ is the depressurization time constant, taken as 500 seconds for thr ETGBR and its variants: this is a conservative re-estimate of the 900 second figure quoted earlier for ETGBR in section 7.1. P_0 is the initial steady state pressure.

6. The coolant always behaves as an ideal gas and the flow rate during the transient is governed by pressure and temperature as follows:

$$W_n = W_{n-1} \times P_n/P_{n-1} \times T_n/T_{n-1}$$

where: W is the mass flow rate, P the pressure and T the coolant temperature. Average axial channel conditions are used and n denotes the current time step.

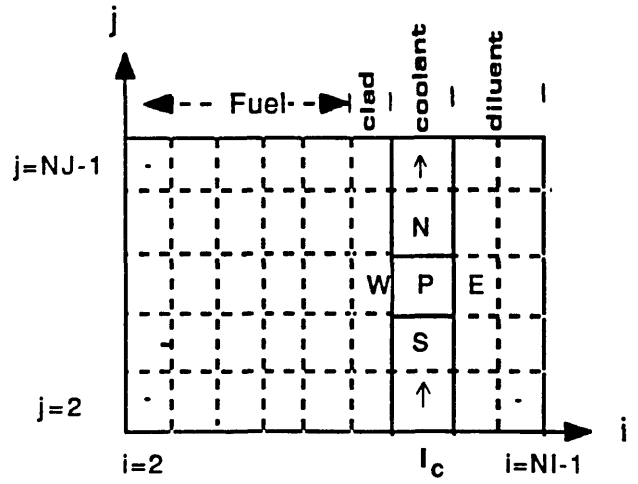

Figure 7.3. The R-Z model of a reactor cell used in TEANT

7. Geometry : The assumption is made that, if this is to represent the hexagonal cluster of the ETGBR and its diluted variants, then each pin is assigned a portion of the outer wrapper or diluent (moderator). This may not be a very sound assumption, but is reasonable for comparisons and is better than any lumped-sum technique. Alternatively, with a mixed pin type cluster, the same geometry may be taken to be one with a fuel rod surrounded by a ring of diluent rods where the diluent rods are smeared. The geometrical model common to both methods of dilution is shown in figure (7.3).

With these assumptions, the program TEANT was written to study the transient temperature response in a depressurization event, with full power changing to decay heating at a specified trip time. A full listing of the program is given in appendix (7) where details of the calculational procedure are given as well. It must be added that the program builds on a simple version of the TEACH-C program available at Imperial College [9].

Figure (7.4) shows the change in maximum clad temperature following the start of a depressurization. Two time constants are used and the figure illustrates the importance of making this as long as possible. With the shorter time constant of 250 seconds, a rapid trip would be needed to keep clad temperature below about $850°C$, at least in the first 15 minutes. With the assumed time constant of 500 seconds and a trip time of 4 minutes, the clad temperature slightly exceeds $850°C$ before the trip. A very slow rise in clad temperature then ensues.

In figure (7.5), for the alumina diluted case (V_d/V_f =3), it is seen that with a delayed trip at 4 minutes, and a τ of 250 seconds, the maximum clad temperature at 20 minutes from transient initiation is $1200°C$ (compared to $1500°C$ for the standard ETGBR case). If the trip were to take place earlier, at 2 minutes, the peak clad temperature at 20 minutes would be reduced by only about $30°C$. Thus the depressurization time constant is seen to control the transient and in this case, with τ taken to be 500 seconds, the maximum clad temperature at 20 minutes is limited to only $500°C$.

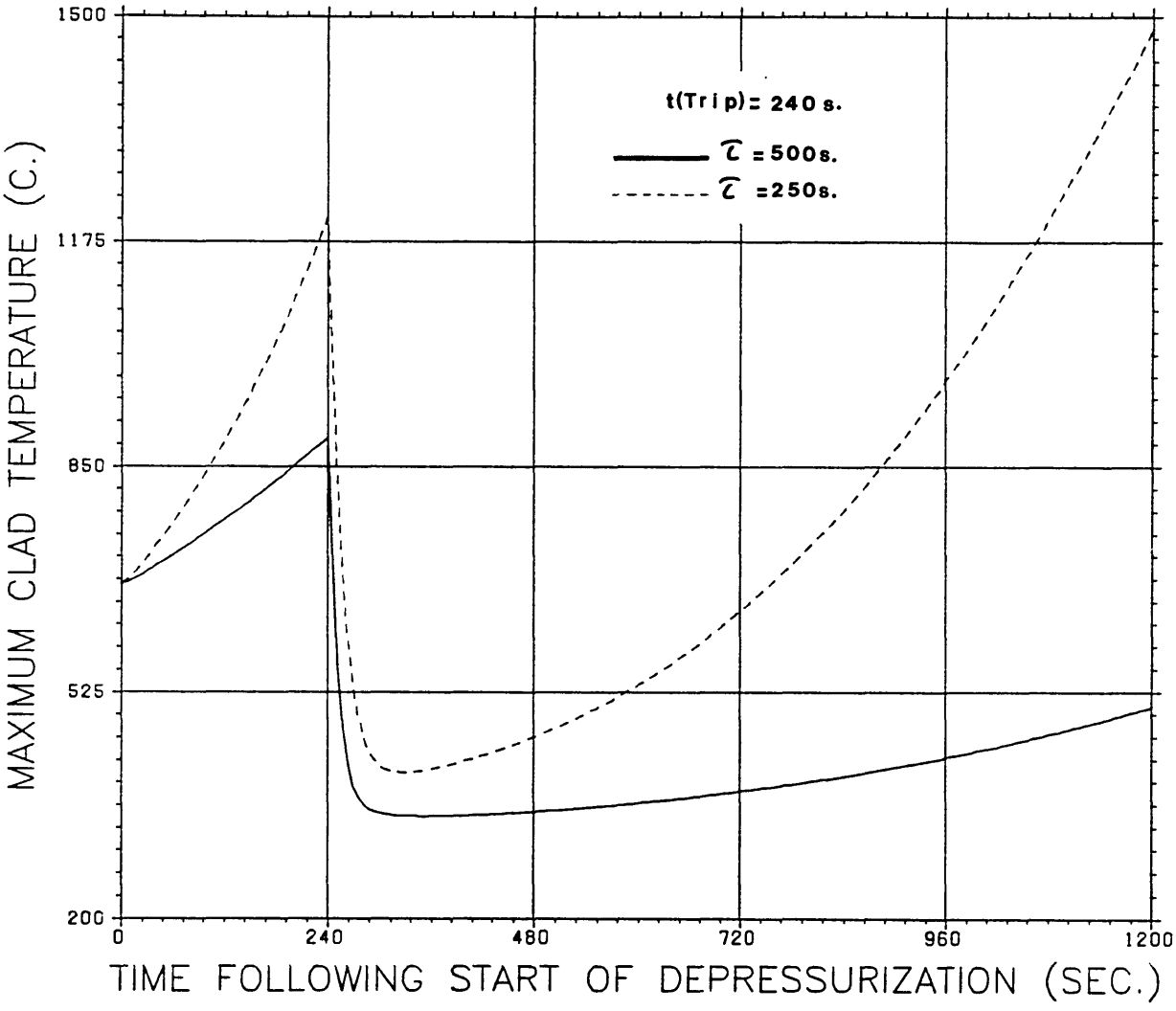

Figure 7.4. The effect of depressurization time constant (τ) on transient clad temperature for standard ETGBR

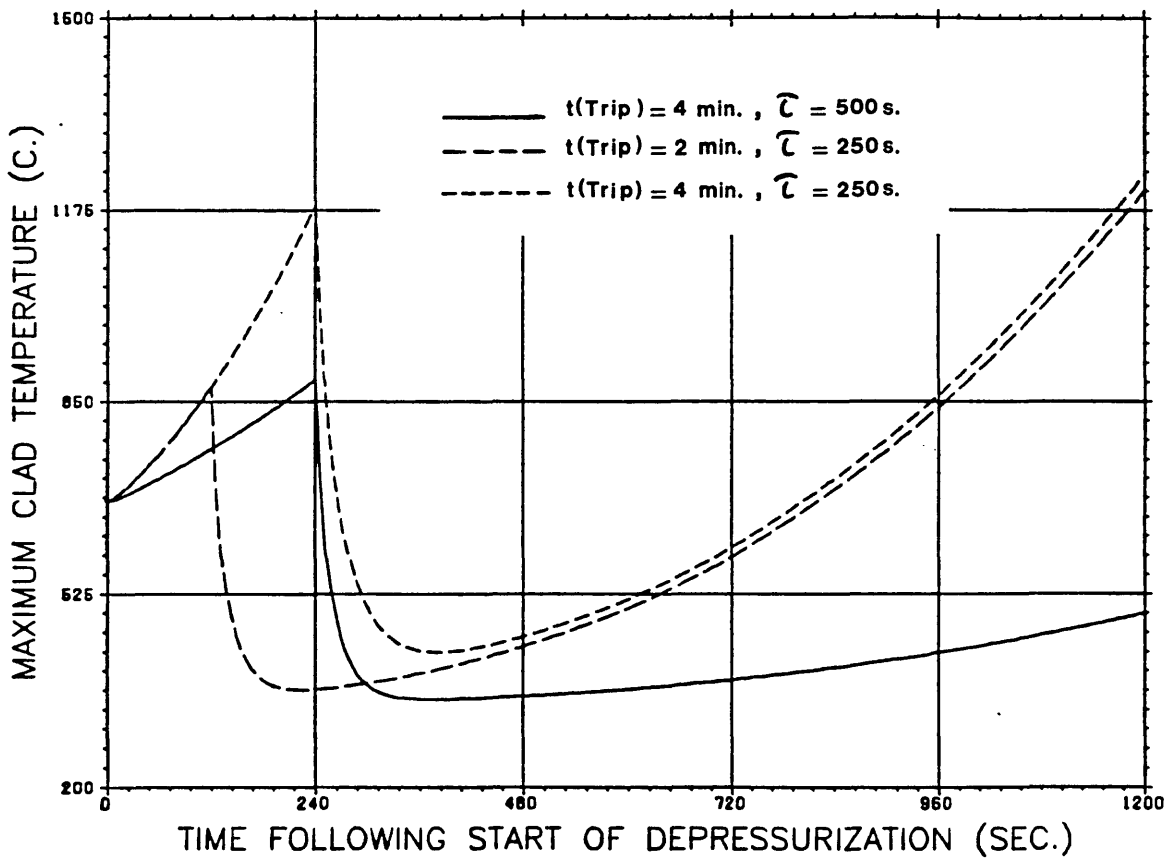

Figure 7.5. Effect of trip time and depressurization time constant on transient clad temperatures of alumina diluted DETGBR with V_d/V_f =3.

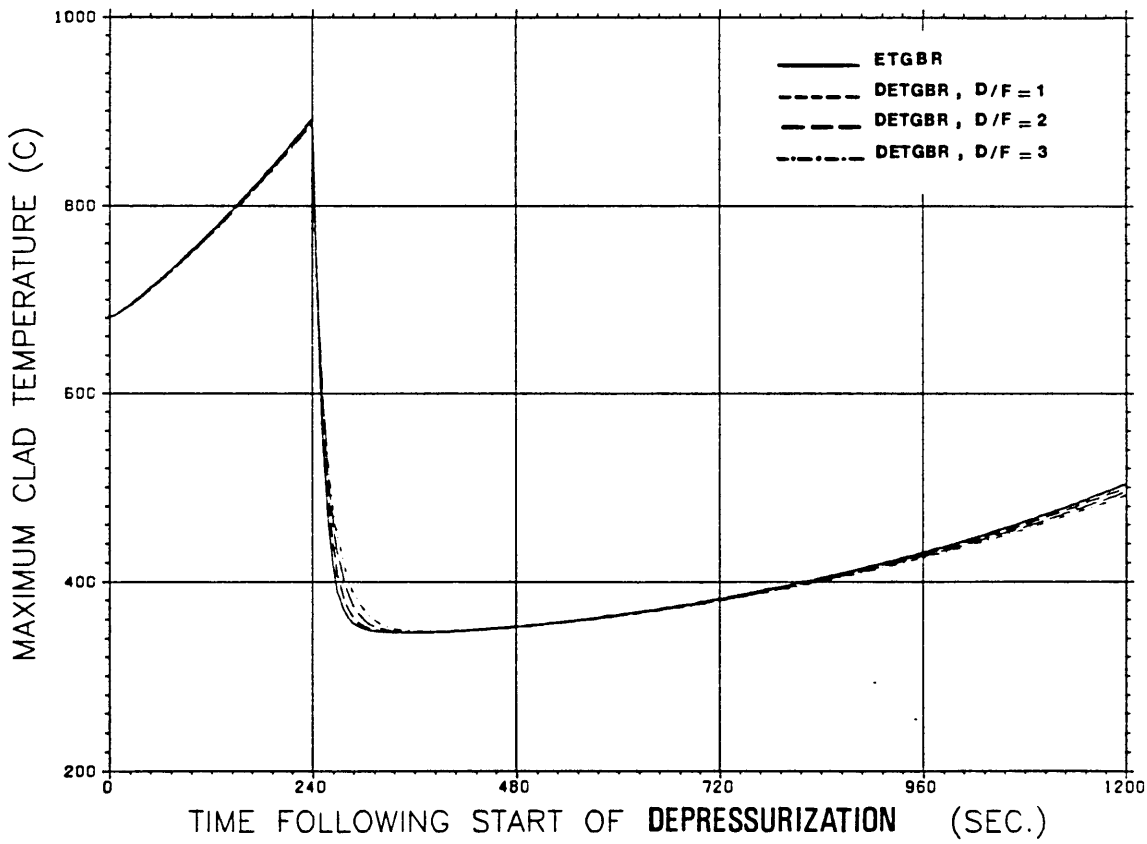

Figure 7.6. Evolution of maximum clad temperature following a depressurization event with τ of 500 s. and trip at 4 minutes. Standard ETGBR and alumina diluted ETGBR at three dilutions shown

With the small dilutions used (for DETGBR), some reduction of temperature rise is possible. Figure (7.6) shows this for alumina dilution cases V_d/V_f of 1, 2, and 3. The actual change is not very striking but interestingly does increase with time. For the V_d/V_f =3 case, the clad temperature at 20 minutes is reduced by about $25°C$. It must be emphasized that these calculations are only valid within the limits of the assumptions made but are indicative of the dependence of temperature transient upon dilution.

7.5 A FULLY DEPRESSURIZED CASE WITH RADIATIVE HEAT TRANSFER ONLY

A limiting calculation is that where the only heat transfer from the fuel rod is by radiation to the diluent (moderator) annulus, and represents a situation where the coolant is lost immediately in a hypothetical deppressurization transient. Although this is an unrealistic situation, it gives additional insight into the value of non-fuel materials in proximity to the fuel. The calculation is performed as in the previous section but using a specially modified version of the program simplified by the removal of convective heat transfer. The geometry studied was the same as shown in figure (7.3) and was modelled in a similar manner. Emissivities used were calculated using the annular geometry given. Some of the calculational techniques used are given in the appendix.

Figure (7.7) shows the change in the maximum clad temperature following the tripping of the reactor. It is seen that an increase in diluent material amount causes a significant reduction in the rate of rise of the maximum clad temperature. Alumina, with its high heat capacity gives the slowest rise of temperature for a given amount of diluent. Alumina at a V_d/V_f ratio 2 is superior to graphite at the higher V_d/V_f of 3. With alumina at V_d/V_f of 2 the maximum clad temperature 5 minutes after the start of the transient is slightly in excess of $1000°C$, nearly $100°C$ lower than the case for graphite at V_d/V_f of 3 at that time.

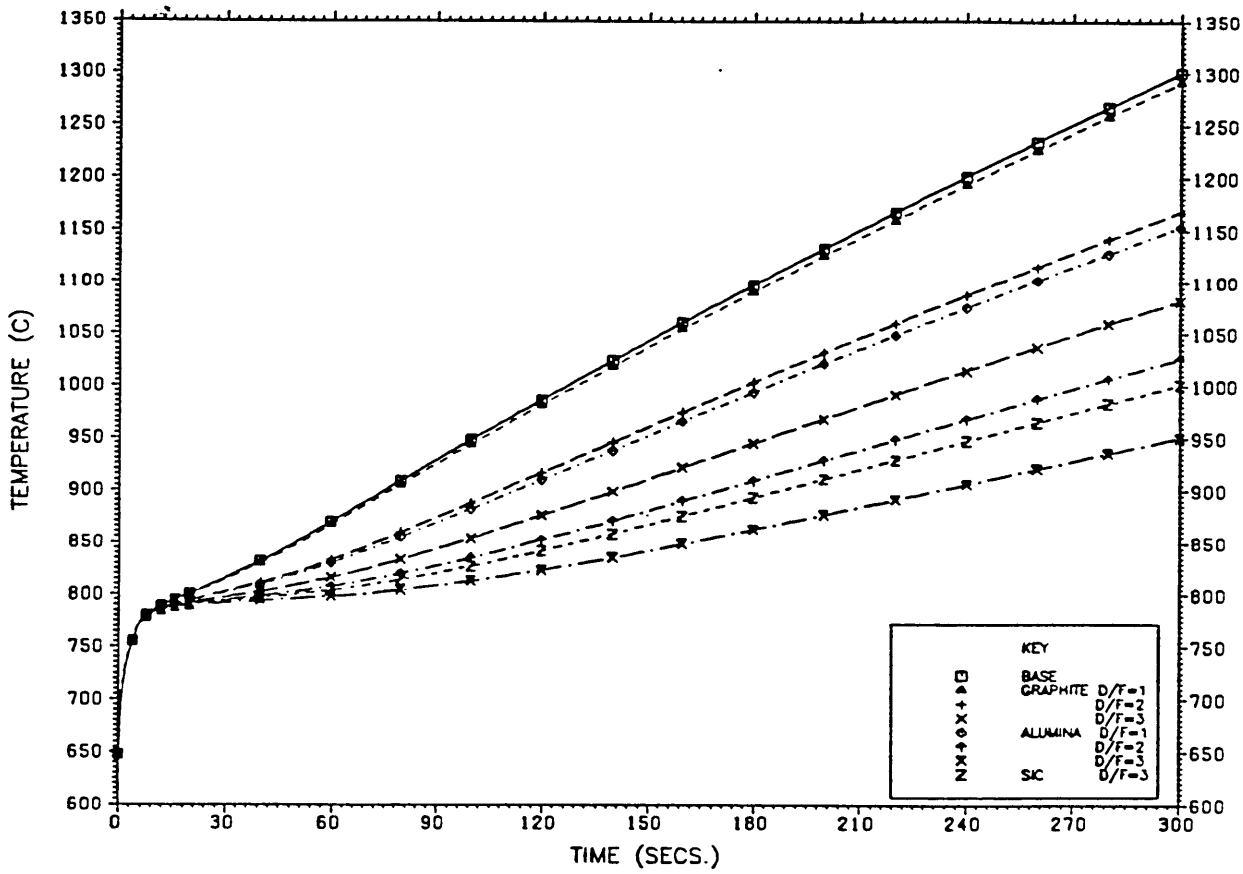

Figure 7.7. Evolution of maximum clad temperature following imediate total loss of coolant and decay heat from onset of transient. Radiative transfer between clad surface and diluent ring considered only for several diluents and dilution ratios

7.6 AGR REALISTIC DEPRESSURIZATION TRANSIENT

KINAGRAX Code Features

KINAGRAX [10], a one dimensional AGR kinetic program has been utilized to study a realistic depressurization scenario. The program, developed by the CEGB, includes many features most prominent of which are:

1. Detailed heat transfer model with up to four rings of rods, inner and outer graphite sleeves, four streams of downflowing coolant with a by-pass coolant, and a bulk moderator as well as an interstitial moderator brick.
2. Radiation between all fuel rings and inner sleeve, between the two sleeves, between outer sleeve and main moderator, and between main moderator and interstitial brick, is allowed for.
3. Tabular treatment of convective heat transfer coefficients and coolant specific heats is included.
4. Steady state is computed by either: (a) flux shape specification with criticality attained by adjusting fixed absorber at each mesh point; (b) source power case with flux and fixed absorber specified at each mesh point, the source strength being calculated at each mesh point; (c) eigenvalue problem in which true criticality searches are made on either k_∞ or uniform fixed absorber (the first is used in the current calculations)
5. Normalization is on: (a) specified gas outlet temperature; (b) specified gas outlet temperature together with specified maximum can temperature; (c) specified channel power (this is the case used in the current calculations); (d) other options may be found in the KINAGRAX reference.
6. During the transient changes may be made to : coolant inlet, bypass coolant flow, demanded outlet temperature, coolant flow rates of any flow channel, etc.

Transient Scenario

The modelled scenario is shown in figure (7.8). One minute following the initiation of depressurization, the reactor trips from full power. Pressure falls from an operating value of 41.4 bars with a time constant of 221 seconds. Decay

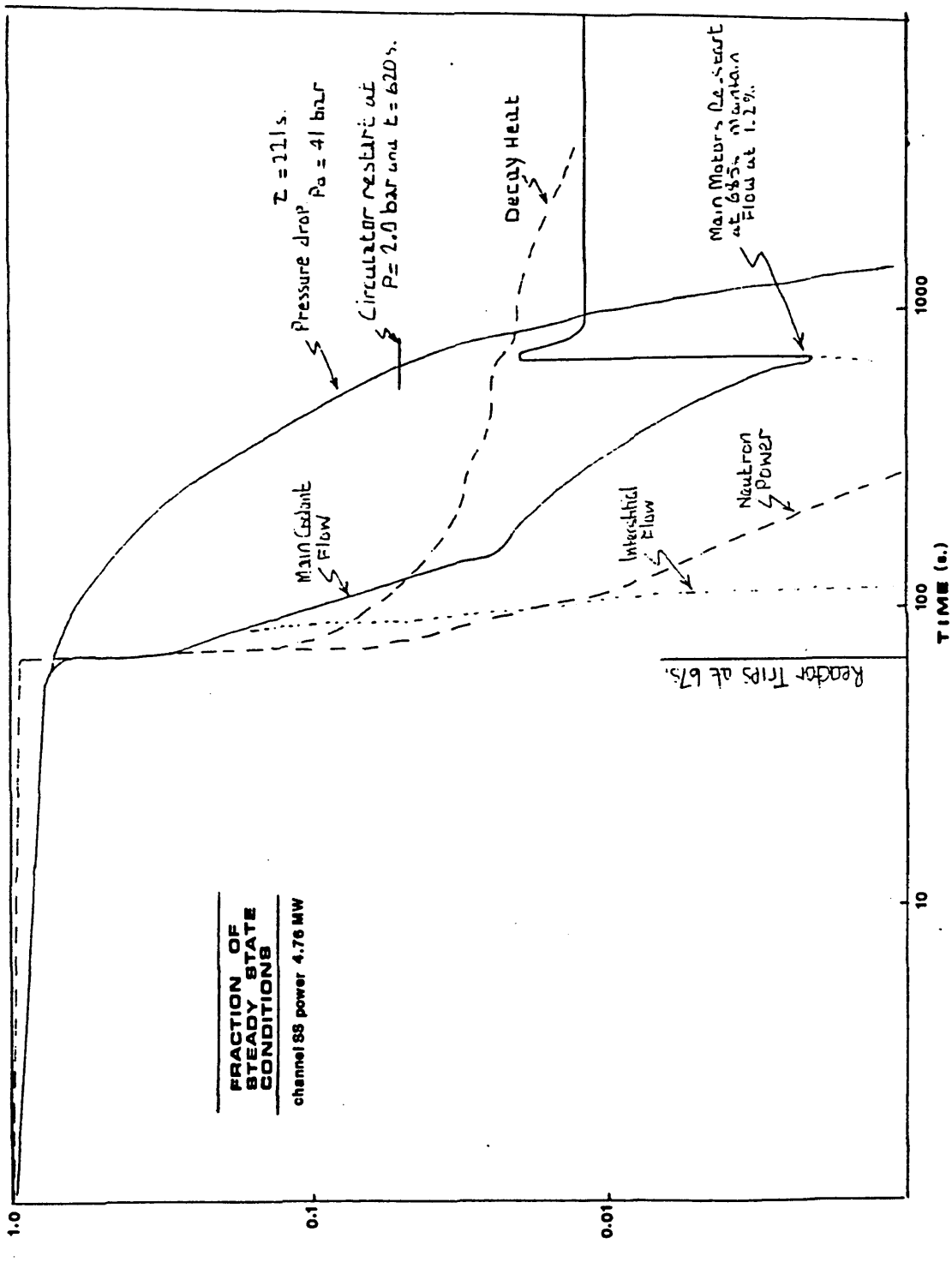

Figure 7.8. The realistic depressurization transient scenario studied with KINAGRAX

heat and the residual neutron power are shown. With the main motors shut down initially, gas circulation coasts down as shown. At 685 seconds, the main motors are re-started and flow is maintained at 1.2% of full flow.

Using KINAGRAX, it was possible to study the effect of reducing the main moderator volume, on the temperature response of an AGR in the event of a depressurization transient. Two reactor types were studied: a standard AGR lattice and a Half-AGR lattice.

The Half-AGR reactor was defined as one with roughly half the amount of bulk moderator graphite per fuel channel. Fuel channel and associated sleeves were kept unaltered. It is realized that this alteration leads, as expected to the need for higher enrichment. WIMS-D4 was used to ascertain the required enrichment for a Half-AGR: a value of 4.0 % U-235 was found to give a burnup of 18.6 GWd/t with a BOL k_{eff} of 1.13.

Several modifications were introduced into the KINAGRAX AGR data to simulate the half-AGR case. Keeping all other parameters unchanged, the changes introduced to give the Half-AGR case are as follows:

1. The main moderator brick radius was altered from the AGR value of 22.745 cm. to 18.70 cm., such that the main moderator brick area was halved and its inner radius kept at the AGR value 13.495 cm. This ensured the constancy of wetted areas and heat transfer coefficients.

2. The cross-sectional area of re-entrant cooling flow between interstitial brick and main brick was changed due to the decrease in the outer radius of the main brick. The outer radius was reduced by 17.8% and a notional change in the re-entrant flow area would in this proportion give a value of 100.38 cm^2 (A_{h2}).(Other values on the outside of the main brick also are changed, these are: S_h=174.1, $\rho_{(m3)}$=117.6)

3. The weight of main brick per unit length of channel reduces to 822.42 kg. (W_{m3}) for the Half-AGR.

4. It was decided against changing the parameters that include the effect of reactivity coefficient. Although the reduction of moderator causes an increase in the

reactivity of the lattice, the enrichment increase envisiged for the Half-AGR may offset this.

5. The proportions of heat generated in each ring of the cluster were re-evaluated based on a WIMS-D4 calculation of a Half-AGR with an increased enrichment giving roughly the same k_{eff} (BOL).(The values of the KINAGRAX parameters in this respect were: $\nu_{f1} = 0.0201, \nu_{f2} = 0.0207, \nu_{f3} = 0.02279, \xi_{f1} = 0.0246, \xi_{f2} = 0.0253, \xi_{f3} = 0.0278, \nu_{m3} = 0.0759, \xi_{m3} = 0.0172$ (see reference 10))

Half-AGR Transient Response

The response of the Half-AGR core to the depressurization scenario given above is shown in figure (7.9a). Also shown for comparison is the response of the AGR base case. The Half-AGR has approximately the same maximum clad temperature as the base AGR at the time the reactor trips (67s.). As the flow deteriorates the next peak occurs as the main motors are re-started to recover the flow to 1.2% of full flow (an established practice). It is at this second peak that the decreased graphite amount leads to higher maximum clad temperature for the Half-AGR case. The figure shows, however, that even for the Half-AGR the post-trip maximum clad temperature is kept at below $825°C$. It must be noted also that this peak occurs 685s. (11.5 minutes) after the start of the transient.

The moderator response to the transient is shown in figure (7.9b). Initially, the Half-AGR has a lower moderator temperature ($310°C$ vs $350°C$) due to increased interstitial flow area. After the reactor trips and as the flow rate progressively decreases, the Half-AGR maximum moderator temperature rises faster than the base AGR does. The raising of the flow rate to 1.2% at 685s.(when it had fell to less than 0.3%) does not appear to significantly arrest the rise. Both the AGR and the Half-AGR maximum moderator temperatures reach a value of $400°C$ at approximately 17 minutes after transient initiation. Only after this time does the Half-AGR moderator temperature begin to significantly surpass that of the AGR. It is therefore apparent that the Half-AGR case does not lead to unmanageable temperatures and gives ample time, just as in AGR, for operator intervention.

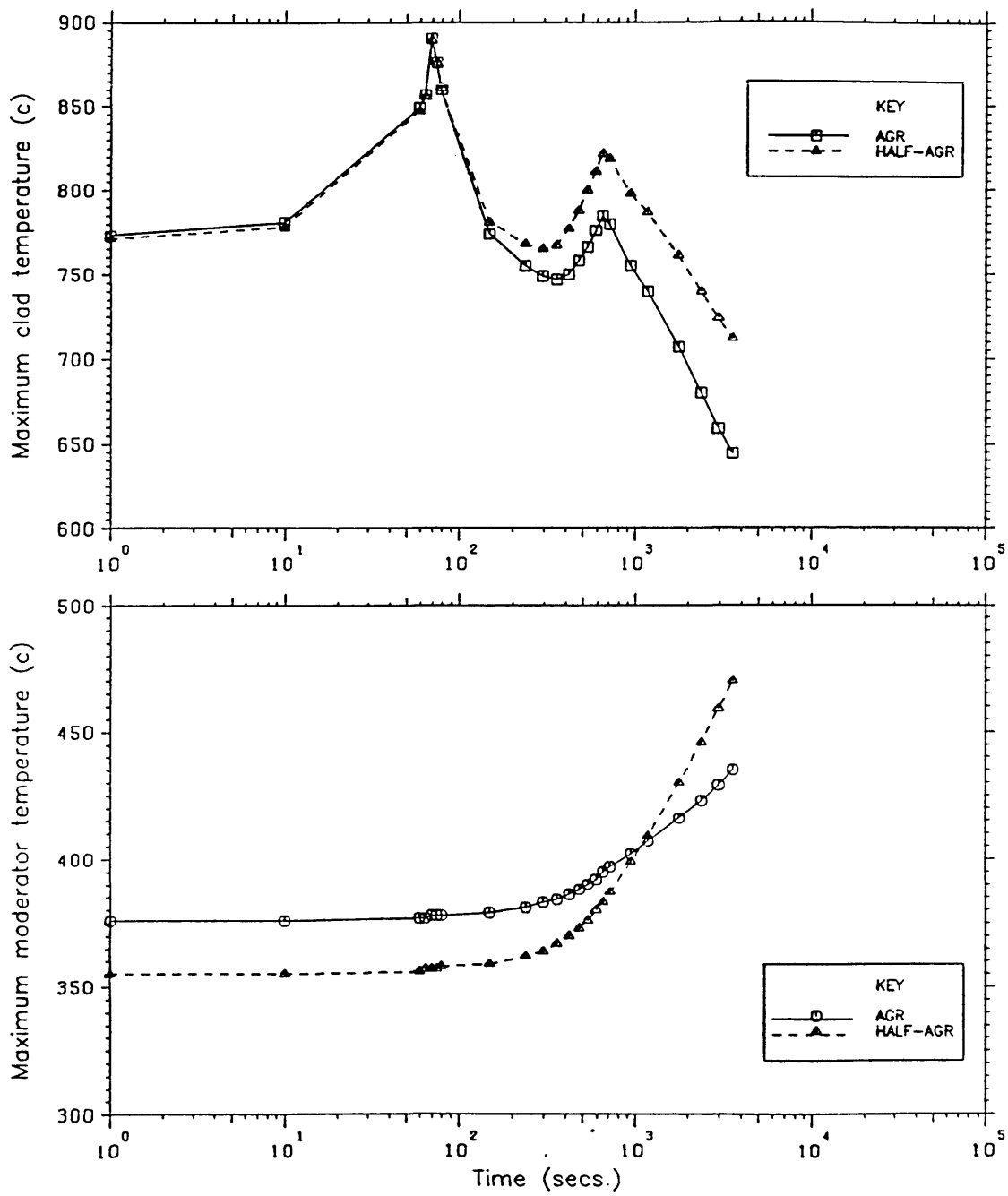

Figure 7.9. The transient response of the (a) maximum clad and the (b) moderator temperatures in a depressurization event. AGR and Half-AGR cores are shown

7.7 MATERIALS CONSIDERATIONS

The selection of materials for a nuclear reactor is a very difficult task. Experience gained with one material over prolonged usage is not readily extended to other materials. In this thesis there is no attempt to study any material design aspects in detail but merely to give an outline discussion in order to help place the concept of dilution in perspective. Clearly the intense neutron field and high temperature environment could impose severe limits on material performance. In a fast spectrum this is especially the case.

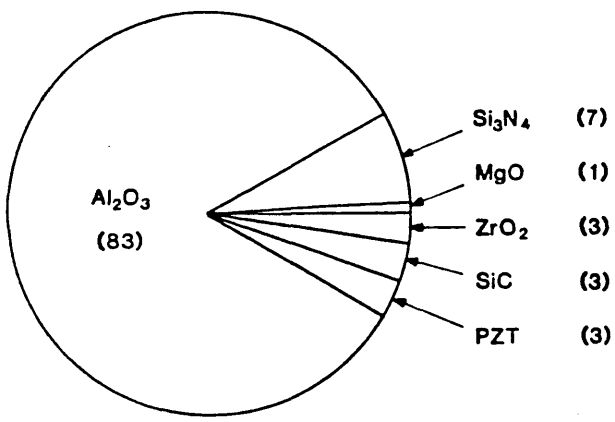

Figure 7.10. Alumina's share in the european ceramic market in 1987

Alumina not only has excellent heat capacity to influence heat transport in transients, but is probably the most readily available ceramic material and possibly one of the longest under developement. Figure (7.10) shows alumina to have 83% of the European ceramic market and its main usage covers several fields such as spark plugs, wear resistant parts, and cutting tool tips [11].

The properties of some of the more important engineering ceramics are summarized in table (7.5). For most of these materials developement has been recent and is continuing.

Table (7.5): Mechanical and physical properties of important ceramics

Material	Young's modulus (GPa)	Bend strength (MPa)	Density (kg/m^3)	Thermal expansion ($10^{-6}\ K^{-1}$	thermal conductivity (W/m.K)
Si_3N_4	310	700	3200	3.2	18
SiC	410	500	3100	4.3	84
sialon	300	860	3200	3.2	22
alumina	380	400	3900	8.0	8
zirconia toughened alumina	360	600	4100	8.5	7
toughened zirconia polycrystals	220	1000	5500	9.8	2
alumina toughened zirconia	250	2400	5000	9.0	4

It can be seen from the table that the high thermal conductivity, low thermal expansion materials (e.g. SiC), have in general less fracture toughness and bend strength. On the other hand, alumina has lower thermal conductivity and higher thermal expansion but has a higher density and potentially has, alone, or as a matrix material with zirconia, the highest strength of any ceramic (see reference 11).

The properties in table (7.5) are given for room temperature. At higher temperature, the strength of ceramics falls appreciably. It is, however, interesting to note that ceramics which have the drawback of being brittle under normal conditions, tend to become more plastic as temperature increases [12].

It has been reported that alumina may suffer up to 65% volume increase at intense neutron fluence ($10^{26}n/m2$) (>0.1 MeV) at a temperature of 1100K [13]; materials with lower volume swelling reported, for the same neutron fluence, include Si_3N_4 and $MgAl_2O_4$. These, however, are still fairly recent materials and relatively untested, in addition to their not being available on a large scale.

Table (7.5) indicates that an interesting ceramic for reactor application (or as a reactor diluent in our case) may be SiC. Extensive use as a block diluent

is probably not possible in the present due to the high cost although it's use in pebble-bed HTR's has been widely adopted. (see reference 11).
In brief, alumina, if to be usable as a diluent in the ETGBR must be:
(1) Used in relatively small blocks in order to limit thermal stress due to its low thermal conductivity. (hence the outline design uses small $V_d/V_f = 2.0$).
(2) Replaced frequently to limit the swelling problem. (hence replaced at the time of refuelling).

7.8 CONCLUSIONS

It has been shown that the thermal inertia of the ETGBR can be increased by the inclusion of a diluent; a non-fuel material equivalent to the AGR graphite moderator in nature, into the core. When convective heat transfer only between fuel and coolant was considered, some reduction in the rate of rise of the clad temperature was demonstrated for a shutdown, depressurization transient. With only radiation transfer considered, as in a full loss of cooling situation, the advantage of alumina over graphite in reducing the clad temperature rise was shown clearly. Both diluents were shown to retard considerably the transient temperature rise in this case.

The program written to perform the above calculations was a simple tool to assess approximately the transient temperature response of a fuel channel linked to a boiler of fixed heat transfer capacity. A furthur calculation was presented which showed that if an AGR, with its large graphite mass, was redesigned with half the moderator, the clad and moderator temperature in a transient depressurization scenario would still be within safety limits.

The chapter indicates alumina as a possible diluent for the ETGBR, but points to the need to further consider the material engineering aspects.

REFERENCES

1. Waltar A. E. , Reynolds A. B. , *Fast breeder reactors*, p. 507, Pergamon Press, 1981

2. Waltar A. E. , Reynolds A. B. , *Fast breeder reactors*, p. 737 Pergamon Press, 1981

3. Lewis E. E. , *Nuclear power reactor safety*, p. 402, John Wiley, 1977

4. Gratton C. P. , Horsley G. W. , *A gas-cooled fast reactor with direct cycle potential*, Symp. on Advanced and High Temperature Gas- Cooled Reactors, p. 376, Julich, 1968

5. Kemmish W. B. , Quick M. V. , Hirst I. L. , *The safety of CO_2 cooled breeder reactors based on existing gas cooled reactor technology*, Progress in Nuclear Energy, Vol. 10, no. 1, pp. 1-17, 1982

6. Gratton C. P. , Askew J. R. , and Goddard A. J. H. , Personal communication, 1984

7. Stewart H. B. , Rickard C. L. , and Melese G. B. , *Gas cooled reactor technology*, pp. 23-38, Advances in Nuclear Science and Technology, 1968

8. Dent K. H. , Pexton A. F. , Preston I. M. H. , and Southwood J. R. M. , *Status of gas-cooled reactors in the UK*, Conf. on Gas Cooled Reactors today p. 25, JBNES, London 1982

9. Gosman A. D. , Launder B. E. , and Reece G. J. , *Computer-aided engineering*, John Wiley 1985

10. Ellis J. , *KINAGRAX: A one-dimensional advanced gas-cooled reactor kinetic program*, CEGB report RD/C/N109,JNPC/RKWP/P374

11. Davidge R. W. , *Engineering ceramics in heat engines*, ATOM, p. 9, May 1987

12. Glastone S. , and Sesonske A. , *Nuclear reactor engineering*, p. 505, Van Nostrand Reinhold, 1981

13. Clinard F. W. , Hurley G. F. , *Neutron induced damage in MgO, Al_2O_3 and $MgAl_2O_4$ ceramics*, Jnl. of Nuclear Materials, pp. 655-670, No. s 108 and 109, 1982

CHAPTER 8.

SUMMARY AND CONCLUSIONS

The prime objective of this thesis has been to investigate the possible development potential of the gas-cooled reactor concept at a time when its dominance in the U.K. is challenged by the PWR. No attempt has been made to present an optimum design and only scoping calculations and comparisons were reported.

With the aim of enhancing neutronic performance, the long-term developement of the AGR was assumed, to be towards achieving a fast spectrum reactor. Between the present AGR and the ultimate gas cooled fast reactor lie a range of 'intermediate' designs: Intermediate, not wholly in the sense of neutron spectrum, but also in terms of technological and economic criteria.

With such a range of systems to investigate it was judged that a single neutronic code would be appropriate. The code selected was WIMS, in its two versions WIMS-D4 and WIMS-E. Although WIMS and its data library had been used extensively for thermal reactors and had been continuously validated and updated, it had never been tested sufficiently for fast reactors. As a part of the work, it was necessary to perform validation runs for WIMS with whatever benchmark cases were available. The general result was, contrary to initial expectations, not completely satisfactory: WIMS was shown to overpredict significantly the reactivity-lifetime (burnup) of fast systems. Nevertheless, scoping calculations were carried out using WIMS for the main study, since reaction rate predictions for fast cores were found to be in reasonable agreement with the results from the use of a dedicated fast reactor code.

Attention was focussed in chapter 3 on the AGR and the immediate moderated variants. The AGR model itself was established and the main neutronic parameters were calculated satisfactorily. The flexibility of the AGR, being a gas-cooled reactor, was demonstrated by studying enrichment variation and the ensuing consequences. Departure from the geometric design of the AGR was then studied by the introduction of the Mixed Spectrum Reactor (MSR) variants. (changing geometry in a GCR is in principle quite straightforward since the coolant plays a

minor role in determining reactivity). With the MSR two advantageous changes relative to AGR were possible: first, the use of large fuelled zones facilitated the use of mixed Pu oxide in place of UO_2 since Pu-239 has a higher η at higher energy; second, the graphite to fuel ratio is less, giving further spectrum 'hardening' and leading to higher conversion ratios. The MSR, however, suffered from two drawbacks: first, large fuel channel power peaking; second, possible difficulty in refuelling such a core with its complex fuel and graphite hexagonal components. As possible remedies to these problems two concepts were presented. A possible solution to the first problem was explored by the use of alumina in place of graphite, resulting in the so-called alumina-MSR. With alumina, at the expense of some increase in enrichment of the outer hexagons of the module, the power peaking was eliminated. This was accomplished using only two enrichments, whereas for the MSR, multiple differential enrichment was seen to be necessary if the peaking problem was to be removed.

Although the use of a two enrichment MSR module eases the refuelling problem, especially if batch refuelling were adopted, a design bearing a closer relationship to AGR geometries was investigated. The prismatic or integral block AGR (IBAGR) is a direct derivative of AGR incorporating an integral fuel channel/moderator block derived from HTR concepts. This design has been presented elsewhere, and in this thesis the basic neutronic parameters of the IBAGR were calculated and compared with the other work and with AGR.

Chapter 4 introduces the final stage of a gas cooled reactor and further presents the ETGBR as a breeder capable of fitting into the current economic and technical environment. Although, from the point of view of neutronics, the next step from the AGR and its immediate derivates are the diluted designs presented in chapter 5, it was judged best to introduce ETGBR calculations first since the later studies depend on them. It was shown that using WIMS in ETGBR calculations gave significant overprediction of reactivity-lifetime. This feature, although already indicated in chapter 2, was of a greater extent than had been expected. Parameters affecting predicted burnup were studied and the conclusion again was

that the calculation method was valid but that WIMS data was inadequate for very 'hard' systems in which the fuel loading is high (> 20% volume).

Building on AGR experience, the ETGBR was modified to incorporate a diluent: a non-fuel in-core material. The diluted-ETGBR (DETGBR) concept was to have the following features: (a) retain a sufficiently fast spectrum thus limiting the amount of diluent introduced. (b) have enrichments not over 20%: the antiproliferation limit. (c) burnups greater than PWR (> 35 GWd/t). In fact at 47.8 MW/t fuel rating up to 60 GWd/t was realizable. (d) replaceable diluent material at refuelling, leading to an integral block design. (e) A high internal conversion ratio (> 0.75) but not necassarily a breeding ratio in excess of 1.10. Towards the last feature, the introduction of partially blanketted DETGBRs was highlighted. (f) the diluent material was to have a high specific heat capacity, a high melting point, and not to interact chemically with CO_2 to any significant extent. Alumina met these criteria, although it clearly has disadvantages for reactor core applications.

Two other methods of introducing diluent into the ETGBR core were considered. A method incorporating subassemblies of mixed fuel and diluent pins was stressed as a way of obtaining minimum dilution ($V_d/V_f = 0.5$), while having the fuel and diluent in close proximity by a suitable layout of the rods. The small amount of diluent, however raises the question of its value in transient situations. For greater dilution a heterogeneous arrangement of fuel and diluent subassemblies was suggested. This was not analyzed in detail due to difficulties with neutronic results from WIMS, notably in the generation of a heterogeneous breeder design.

The main motive behind the introduction of the diluted ETGBR concept of chapter 5 was the belief that a large in-core heat sink, in the form of a moderator or diluent, tends to retard the rate of temperature rise in the core following a deppresurization accident in a shut down reactor. This was tested explicitly in chapter 7 by the coding of two programs: (a) TEANT, which follows a shut-down depressurization event in a reactor primary loop composed of an average single fuel channel and a boiler of fixed heat removal capabilty. The program only allowed,

at the present stage of development convective heat transfer between fuel and coolant. (b) TEAR, a simple fully isolated fuel channel program, starting from steady state and allowing only radiative transfer between clad and moderator rings in a regime governed by decay heating. With both programs different materials were compared, notably graphite and alumina. The advantage of alumina was clear in TEAR but less so in TEANT. Nevertheless, the value of an in-core heat sink: a diluent, was demonstrated. The case (b) benefits, would in practise be supplemented by circulator restart. As a final study of the value of the moderator, two realistic KINAGRAX runs were obtained for a depressurization scenario. One for a standard AGR channel and one were the moderator brick volume was halved. The result showed that maximum clad and moderator temperatures are still within the allowable limits. There are thus good indications that AGR variants, with reduced moderator volume, would conform to safety standards.

In conclusion, it has been indicated that the gas-cooled reactor has not reached the end of its development. Alternative routes have been presented. The diluted-ETGBR (DETGBR) was recomended as a target design featuring, as much as possible the fast reactor neutron economy, a measure of the AGR thermal inertia, and a minimum of additional technological and cost expenditure. The economic penalty of increased enrichment, however, must be borne in mind.

The recommended areas for further study can be listed as follows: (1) the applicability of the WIMS library to highly-loaded fast reactor cores and its modification (the 1981 WIMS library is most recent version) (2) the use of a detailed code linking neutronics and thermal-hydraulics for detailed assessment of the introduced DETGBR designs. A model with at least the same geometrical detail as WIMS to study heat transfer is the minimum requirement. (3) a depressurization transient comparison between the ETGBR, DETGBR design, and the other dilution methods using diluent pins and heterogeneous cores. (4) an assessment of the economics of introducing the diluted ETGBR variants either as full breeders or with either axial or radial blankets removed.

Appendix (1): Effect of WIMS Resonance Methods on Gas-Cooled Fast Systems

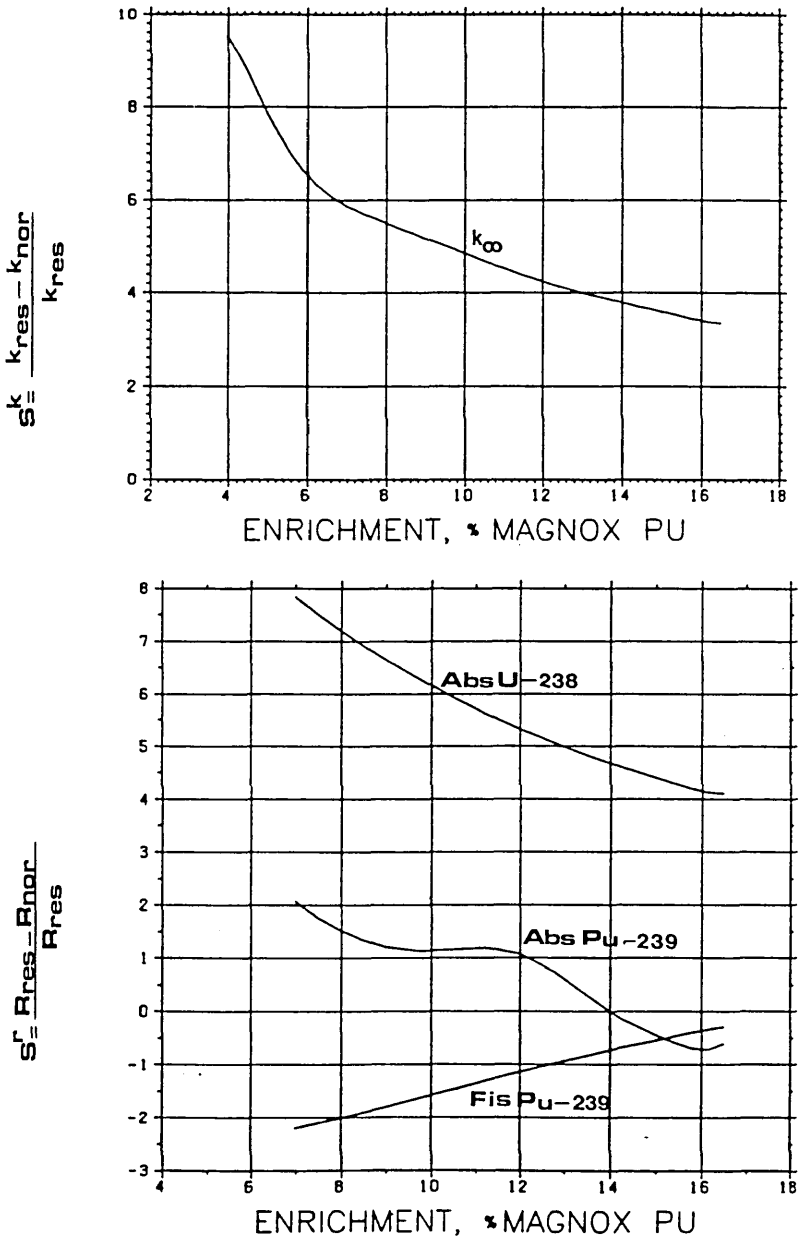

Figure A.1.1. Dependence of WIMS resonance calculations on enrichment for (a) k_∞ (b) Absorbtions and Fissions in U-238 and Pu-239. (ETGBR lattice).

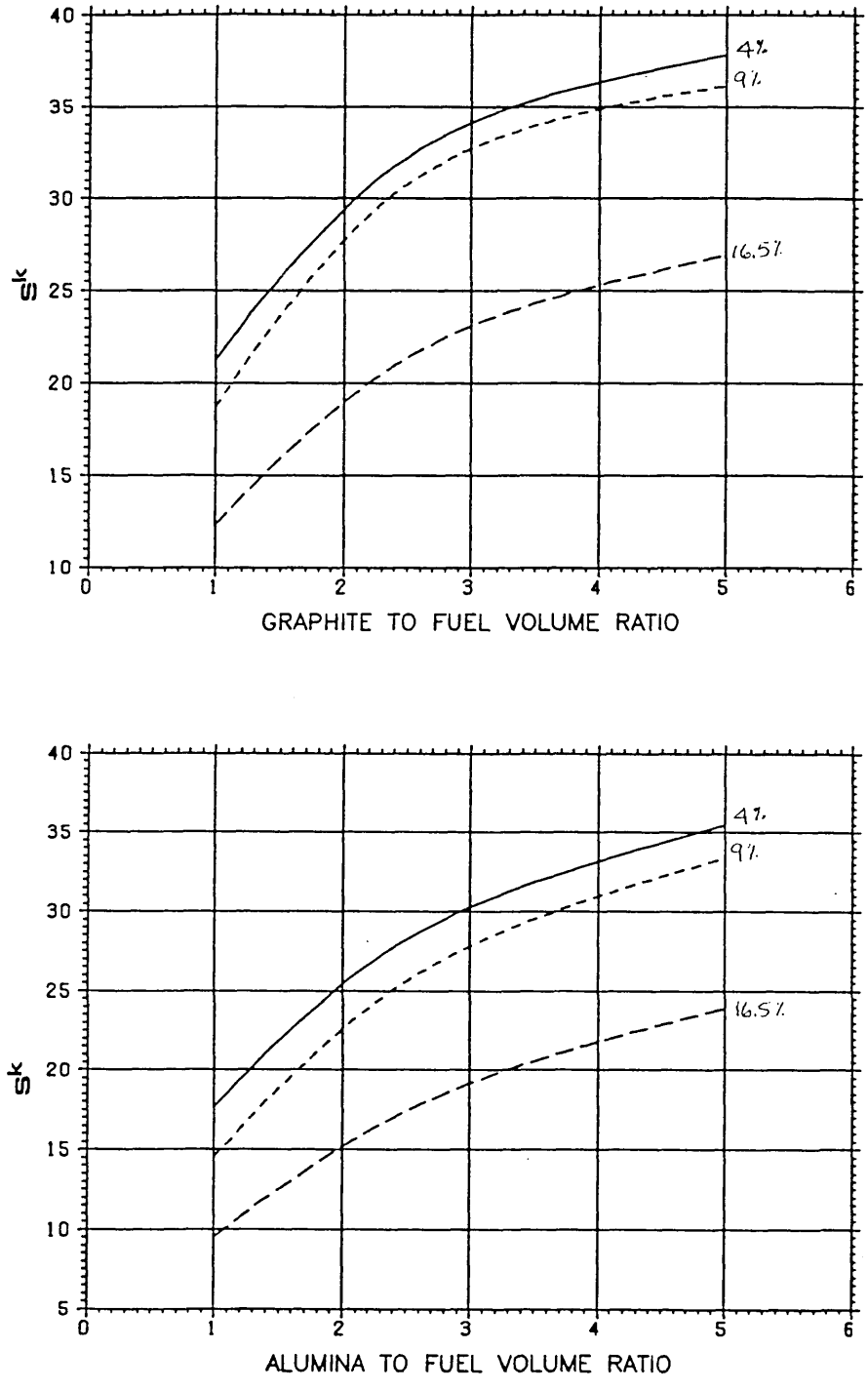

Figure A.1.2. Dependence of WIMS resonance calculations on moderation for (a) k_∞ (b) Absorbtions and Fissions in U-238 and Pu-239. (moderated ETGBR lattice, also see chapter 5).

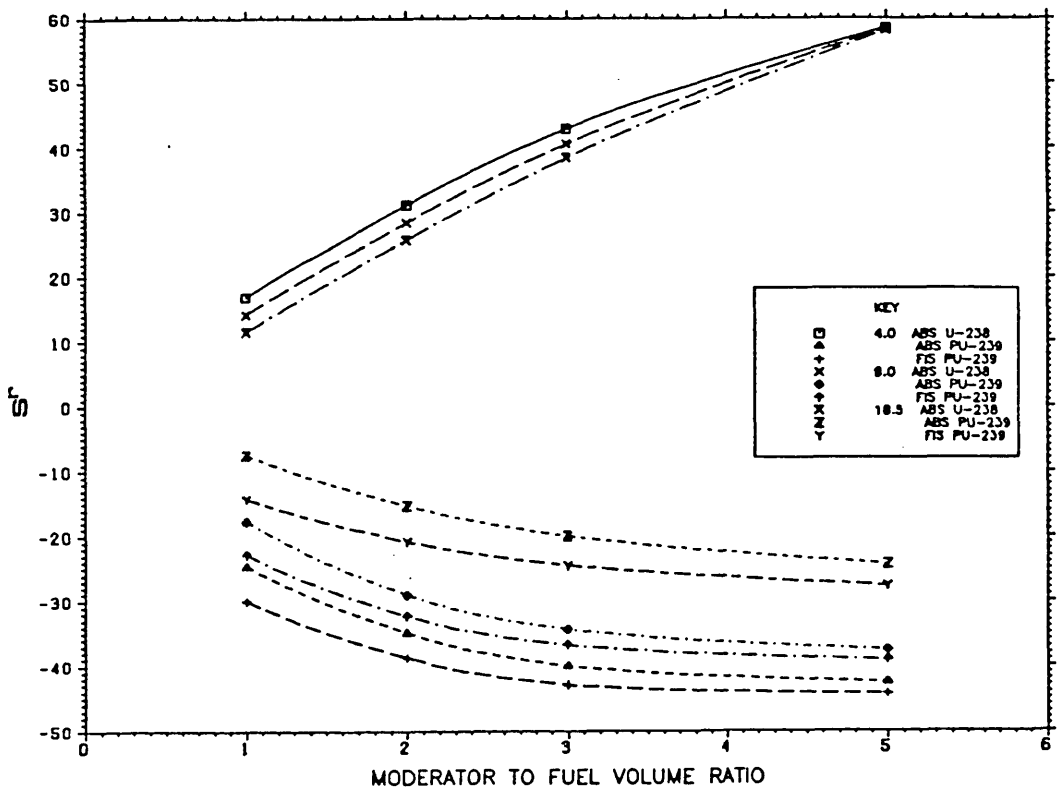

Figure A.1.3. Effect of moderation ratio on the relative difference in reaction rates calculated with and without resonance shielding included. Absorbtions and fissions in U-238 and Pu-239, at three enrichments considered. (graphite moderation of a ETGBR lattice).

Appendix (2): WIMS Input Files for LWHCR.

(a) WIMS-D4 listing of LWHCR calculation

```
1  //UMEMN26P JOB 'NUWAYHID,IC',MSGLEVEL=(1,1),MSGCLASS=X,
2  //      TIME=(,10),PRTY=3,NOTIFY=UMEMN26
3  //*PROCLIB=UMEMN26.PROC.LB
4  // EXEC RUNWMD4,
5  //      LBR='UMEMN26.WDN26B.DATA',REGION=1300K
6  //FT08F001  DD UNIT=TEMP,SPACE=(3152,(200,5),,,ROUND),
7  //      DCB=(RECFM=VBS,BLKSIZE=1604,LRECL=1600,BUFNO=1)
8  //G.FT06F001 DD SYSOUT=*
9  //G.SYSIN DD *
10 SAVE -1 1
11 WIMSDTOWIMSEPINCELLD
12 CELL 6        * PIN-CELL
13 SEQUENCE 2    * PERS
14 NGROUP 7 3
15 NTHERMAL 14
16 NREG 3
17 NMESH 4
18 NMAT 3
19 NREACT 6
20 PREOUT
21 INITIATE
22 ** PIN CELL TEST OF LWHCR CASE (RONEN ET AL)
23 SUPPRESS 0 0 1
24 MATE 1 -1 1178 1 1235.4 4.215E-05 3238.5 2.077E-02 $
25  3239.1 1.505E-3 1240 6.890E-4 241 2.445E-4 242 1.582E-4 $
26  16 4.682E-2                    *** ENR = 7.51 % 239+241 (RONEN)
27 MATER 2 7.96 600 2 2056 65.18 52 17.0 58 12.50 93 2.50 $
28  55 2.00 29 0.75 2012 0.07     *** S.S. AS I DEFINE IT (TEMP?)
29 MATER 3 0.7328 576 3 3001 11.19 16 88.18  **NOTE H2O DENS
30 ANNU 1 0.4705 1
31 ANNU 2 0.5105 2
32 ANNU 3 0.5725 3     * P=1.090
33 FEWGROUP 3 4 5 14 27 45 69
34 *FEWGROUP 3 4 5 15 27 45 69 (RONEN)
35 MESH 2 1 1
36 BEGINC
37 PARTIT 14 27 69
38 THERMAL 2
39 REACT 1235 1178 3238 1178 3239 1178 1240 1178 $
40 241 1178 242 1178
41 PRINTC 1 1 0 0
42 BUCK 1.612E-4 2.039E-4
43 DIFF 4 7 1
44 LEAK 5
45 BEGINC
46 /*
47
```

(b) WIMS-E listing of LWHCR calculation

```
1  //UMEMN26M JOB 'NUWAYHID-IC',MSGLEVEL=(1,1),MSGCLASS=X,
2  //      TIME=(,10),PRTY=5,NOTIFY=UMEMN26
3  //*PROCLIB=UMEMN26.PROC.LB
4  // EXEC LSWIMSEO,LL1=I1,LL2=I2,
5  //      D1='DISP=(,DELETE),UNIT=DISC',D2='DISP=(,DELETE),UNIT=DISC',
6  //      LIB='UMEMN26.WEN34B.DATA',REGION=1500K
7  //G.FT06F001 DD SYSOUT=*
8  //G.SYSIN DD *
9  *******
```

```
WHEAD 1
NMAT 3 NREG 3 NMESH 3 ENDP CENT
* LWHCR PIN-CELL (RONEN ET AL)
ANNU 1 0.4705 1
ANNU 2 0.5105 2
ANNU 3 0.5725 3
MATE 1 -1 1178 1 235 4.215E-05 3238 2.077E-02 $
 3239 1.505E-3 1240 6.890E-4 241 2.445E-4 242 1.582E-4 $
 16 4.682E-2                    *** ENR = 7.51 % 239+241 (RONEN)
MATER 2 7.96 600 2 2056 65.18 52 17.0 58 12.50 93 2.50 $
 55 2.00 29 0.75 2012 0.07     *** S.S. AS I DEFINE IT (TEMP?)
MATER 3 0.7328 576 3 2001 11.19 16 88.18  **NOTE H2O DENS
BEGIN
WPERS 1 PRINT 0 BEGIN
WPERS 1 BUCK 3.651E-4 PRINT 0 BEGIN
WSMEAR 1 2
MATE 1 MESH 1 ENDP
NEWMAT 1 1 2 3 MCODE 1 BEGIN
WPERS 2 BUCK 3.651E-4 PRINT 0 BEGIN
WCOND 2 1
GROUPS 7 ENDP
PART 3 4 5 14 27 45 69
BEGIN
WPERS 2 PRINT 0 BEGIN
*******
WSNAP 1
* ETGBR - RZ ZONC C1+C2
GEOMETRY ZCURR 2 3
MESH R 10*18.942
      Z 10*22.0
MAP SHOW ALL 1
DUMMY
CONSTANTS SHOW GROUPS 7
SCATTER DOWN 6
SCATTER UP 6
WMAT 1
SOLVE
PRINT PHI J I K G
RETURN
WLINK 1
WIMS MAP FLUX BEGIN
WWED 1 OPTION 4 BEGIN
STOP
/*
```

Appendix (3): WIMS-E Calculation of Reference ETGBR

Listing of WIMS-E input for an ETGBR model with the same geometry and volume fractions as that described in AEEW-M1669 (see 2.1.3). The listing is for the begining of life (BOL) condition.

```
//UMEMN26E JOB 'NUWAYHID,IC',MSGLEVEL=(1,1),MSGCLASS=X,
//     TIME=(1,20),PRTY=8
//*PROCLIB=UMEMN26.PROC.LB
// EXEC LSWIMSEO,LL1=ETH1,LL2=ETH2,LL3=ETH3,
//      LL4=ETH4,LL5=ETH5,
//      D1='DISP=(,DELETE),UNIT=DISC',D2='DISP=(,DELETE),UNIT=DISC',
//      D3='DISP=(,DELETE),UNIT=DISC',D4='DISP=(,DELETE),UNIT=DISC',
//      D5='DISP=(,DELETE),UNIT=DISC',
//     NBF=150,
//      LIB='UMEMN26.WEN34B.DATA',REGION=1900K
//G.FT06F001 DD SYSOUT=*
//G.SYSIN DD *
NCYCLE 1 4
WHEAD 0 1 0 1
NMAT 3 NREG 3 NMESH 3 ENDP CENT
* ETGBR PIN-CELLS AT AEEW-M1669 VOL FRQNS EACH MAT
ANNU 1 0.3500 1
ANNU 2 0.3850 2
ANNU 3 0.5846 3
GOTO 1 2
GOTO 2 3
GOTO 3 4
MATE 1 -1 1000 1 235 2.0834E-5 3238 2.0813E-2 3239 2.9806E-3
1240 6.2965E-4 241 1.0059E-4 242 1.4903E-5 16 .04912     *C1
MATE 2 7.96 850 2 2056 65.18 52 17.0
58 12.50 93 2.50 55 2.00 29 0.75 2012 0.07
MATE 3 -1 750 3 2012 4.2288E-4 16 8.4576E-4
GOTO 10 1 2 3 4
POINT 1
MATE 1 -1 1000 1 235 1.9301E-5 3238 1.9282E-2 3239 4.2066E-3
1240 8.8863E-4 241 1.4197E-4 242 2.1033E-5 16 0.04912     *C2
MATE 2 7.96 850 2 2056 65.18 52 17.0
58 12.50 93 2.50 55 2.00 29 0.75 2012 0.07
MATE 3 -1 750 3 2012 4.2288E-4 16 8.4576E-4
GOTO 10 1 2 3 4
POINT 2
MATE 1 -1 900 1 235 9.7795E-5 3238 2.4351E-2 16 0.048897
MATE 2 7.96 750 2 2056 65.18 52 17.0
58 12.50 93 2.50 55 2.00 29 0.75 2012 0.07
MATE 3 -1 650 3 2012 4.2288E-4 16 8.4576E-4
GOTO 10 1 2 3 4
POINT 3
MATE 1 -1 900 1 235 4.2990E-5 3238 2.0705E-2 16 0.021495
MATE 2 7.96 750 2 2056 65.18 52 17.0
58 12.50 93 2.50 55 2.00 29 0.75 2012 0.07
MATE 3 -1 650 3 2012 4.2288E-4 16 8.4576E-4
POINT 10
BEGIN
WPERS 1 0 1 0
*BUCKL 1.261E-4
BEGIN
WSMEAR 1 2 1 1
MATE 1 MESH 1 ENDP
NEWMAT 1 1 2 3
QUAL 1 1
FACTORS 0.564190 1.851935 1.1626640
QUAL 1 2
FACTORS 0.618232 1.894440 1.1227560
QUAL 1 3
FACTORS 0.606236 1.907730 1.0302200
QUAL 1 4
FACTORS 0.664544 1.881162 1.1082750
MCODE 1 BEGIN
WPERS 2 0 1 0
BEGIN
WCOND 2 1 1 1
```

```
GROUPS 7 ENDP
*PART 2 3 4 5 6 7 8 9 10 11 12 13 14 16 18
*22 24 27 69 BEGIN
PART 4 7 14 18 22 27 69 BEGIN
WPERS 1 0 1 0
*BUCKL 1.261E-4
BEGIN
*QUAL 2 1
*WWED 2
*BEGIN
FINISH
WMERGE 1 2 3 4 5
NOIF 4 ENDP
BEGIN
WHEAD 1
NMAT 3 NREG 3 NMESH 3 ENDP CENT
MATE 1 -1 900 1 235 4.2990E-5 3238 .010705 16 .021495  *RB
MATE 2 7.96 750 2 2056 65.18 52 17.00
58 12.50 93 2.50 55 2.00 29 0.75 2012 0.07
MATE 3 -1 650 3 2012 4.2288E-4 16 8.4576E-4
ANNU 1 1.0500 1
ANNU 2 1.0850 2
ANNU 3 1.2207 3
BEGIN
WPERS 1
*BUCKL 1.261E-4
BEGIN
WSMEAR 1 2
MATE 1 MESH 1 ENDP
NEWMAT 1 1 2 3
FACTORS 0.59415 3.57349 1.81547
MCODE 1 BEGIN
WPERS 2 BEGIN
WCOND 2 1
GROUPS 7 ENDP
PART 4 7 14 18 22 27 69 BEGIN
*PART 2 3 4 5 6 7 8 9 10 11 12 13 14 16 18
*22 24 27 69 BEGIN
WPERS 1
*BUCKL 1.261E-4
BEGIN
WHEAD 3
NMAT 1 NREG 1 NMESH 1 ENDP CENT
MATE 1 7.96 750 2 2056 1.0      * ZONE R
ANNU 1 1.085 1 BEGIN
FFACE 2
WCOND 3 4
GROUPS 7 SUBF ENDP
PART 4 7 14 18 22 27 69
*PART 2 3 4 5 6 7 8 9 10 11 12 13 14 16 18
*22 24 27 69
COND 1 1 1
BEGIN
WMERGE 5 1 4 3
NOIF 3  ENDP
BEGIN
WSNAP 3
* ETGBR - RZ
GEOMETRY ZCURR 2 3
MESH R 10*14.231 4*11.44 4*11.894 3*17.14
      Z 5*14.0 4*15.0 3*26.67
MAP SHOW ALL 6
T 1 B 1 1 10 5
T 2 B 11 1 14 5
T 3 B 1 6 10 9
T 4 B 11 6 14 9
T 5 B 15 1 18 9  DUMMY
CONSTANTS SHOW GROUPS 7
SCATTER DOWN 6
SCATTER UP -1
WMAT 1
SOLVE
RETURN
WLINK 3
WIMS MAP FLUX
BEGIN
WWED 3
```

```
144 OPTION 4
145 BEGIN
146 WWIRE 3
147 REAC 235 1110 14 19 REAC 3238 1110 14 19
148 REAC 3239 1110 14 19 REAC 1240 1110 14 19
149 REAC 241 1110 14 19 REAC 242 1110 14 19
150 BEGIN
151 STOP
152 /*
153 /
```

Appendix (4): WIMS-D4/WIMS-E Calculation of ETGBR and DETGBR

Listing of the input of an ETGBR or DETGBR calculation using the WIMS-D4/ WIMS-E method. Two parts thus follow: Part (1) shows the WIMS-D4 data generation for an alumina DETGBR with D/F of 2.0 followed by translation into WIMS-E format and cataloging of the data. Part(2) gives a WIMS-E/WSNAP calculation of the same data in hexagonal-Z geometry. In the lattice-cell determinations part (1) gives all required details.

Part 1

```
1 //UMEMN26L JOB 'R.Y.N.-IC',MSGLEVEL=(1,1),MSGCLASS=X
2 //   TIME=(1,29),PRTY=1
3 //*PROCLIB=UMEMN26.PROC.LB
4 // EXEC RUNWND4,FILE=TEMP,DISP='DISP=(NEW,PASS),UNIT=DISC',
5 //      LBR='UMEMN26.WDN26B.DATA',REGION=1900K
6 //FT03F001  DD UNIT=TEMP,SPACE=(3152,(200,5),,,ROUND),
7 //      DCB=(RECFM=VBS,BLKSIZE=1604,LRECL=1600,BUFNO=1)
8 //SYSIN DD *
9 PRIME 0
10 SAVE 1 1
11 WIMSDTOWIMSECLUSTER2
12 CELL 7
13 SEQUENCE 2
14 NREACT 3
15 NGROUP 19 19
16 NTHERMAL 14
17 NREG 9 7
18 NMESH 16
19 NMAT 6 2
20 NRODS 1 1 1 1 8 2 1
21 PREOUT
22 INITIATE
23 COOLANT 4
24 *************** PURE MAG PU FUEL ************************
25 MATER 1 -1 1000 1 1235.4 2.012615E-05 3238.5 2.010603E-02 $
26 3239.1 3.534348E-03 1240 7.466310E-04 241 1.192842E-04 $
27 242 1.767174E-05 16 4.908818E-02  **E=18.0%
28 MATE 2=1
29 MATER 3 7.96 650 2 2056 65.18 52 17.0 58 12.50 93 2.50 $
30  55 2.00 29 0.75 2012 0.07
31 MATER 4 -1 650 3 2012 4.2288E-4 16 8.4576E-4
32 MATER 5 7.96 650 4 2056 65.18 52 17.0 58 12.50 93 2.50 $
33  55 2.00 29 0.75 2012 0.07
34 *MATER 6 1.7 650 4 2012 1.0              * GRAPHITE
35 MATER 6 -1 650 4 27 .06678 16 .07017    * ALUMINA
```

```
ANNU 1 0.3850 3 *
ANNU 2 1.5687 4 *
ANNU 3 2.6145 4 *
ANNU 4 3.6603 4 *
ANNU 5 4.7061 4 *
ANNU 6 5.7519 4 *
ANNU 7 6.7977 4 *
ANNU 8 7.8435 4 *
*ANNU 9 8.2635 5 * BASE SS WRAP
*ANNU 9 9.0612 6 * M/F=1.0
ANNU 9 10.130 6 * M/F=2.0
*ANNU 9 11.090 6 * M/F=3.0
*ANNU 9 12.822 6 * M/F=5.0
******************
RODSUB 1 1 0.350 1
RODSUB 1 2 0.390 3
RODSUB 2 1 0.350 1
RODSUB 2 2 0.385 3
RODSUB 3 1 0.350 1
RODSUB 3 2 0.390 3
RODSUB 4 1 0.350 1
RODSUB 4 2 0.385 3
RODSUB 5 1 0.350 1
RODSUB 5 2 0.390 3
RODSUB 6 1 0.350 1
RODSUB 6 2 0.385 3
RODSUB 7 1 0.365 3
RODSUB 8 1 0.350 2
RODSUB 8 2 0.390 3
******************
ARRAY 1 1 6  0.9768 0
ARRAY 2 1 12 2.0916 .261799
ARRAY 3 1 18 3.1374 0
ARRAY 4 1 24 4.1832 .130899
ARRAY 5 1 30 5.2290 0
ARRAY 6 1 32 6.2748 .0981747
ARRAY 7 1 4  6.2748 0
ARRAY 8 1 42 7.3206 .074799
MESH 1 2 2 2 2 2 2 2 1
FEWGR 2 3 4 5 6 7 8 9 10 11 12 13 14 $
16 18 22 24 27 69
SUPP 0 0 1 1
BUCK 3.14E-4 5.035E-4  ** D/F=2 OUTER CORE
DBSQ -11 3.14E-4 5.035E-4 3.14E-4 5.035E-4 3.14E-4 5.035E-4 $
    3.14E-4 5.035E-4 3.14E-4 5.035E-4 3.14E-4 5.035E-4 $
    3.14E-4 5.035E-4 3.14E-4 5.035E-4 3.14E-4 5.035E-4 $
    3.14E-4 5.035E-4 3.14E-4 5.035E-4 3.14E-4 5.035E-4 $
    3.14E-4 5.035E-4 3.14E-4 5.035E-4 3.14E-4 5.035E-4 $
    3.14E-4 5.035E-4 3.14E-4 5.035E-4 3.14E-4 5.035E-4 $
    3.14E-4 5.035E-4
POWERC 1 33.82 36.50 10
DWRITE
BEGINC
BUCK 3.14E-4 5.035E-4  ** D/F=2 OUTER CORE
DIFF 1 1 7.8435
REACT 135 1000 1235 1000 3239 1000
PART 2 3 4 5 6 7 8 9 10 11 12 13 14 $
16 18 22 24 27 69
THERMAL 1
PRINTC 1 1 1 0
BEGINC
**
BEGINC   * 1 YR FILE  (SEQ 2)
BEGINC  *2SR***
BEGINC   * 2 YR FILE  (SEQ 3)
BEGINC  *3SR***
BEGINC   * 3 YR FILE
BEGINC  *4SR***
BEGINC   * 4 YR FILE
BEGINC  *5SR***
BEGINC   * 5 YR FILE
BEGINC  *6SR***
BEGINC   * 6 YR FILE
BEGINC  *7SR***
BEGINC   * 7 YR FILE
BEGINC  *8SR***
POWERC 0 0
```

```
113 BEGINC   * 8 YR FILE
114 BEGINC
115 *********
116 /*
117 // EXEC LSWIMSEO,LL1=I1,LL2=AHO,
118 //    LL3=I3,LL4=AH2,LL5=I5,LL6=AH4,LL7=I7,LL8=AH6,
119 //    D1='DISP=(,DELETE),UNIT=DISC',D2='DISP=(NEW,CATLG),UNIT=DISC',
120 //    D3='DISP=(,DELETE),UNIT=DISC',D4='DISP=(,DELETE),UNIT=DISC',
121 //    D5='DISP=(,DELETE),UNIT=DISC',D6='DISP=(,DELETE),UNIT=DISC',
122 //    D7='DISP=(,DELETE),UNIT=DISC',D8='DISP=(,DELETE),UNIT=DISC',
123 //    LIB='UMEMN26.WEN34B.DATA',REGION=1995K
124 //G.FT06F001 DD SYSOUT=*
125 //G.FT71F001 DD DISP=SHR,DSN=UMEMN26.TEMP.DATA
126 //G.SYSIN DD *
127 WFORTE 1 3 5 7
128 SEQ  1 3 5 7
129 BEGIN
130 WMIX 1
131 WMIX 3
132 WMIX 5
133 WMIX 7
134 WSMEAR 1 2
135 MATE 1 MESH 1 ENDP
136 NEWMAT 1 1 2 3 4 5 6 7 8 9 10 11 12 13
137 14 15 16 17 18 19 20 21 22 23
138 MCODE 1 BEGIN
139 WSMEAR 3 4
140 MATE 1 MESH 1 ENDP
141 NEWMAT 1 1 2 3 4 5 6 7 8 9 10 11 12 13
142 14 15 16 17 18 19 20 21 22 23
143 MCODE 1 BEGIN
144 WSMEAR 5 6
145 MATE 1 MESH 1 ENDP
146 NEWMAT 1 1 2 3 4 5 6 7 8 9 10 11 12 13
147 14 15 16 17 18 19 20 21 22 23
148 MCODE 1 BEGIN
149 WSMEAR 7 8
150 MATE 1 MESH 1 ENDP
151 NEWMAT 1 1 2 3 4 5 6 7 8 9 10 11 12 13
152 14 15 16 17 18 19 20 21 22 23
153 MCODE 1 BEGIN
154 STOP
155 /*
156 /
```

Part 2

```
 1 //UMEMN26L JOB 'NUWAYHID-I.C.',MSGLEVEL=(1,1),MSGCLASS=X,
 2 //       TIME=(3,59),PRTY=1
 3 //*PROCLIB=UMEMN26.PROC.LB
 4 // EXEC LSWIMSEO,LL1=I1,LL2=I2,LL3=AR,LL4=RR,LL5=I5,
 5 //       LL6=I6,LL7=I7,LL8=ALO,LL9=AHO,LL10=ABO,LL11=RBO,
 6 //       D1='DISP=(,DELETE),UNIT=DISC',D2='DISP=(,DELETE),UNIT=DISC',
 7 //       D3='DISP=(,DELETE),UNIT=DISC',D4='DISP=(,DELETE),UNIT=DISC',
 8 //       D5='DISP=(,DELETE),UNIT=DISC',D6='DISP=(,DELETE),UNIT=DISC',
 9 //       D7='DISP=(,DELETE),UNIT=DISC',D8='DISP=OLD,UNIT=DISC',
10 //       D9='DISP=OLD,UNIT=DISC',D10='DISP=OLD,UNIT=DISC',
11 //       D11='DISP=OLD,UNIT=DISC',
12 //       SP1='(TRK,(3,1),RLSE)',SP2='(TRK,(6,3),RLSE)',
13 //*       BSF=6160,NBF=180,BSX=6160,NBX=180,
14 //       SPW='(6160,(120,40),RLSE)',
15 //       LIB='UMEMN26.WEN34B.DATA',REGION=2200K
16 //G.FT06F001 DD SYSOUT=*
17 //G.SYSIN DD *
18 **********-------------GENERATE REFL DATA FOR GIVEN ENRICH
19 WHEAD 1
20 BURN
21 NMAT 3 NREG 3 NMESH 3 ENDP CENT PRINT 0
22 ANNU 1 0.3500 1 ANNU 2 0.3850 2 ANNU 3 0.5899 3
23 MATER 1 -1 1000 1 235 2.098792E-05 3238 2.096693E-02
24 3239 2.847483E-03 1240 6.015307E-04 241 9.610255E-05
25 242 1.423741E-05 16 4.909454E-02  ** E=14.5%
26 MATE 2 7.96 850 2 2056 65.18 52 17.0
27 58 12.50 93 2.50 55 2.00 29 0.75 2012 0.07
```

```
MATE 3 -1 750 3 2012 4.2288E-4 16 8.4576E-4
BEGIN
WPERS 1 BEGIN
WBRNUP 1 3
RATING 1 47.8 CENT
BUCK 19 2.13E-4 5.035E-4 0.0 0.0
STEPS 1 .001  BEGIN    ** BNUP IS APPROX TO GET REFL ONLY
WMIX 3
WSMEAR 3 2
MATE 1 MESH 1 ENDP
NEWMAT 1 1 2 3
FACTORS 0.835220 2.309250 0.931920
MCODE 1 BEGIN
WPERS 2 BEGIN        ** 69 GP BURNT C1 DATA ON    --(2)
*****************************************************
WHEAD 1
BURN
NMAT 3 NREG 3 NMESH 3 ENDP CENT PRINT 0
ANNU 1 0.3500 1 ANNU 2 0.3850 2 ANNU 3 0.5899 3NMATER 1 -1 1000 1 235 2.012615E-05 3238 2.010603E-02
3239 3.534348E-03 1240 7.466310E-04 241 1.192842E-04
242 1.767174E-05 16 4.908818E-02 **E=18.0%
MATE 2 7.96 850 2 2056 65.18 52 17.0
58 12.50 93 2.50 55 2.00 29 0.75 2012 0.07
MATE 3 -1 750 3 2012 4.2288E-4 16 8.4576E-4
BEGIN
WPERS 1 BEGIN
WBRNUP 1 3
RATING 1 47.8 CENT
BUCK 19 2.13E-4 5.035E-4 0.0 0.0
STEPS 1 0.001  BEGIN    ** BNUP IS APPROX TO GET REFL ONLY
WMIX 3
WSMEAR 3 4
MATE 1 MESH 1 ENDP
NEWMAT 1 1 2 3
FACTORS 0.835220 2.309250 0.931920
MCODE 1 BEGIN
WPERS 4 BEGIN        ** 69 GP BURNT C2 DATA ON    --(4)
*****************************************************
***   AB DATA WITH BURNUP
WHEAD 1
BURN
NMAT 3 NREG 3 NMESH 3 ENDP CENT PRINT 0
ANNU 1 0.3500 1 ANNU 2 0.3850 2 ANNU 3 0.5899 3
MATER 1 -1 750 1 235 9.7795E-5 3238 2.4351E-2 16 0.048897  **AB
MATE 2 7.96 850 2 2056 65.18 52 17.0
58 12.50 93 2.50 55 2.00 29 0.75 2012 0.07
MATE 3 -1 750 3 2012 4.2288E-4 16 8.4576E-4
BEGIN
WPERS 1 BEGIN
WBRNUP 1 3
RATING 1 2.51 CENT
BUCK 19 2.13E-4 1.20E-2 0.0 0.0  *** AB
STEPS 1 0.001  BEGIN    ** BNUP IS APPROX
WMIX 3
WSMEAR 3 5
MATE 1 MESH 1 ENDP
NEWMAT 1 1 2 3
FACTORS 0.835220 2.309250 0.931920
MCODE 1 BEGIN
WPERS 5 BEGIN        ** 69 GP BURNT AB DATA ON     --(5)
*****************************************************
***   RB DATA WITH BURNUP
WHEAD 1
BURN
NMAT 3 NREG 3 NMESH 3 ENDP CENT PRINT 0
ANNU 1 1.050 1 ANNU 2 1.0850 2 ANNU 3 1.220 3
MATER 1 -1 850 1 235 9.7795E-5 3238 2.4351E-2 16 0.048897  **RB
MATE 2 7.96 850 2 2056 65.18 52 17.0
58 12.50 93 2.50 55 2.00 29 0.75 2012 0.07
MATE 3 -1 750 3 2012 4.2288E-4 16 8.4576E-4
BEGIN
WPERS 1 BEGIN
WBRNUP 1 3
RATING 1 2.51 CENT
BUCK 19 5.6E-4 2.535E-4 0.0 0.0  *** RB
STEPS 1 0.001  BEGIN    ** BNUP IS APPROX
WMIX 3
```

```
105 WSMEAR 3 1
106 MATE 1 MESH 1 ENDP
107 NEWMAT 1 1 2 3
108 FACTORS 0.68340 2.9180 1.6570
109 MCODE 1 BEGIN
110 WPERS 1 BEGIN        ** 69 GP BURNT RB DATA ON       --(1)
111 ******************************************************
112 WHEAD 3
113 NMAT 1 NREG 1 NMESH 1 ENDP CENT PRINT 0
114 MATE 1 7.96 650 2 2056 1.0     * ZONE REF
115 ANNU 1 1.220 1 BEGIN
116 **
117 WMERGE 2 4 1 3 6
118 NOIF 4 ENDP BEGIN  ** C1+C2+RB+REF  69 BURNED
119 **
120 WMERGE 2 5 3 7
121 NOIF 3 ENDP BEGIN  ** C1+AB+REF     69 BURNED
122 ************ 1-D ******************************
123 WHEAD 2   ** GEOMETRY EXACT/MATERIAL APPROX BUT READ LATER EXACTLY
124 NMAT 4 NREG 4 NMESH 50 ENDP CENT PRINT 0
125 MATER 1 -1 1000 1 235 2.098792E-05 3238 2.096693E-02
126 3239 2.847483E-03 1240 6.015307E-04 241 9.610255E-05
127 242 1.423741E-05 16 4.909454E-02  **E=14.5%
128 MATER 2 -1 1000 1 235 2.012615E-05 3238 2.010603E-02
129 3239 3.534348E-03 1240 7.466310E-04 241 1.192842E-04
130 242 1.767174E-05 16 4.908818E-02  **E=18.0%
131 MATER 3 -1 850 1 235 9.7795E-5 3238 2.4351E-2 16 0.048897  **RB
132 MATE 4 7.96 650 2 2056 1.0                          *REF
133 *ANNU 1 121.73 1 ANNU 2 164.45 2
134 *ANNU 3 193.09 3  ANNU 4 207.41  4    ** STAND
135 ANNU 1 149.22 1 ANNU 2 201.580 2
136 ANNU 3 236.7 3 ANNU 4 251.0  4    ** D/F=2
137 MESH 20 10 10 10 BEGIN
138 **
139 WINTER 6 2
140 COPY FILE 1 2 3 BEGIN
141 WPERS 2 FREE PRINT 0 BEGIN
142 **
143 WCOND 2 3
144 GROUPS 19 ENDP PRINT 0
145 PART 2 3 4 5 6 7 8 9 10 11 12 13 14
146 16 18 22 24 27 69 BEGIN
147 WSMEAR 3 4
148 MATE 1 MESH 1 ENDP PRINT 0
149 NEWMAT 1 41 42 43 44 45 46 47 48 49 50
150 MCODE 1 BEGIN    ****  REFLECTOR DATA RADIALLY IS --- 4
151 **********--GENERATE AXIAL REFLECTOR DATA
152 WHEAD 2
153 NMAT 3 NREG 3 NMESH 40 ENDP CENT PRINT 0
154 MATER 1 -1 1000 1 235 2.098792E-05 3238 2.096693E-02
155 3239 2.847483E-03 1240 6.015307E-04 241 9.610255E-05
156 242 1.423741E-05 16 4.909454E-02  **E=14.5%
157 MATER 2 -1 750 1 235 9.7795E-5 3238 2.4351E-2
158 16 0.048897                        ** AB
159 MATE 3 7.96 650 2 2056 1.0         **REF
160 ANNU 1 70.0 1 ANNU 2 98.64 2
161 ANNU 3 112.96 3
162 MESH 20 10 10 BEGIN
163 **
164 WINTER 7 2
165 COPY FILE 1 2 3 BEGIN
166 WPERS 2 FREE PRINT 0 BEGIN
167 **
168 WCOND 2 3
169 GROUPS 19 ENDP PRINT 0
170 PART 2 3 4 5 6 7 8 9 10 11 12 13 14
171 16 18 22 24 27 69 BEGIN
172 WSMEAR 3 2
173 MATE 1 MESH 1 ENDP
174 NEWMAT 1 31 32 33 34 35 36 37 38 39 40
175 MCODE 1 BEGIN     **** REFLECTOR DATA AXIALLY IS ----- 2
176 **
177 *********------------- SNAP CALCS ON REFL+NON REFL CASES
178 WMERGE 8 9 10 11 4 2 1
179 NOIF 6 ENDP BEGIN       ** ZONES C1+C2+AB+RB+RR+AR
180 *******  SNAP CALCS
181 ** HEX SIZES(S): 9.087 STAN, 11.14 D/F=2
```

```
WSNAP 1
* DIL ETGBR
GEOMETRY CYCLIC S
ZCURR 8
MESH HEX 11.14 15 14
    Z 2*7.16 2*14.32 4*17.5
MAP PLANE 1
R 1 1 6 6 6 6 6 6 6 6 6 6 6 6 6 6 6
      0 0 6 6 6 6 6 6 6 6 6 6 6 6 6
      0 0 0 6 6 6 6 6 6 6 6 6 6 6 6
      0 0 0 0 6 6 6 6 6 6 6 6 6 6 6
      0 0 0 0 0 6 6 6 6 6 6 6 6 6 6
      0 0 0 0 0 0 6 6 6 6 6 6 6 6 6
      0 0 0 0 0 0 0 6 6 6 6 6 6 6 6
      0 0 0 0 0 0 0 0 6 6 6 6 6 6 6
      0 0 0 0 0 0 0 0 0 6 6 6 6 6 6
      0 0 0 0 0 0 0 0 0 0 6 6 6 6 6
      0 0 0 0 0 0 0 0 0 0 0 6 6 6 6
      0 0 0 0 0 0 0 0 0 0 0 0 6 6 6
      0 0 0 0 0 0 0 0 0 0 0 0 0 6 6
      0 0 0 0 0 0 0 0 0 0 0 0 0 0 6
MAP PLANE 3
R 1 1 3 3 3 3 3 3 3 3 3 3 3 4 4 5
      0 0 3 3 3 3 3 3 3 3 3 3 4 4 5
      0 0 0 3 3 3 3 3 3 3 3 3 4 4 5
      0 0 0 0 3 3 3 3 3 3 3 3 4 4 5
      0 0 0 0 0 3 3 3 3 3 3 3 4 4 5
      0 0 0 0 0 0 3 3 3 3 3 3 4 4 5
      0 0 0 0 0 0 0 3 3 3 3 3 4 4 5
      0 0 0 0 0 0 0 0 3 3 3 3 4 4 5
      0 0 0 0 0 0 0 0 0 3 3 3 4 4 5
      0 0 0 0 0 0 0 0 0 0 3 3 4 4 5
      0 0 0 0 0 0 0 0 0 0 0 3 4 4 5
      0 0 0 0 0 0 0 0 0 0 0 0 4 4 5
      0 0 0 0 0 0 0 0 0 0 0 0 0 4 5
      0 0 0 0 0 0 0 0 0 0 0 0 0 0 5
      SHOW DUMMY
    PLANE 5
R 1 1 1 1 1 1 1 1 1 1 1 2 2 2 4 4 5
      0 0 1 1 1 1 1 1 1 2 2 2 4 4 5
      0 0 0 1 1 1 1 1 1 2 2 2 4 4 5
      0 0 0 0 1 1 1 1 1 2 2 2 4 4 5
      0 0 0 0 0 1 1 1 1 2 2 2 4 4 5
      0 0 0 0 0 0 1 1 1 2 2 2 4 4 5
      0 0 0 0 0 0 0 1 1 2 2 2 4 4 5
      0 0 0 0 0 0 0 0 1 2 2 2 4 4 5
      0 0 0 0 0 0 0 0 0 2 2 2 4 4 5
      0 0 0 0 0 0 0 0 0 0 2 2 4 4 5
      0 0 0 0 0 0 0 0 0 0 0 2 4 4 5
      0 0 0 0 0 0 0 0 0 0 0 0 4 4 5
      0 0 0 0 0 0 0 0 0 0 0 0 0 4 5
      0 0 0 0 0 0 0 0 0 0 0 0 0 0 5
      SHOW DUMMY
CONSTANTS SHOW GROUPS 10
WEIGHTS 280
SCATTER DOWN 18
SCATTER UP -1
WHAT 1
SOLVE
PRINT LC J I K S
RETURN
** EDITS HERE:WWED/WWIRE
STOP
/*
/
```

Appendix (5): The Multi-Cell WIMS Calculation of a Heterogeneously Diluted Core

Listing of the WIMS-D4 Multi-Cell input modelling of a heterogeneously diluted ETGBR as explained in chapter 6 , section 2.

```
1  //UMEMN26C JOB 'R.Y.N.-IC',MSGLEVEL=(1,1),MSGCLASS=X,
2  //       TIME=(,15),PRTY=8,NOTIFY=UMEMN26
3  //*PROCLIB=UMEMN26.PROC.LB
4  // EXEC RUNWMD4,FILE=TA,DISP='DISP=(NEW,PASS),UNIT=DISC',
5  //       LBR='UMEMN26.WDN26B.DATA',REGION=1800K
6  //FT03F001  DD UNIT=TEMP,SPACE=(3152,(200,5),,,ROUND),
7  //       DCB=(RECFM=VBS,BLKSIZE=1604,LRECL=1600,BUFNO=1)
8  //SYSIN DD *
9  PRIME 0
10 SAVE 1 1
11 WIMSDMULTICELLUSTER2
12 CELL 7
13 SEQUENCE 2
14 NREACT 3
15 NGROUP 19 19
16 NREG 9 14
17 NMESH 46
18 NMAT 5 2
19 NRODS 1 1 1 1 14 2 1
20 NCELL 2
21 NTHERMAL 14
22 PREOUT
23 INITIATE
24 COOLANT 3
25 **----------------------------------------
26 ** FUEL
27 MATER 1 -1 1000 1 1235.4 2.012615E-05 3238.5 2.010603E-02 $
28 3239.1 3.534348E-03 1240 7.466310E-04 241 1.192842E-04 $
29 242 1.767174E-05 16 4.908818E-02   **E=18%
30 **----------------------------------------
31 MATER 2 7.96 850 2 2056 65.18 52 17.0 58 12.50 93 2.50 $
32  55 2.00 29 0.75 2012 0.07  ** CLAD
33 MATER 3 -1 750 3 2012 4.2288E-4 16 8.4576E-4  ** COOLANT
34 MATER 4 7.96 750 4 2056 65.18 52 17.0 58 12.50 93 2.50 $
35  55 2.00 29 0.75 2012 0.07  ** WRAPPER
36 ** DILUENT/MODERATOR BLOCK MATERIAL
37 *MATER 5 1.8 750 1 2012 99.9999 1235 1E-15            * GRAP
38 MATER 5 -1 750 1 27 .06678 16 .07017 1235 1E-15       * ALUM
39 *MATER 5 -1 850 1 1235.4 9.7796E-5 3238.5 2.3471E-2 $ * DEP U
40 *16 0.048898
41 *** CONTROL ROD VACANCY MATERIAL IS CO2 WITH A DASH OF FUEL
42 *MATER 5 -1 750 1 2012 4.2288E-4 16 8.4576E-4 1235 1.E-15
43 ***
44 RODSUB 1 1 0.350 1
45 RODSUB 1 2 0.390 2
46 RODSUB 2 1 0.350 1
47 RODSUB 2 2 0.385 2
48 RODSUB 3 1 0.350 1
49 RODSUB 3 2 0.390 2
50 RODSUB 4 1 0.350 1
51 RODSUB 4 2 0.385 2
52 RODSUB 5 1 0.350 1
53 RODSUB 5 2 0.390 2
54 RODSUB 6 1 0.350 1
55 RODSUB 6 2 0.385 2
56 RODSUB 7 1 0.350 1
57 RODSUB 7 2 0.390 2
58 **
59 RODSUB 8  1 0.430 5
60 RODSUB 9  1 0.430 5
61 RODSUB 10 1 0.430 5
62 RODSUB 11 1 0.430 5
63 RODSUB 12 1 0.430 5
64 RODSUB 13 1 0.430 5
65 RODSUB 14 1 0.430 5
66 ***************************
```

```
CELL 1 2  * CORE SUBASSEM
ANNU 1 0.3850 2  *
ANNU 2 1.5687 3  *
ANNU 3 2.6145 3  *
ANNU 4 3.6603 3  *
ANNU 5 4.7061 3  *
ANNU 6 5.7519 3  *
ANNU 7 6.7977 3  *
ANNU 8 7.8435 3  *
ANNU 9 8.2635 4  * BASE SS WRAP
ARRAY 1 1 6  0.9768 0
ARRAY 2 1 12 2.0916 .261799
ARRAY 3 1 18 3.1374 0
ARRAY 4 1 24 4.1832 .130899
ARRAY 5 1 30 5.2290 0
ARRAY 6 1 36 6.2748 .0981747
ARRAY 7 1 42 7.3206 0
MESH 1 3 3 3 3 3 3 3 1
PCELL 1 0.50 0.50
******************************
CELL 2 1  * DILUENT PINS
ANNU 1 0.3850 2  *
ANNU 2 1.5687 3  *
ANNU 3 2.6145 3  *
ANNU 4 3.6603 3  *
ANNU 5 4.7061 3  *
ANNU 6 5.7519 3  *
ANNU 7 6.7977 3  *
ANNU 8 7.8435 3  *
ANNU 9 8.2635 4  * BASE SS WRAP
ARRAY 8 1 6  0.9768 0
ARRAY 9 1 12 2.0916 .2617B9
ARRAY 10 1 18 3.1374 0
ARRAY 11 1 24 4.1832 .130899
ARRAY 12 1 30 5.2290 0
ARRAY 13 1 36 6.2748 .0981747
ARRAY 14 1 42 7.3206 0
MESH 1 3 3 3 3 3 3 3 1
PCELL 2 1.0 0.0
************************
**** GEOM : VD/VF = 1.77
*CELL 2 1 * DILUENT BLOCK IS SOLID
*ANNU 1 1.0000  3
*ANNU 2 8.2635  5  *NO WRAP
*MESH 1 10
*PCELL 2 1.0 0.0
************************
*CELL 2 1 * CR VACANCY BLOCK
*ANNU 1 7.6335  5
*ANNU 2 8.2635  4  *WRAP THICK=0.6CM
*MESH 19 1
*PCELL 2 1.0 0.0
*****************************
FEWGR 2 3 4 5 6 7 8 9 10 11 12 13 14 $
16 18 22 24 27 69
SUPP  0 0 1
POWERC 1 47.8 0.001 1      *C1
*POWERC 1 33.8 18.25 10      * C2
BUCK 2.13E-4 5.035E-4
BEGINC
REACTION 135 1000 1235 1000 3239 1000
PARTIT 2 3 4 5 6 7 8 9 10 11 12 13 14 $
16 18 22 24 27 69
BUCK 2.13E-4 5.035E-4
THERMAL 1
PRINTC 1 1 1 1
BEGINC
**
POWERC 0
BEGINC
BEGINC
/*
// EXEC LSWIMSEO,LL1=I1,LL2=FALO,LL3=ALO,
//  D1='DISP=(,DELETE),UNIT=DISC',
//  D2='DISP=(NEW,CATLG),UNIT=DISC',
//  D3='DISP=(NEW,CATLG),UNIT=DISC',
//  LIB='UMEMN26.WEN34B.DATA',REGION=1800K
```

```
144 //G.FT06F001 DD SYSOUT=*
145 //G.FT71F001 DD DISP=SHR,DSN=UMEMN26.TA.DATA
146 //G.SYSIN DD *
147 WFORTE 1
148 SEQ 2 BEGIN
149 WMIX 1
150 WSMEAR 1 2
151 MATE 1 MESH 1 ENDP
152 NEWMAT 1 1 2 3 4 5 6 7 8 9 10 11 12 13 14 15 16
153 17 18 19 20 21 22 23
154 MCODE 1 BEGIN
155 WSMEAR 1 3
156 MATE 1 MESH 1 ENDP
157 NEWMAT 1 24 25 26 27 28 29 30 31 32 33 34 35
158 36 37 38 39 40 41 42 43 44 45 46
159 MCODE 1 BEGIN
160 STOP
161 /*
162 /
```

Appendix (6): Methods and assumptions in TEANT

A general explanation of the calculation methods and assumptions in the depressurization transient program TEANT.

1. The nature of the problem solved and the general solution technique.

The program TEANT retains the basic methods and prescriptions of the finite difference scheme TEACH-C mentioned in chapter 7 - hence the naming TEANT : TEA-Nuclear-transient. TEACH-C is a particularly simple and convenient method of solving the equation of heat conduction, which is (in R-Z geometry):

$$\rho C_v r \frac{\partial T}{\partial t} - \frac{\delta}{\partial z} rk \frac{\partial T}{\partial z} - \frac{\delta}{\partial r} rk \frac{\partial T}{\partial r} - rs = 0$$

With some simple manipulation (see reference , p. for details) the equation can be put in the convenient form:

$$D_P(T_P - T_P^{old}) + A_N(T_P - T_N) + A_S(T_P - T_S)$$

$$+A_E(T_P - T_E) + A_W(T_P - T_W) - (B_P\ T_P + C_P) = 0$$

Where P,N,S,E,W are the locations of the central node, its north, south, east, and west neighbours respectively. A_i are the thermal conductances (reciprocal thermal resistances) and D_P is the capacitance of the node. These are given by:

$$A_i = \frac{k_i + k_P}{2} \frac{a_i}{\delta r_i P}$$

and,

$$D_P = \rho C_P V_P / \partial t$$

The equation can be further recast into a form amenable to solution as follows:

$$(A_P - S_P)T_P = \sum_i A_i T_i + S_u$$

with,

$$A_P = \sum_i A_i$$

$$S_u = C_P + D_P T_P^{old}$$

$$S_P = B_P - D_P$$

Where now the source terms are contained in S_u and S_P and are controlled through the terms B_P and C_P.

With this setup it becomes relatively simple to impose boundary conditions by suppressing the normal conduction term via the zeroing of the relavant A_i. This is then followed , usually, by redifinition of the A_i for the face, or by modifying the heat flow term through S_u and S_P with aknowledge of B_P and C_P at the relavant face.

2. Boundary conditions for the TEANT problem

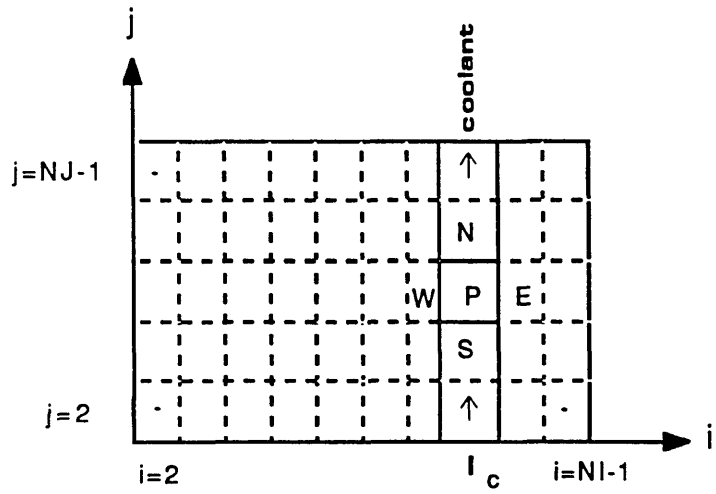

Figure A.6.1. The R-Z solution domains of TEANT. Fuel, clad, coolant, and diluent are shown.

The solution domain of the problem solved by TEANT is shown in the diagram. An energy balance on node P clarifies the situation.

$$\frac{T_W - T_P}{R_W} + \frac{T_E - T_P}{R_E} = \dot{m} C_P (T_P - T_N)$$

where $\dot{m}$ is the mass flow rate (kg/s) per coolant channel.

The heat flow to the E-W sides are incorporated by first setting for all j :

$$A_W(I_c, j) = 0 \quad and \quad A_E(I_c, j) = 0$$

as well as,

$$A_W(I_{c+1}, j) = 0 \quad and \quad A_E(I_{c-1}, j) = 0$$

The A's are then modified to include the convective boundary condition as well as the remaining half-cell conduction. Hence,

$$A_E(I_{c-1}, j) = 1/R_f \quad and \quad A_W(I_c, j) = A_E(I_{c-1}, j)$$

also,

$$A_W(I_{c+1}, j) = 1/R_m \quad and \quad A_E(I_c, j) = A_W(I_{c+1}, j)$$

The heat flow resistances on the fuel side R_f and on the diluent side R_m are given by:

$$R_f = \frac{\delta_{rWP}}{2a_{NS}\bar{k}_{WP}} + \frac{1}{h_f a_{NS}}$$

and,

$$R_m = \frac{\delta_{rPE}}{2a_{NS}\bar{k}_{PE}} + \frac{1}{h_m a_{NS}}$$

where h_f and h_m are the convective heat transfer coefficients on the fuel and moderator(diluent) sides respectively.

To complete the energy balance, the heat flow in the along the coolant channel is considered. For all coolant nodes, except the bottom one the north boundary conduction term is cancelled by requiring:

$$A_N(I_c, j) = 0 \quad , for\ j\ from\ 2\ to\ NJ - 1$$

A flow term is then introduced into these nodes by putting:

$$A_S(I_c, j) = \frac{\dot{m}C_P}{2\pi}$$

where the 2π modifies the flow to be per unit angle so as to be consistent with the remainder of the TEACH-C formulation (i.e. note the original difference equation)

For the lower most coolant mesh, a special treatment is required since it contains an external source incorporating the current inlet temperature. This is accounted for by modifying the source terms as follows:

$$S_u = S_u + \frac{\dot{m}C_P}{2\pi T_{in}}$$

and,

$$S_P = S_P - \frac{\dot{m}C_P}{2\pi}$$

3. Solution of the difference equations

There is probably no need to present the details of the solution technique adopted in TEACH-C since it is very well documented in the reference [79]. It suffices to say here that the TDMA is used. The only difference TEANT entails is the replacement of the block adjustment routine by a horizontal W-E iteration sweep following the conventional S-N sweep in TEACH-C. This was found to give quiker convergence altough the reasons behind this were not studied in this thesis.

4. The calculational route of TEANT

The problem solved by TEANT, as explained starts with asteady state, full power and full pressure (full flow) step. A hypothetical transient is then considered with the the pressure falling exponentialy with a given period. The full power heat may be altered to become decay heat, a function of time, at any stage of the transient.

The general setup of the TEANT calculation, disregarding the details of the finite difference solution, is shown in the diagram.

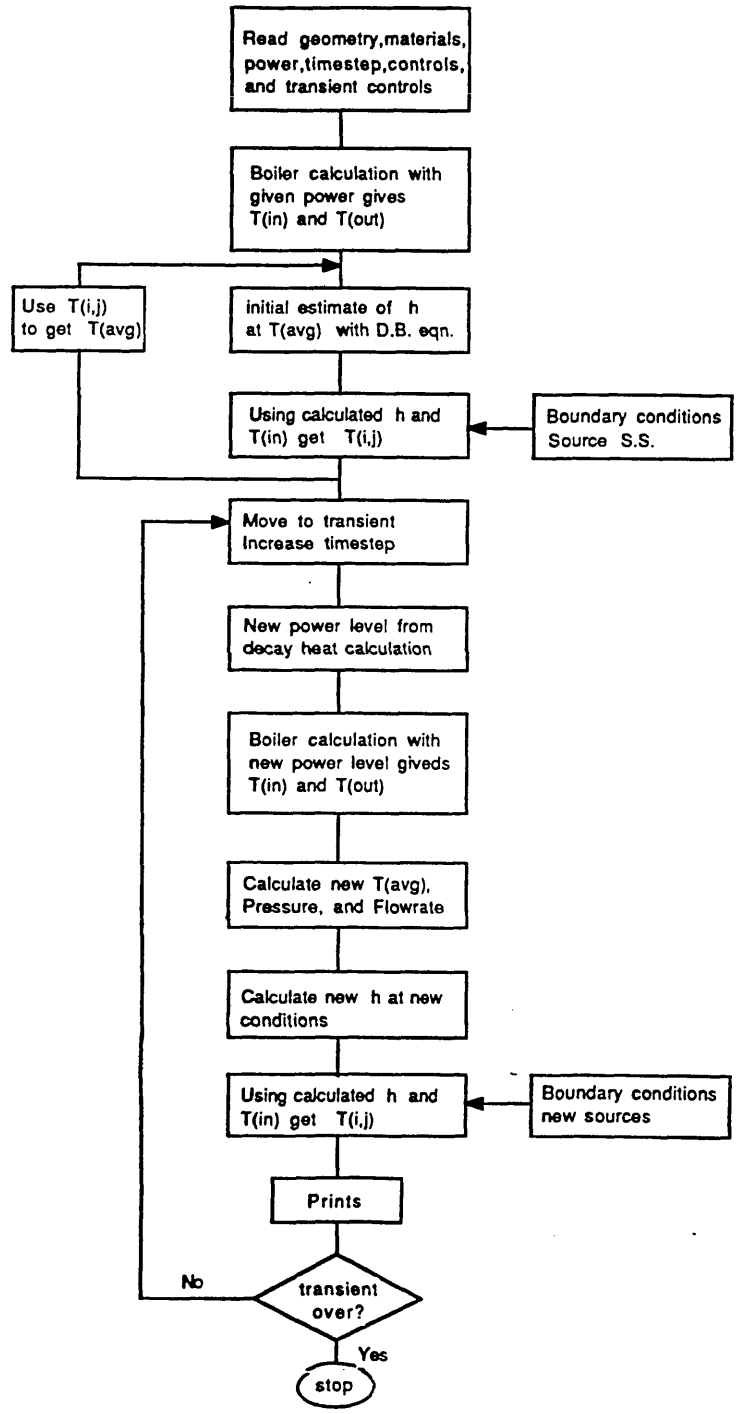

Figure A.6.2. The TEANT general calculational route.

5. Simple Treatment of boilers

An energy balance on a boiler has the simplified form:

$$T_{in}^{B} = T_{out}^{B} + \dot{Q}_B / \dot{m}_B C_p$$

where $\dot{Q}_B$ is the heat input to a single boiler and the other terms are self-explanatory.

Assuming the secondary side(steam side) stays at the saturation temperature, which is not an unreasonable assumption. Then,

$$T_{out}^{B} - T_{sat} = (T_{in}^{B} - T_{sat}) e^{-Ah/\dot{m}_B C_p}$$

Combining the last two equations gives T_{in}^{B} in terms of T_{sat} :

$$T_{in}^{B} = T_{sat} + (\dot{Q}_B / \dot{m}_B C_p)(1 - e^{-Ah/\dot{m}_B C_p})^{-1}$$

since,

$$T_{out}^{core} = T_{in}^{core} - \dot{Q}_B / \dot{m}_B C_p$$

and,

$$T_{in}^{B} = T_{out}^{core}$$

It is possible to calculate T_{in}^{core} of the present time step from T_{out}^{core} of the previous step.

For the cases performed by TEANT the number of boilers assumed were 12, the total mass flow rate was 5750 kg/s, the boiler heat transfer area was $2.6 \times 10^4 cm^2$, and the saturation temperature of steam at 169 bars was $270°C$.

6. The accuracy of TEANT

Although the equation solved by TEANT, based on TEACH-C guidelines is an implicit one, it still requires some optimization especially as far as transient time step is concerned. Extensive computing time is avoided by selection of a somewhat optimized time step, although this was not fully carried through. Nevertheless, the figure shows an standard ETGBR transient with trip at 120s. and a τ of

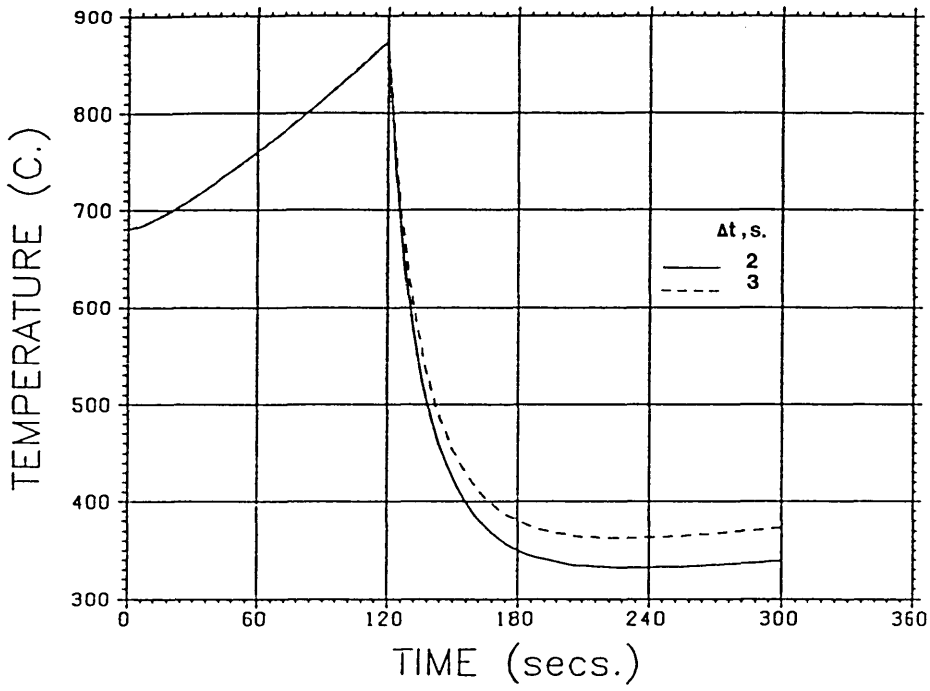

Figure A.6.3. Effect of time step on transient temperature in TEANT (base case).

250s. Reducing the time step from 3s. to 2s. showed increasingly divergent clad temperatures as the the transient proceeds. The 2s. time step was taken for all the calculation reported since a 1s. time step gave only a small difference and would cause the runs to be time consuming.

Appendix (7): The nuclear transient program TEANT

The following pages contain a listing of the program TEANT used in chapter 7 to study depressurization transients in fuel rods with differing amounts of diluent material surrounding the coolant.

A sample input file for TEANT is first given below showing the meshing as midgrid points. Material identification and other control values are shown.

```
 1  OUTPUT FILE NAME IS
 2 ALX5
 3  NI      NJ    ICHAN
 4  13      7       8
 5  URFT        SORMAX     DT
 6  1.000       1.E-6      3.00
 7  MAXIT  MAXSTP   MAXERR   NITPRI   NSTPRI
 8  100    400       100       100      2
 9  IMON   JMON
10    9      6
11 X CO-ORDINATES
12 -.035 .035 .105 .175 .245 .315 .368 .532 .637 .702 .824 .946 1.107
13 Y CO-ORDINATES
14 -14. 14. 42. 70. 98. 126. 154.
15 MATERIAL CONFIGURATION
16  0  0  0  0  0  0  0  0  0  0  0  0  0
17  0  1  1  1  1  1  2  0  5  5  5  5  0
18  0  1  1  1  1  1  2  0  5  5  5  5  0
19  0  1  1  1  1  1  2  0  5  5  5  5  0
20  0  1  1  1  1  1  2  0  5  5  5  5  0
21  0  1  1  1  1  1  2  0  5  5  5  5  0
22  0  0  0  0  0  0  0  0  0  0  0  0  0
23  FULL-FLOW / CHANS / RODS / POWER / TSAT
24  5750. 397. 168. 1680. 270.
25 DEPRES. TIME CONST. / TRIP FROM FULL POWER
26 500.0 240.0
27
28 ************* ADDITIONAL INFO ************
29 NOTE 1: X COORDS.
30 STANDARD
31  -.035 .035 .105 .175 .245 .315 .368 .532 .637 .645 .653 .661 .672
32 D/F=1
33  -.035 .035 .105 .175 .245 .315 .368 .532 .637 .655 .682 .710 .746
34 D/F=2
35  -.035 .035 .105 .175 .245 .315 .368 .532 .637 .668 .722 .776 .845
36 D/F=3
37  -.035 .035 .105 .175 .245 .315 .368 .532 .637 .688 .758 .836 .935
38  -.035 .035 .105 .175 .245 .315 .3675 .5324 .6938 .8144 .9350
39 D/F=5
40  -.035 .035 .105 .175 .245 .315 .368 .532 .637 .702 .824 .946 1.107
41 NOTE 2: 3 IS S.S.
42         4 IS GRAPHITE
43         5 IS ALUMINA
44         6 IS SIC
```

```
      PROGRAM MAIN
CCCCCCCCCCCCCCCCCCCCCCCCCCCCCCCCCCCCCCCCCCCCCCCCCCCCCCCCCCCCCCCCCCCCCCC
C TRANSIENT FUEL ROD CHANNEL WITH DEPRESSURIZATION AND DECAY HEAT     C
C AT SHUTDOWN  USES  TDMA SOLVER OF THE TEACH-C PROGRAM               C
C R Y NUNAYHID / IMPERIAL COLLEGE                                     C
CCCCCCCCCCCCCCCCCCCCCCCCCCCCCCCCCCCCCCCCCCCCCCCCCCCCCCCCCCCCCCCCCCCCCCC
      PARAMETER(MAXNI=20,MAXNJ=20)
      PARAMETER(NMAT=6)
      PARAMETER(TZERO=1 OE-04)
      REAL
     & EPS1(O NMAT),EPS2(O NMAT),
     & GAMN(O NMAT),DENSIT(O NMAT),CP(O NMAT),
     & HEAT(O NMAT),SHEAT,DX,DY,
     & RX(MAXNI),RU(MAXNI),X(MAXNI),Y(MAXNJ),DXEP(MAXNI),DXPW(MAXNI),
     & DYNP(MAXNJ),DYPS(MAXNJ),SNS(MAXNJ),SEW(MAXNI),XU(MAXNI),
     & YV(MAXNJ),RY(MAXNJ),RV(MAXNJ)
      REAL TF(MAXNJ),QLOCAL(MAXNJ),RESFUL(MAXNJ),
     & RESMOD(MAXNJ),TFOLD(MAXNJ)
      INTEGER
     & NI,NJ,NIM1,NJM1,ICHAN,IMAT(MAXNI,MAXNJ),NITER
      REAL
     & T(MAXNI,MAXNJ),TOLD(MAXNI,MAXNJ),DT,RESORT,URFT,TIME,
     & AP(MAXNI,MAXNJ),AN(MAXNI,MAXNJ),AS(MAXNI,MAXNJ),AE(MAXNI,MAXNJ),
     & AW(MAXNI,MAXNJ),SU(MAXNI,MAXNJ),SP(MAXNI,MAXNJ)
      LOGICAL INCYLY,INCYLX,INPRO,INTIME
      COMMON /TEMP/   T,GAMN,TOLD,DENSIT,CP,EPS1,EPS2
      COMMON /CONVAR/ NI,NJ,NIM1,NJM1,ICHAN,DT,RESORT,URFT,SHEAT
      COMMON /GEOM/ NITER, DX, DY, RX, RU, X, Y, DXEP, DXPW, DYNP, DYPS,
     &               SNS, SEW, XU, YV, RY, RV, JN, JN
      COMMON /COEF/   AP, AN, AS, AE, AW, SU, SP
      COMMON /DNDATA/ DN, HEAT, IMAT
      COMMON /LOGON/  INCYLX,INCYLY,INTIME
      COMMON /FLUID/  FLOW,CHAN,ROD
      COMMON /RESIST/ RESFUL,RESMOD
      COMMON /CONT/ MAXIT,MAXSTP,NSTEP,MAXERR,NITPRI,NSTPRI,SORMAX,
     &               INOW,JNOW,NXTEMP
C
      CHARACTER HEDT*50,HEDI*50,HEDIT*50,HEDM*50,TT*1,SFILE*80
      DATA HEDT /'       TEMPERATURE (C)                   '/
      DATA HEDIT/'  INTERMEDIATE TEMPERATURE (C)           '/
      DATA HEDI /'     INITIAL TEMPERATURE (C)             '/
      DATA HEDM /'      MATERIAL CONFIGURATION             '/
C
C ......SPECIFY GRID, PROGRAM CONTROL AND MONITOR    .....C
      OPEN(7,FILE='TEAD')
      READ(7,*)
      READ(7,10) SFILE
      READ(7,*)
      READ(7,*)  NI,NJ,ICHAN
      READ(7,*)
      READ(7,*)  URFT,SORMAX,DT
      READ(7,*)
      READ(7,*)  MAXIT,MAXSTP,MAXERR,NITPRI,NSTPRI
      READ(7,*)
      READ(7,*)  INOW,JNOW
C READS X AND Y CO-ORDINATES
      READ(7,*)
      READ(7,*)  (X(II),II=1,NI)
      READ(7,*)
      READ(7,*)  (Y(JJ),JJ=1,NJ)
C READS IMAT CO-ORDINATES
      READ(7,*)
      DO 100 J=1,NJ
       READ(7,*) (IMAT(II,J),II=1,NI)
 100  CONTINUE
      NIM1 = NI - 1
      NJM1 = NJ - 1
      DO 862 II=1,NI
 862   X(II)=X(II)*1 0E-03
      DO 863 JJ=1,NJ
 863   Y(JJ)=Y(JJ)*1 0E-03
C
      DO 101 JJ=1,NJ
       DO 101 II=1,NI
        T(II,JJ)=0 0
 101  CONTINUE
C
C READ FULL FLOW,CHANNELS,RODS/CHAN,Q,AND TS
      READ(7,*)
      READ(7,*)  FFLOW,CHAN,ROD,Q,TS
      READ(7,*)
      READ(7,*) TAU,TTRIP
C
      TTRIP=TTRIP+TZERO
      Q=Q*1 OE+06
      SHEAT = 1 OE+30
      PI = 4 0 * ATAN(1 0)
      FLOW=FFLOW/(CHAN*ROD)
C
      SORTEM=SORMAX
      NXTEMP=MAXSTP
C
C BOOLEAN INITIALISATION
      INCYLX =  TRUE
      INCYLY =  FALSE
      INPRO  =  FALSE
      INTIME =  FALSE
      OPEN(2,FILE='TRUC')
      OPEN(8,FILE='TOUT')
      OPEN(9,FILE=SFILE)
C
C                   ... MAIN CONTROL SEGMENT               .C
C
      CALL INIT
      NSTEP=1
      MAXSTP=1
      TIME=TZERO
C
      DO 3333 IT=1,2
      CALL QLOC(Q,QLOCAL,QFLUID)
      CALL BOILER(Q,QFLUID,TS,TOUCOR,TINCOR)
      CALL FLUIDT(TINCOR,TOUCOR,Q,QLOCAL,TF,QFLUID)
      CALL CONVEC(TINCOR,TOUCOR,TF,TFOLD,TIME,IT,S,POLD,TAU)
      IF(IT EQ 2) GO TO 333
      CALL START(Q,TIME,S,TF)
 333  CONTINUE
      CALL SOLVC(Q,TIME,S,TF,QLOCAL,QFLUID,TINCOR,TOUCOR,TTRIP)
 3333 CONTINUE
C
C MOVE TO TRANSIENT CALCULATION
C
      INTIME =  TRUE
      SORMAX=SORTEM
      MAXSTP=NXTEMP
      DO 30 NSTEP= 1,MAXSTP
      TIME=TIME+DT
C     IF(NSTEP EQ 10) NSTPRI =10
      CALL BOILER(Q,QFLUID,TS,TOUCOR,TINCOR)
      CALL FLUIDT(TINCOR,TOUCOR,Q,QLOCAL,TF,QFLUID)
      CALL CONVEC(TINCOR,TOUCOR,TF,TFOLD,TIME,IT,S,POLD,TAU)
      CALL SOLVC(Q,TIME,S,TF,QLOCAL,QFLUID,TINCOR,TOUCOR,TTRIP)
 30   CONTINUE
C
 10   FORMAT(A80)
      CLOSE(UNIT=9)
      STOP
      END
C..........................................................C
C-----------------------------------------------------------C
      SUBROUTINE START(Q,TIME,S,TF)
      PARAMETER(MAXNI=20,MAXNJ=20)
      PARAMETER(NMAT=6)
      PARAMETER(TZERO=1 0E-04)
      REAL
     & EPS1(O NMAT),EPS2(O NMAT),
     & GAMN(O NMAT),DENSIT(O NMAT),CP(O NMAT),
     & HEAT(O NMAT),SHEAT,DX,DY,
     & RX(MAXNI),RU(MAXNI),X(MAXNI),Y(MAXNJ),DXEP(MAXNI),DXPW(MAXNI),
     & DYNP(MAXNJ),DYPS(MAXNJ),SNS(MAXNJ),SEW(MAXNI),XU(MAXNI),
     & YV(MAXNJ),RY(MAXNJ),RV(MAXNJ)
      REAL TF(MAXNJ),QLOCAL(MAXNJ),RESFUL(MAXNJ),
     & RESMOD(MAXNJ),TFOLD(MAXNJ)
      INTEGER
     & NI,NJ,NIM1,NJM1,ICHAN,IMAT(MAXNI,MAXNJ),NITER
      REAL
     & T(MAXNI,MAXNJ),TOLD(MAXNI,MAXNJ),DT,RESORT,URFT,TIME,
     & AP(MAXNI,MAXNJ),AN(MAXNI,MAXNJ),AS(MAXNI,MAXNJ),AE(MAXNI,MAXNJ),
     & AW(MAXNI,MAXNJ),SU(MAXNI,MAXNJ),SP(MAXNI,MAXNJ)
      LOGICAL INCYLY,INCYLX,INPRO,INTIME
      COMMON /TEMP/   T,GAMN,TOLD,DENSIT,CP,EPS1,EPS2
      COMMON /CONVAR/ NI,NJ,NIM1,NJM1,ICHAN,DT,RESORT,URFT,SHEAT
      COMMON /GEOM/ NITER, DX, DY, RX, RU, X, Y, DXEP, DXPW, DYNP, DYPS,
     &               SNS, SEW, XU, YV, RY, RV, JN, JN
      COMMON /COEF/   AP, AN, AS, AE, AW, SU, SP
      COMMON /DNDATA/ DN, HEAT, IMAT
      COMMON /LOGON/  INCYLX,INCYLY,INTIME
      COMMON /FLUID/  FLOW,CHAN,ROD
      COMMON /RESIST/ RESFUL,RESMOD
      COMMON /CONT/ MAXIT,MAXSTP,NSTEP,MAXERR,NITPRI,NSTPRI,SORMAX,
     &               INOW,JNOW,NXTEMP
C
      CHARACTER HEDT*50,HEDI*50,HEDIT*50,HEDM*50,TT*1,SFILE*80
      DATA HEDT /'       TEMPERATURE (C)                   '/
      DATA HEDIT/'  INTERMEDIATE TEMPERATURE (C)           '/
      DATA HEDI /'     INITIAL TEMPERATURE (C)             '/
      DATA HEDM /'      MATERIAL CONFIGURATION             '/
C
C INITIAL OUTPUT
      WRITE(2,3000) DT,URFT,NI,NJ
      WRITE(2,4100)
      WRITE(2,4200)  (II,GAMN(II),DENSIT(II),CP(II),II=0,NMAT)
      CALL CONOUT(MAXNI,MAXNJ,NI,NJ,IMAT,HEDM)
CC    CALL PRINT(MAXNI,MAXNJ,1,1,NI,NJ,X,Y,T,TIME,HEDI)
      WRITE(2,3100) INOW,JNOW
C
C THE SS HEAT OUTPUT IS GIVEN AS
       PI=4 0*ATAN(1 0)
       HZ=YV(NJ)
       QC=Q/(CHAN*ROD)
       RAT=QC/HZ
       HEAT(0)=0 0
       AF= PI*(RU(ICHAN-1))**2
       DO 111 IN=1,NMAT
        IF(IN EQ 1)THEN
        HEAT(IN)= (RAT/AF)
        ELSE
        HEAT(IN)=0 0
        ENDIF
 111   CONTINUE
        WRITE(2,*)'HEAT(1)= ',HEAT(1)
       RETURN
 3000 FORMAT(//27X,'* MODIFIED TEACH-C TRANSIENT CODE     * ',
     &        /27X,'*  (NTTC)  .  REACTOR ROD CHANNEL WITH *
     &        '/27X,'* DEPRES  AT SHUTDOWN WITH DECAY HEAT *'/
     &/20X,' INITIAL TIME STEP, DT -------------------------*',1PE12.3
     &/20X,' RELAXATION FACTOR, URFT------------------------*',1PE12 3
     &/20X,' NO  OF NODES IN DIRECTION R, NI --------------*',3X,I3
     &/20X,' NO  OF NODES IN DIRECTION Z, NJ --------------*',3X,I3)
 3100 FORMAT(/20X,'NITER',3X,'RESORT',3X,'T(',I2,',',I2,')',3X,' TIME ',
     &  8X,'DT')
 4100 FORMAT(///'          IMAT       GAMN        DENSIT        CP   ',
     &        /'       --------------------------------------------')
 4200 FORMAT(11X,I1,1PE12 3)
       END
C--------- SOLUTION OF SS AND TIME ITERATION LOOPS ------------C
      SUBROUTINE SOLVC(Q,TIME,S,TF,QLOCAL,QFLUID,TINCOR,TOUCOR,TTRIP)
      PARAMETER(MAXNI=20,MAXNJ=20)
      PARAMETER(NMAT=6)
      PARAMETER(TZERO=1 OE-04)
      REAL
     & EPS1(O NMAT),EPS2(O NMAT),
     & GAMN(O NMAT),DENSIT(O NMAT),CP(O NMAT),
     & HEAT(O NMAT),SHEAT,DX,DY,
     & RX(MAXNI),RU(MAXNI),X(MAXNI),Y(MAXNJ),DXEP(MAXNI),DXPW(MAXNI),
     & DYNP(MAXNJ),DYPS(MAXNJ),SNS(MAXNJ),SEW(MAXNI),XU(MAXNI),
     & YV(MAXNJ),RY(MAXNJ),RV(MAXNJ)
      REAL TF(MAXNJ),QLOCAL(MAXNJ),RESFUL(MAXNJ),
     & RESMOD(MAXNJ),TFOLD(MAXNJ)
```

```
      INTEGER
     &  NI,NJ,NIM1,NJM1,ICHAN,IMAT(MAXNI,MAXNJ),NITER
      REAL
     &  T(MAXNI,MAXNJ),TOLD(MAXNI,MAXNJ),DT,RESORT,URFT,TIME,
     &  AP(MAXNI,MAXNJ),AN(MAXNI,MAXNJ),AS(MAXNI,MAXNJ),AE(MAXNI,MAXNJ),
     &  AW(MAXNI,MAXNJ),SU(MAXNI,MAXNJ),SP(MAXNI,MAXNJ)
      LOGICAL INCYLY,INCYLX,INPRO,INTIME
      COMMON /TEMP/   T,GAMH,TOLD,DENSIT,CP,EPS1,EPS2
      COMMON /CONVAR/ NI,NJ,NIM1,NJM1,ICHAN,DT,RESORT,URFT,GREAT
      COMMON /GEOM/ NITER, DX, DY, RX, RU, X, Y, DXEP, DXPW, DYNP, DYPS,
     &                 SNS, SEW, XU, YV, RY, RV, JS, JN
      COMMON /COEF/   AP, AN, AS, AE, AW, SU, SP
      COMMON /DHDATA/ DH, HEAT, IMAT
      COMMON /LOGCOM/  INCYLX,INCYLY,INTIME
      COMMON /FLUID/  FLOW,CHAN,ROD
      COMMON /RESIST/ RESFUL,RESMOD
      COMMON /CONT/ MAXIT,MAXSTP,NSTEP,MAXERR,NITPRI,NSTPRI,SORMAX,
     &                 IMON,JMON,NXTEMP
C
       CHARACTER HEDT*80,HEDI*80,HEDIT*80,HEDM*80,TT*1,NFILE*80
       DATA HEDT /'         TEMPERATURE (C)              '/
       DATA HEDIT/'     INTERMEDIATE TEMPERATURES (C)    '/
       DATA HEDI /'        INITIAL TEMPERATURES (C)      '/
       DATA HEDM /'       MATERIAL CONFIGURATION         '/
C
       PI=4.0*ATAN(1.0)
C  SKIP OVER CALCHR FOR STEADY STATE
       IF( NOT INTIME) GO TO 1130
C
C  CALCULATES NEW DECAY HEATING SOURCES
         CALL CALCHR (TIME-DT,TIME,Q,TTRIP)
         DO 1020 I=1,NI
           DO 1010 J=1,NJ
             TOLD(I,J)=T(I,J)
 1010      CONTINUE
 1020    CONTINUE
C
 1130    CONTINUE
C
         SNORM=1.0
CCNORMALIZE BY HEAT FLUX INTO CHANNEL
CC       IF(INTIME) THEN
CC        SNORM = QFLUID*(2.0*PI)
CC       ELSE
CC        SNORM = QFLUID
CC       ENDIF
C
         DO 1100 NITER=1,MAXIT
C
C UPDATE TEMPERATURES AND START OF INNER ITERATION LOOP
         CALL CALCT(TF,Q,TINCOR,TOUCOR)
C
C NORMALISING OF RESIDUAL  SOURCE AND INTERMEDIATE OUTPUT
         RESORT = RESORT/SNORM
         SOURCE = RESORT
         WRITE(2,8200) NITER,RESORT,T(IMON,JMON),TIME,DT
         IF (MOD(NITER,NITPRI) EQ 0) THEN
          CALL PRINT(MAXNI,MAXNJ,1,1,NI,NJ,X,Y,T,TIME,HEDIT)
          WRITE(2,8100) IMON,JMON
         ENDIF
C
C TERMINATION TESTS
         IF(SOURCE LE SORMAX) GOTO 1300
C
C EXIT CALCULATION IF SOURCE IS LARGE AFTER MAXERR ITERATIONS
         IF(NITER LE MAXERR AND SOURCE.LT.1.0E+6) GO TO 1100
         WRITE (*,8800) MAXERR
         GO TO 1200
 1100   CONTINUE
C
C END OF INNER ITERATION LOOP
         WRITE (*,8900)
         WRITE(2,*)'END OF INNER'
         GO TO 1200
C
C OUTPUT CONVERGED SOLUTION AT INTERVALS SPECIFIED BY NSTPRI
 1300   IF (MOD(NSTEP,NSTPRI) NE  0
     &               OR MOD(NITER,NITPRI) EQ 0) GOTO 1001
         CALL PRINT(MAXNI,MAXNJ,1,1,NI,NJ,X,Y,T,TIME,HEDT)
         IF (NSTEP NE MAXSTP) WRITE (2,8100) IMON,JMON
C
 1001   CONTINUE
C
C RECALCULATE QFLUID FOR NEXT BOILER INPUT
         CALL FUELHT(TF,QLOCAL,QFLUID,TINCOR,TOUCOR)
C
C END OF OUTER LOOP
C FINAL OPERATIONS AND OUTPUT
C
 1200 CONTINUE
      IF (MOD(NITER,NITPRI) NE 0 AND MOD(MAXSTP,NSTPRI) NE 0)
     &   CALL PRINT(MAXNI,MAXNJ,1,1,NI,NJ,X,Y,T,TIME,HEDT)
C   FORMAT STATEMENTS
 8100 FORMAT(/2NX,'NITER',5X,'RESORT',6X,'T(',I3,',',I3,')',8X,' TIME ',
     &  8X,'DT')
 8200 FORMAT(I8 ,2NX,I8,1P4E12.5)
 8800 FORMAT(//'SOURCE IS LARGE AFTER MORE THAN ',I8,' ITERATIONS',
     &       /'         - CALCULTION TERMINATED - ')
 8900 FORMAT(//'            - CAUTION -'/' CONVERGENCE CRITERION NOT',
     &      'SATISFIED WHEN THE PROGRAM TERMINATED AT NITER = MAXIT ')
      RETURN
      END
C--------------------- SOLUTION OF ENERGY EQUATIONS ------------C
      SUBROUTINE CALCT(TF,Q,TINCOR,TOUCOR)
      PARAMETER(MAXNI=20,MAXNJ=20)
      PARAMETER(NMAT=8)
      PARAMETER(TZERO=1.0E-04)
      REAL
     &  EPS1(0:NMAT),EPS2(0:NMAT),
     &  GAMH(0:NMAT),DENSIT(0:NMAT),CP(0:NMAT),
     &  HEAT(0:NMAT),GREAT,DX,DY,
     &  RX(MAXNI),RU(MAXNI),X(MAXNI),Y(MAXNJ),DXEP(MAXNI),DXPW(MAXNI),
     &  DYNP(MAXNJ),DYPS(MAXNJ),SNS(MAXNJ),SEW(MAXNI),XU(MAXNI),
     &  YV(MAXNJ),RY(MAXNJ),RV(MAXNJ)
      REAL TF(MAXNJ),QLOCAL(MAXNJ),RESFUL(MAXNJ),
     &  RESMOD(MAXNJ),TFOLD(MAXNJ)
      INTEGER
     &  NI,NJ,NIM1,NJM1,ICHAN,IMAT(MAXNI,MAXNJ),NITER
      REAL
     &  T(MAXNI,MAXNJ),TOLD(MAXNI,MAXNJ),DT,RESORT,URFT,TIME,
     &  AP(MAXNI,MAXNJ),AN(MAXNI,MAXNJ),AS(MAXNI,MAXNJ),AE(MAXNI,MAXNJ),
     &  AW(MAXNI,MAXNJ),SU(MAXNI,MAXNJ),SP(MAXNI,MAXNJ)
      LOGICAL INCYLY,INCYLX,INPRO,INTIME
      COMMON /TEMP/   T,GAMH,TOLD,DENSIT,CP,EPS1,EPS2
      COMMON /CONVAR/ NI,NJ,NIM1,NJM1,ICHAN,DT,RESORT,URFT,GREAT
      COMMON /GEOM/ NITER, DX, DY, RX, RU, X, Y, DXEP, DXPW, DYNP, DYPS,
     &                 SNS, SEW, XU, YV, RY, RV, JS, JN
      COMMON /COEF/   AP, AN, AS, AE, AW, SU, SP
      COMMON /DHDATA/ DH, HEAT, IMAT
      COMMON /LOGCOM/  INCYLX,INCYLY,INTIME
      COMMON /FLUID/  FLOW,CHAN,ROD
      COMMON /RESIST/ RESFUL,RESMOD
      COMMON /CONT/ MAXIT,MAXSTP,NSTEP,MAXERR,NITPRI,NSTPRI,SORMAX,
     &                 IMON,JMON,NXTEMP
C
C  ASSEMBLY OF COEFFICIENTS
C
      DO 100 I = 2,NIM1
        DO 101 J = 2,NJM1
C-----COMPUTE AREAS AND VOLUMES
          AREAN = RV(J+1) * SEW(I) * RX(I)
          AREAS = RV(J)   * SEW(I)  * RX(I)
          AREAE = RY(J) * SNS(J) * RU(I+1)
          AREAW = RY(J) * SNS(J) * RU(I)
          VOL = RY(J) * SNS(J) * SEW(I) * RX(I)
C---- CALCULATE DIFFUSION COEFFICIENTS
          GAMN = 0.5 * (GAMH(IMAT(I,J)) + GAMH(IMAT(I,J+1)))
          GAMS = 0.5 * (GAMH(IMAT(I,J)) + GAMH(IMAT(I,J-1)))
          GAME = 0.5 * (GAMH(IMAT(I,J)) + GAMH(IMAT(I+1,J)))
          GAMW = 0.5 * (GAMH(IMAT(I,J)) + GAMH(IMAT(I-1,J)))
          DN = GAMN * AREAN/DYNP(J)
          DS = GAMS * AREAS/DYPS(J)
          DE = GAME * AREAE/DXEP(I)
          DW = GAMW * AREAW/DXPW(I)
C
C   SOURCE TERMS
C   UPDATES SU AND SP FOR TIME DEPENDANT HEAT SOURCES
          SU(I,J) = 0.0
          SP(I,J) = 0.0
          IF (INTIME)  THEN
            B = DENSIT(IMAT(I,J))*CP(IMAT(I,J))*VOL/DT
            SU(I,J) = B*TOLD(I,J) + (VOL * HEAT(IMAT(I,J)))
            SP(I,J) = - B
          ELSE
            B = 0.0
            SU(I,J) = VOL * HEAT(IMAT(I,J))
            SP(I,J) = 0.0
          ENDIF
C
C     ASSEMBLE MAIN COEFFICIENTS
          AN(I,J) = DN
          AS(I,J) = DS
          AW(I,J) = DW
          AE(I,J) = DE
  101   CONTINUE
  100 CONTINUE
C
C  PROBLEM MODIFICATIONS
        CALL PROMOD(TF,Q,TINCOR,TOUCOR)
C
C  FINAL COEFFICIENT ASSEMBLY + RESIDUAL SOURCE CALCULATION
        RESORT = 0.0
        DO 300 I = 2,NIM1
          DO 301 J = 2,NJM1
            AP(I,J) = AN(I,J)+AS(I,J)+AE(I,J)+AW(I,J)-SP(I,J)
            RESOR = AN(I,J)*T(I,J+1)+AS(I,J)*T(I,J-1)+AE(I,J)*T(I+1,J)
     &               +AW(I,J)*T(I-1,J)-AP(I,J)*T(I,J)+SU(I,J)
            VOL = RY(J)*SNS(J)*SEW(I)*RX(I)
            SORVOL = GREAT*VOL
            IF (-SP(I,J) GT 0.5*SORVOL) RESOR = RESOR/SORVOL
            RESORT = RESORT+ABS(RESOR)
C   UNDER-RELAXATION
            AP(I,J) = AP(I,J)/URFT
            SU(I,J) = SU(I,J)+(1.0 - URFT)*AP(I,J)*T(I,J)
  301   CONTINUE
  300 CONTINUE
C
C   SOLUTION OF DIFFERENCE EQUATIONS
        CALL LISOLV(2,2,T)
        RETURN
        END
C
C--------- LINE SOLVER ------------------------------------------C
        SUBROUTINE LISOLV(ISTART,JSTART,PHI)
CSUBROUTINE USES THE TRI-DIAGONAL MATRIX ALGORITHM IN ORDER TO SOLVE
CTHE SIMULTANEOUS EQUATIONS BY LINE ITERATION  THE BLOCK ADJUSTMENT
CPROCEDURE HAS ALSO BEEN ADDED
C
        PARAMETER(MAXNI=20,MAXNJ=20)
        PARAMETER(NMAT=8)
        PARAMETER(TZERO=1.0E-04)
        INTEGER
     &  NI,NJ,NIM1,NJM1,ICHAN,IMAT(MAXNI,MAXNJ),NITER
        REAL
     &  T(MAXNI,MAXNJ),TOLD(MAXNI,MAXNJ),DT,RESORT,URFT,TIME,
     &  AP(MAXNI,MAXNJ),AN(MAXNI,MAXNJ),AS(MAXNI,MAXNJ),
     &  AE(MAXNI,MAXNJ),SP(MAXNI,MAXNJ),
     &  AW(MAXNI,MAXNJ),SU(MAXNI,MAXNJ),
     &  AB(MAXNI),BB(MAXNI),CB(MAXNI),DB(MAXNI),PHI(MAXNI,MAXNJ),
     &  A(MAXNJ),B(MAXNJ),C(MAXNJ),D(MAXNJ),TERM
        LOGICAL INCYLY,INCYLX,INPRO,INTIME
        COMMON /CONVAR/ NI,NJ,NIM1,NJM1,ICHAN,DT,RESORT,URFT,GREAT
        COMMON /COEF/   AP, AN, AS, AE, AW, SU, SP
C
C     SWEEP/TRAVERSE SEQUENCE
        JSTM1 = JSTART-1
        A(JSTM1) = 0.0
C
```

```
C       COMMENCE S-N SWEEP --------
        DO 100 I = ISTART,NIM1
          C(JSTM1) = PHI(I,JSTM1)
C
C       COMMENCE S-N TRAVERSE
          DO 101 J = JSTART,NJM1
C
          IF(I.EQ.ICHAN) THEN
          ENDIF
C       ASSEMBLE TDMA COEFFICIENTS
            A(J) = AN(I,J)
            B(J) = AS(I,J)
            C(J) = AE(I,J)*PHI(I+1,J)+AW(I,J)*PHI(I-1,J)+SU(I,J)
            D(J) = AP(I,J)
C
C       CALCULATE COEFFICIENTS OF RECURRENCE FORMULA
            IF ((D(J)-B(J)*A(J-1)) .EQ. 0.0) THEN
              TERM = 0.0
            ELSE
              TERM = 1.0 / (D(J)-B(J)*A(J-1))
            ENDIF
            A(J) = A(J)*TERM
            C(J) = (C(J)+B(J)*C(J-1))*TERM
  101   CONTINUE
C
C       OBTAIN NEW T'S
          DO 102 JJ = JSTART,NJM1
            J = NJ+JSTM1-JJ
            PHI(I,J) = A(J)*PHI(I,J+1)+C(J)
  102   CONTINUE
  100 CONTINUE
C
C
        ISTM1 = ISTART-1
        A(ISTM1) = 0.0
C
C       COMMENCE W-E SWEEP --------
        DO 200 J = JSTART,NJM1
          C(ISTM1) = PHI(ISTM1,J)
C
C       COMMENCE W-E TRAVERSE
          DO 201 I = ISTART,NIM1
C
C       ASSEMBLE TDMA COEFFICIENTS
            A(I) = AE(I,J)
            B(I) = AW(I,J)
            C(I) = AN(I,J)*PHI(I,J+1)+AS(I,J)*PHI(I,J-1)+SU(I,J)
            D(I) = AP(I,J)
C
C       CALCULATE COEFFICIENTS OF RECURRENCE FORMULA
            IF ((D(I)-B(I)*A(I-1)) .EQ. 0.0) THEN
              TERM = 0.0
            ELSE
              TERM = 1.0 / (D(I)-B(I)*A(I-1))
            ENDIF
            A(I) = A(I)*TERM
            C(I) = (C(I)+B(I)*C(I-1))*TERM
  201   CONTINUE
C
C       OBTAIN NEW T'S
          DO 202 II = ISTART,NIM1
            I = NI+ISTM1-II
            PHI(I,J) = A(I)*PHI(I+1,J)+C(I)
  202   CONTINUE
  200 CONTINUE
C
CCC INITIALISES THE BLOCK ADJUSTMENT COEFFICIENTS
C   (BLOCK ADJUSTMENT ALGORITHM ONLY APPLICABLE FOR N>3)
C   (W-E SWEEP FOLLOWED BY S-N SWEEP REPLACED SAA-FASTER)
C
C       IF (NI.LE.3) GO TO 1000
C       DO 80 K = 1,NI
C         AB(K) = 0.0
C         BB(K) = 0.0
C         CB(K) = 0.0
C         DB(K) = 0.0
```

```
C 80  CONTINUE
C       BLOCK ADJUSTMENT PROCEDURE
C       DO 200 I = ISTART,NIM1
C         DO 110 J = JSTART,NJM1
C           AB(I) = AB(I) + AE(I,J)
C           BB(I) = BB(I) + AW(I,J)
C           CB(I) = CB(I) + AN(I,J)*PHI(I,J+1) + AS(I,J)*PHI(I,J-1)
C    &                    + AE(I,J)*PHI(I+1,J) + AW(I,J)*PHI(I-1,J)
C    &                    - AP(I,J)*PHI(I,J)   + SU(I,J)
C           DB(I) = DB(I) + AE(I,J) + AW(I,J) - SP(I,J)
C 110   CONTINUE
C 200 CONTINUE
C       AB(JSTM1) = 0.0
C       CB(JSTM1) = 0.0
C       DO 115 I = ISTART,NIM1
C         IF ((DB(I)-BB(I)*AB(I-1)) .EQ. 0.0) THEN
C           TERM = 0.0
C         ELSE
C           TERM = 1.0 / (DB(I)-BB(I)*AB(I-1))
C         ENDIF
C         AB(I) = AB(I)*TERM
C         CB(I) = (CB(I)+BB(I)*CB(I-1))*TERM
C 115 CONTINUE
C       BB(NI) = 0.0
C       DO 120 JJ = ISTART,NIM1
C         I = NI+JSTM1-JJ
C         BB(I) = AB(I)*BB(I+1)+CB(I)
C 120 CONTINUE
C       DO 180 I = ISTART,NIM1
C         DO 125 J = JSTART,NJM1
C           PHI(I,J) = PHI(I,J)+BB(I)
C 125   CONTINUE
C 180 CONTINUE
C1000 CONTINUE
C
        RETURN
        END
C------------------------- PROBLEM MODIFICATION ----------------C
        SUBROUTINE PROMOD(TF,N,TINCOR,TOUCOR)
C
        PARAMETER(MAXNI=20,MAXNJ=20)
        PARAMETER(NMAT=6)
        PARAMETER(TZERO=1.0E-04)
        REAL
     &  EPS1(0:NMAT),EPS2(0:NMAT),
     &  GAMH(0:NMAT),DENSIT(0:NMAT),CP(0:NMAT),
     &  HEAT(0:NMAT),GHEAT,DX,DY,
     &  RX(MAXNI),RU(MAXNI),X(MAXNI),Y(MAXNJ),DXEP(MAXNI),DXPW(MAXNI),
     &  DYNP(MAXNJ),DYPS(MAXNJ),SNS(MAXNJ),SEW(MAXNI),XU(MAXNI),
     &  YV(MAXNJ),RY(MAXNJ),RV(MAXNJ)
        REAL TF(MAXNJ),RESFUL(MAXNJ),RESMOD(MAXNJ),
     &  TFOLD(MAXNJ),RESF(MAXNJ),RESM(MAXNJ)
        INTEGER
     &  NI,NJ,NIM1,NJM1,ICHAN,IMAT(MAXNI,MAXNJ),NITER
        REAL
     &  T(MAXNI,MAXNJ),TOLD(MAXNI,MAXNJ),DT,RESORT,URFT,TIME,
     &  AP(MAXNI,MAXNJ),AN(MAXNI,MAXNJ),AS(MAXNI,MAXNJ),AE(MAXNI,MAXNJ),
     &  AW(MAXNI,MAXNJ),SU(MAXNI,MAXNJ),SP(MAXNI,MAXNJ)
        LOGICAL INCYLY,INCYLX,INPRO,INTIME
        COMMON /TEMP/   T,GAMH,TOLD,DENSIT,CP,EPS1,EPS2
        COMMON /CONVAR/ NI,NJ,NIM1,NJM1,ICHAN,DT,RESORT,URFT,GHEAT
        COMMON /GEOM/ NITER, DX, DY, RX, RU, X, Y, DXEP, DXPW, DYNP, DYPS,
     &                SNS, SEW, XU, YV, RY, RV, JS, JN
        COMMON /COEF/   AP, AN, AS, AE, AW, SU, SP
        COMMON /DMDATA/ DN, HEAT, IMAT
        COMMON /LGCOM/  INCYLX,INCYLY,INTIME
        COMMON /FLUID/  FLOW,CHAN,ROD
        COMMON /RESIST/ RESFUL,RESMOD
C
C     BOUNDARY PROPERTIES
C
          PI=4.0*ATAN(1.0)
          SIGMA = 5.67E-08
          KEL = 273.000
C--SET EXTERNAL NORTH&SOUTH COEFFS TO ZERO
        DO 100 I=2,NIM1
```

```
          AN(I,NJM1) = 0.0
          AS(I,2) = 0.0
  100 CONTINUE
C--SET EXTERNAL SIDE COEFFS TO ZERO
        DO 200 J=2,NJM1
          AW(2,J) = 0.0
          AE(NIM1,J) = 0.0
  200 CONTINUE
C
C--INNER BOUNDARIES ZEROED
          DO 202 J=2,NJM1
            SU(ICHAN,J) = 0.0
            SP(ICHAN,J) = 0.0
  202   CONTINUE
C
CC COND/V  INTERNAL BOUNDARY CONDS
            DO 300 J=2,NJM1
            DXE=RU(ICHAN)-RX(ICHAN-1)
            DF=GAMH(IMAT(ICHAN-1,J)) *SNS(J) *RU(ICHAN)/DXE
            HAF=H*SNS(J)*RU(ICHAN)
            RESF(J)= 1.0/DF + 1.0/HAF
                    RESFUL(J)=RESF(J)/(2.*PI)
            AE(ICHAN-1,J)= 1.0/RESF(J)
            AW(ICHAN,J)= AE(ICHAN-1,J)
C
            DXW=RX(ICHAN+1)-RU(ICHAN+1)
            DM=GAMH(IMAT(ICHAN+1,J))*SNS(J)*RU(ICHAN+1)/DXW
            HAM=H*SNS(J)*RU(ICHAN+1)
            RESM(J)= 1.0/DM + 1.0/HAM
                    RESMOD(J)=RESM(J)/(2.*PI)
            AW(ICHAN+1,J)= 1.0/RESM(J)
            AE(ICHAN,J)= AW(ICHAN+1,J)
C
C FLUID CHANNEL IS PART OF DOMAIN BUT LOWER NODE HAS A SOURCE IN IT
C AFLOW IS FLOW PER UNIT ANGLE TO BE CONSISTENT WITH COEFS
              CCP=1100.0
              AFLOW=FLOW*CCP/(2.*PI)
            AN(ICHAN,J)= 0.0
            AS(ICHAN,J)= AFLOW
            IF(J.EQ.2) THEN
             AS(ICHAN,J)=0.0
             SU(ICHAN,J)=SU(ICHAN,J)+AFLOW*TINCOR
             SP(ICHAN,J)=SP(ICHAN,J)-AFLOW
            ENDIF
C
  300       CONTINUE
CCCCCC RADIATIVE TRANSFER NEGLECTED PRESENTLY CCCC
C           IF(.NOT.INTIME)GO TO 800
CC RAD
C           AE(ICHAN-1,J) = 0.0
C           E1 = EPS1(IMAT(ICHAN-1,J))
C           ALPHA = E1 * SIGMA * ( (T(ICHAN-1,J)+KEL + T(ICHAN+1,J) +
C    &        KEL)*((T(ICHAN-1,J)+KEL)**2 + (T(ICHAN+1,J)+KEL)**2) )
C           RES =  DXE/(GAMH(IMAT(ICHAN-1,J))*SNS(J)*RU(ICHAN))
C    &              + 1.0/( ALPHA * SNS(J) * RU(ICHAN))
C           SU(ICHAN-1,J) = SU(ICHAN-1,J) +  T(ICHAN+1,J)/RES
C           SP(ICHAN-1,J) = SP(ICHAN-1,J) - 1.0/RES
C
C           AW(ICHAN+1,J) = 0.0
C           E2 = EPS2(IMAT(ICHAN+1,J))
C           ALPHA = E2 * SIGMA * ( (T(ICHAN-1,J)+KEL + T(ICHAN+1,J) +
C    &        KEL)*((T(ICHAN-1,J)+KEL)**2 + (T(ICHAN+1,J)+KEL)**2) )
C           RES =  DXW/(GAMH(IMAT(ICHAN+1,J))*SNS(J)*RU(ICHAN+1))
C    &              + 1.0/( ALPHA * SNS(J) * RU(ICHAN+1))
C           SU(ICHAN+1,J) = SU(ICHAN+1,J) +  T(ICHAN-1,J)/RES
C           SP(ICHAN+1,J) = SP(ICHAN+1,J) - 1.0/RES
C 800       CONTINUE
CCCCCCCCCCCCCCCCCCCCCCCCCCCCCCCCCCCCCCCCCCCCCCCCCCCCCCCCCC
        RETURN
        END
C
C------------ DATA FOR EACH OF THE MATERIALS ENTERED HERE ------C
        BLOCK DATA DEVALU
C
        PARAMETER(MAXNI=20,MAXNJ=20)
        PARAMETER(NMAT=6)
```

```
      PARAMETER(ZERO=1 0E-04)
      REAL
     &  EPS1(0 :MAT),EPS2(0 :MAT),
     &  GAMS(0 :MAT),DENSIT(0 :MAT),CP(0 :MAT),
     &  HEAT(0 :MAT),GREAT
      INTEGER
     &  NI,NJ,NIM1,NJM1,ICHAR,IMAT(MAXNI,MAXNJ),NITER
      REAL
     &  T(MAXNI,MAXNJ),TOLD(MAXNI,MAXNJ),DT,RESORT,URFT,TIME,
     &  AP(MAXNI,MAXNJ),AN(MAXNI,MAXNJ),AS(MAXNI,MAXNJ),AE(MAXNI,MAXNJ),
     &  AW(MAXNI,MAXNJ),SU(MAXNI,MAXNJ),SP(MAXNI,MAXNJ)
      LOGICAL IPCYLY,IPCYLX,IPPRO,IPTIME
      COMMON /TEMP/   T, GAMS, TOLD, DENSIT, CP,EPS1,EPS2
      COMMON /CONVAR/ NI,NJ,NIM1,NJM1,ICHAR,DT,RESORT,URFT,GREAT
      COMMON /DMDATA/ DB, HEAT, IMAT
C
      DATA HEAT(0)   / 0 0  /
      DATA GAMS(0)   / 0 0  /
      DATA DENSIT(0) / 0 0  /
      DATA CP(0)     / 0 0  /
      DATA EPS1(0)   / 0 0  /
      DATA EPS2(0)   / 0 0  /
C
C   1  U02    DATA (DECAY DATA IS 'CALCSR')
      DATA GAMS(1)   / 2 430  /
      DATA DENSIT(1) / 10500 0/
      DATA CP(1)     / 235 0  /
      DATA EPS1(1)   / 0 400  /
      DATA EPS2(1)   / 0 400  /
C
C   2.  S.S  CLAD  DATA
      DATA GAMS(2)   / 31 80  /
      DATA DENSIT(2) / 7980 0 /
      DATA CP(2)     / 500 0  /
      DATA EPS1(2)   / 0 011  /
      DATA EPS2(2)   / 0 080  /
C
C   3.  MODERATOR/DILUENT DATA
C       H 0    DATA
      DATA GAMS(3)   / 31 5   /
      DATA DENSIT(3) / 7980 0 /
      DATA CP(3)     / 500 0  /
      DATA EPS1(3)   / 0 011  /
      DATA EPS2(3)   / 0 080  /
C       GRAPHITE DATA
      DATA GAMS(4)   / 80 0   /
      DATA DENSIT(4) / 1700 0 /
      DATA CP(4)     / 1867   /
      DATA EPS1(4)   / 0 804  /
      DATA EPS2(4)   / 0 080  /
C       ALUMINA DATA
      DATA GAMS(5)   / 7 00   /
      DATA DENSIT(5) / 3750 0 /
      DATA CP(5)     / 1382 0 /
      DATA EPS1(5)   / 0 723  /
      DATA EPS2(5)   / 0 033  /
C       SIC DATA
      DATA GAMS(6)   / 45 00  /
      DATA DENSIT(6) / 3200 0 /
      DATA CP(6)     / 1320 0 /
      DATA EPS1(6)   / 0 730  /
      DATA EPS2(6)   / 0 030  /
C
      END
C
C----------------- OUTPUT OF MATERIAL FIELD ------------------C
      SUBROUTINE CONOUT(MAXNI,MAXNJ,NI,NJ,IMAT,HEADT)
      DIMENSION IMAT(MAXNI,MAXNJ)
      CHARACTER F*11,HEADT*(*)
      DATA F   / '(YY(2X,I1))' /
C
      WRITE(3,100) HEADT
      DO 500 J = 1,NJ
        LISTA = 1
  250   CONTINUE
        LISEND = LISTA + (LISLIN - 1)
        LISEND = MIN0(LISEND,NI)
        IF4 = LISEND
        WRITE(F(2 3),FMT='(I3)') LISEND
        WRITE(3,FMT=F) (IMAT(II,J),II=LISTA,LISEND)
        LISTA = LISEND + 1
        IF (LISEND LT NI) GO TO 250
  500 CONTINUE
  100 FORMAT(///101,A80/)
      RETURN
      END
C
C----------------- OUTPUT OF DEPENDANT-VARIABLE FIELDS --------C
      SUBROUTINE PRINT(MAXNI,MAXNJ,ISTART,JSTART,NI,NJ,X,Y,PSI,TIME
     &,HEAD)
      REAL  PSI(MAXNI,MAXNJ),STORE(80)
      REAL  X(MAXNI),Y(MAXNJ)
      CHARACTER NI*4,NY*4,F*28,FD*28,HEAD*(*)
      DATA F/  '(/1X ,A8,''Y=''(1X,7X),A8)'/
      DATA FD/ '(1X ,1X,''Y=''(1PE10 3),G11 3)' /
      DATA NI,NY/' I =  ',' Y =  '/
        WRITE(8,*) TIME,PSI(7,6)
C
        WRITE(8,*)'.....'
      DO 80 I=2,NI-1
        WRITE(8,1500) X(I),PSI(I,6)
   80   CONTINUE
 1500  FORMAT(2X,3(1PE12 6,6X))
C       WRITE(8,*)'.....'
      ISKIP=1
      JSKIP=1
      LIMLIN = 10
      LISTA = ISTART
      WRITE(2,110) HEAD
  100 CONTINUE
      LISEND = LISTA + (LIMLIN - 1) * ISKIP
      LISEND = MIN0(NI,LISEND)
      IF4 = (LISEND-LISTA)/ISKIP + 1
      WRITE(F(10 11),FMT='(I2)') IF4
      WRITE(FD(8 10),FMT='(I3)') IF4
      WRITE(3,FMT=F) NI, (I,I=LISTA,LISEND,ISKIP), NY
      WRITE(3,113)
      DO 101 JJ=JSTART,NJ,JSKIP
        J = JSTART+NJ-JJ
        IS = 0
        DO 120 I = LISTA,LISEND,ISKIP
          A=PSI(I,J)
          IF (ABS(A) LT 1 0E-20) A = 0 0
          IS = IS+1
          STORE(IS) = A
  120   CONTINUE
        WRITE(3,FMT=FD)  J,(STORE(I),I=1,IS),Y(J)
  101  CONTINUE
      WRITE(2,114) (X(I),I=LISTA,LISEND,ISKIP)
      LISTA = LISEND+ISKIP
      IF (LISEND LT NI) GO TO 100
  110 FORMAT(//40('-'),7X,A80,7X,40('-'))
  112 FORMAT(' J')
  114 FORMAT(/' X = ',1P80 8,11610 8)
      RETURN
      END
C
C------------------------ INITIALISATION OPERATIONS ----------C
      SUBROUTINE INIT
      PARAMETER(MAXNI=20,MAXNJ=20)
      PARAMETER(NMAT=8)
      PARAMETER(ZERO=1 0E-04)
      REAL
     &  EPS1(0 :MAT),EPS2(0 :MAT),
     &  GAMS(0 :MAT),DENSIT(0 :MAT),CP(0 :MAT),
     &  HEAT(0 :MAT),GREAT,DX,DY,
     &  XI(MAXNI),SU(MAXNI),X(MAXNI),Y(MAXNJ),DXEP(MAXNI),DXPW(MAXNI),
     &  DYSP(MAXNJ),DYPN(MAXNJ),SNS(MAXNJ),SEW(MAXNI),XU(MAXNI),
     &  YV(MAXNJ),SY(MAXNJ),SV(MAXNJ)
      INTEGER
     &  NI,NJ,NIM1,NJM1,ICHAR,IMAT(MAXNI,MAXNJ),NITER
      REAL
     &  T(MAXNI,MAXNJ),TOLD(MAXNI,MAXNJ),DT,RESORT,URFT,TIME,
     &  AP(MAXNI,MAXNJ),AN(MAXNI,MAXNJ),AS(MAXNI,MAXNJ),AE(MAXNI,MAXNJ),
     &  AW(MAXNI,MAXNJ),SU(MAXNI,MAXNJ),SP(MAXNI,MAXNJ)
      LOGICAL IPCYLY,IPCYLX,IPPRO,IPTIME
      COMMON /TEMP/   T, GAMS, TOLD, DENSIT, CP,EPS1,EPS2
      COMMON /CONVAR/ NI,NJ,NIM1,NJM1,ICHAR,DT,RESORT,URFT,GREAT
      COMMON /GEOM/ NITER, DX, DY, XI, SU, X, Y, DXEP, DXPW, DYSP, DYPN,
     &             SNS, SEW, XU, YV, SY, SV, JN, JS
      COMMON /COEF/   AP, AN, AS, AE, AW, SU, SP
      COMMON /DMDATA/ DB, HEAT, IMAT
      COMMON /LOGOM/  IPCYLX,IPCYLY,IPTIME
C
C CALCULATE GEOMETRICAL QUANTITIES
C
      IF(IPCYLX AND IPCYLY) GO TO 1800
      DO 100 I = 1,NI
        XI(I) = 1 0
        IF(IPCYLX) XI(I) = X(I)
  100 CONTINUE
      DO 300 J = 1,NJ
        SY(J) = 1 0
        IF(IPCYLY) SY(J) = Y(J)
  300 CONTINUE
      DXPW(1) = 0 0
      DXEP(NI) = 0 0
      DO 200 I = 1,NIM1
        DXEP(I) = X(I+1)-X(I)
        DXPW(I+1) = DXEP(I)
  200 CONTINUE
      DYPN(1) = 0 0
      DYSP(NJ) = 0 0
      DO 400 J = 1,NJM1
        DYSP(J) = Y(J+1)-Y(J)
        DYPN(J+1) = DYSP(J)
  400 CONTINUE
      SEW(1) = 0 0
      SEW(NI) = 0 0
      DO 500 I = 2,NIM1
        SEW(I) = 0 5*(DXEP(I)+DXPW(I))
  500 CONTINUE
      SNS(1) = 0 0
      SNS(NJ) = 0 0
      DO 600 J = 2,NJM1
        SNS(J) = 0 5*(DYSP(J)+DYPN(J))
  600 CONTINUE
      XU(1) = 0 0
      SU(1) = 0 0
      DO 700 I = 2,NI
        SU(I) = 0 5*(SX(I)+SX(I-1))
        XU(I) = 0 5*(X(I)+X(I-1))
  700 CONTINUE
      YV(1) = 0 0
      SV(1) = 0 0
      DO 800 J = 2,NJ
        SV(J) = 0 5*(SY(J)+SY(J-1))
        YV(J) = 0 5*(Y(J)+Y(J-1))
  800 CONTINUE
C
C  MODIFY BOUNDRY VALUES OF X AND Y
C  SET VARIABLES TO ZERO
C
      X(1) = XU(2)
      IF (X(1) LT (XU(NI)-XU(2))*1 0E-08) X(1) = 0 0
      X(NI) = XU(NI)
      Y(1) = YV(2)
      IF (Y(1) LT (YV(NJ)-YV(2))*1 0E-08) Y(1) = 0 0
      Y(NJ) = YV(NJ)
      DO 1000 I = 1,MAXNI
        DO 900 J = 1,MAXNJ
          AE(I,J) = 0 0
          AW(I,J) = 0 0
          AN(I,J) = 0 0
          AS(I,J) = 0 0
          SU(I,J) = 0 0
          SP(I,J) = 0 0
```

```
            TOLD(I,J) = 0.0
  900     CONTINUE
 1000 CONTINUE
C
        RETURN
 1900 WRITE(2,8000)
        STOP
 8000 FORMAT(//10X,'INCYLX AND INCYLY SET TO TRUE'
     &//'  - PROGRAM TERMINATED - ')
        END
C--------------- DECAY HEAT CALCULATION -----------------------C
        SUBROUTINE CALCDH (OLDTM,TNEW,Q,TTRIP)
C
C  CALCULATES THE NEW DECAY HEAT SOURCE COEFFICIENTS OVER
C  THE TIME STEP BETWEEN 'OLDTM' AND 'TNEW'  THE MATERIAL
C  DATA IS IN BLOCK DATA  AN ANALYTIC EQN IS USED  (WINTERTON)
C
        PARAMETER(MAXNI=20,MAXNJ=20)
        PARAMETER(NMAT=6)
        PARAMETER(TZERO=1.0E-04)
        REAL
     &  HEAT(0:NMAT),GHEAT,DX,DY,
     &  RX(MAXNI),RU(MAXNI),X(MAXNI),Y(MAXNJ),DXEP(MAXNI),DXPW(MAXNI),
     &  DYNP(MAXNJ),DYPS(MAXNJ),SNS(MAXNJ),SEW(MAXNI),XU(MAXNI),
     &  YV(MAXNJ),RY(MAXNJ),RV(MAXNJ)
        INTEGER
     &  NI,NJ,NIM1,NJM1,ICHAN,IMAT(MAXNI,MAXNJ),NITER
        REAL OLDTM,TNEW
        LOGICAL INCYLY,INCYLX,INPRO,INTIME
        COMMON /CONVAR/ NI,NJ,NIM1,NJM1,ICHAN,DT,RESORT,URFT,GHEAT
        COMMON /GEOM/ NITER, DX, DY, RX, RU, X, Y, DXEP, DXPW, DYNP, DYPS,
     &                SNS, SEW, XU, YV, RY, RV, JS, JN
        COMMON /LGEOM/ INCYLX,INCYLY,INTIME
        COMMON /DHDATA/ DH, HEAT, IMAT
        COMMON /FLUID/ FLOW,CHAN,ROD
C
        PI=4.0*ATAN(1.0)
        HZ= YV(NJ)
        QC= Q/(CHAN*ROD)
        AF=PI*(RU(ICHAN-1))**2
        RAT= QC/HZ
        T01 = 0.1
        T10 = 10.0
        IF(TNEW.GT.TTRIP) THEN
          TN=TNEW-TTRIP
          IF(OLDTM.GE.TTRIP) THEN
            OT=OLDTM-TTRIP
          ELSE
            OT=0.0
          ENDIF
        ENDIF
C
        DO 400 IM=1,NMAT
C
         IF(IM.EQ.1) THEN
          IF(TNEW.GT.TTRIP) THEN
             DH0=0.00700
C
           IF (TN.LT.T01) THEN
             HEAT(IM) =  DH0
           ELSEIF (TN.LE.T10 .AND. OT.LT.T01) THEN
             HEAT(IM) =DH1(TN)-DH0
           ELSEIF (TN.LE.T10 .AND. OT.GE.T01) THEN
             HEAT(IM) =DH1(TN) -DH1(OT)
           ELSEIF (TN.GT.T10 .AND. OT .LE. T10) THEN
             HEAT(IM) =DH1(T10) - DH1(OT) + DH2(TN) - DH1(T10)
           ELSE
             HEAT(IM) = DH2(TN) - DH2(OT)
           ENDIF
C
         ELSE
         HEAT(IM)=1.0
         ENDIF
        ELSE
        HEAT(IM) = 0.0
        ENDIF
C RATING AT RAT W/M AND  FUEL CM RADIUS ROD GIVES (W/M3)
C FOR A CORE OF HZ HEIGHT AND CHAN-ROD PINS
        HEAT(IM)=  HEAT(IM)*(RAT/AF)
C
        IF(IM.NE.1) GO TO 400
        WRITE(2,888) IM,HEAT(IM)
        WRITE(*,*) 'HEAT=  ',HEAT(IM)
        WRITE(*,*)'---  -- ---- -- - '
  888   FORMAT(' HEAT(',I1,')= ',1PE10.3)
C
  400   CONTINUE
        RETURN
        END
C
C  DH1 DECAY HEAT ANALYTICAL FUNCTION
        REAL FUNCTION DH1(T)
        REAL T
        DH1 =  0.007 + 0.0843*((T**0.2661)-0.11686)
        RETURN
        END
C
C  DH1 DECAY HEAT ANALYTICAL FUNCTION
        REAL FUNCTION DH2(T)
        REAL T
        DH2 = 0.6648 + 0.0888*((T**0.2193)-6.986)
        RETURN
        END
C--------------- INIT ESTIMATE OF HEAT FLUX TO COOLANT ---------C
        SUBROUTINE QLOC(Q,QLOCAL,QFLUID)
        PARAMETER(MAXNI=20,MAXNJ=20)
        REAL
     &  RX(MAXNI),RU(MAXNI),X(MAXNI),Y(MAXNJ),DXEP(MAXNI),DXPW(MAXNI),
     &  DYNP(MAXNJ),DYPS(MAXNJ),SNS(MAXNJ),SEW(MAXNI),XU(MAXNI),
     &  YV(MAXNJ),RY(MAXNJ),RV(MAXNJ)
        REAL TF(MAXNJ),QLOCAL(MAXNJ)
        LOGICAL INCYLY,INCYLX,INPRO,INTIME
        COMMON /CONVAR/ NI,NJ,NIM1,NJM1,ICHAN,DT,RESORT,URFT,GHEAT
        COMMON /GEOM/ NITER, DX, DY, RX, RU, X, Y, DXEP, DXPW, DYNP, DYPS,
     &                SNS, SEW, XU, YV, RY, RV, JS, JN
        COMMON /FLUID/ FLOW,CHAN,ROD
C
        HZ= YV(NJ)
        QC= Q/(CHAN*ROD)
        RAT= QC/HZ
C
        QFLUID=0.0
        DO 15 IZ=2, NJM1
        QLOCAL(IZ) = RAT * SNS(IZ)
        QFLUID=QFLUID+QLOCAL(IZ)
  15    CONTINUE
C
        RETURN
        END
C-------------------------------------------------------------C
        SUBROUTINE FUELHT(TF,QLOCAL,QFLUID,TINCOR,TOUCOR)
        PARAMETER(MAXNI=20,MAXNJ=20)
        PARAMETER(NMAT=6)
C THE TRANSIENT HEAT INTO COOLANT CHANNEL FROM
C THE FUELMOD VIA THE INTERFACE RESISTANCES
        REAL
     &  EPS1(0:NMAT),EPS2(0:NMAT),
     &  GAMH(0:NMAT),DENSIT(0:NMAT),CP(0:NMAT),
     &  RX(MAXNI),RU(MAXNI),X(MAXNI),Y(MAXNJ),DXEP(MAXNI),DXPW(MAXNI),
     &  DYNP(MAXNJ),DYPS(MAXNJ),SNS(MAXNJ),SEW(MAXNI),XU(MAXNI),
     &  YV(MAXNJ),RY(MAXNJ),RV(MAXNJ)
        REAL TF(MAXNJ),QLOCAL(MAXNJ),RESFUL(MAXNJ),
     &  RESMOD(MAXNJ)
        REAL T(MAXNI,MAXNJ),TOLD(MAXNI,MAXNJ),DT,RESORT,URFT,
     &  TIME
        COMMON /TEMP/   T, GAMH  TOLD, DENSIT, CP,EPS1,EPS2
        COMMON /CONVAR/ NI,NJ,NIM1,NJM1,ICHAN,DT,RESORT,URFT,GHEAT
        COMMON /RESIST/ RESFUL RESMOD
C
        QFLUID=0.0
        WRITE(2,*)'------ '
        WRITE(2,*)' IN FUELHT '
        DO 10 IZ=2,NJM1
        QLOCAL(IZ)=( (T(ICHAN-1,IZ)-T(ICHAN,IZ))/RESFUL(IZ)
       & +(T(ICHAN+1,IZ)-T(ICHAN,IZ))/RESMOD(IZ) )
        QFLUID=QFLUID+QLOCAL(IZ)
        WRITE(2,*)'RESFUL(IZ) ',RESFUL(IZ),' RESMOD(IZ) ',RESMOD(IZ)
        WRITE(2,*)' QLOCAL(IZ) ',QLOCAL(IZ)
   10   CONTINUE
        WRITE(2,*)'QFLUID ',QFLUID
        WRITE(2,*)'------ '
C
        RETURN
        END
C-------------------------------------------------------------C
        SUBROUTINE FLUIDT(TIN,TOUT,Q,QLOCAL,TF,QFLUID)
        PARAMETER(MAXNI=20,MAXNJ=20)
        REAL TF(MAXNJ),QLOCAL(MAXNJ)
        COMMON /CONVAR/ NI,NJ,NIM1,NJM1,ICHAN,DT,RESORT,URFT,GHEAT
        COMMON /FLUID/ FLOW,CHAN,ROD
C
C CALCULATES TEMPERATURE FIELD IN COOLANT IN CORE
C QLOCAL IS THE LOCAL HEAT-TRANSFER RATE AND Q IS THE TOTAL
C NOTE THAT THIS RETURNS MID-SECTION VALUES
C
C Q IS NOW MODIFIED TO BE TOTAL OUTPUT PER SINGLE PIN
         QO= Q/(CHAN-ROD)
C
         TOUTLO=TIN
        WRITE(2,*)'------  IN FLUIDT '
         WRITE(2,*)'TIN/TOUT ',TIN,'/',TOUT
         DO 20 IZ=2,NJM1
         TFDIFF=0.5*(TOUT-TIN)*QLOCAL(IZ)/QFLUID
         TF(IZ)=TOUTLO+TFDIFF
        WRITE(2,*)'TFLUID(',IZ,')=',TF(IZ),' QLOCAL(',IZ,')=',QLOCAL(IZ)
         TOUTLO=TF(IZ)+TFDIFF
   20    CONTINUE
        WRITE(2,*)'------ '
         RETURN
         END
C-------------------------------------------------------------C
        SUBROUTINE CONVEC(TINCOR,TOUCOR,TF,TFOLD,TIME,IT,S,POLD,TAU)
        PARAMETER(MAXNI=20,MAXNJ=20)
        PARAMETER(NMAT=6)
        REAL
     &  EPS1(0:NMAT),EPS2(0:NMAT),
     &  GAMH(0:NMAT),DENSIT(0:NMAT),CP(0:NMAT),
     &  HEAT(0:NMAT),GHEAT,DX,DY,
     &  RX(MAXNI),RU(MAXNI),X(MAXNI),Y(MAXNJ),DXEP(MAXNI),DXPW(MAXNI),
     &  DYNP(MAXNJ),DYPS(MAXNJ),SNS(MAXNJ),SEW(MAXNI),XU(MAXNI),
     &  YV(MAXNJ),RY(MAXNJ),RV(MAXNJ),
     &  T(MAXNI,MAXNJ),TOLD(MAXNI,MAXNJ)
        REAL TF(MAXNJ),TFOLD(MAXNJ),QLOCAL(MAXNJ)
        LOGICAL INCYLY,INCYLX,INPRO,INTIME
        COMMON /TEMP/  T,GAMH,TOLD,DENSIT,CP,EPS1,EPS2
        COMMON /CONVAR/ NI,NJ,NIM1,NJM1,ICHAN,DT,RESORT,URFT,GHEAT
        COMMON /GEOM/ NITER, DX  DY, RX, RU, X, Y, DXEP, DXPW, DYNP, DYPS,
     &                SNS, SEW, XU, YV, RY, RV, JS, JN
        COMMON /FLUID/ FLOW,CHAN,ROD
        COMMON /LGEOM/ INCYLX,INCYLY,INTIME
C
          CALL MASFLO(TINCOR,TOUCOR,TF,TFOLD,TIME,TAVG,P,IT,POLD,TAU)
          CALL STCORE(TINCOR,TOUCOR,TAVG,P,S,POLD)
        RETURN
        END
C
        SUBROUTINE MASFLO(TINCOR,TOUCOR,TF,TFOLD,TIME,TAVG,P,IT,POLD,TAU)
        PARAMETER(MAXNI=20,MAXNJ=20)
        PARAMETER(NMAT=6)
        REAL
     &  EPS1(0:NMAT),EPS2(0:NMAT),
     &  GAMH(0:NMAT),DENSIT(0:NMAT),CP(0:NMAT),
     &  HEAT(0:NMAT),GHEAT,DX,DY,
     &  RX(MAXNI),RU(MAXNI),X(MAXNI),Y(MAXNJ),DXEP(MAXNI),DXPW(MAXNI),
     &  DYNP(MAXNJ),DYPS(MAXNJ),SNS(MAXNJ),SEW(MAXNI),XU(MAXNI),
     &  YV(MAXNJ),RY(MAXNJ),RV(MAXNJ)
     &  T(MAXNI,MAXNJ),TOLD(MAXNI,MAXNJ)
        REAL TF(MAXNJ),TFOLD(MAXNJ)
```

```
      LOGICAL INCYLX,INCYLY,INTIME
      COMMON /TEMP/  T,GAMA,TOLD,DENSIT,CP,EPS1,EPS2
      COMMON /CONVAR/  NI,NJ,NIM1,NJM1,ICHAN,DT,REPORT,URFT,GREAT
      COMMON /GEOM/ NITER, DX, DY, RX, RU, X, Y, DXEP, DXPW, DYNP, DYPS,
     &                  SNS, SEW, XU, YV, RY, RV, JS, JN
      COMMON /FLUID/ FLOW,CHAN,ROD
      COMMON /LOGDM/ INCYLX,INCYLY,INTIME
CVCALCULATES THE FLOW RATE AT A GIVEN PRESSURE AND TEMP
CV NOTE USAGE OF FLOW PER SINGLE CHANNEL(FLOW)
C
C------
        IF(IT EQ 1) THEN
         TFOLD(2)=TF(2)
         TFOLD(NJM1)=TF(NJM1)
          TAVG = TF(2) + TF(NJM1) / 2 0
          TOLD(ICHAN,2) = TFOLD(2)
          TOLD(ICHAN,NJM1) = TFOLD(NJM1)
        ELSE
          TAVG = T(ICHAN,2) + T(ICHAN,NJM1) / 2 0
          TOLD(ICHAN,2) = T(ICHAN,2)
          TOLD(ICHAN,NJM1) = T(ICHAN,NJM1)
        ENDIF
C
        IF(INTIME) THEN
          TAVGO = TOLD(ICHAN,2) + TOLD(ICHAN,NJM1) /2 0
        ELSE
          IF(IT EQ 1) THEN
            TAVGO=TFOLD(2)+TFOLD(NJM1)/2 0
          ELSE
            TAVGO=TOLD(ICHAN,2)+TOLD(ICHAN,NJM1)/2 0
          ENDIF
         ENDIF
C-----
        TOLD(ICHAN,2)=T(ICHAN,2)
CV PRESSURE FALL CONSTANT TAU GIVEN
      PO= 40 0
      IF(INTIME) THEN
        P = PO - EXP(-TIME/TAU)
      WRITE(2,*)' TIME  ',TIME,' P  = ',P
CVUSE AVERAGE AXIAL TEMP USED FOR CHAN TO REDETERMINE FLOW
         FLOW = FLOW - (P/POLD) - (TAVGO/TAVG)
      ELSE
       P=PO
      ENDIF
C
      POLD = P
C
       DO 783 II=2,NJM1
       TFOLD(II)=TF(II)
783    CONTINUE
      RETURN
      END
C
      SUBROUTINE HTCORE(TINCOR,TOUCOR,TAVG,P,H,POLD)
      PARAMETER(MAXNI=20,MAXNJ=20)
      PARAMETER(NMAT=8)
      REAL
     &  RX(MAXNI),RU(MAXNI),X(MAXNI),Y(MAXNJ),DXEP(MAXNI),DXPW(MAXNI),
     &  DYNP(MAXNJ),DYPS(MAXNJ),SNS(MAXNJ),SEW(MAXNI),XU(MAXNI),
     &  YV(MAXNJ),RY(MAXNJ),RV(MAXNJ)
      COMMON /CONVAR/ NI,NJ,NIM1,NJM1,ICHAN,DT,REPORT,URFT,GREAT
      COMMON /GEOM/ NITER, DX, DY, RX, RU  X, Y, DXEP, DXPW, DYNP, DYPS,
     &                  SNS, SEW, XU, YV, RY, RV, JS, JN
      COMMON /FLUID/  FLOW,CHAN,ROD
C
CVCALCULATE THE VISCOSITY FOR THE AVERAGE FLUID TEMP
      VST1 =  3 8E-04 + (0 078E-04)*TAVG
      VST2 = 8 88E-04 + (0 088E-04)*TAVG
      AMU2= VST1+(VST1-VST2) - ( P -1 0 )/80 0
C
      AMU=30 0E-06
CVCALCULATE THE THERMAL CONDUCTIVITY FOR THE AVERAGE FLUID TEMP
C     AKT1= (0 078E-5)*TAVG - 3 8E-5
C     AKT2= (1 87E-5) + (0 088E-5)*TAVG
C     AK= AKT2-AKT1
C     AKC= AKT1 + AK*(P - 1 0)/80 0
      AKC=46 0E-03
CVCHANNEL GEOMETRY
      PI=4 0*ATAN(1 0)
      R1 = RU(ICHAN)
      R2 = RU(ICHAN+1)
      AX = PI * (R2**2 - R1**2)
      WP = 2 0*PI*(R1+R2)
C
CVCALCULATE THE HEAT-TRANSFER COEFFICIENT
      CC = 1100 0
      DE = 4 0*AX/WP
      PR = CC * AMU /AKC
      GCORE=(FLOW/AX)
      VELOC=GCORE/31 0
      RE = GCORE*DE / AMU
      WRITE(2,*)'AMU = ',AMU,' AMU2(NOT USED) ',AMU2
      WRITE(2,*)'FLOW(KG/S) PER PIN = ',FLOW,' GCORE(PIN)= ',GCORE
      WRITE(2,*)'VELOC(M/S) ',VELOC,'  RE  = ',RE
CVROUGHENED SURFACE CORRELATION
C     H = 0 064*GCORE*CC* (RE**(-0 2)) * (PR**(-0 6))
      H2= 0 023*GCORE*CC* (RE**(-0.2)) * (PR**(-0 6))
      H=0 023*(AKC/DE)*(RE**0 8)*(PR**0 4)
      WRITE(2,*)'H  =',H
      RETURN
      END
C-------------------------------------------------------------------C
      SUBROUTINE BOILER(Q,QFLUID,TS,TOUCOR,TINCOR)
      REAL MUP,KP,KWALL,ID,NOB
      COMMON /FLUID/  FLOW,CHAN,ROD
CB CALCULATES THE OVER-ALL HEAT-TRANSFER COEFFICIENT FOR THE BOILER
CB AND HENCE THE INLET AND OUTLET TEMPERATURES
CB ASSUMES NEGLIGIBLE SECONDARY RESISTANCE, QUASI-STEADY CONDITIONS
CB AND CONSTANT SECONDARY TEMP
C
CB BOILER CHARACTERISTICS
      DATA KWALL/21 5/,THICK/4 E-4/,OD/2 99E-2/,ID/2 817E-2/
     & ,AHEAT/2 88E04/,AMIN/1 88E01/,NOB/12/
C
      FLOWB= (FLOW*CHAN*ROD)/NOB
CBCOOLANT PROPERTIES
      CCP = 1100
      KP =46 E-3
      MUP=30 E-6
CBHEAT TRANSFER COEFFICIENT
      GB = FLOWB/AMIN
      PR = CCP * MUP /KP
      REP = GB*OD/MUP
      HP =  023*(KP/OD)*(REP**0 84)*(0 87)
      U = 1 0/((1 /HP)+(THICK/KWALL))
CCCCCCCCCCCCCCCCCCCCCCCCCCCCCCCCCCCCCCCCCCCC
CCC CIRCULATOR CC NOT INCLUDED PRESENTLY
CCI   TCUI = TBO
CCI   DELPCU= 0 184*FLOW*(REP**0 2)*(L/(DE*AC))
CCI   CP =1 1
CCI   CV =1 4
CCI   CRATIO = CP/CV
CCI   CPOW = (CRATIO-1 0)/CRATIO
CCI   TCUO = TCUI * ((DELPCU+POLD)/POLD)**CPOW
CCCCCCCCCCCCCCCCCCCCCCCCCCCCCCCCCCCCCCCCCCCC
C CALCULATE TEMPERATURES REQUIRED TO TRANSFER HEAT THROUGH BG
C NOTE I HAVE MADE THIS A CALC PER SINGLE BOILER BY USING
C THE HEAT TRANSFER PER BOILER AND THE FLOW PER BOILER !
      QFLT=QFLUID*CHAN*ROD/NOB
      QB=QFLT
      NTUNIT=AHEAT*U/(FLOWB*CCP)
      NTERM=1 -EXP(-NTUNIT)
      TOUCOR=TS+QB/(FLOWB*CCP*NTERM)
      TINCOR=TOUCOR-QB/(FLOWB*CCP)
         WRITE(2,*)'****** IN BOILER   '
         WRITE(2,*)' RE = ',REP,' U = ',U
         WRITE(2,*)' QFLT= ',QFLT,' NTERM ',NTERM
         WRITE(2,*)' FLOWB = ',FLOWB
      RETURN
      END
```

GLOSSARY

η	number of neutrons produced per neutron absorbed.
DI (or I_d)	discharge irradiation.
DT	core dwell time.
B_r^2	radial geometric buckling.
B_z^2	axial geometric buckling.
k_∞	infinite multiplication factor.
k_{eff}	effective multiplication factor.
ϵ	fast fission factor.
α	ratio of capture to fission.
k^g	g-group evaluated infinite multiplication factor.
k^{69}	69-group evaluated infinite multiplication factor.
1-d	one dimensional.
BOL	beginning-of-life.
EOL	end-of-life.
ICR	internal conversion ratio.
BR	breeding ratio.
dk	difference in multiplication factor.
c.c.	continuous-cycle refuelling.
E-median	median energy of neutron flux spectrum.
V_d/V_f	volume ratio of diluent to fuel.
HM	heavy metal.
L/D	ratio of core length to diameter.
ρ	density.
C_p	specific heat capacity at constant pressure.
ξ	neutron mean lethargy gain per collision.
Σ_s	macroscopic scattering cross-section.
Σ_a	macroscopic absorption cross-section.
$\xi\Sigma_s$	moderating power.
$\xi\Sigma_s/\Sigma_a$	moderating ratio.
MWd/t	Mega-Watt-day per tonne.
kg/GW-yr	kilogram per Giga-Watt-year.
SS316	stainless-steel 316.